PROCEEDINGS OF

APSYM 2008

*Eleventh National Symposium on*

# ANTENNAS AND PROPAGATION

**29-31 December, 2008**

DEPARTMENT OF ELECTRONICS
Cochin University of Science and Technology
Kochi – 682 022

ISBN : 978-81-906050-6-9
Published by The Directorate of Public Relations and Publications for CREMA, Department of Electronics, Cochin University of Science & Technology, Cochin 682022, INDIA and printed at Maptho Printers, South Kalamassery, INDIA.

December 2008

SEARCH

Next Page

**Proceedings of APSYM 2008**
December 29-31, 2008

***Organised by,***

***Department of Electronics***
***Cochin University of Science and Technology***
***Kochi, India***
***Phone: 91 484 2576418***
***Fax : 91 484 2575800***
***URL : www.doe.cusat.edu***

**Editors:**
**Prof. K.G. Nair**
**Prof. P.R.S. Pillai**
**Prof. K. Vasudevan**
**Prof. K.T. Mathew**
**Prof. P. Mohanan**
**Prof. C.K. Aanandan**

**Co-sponsored by**

**University Grants Commission (UGC).**
**All India Council for Technical Education (AICTE).**
**Council of Scientific and Industrial Research(CSIR).**
**Kerala State Council for Science Technology and Environment(Govt. of Kerala).**
**IEEE Student Branch, Kochi.**



**INCLUDE INDEX**
**ISBN : 978-81-906050-6-9**
**Published by The Directorate of Public Relations and Publications for CREMA, Department of Electronics, Cochin University of Science & Technology, Cochin 682022, INDIA and printed at Maptho Printers, South Kalamassery, INDIA.**

SEARCH

Previous Page

Next Page

2

# Chairman Welcomes You

Dear friend,

I cordially invite you to attend the Antennas and Propagation Symposium **(APSYM 2008,** the 11th in the biennial series started science 1988. Your presence and participation in APSYM 2008 will definitely be an event for us to remember for years to come. Over fifty papers are scheduled to be presented during APSYM 2008. All the information about the advance program is available at www.doe.cusat.edu/apsym. The Organising committee have planned an excellent technical programme with a number of invited talks by eminent scientists in the field.

**Chronology of APSYM's**

| Sl. No. | Symposium | Date of Symposium | Number of Papers | Number of Invited talks |
|---|---|---|---|---|
| 1 | APSYM-1988 | Dec. 15- 17- 1988 | 42 | 2 |
| 2 | APSYM-1990 | Nov. 28-30- 1990 | 51 | 10 |
| 3 | APSYM-1992 | Dec. 29-31-1992 | 91 | 2 |
| 4 | APSYM-1994 | Nov.17-19-1994 | 75 | 6 |
| 5 | APSYM-1996 | Nov.01-02-1996 | 42 | 2 |
| 6 | APSYM-1998 | Dec.15-16-1998 | 57 | 1 |
| 7 | APSYM-2000 | Dec.06-08-2000 | 71 | 3 |
| 8 | APSYM-2002 | Dec.09-11-2002 | 84 | 10 |
| 9 | APSYM-2004 | Dec.21-23-2004 | 55 | 4 |
| 10 | APSYM-2006 | Dec.14-16-2006 | 64 | 16 |
| 11 | APSYM-2008 | Dec.29-31-2008 | 50 | 7 |
| 12 | APSYM-2010 | Dec.08-10-2010 | Scheduled | |

Wishing you all a warm welcome once again and hoping very fruitful discussions in the sessions. I look forward to seeing you at APSYM 2008 in Cochin.

*Cochin*
*November 28, 2008*

***Prof. K.G. Nair***

SEARCH

Previous Page

Next Page

3

## *In Memory of Prof. K.C. Gupta*

Dr. Kuldip Chandra Gupta, distinguished educator, dedicated Microwave Scientist and past president of the IEEE Microwave Theory and Techniques Society passed away on 7 February 2007 in Mumbai, India, at the age of 66. The Microwave community has lost an outstanding contributor.

Born on 6 October 1940 at Risalpur in India, he studied electrical communication engineering at the Indian Institute of Science, Bangalore, India, receiving both a first degree (D.I.I.Sc.) in 1961 and the Master's degree in 1962. Following that, he worked at Birla Institute of Technology and Science in Pilani, India, where he received the Ph.D. degree in 1969.

A recipient of numerous awards, he has several well referred books and journal publications to his credit.

Our tributes to this great Indian scientist. He'll be deeply missed by the Microwave family.

SEARCH

Previous Page

Next Page

# Remembering a pioneering Indian scientist

## "It is the invention which is of importance for the mankind, not the inventor"

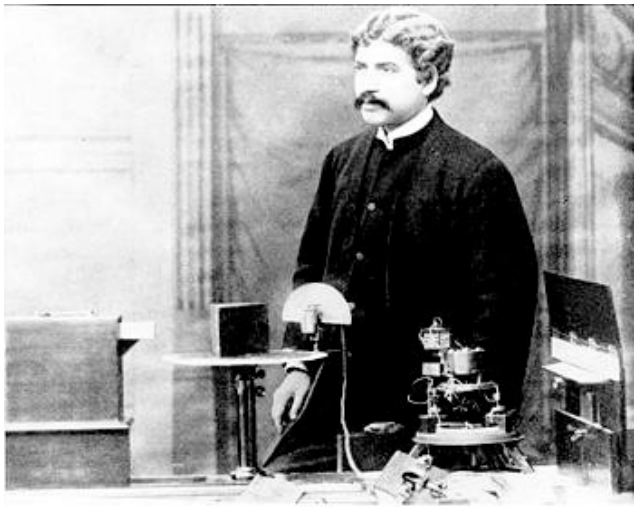

This year we commemorate the 150th birth anniversary of the talented Indian genius Acharya Jagadish Chandra Bose (1858-1937), widely recognized as the first scientist who demonstrated the phenomenon of wireless transmission of electromagnetic waves. His range of interests varied from Physics to Plant sciences. Elected Fellow of the Royal Society on May 13, 1920, he is internationally famous as the father of modern wireless communication.

The Daily Chronicle of England noted in 1896: "J.C. Bose has transmitted signals to a distance of nearly a mile and herein lies the first and obvious and exceedingly valuable application of this new theoretical marvel. Bose was also the first to use a semi-conducting crystal as a detector of radio waves." But unfortunately, the person who, after a prolonged and dedicated research actually explained the origin of radio waves and their characteristics, remained overshadowed in the history of science. However, recently IEEE has given the credit of this invention to this Indian Scientist. Sir J.C.Bose's alma mater, the Christ's College, Cambridge has also recognized his contributions to both Physics and Physiology.

The members of Centre for Electromagnetics and Antennas (CREMA) of Department of Electronics, Cochin University of Science & Technology accolade you sir for your genius inventions in different non correlating field of science. Sir, the great legacy that you left behind remains an inspiration for us and the generations to come.

SEARCH

Previous Page

Next Page

5

## ORGANISING COMMITTEE

| | |
|---|---|
| **Chairman** | **Prof. K.G. Nair**<br>**Emeritus Professor** |
| **Director** | **Prof. K. Vasudevan** |
| **Publications** | **Prof. P.R.S.Pillai** |
| **Registration** | **Prof. K.T. Mathew** |
| **Technical Programme** | **Prof. P. Mohanan** |
| **Local Arrangements** | **Prof. C.K. Aanandan** |

### Members

Dr. Tessamma Thomas
Mr. James Kurian
Dr. Supriya M.H
Mrs. Deepthi Das Krishna
Mrs Lekshmi K.J
Mr. Cyriac M. Odakkal
Mr. Nelson K.J
Dr. Jaimon Yohannan
Ms. Jitha B
Mr. Deepu V
Mrs. Laila Das
Mr. Gopikrishana. M
Mr. Sreenath S
Mr. Jaison Peter
Mrs. Nisha Nassar
Ms. Ann Mary Austin
Mr. Sreejith M. Nair
Ms. Raji S. Nair
Mr. Sujith Raman
Mr. Sarin V.P
Mr. Ullas Kalappura
Mr. Sujith Mathew
Ms. Anju P. Mathews
Mr. Lindo A.O
Mr. Prajas John
Mr. Ananthakrishnan V
Mr. Adrine Correya
Mrs. Shameena V.A

## BOARD OF REFREES

- Prof. K.G. Nair
- Prof. C.S. Sridhar
- Prof. K.T. Mathew
- Prof. K. Vasudevan
- Prof. P. Mohanan
- Prof. C.K. Aanandan
- Dr. M.T. Sebastain
- Prof. K.J. Vinoy
- Prof. G. Guha
- Dr. S. Mridula
- Dr. Binu Paul
- Dr. Joe Jacob

SEARCH

Previous Page

Next Page

## MILESTONES IN THE HISTORY OF ELECTROMAGNETICS

| | | |
|---|---|---|
| 1747 | Benjamin Franklin | Types of Electricity |
| 1773 | Henri Cavendish | Inverse square law |
| 1785 | Coulomb | Law of electric force |
| 1813 | Gauss | Divergence theorem |
| 1820 | Ampere | Ampere's experiment |
| 1826 | Ohm | Ohm's law |
| 1831 | Faraday | Electromagnetic Induction |
| 1837 | Morse | Telegraphy |
| 1855 | Sir William Thomson | Transmission lines theory |
| 1864 | Lord Rayleigh | Theory of Sound Propagation |
| 1865 | James Clerk Maxwell | Electromagnetic field equations |
| 1873 | James Clerk Maxwell | Unified theory of Electricity and Magnetism |
| 1876 | Graham Bell & Gray | Telephone |
| 1883 | Thomas Alva Edison | Electron Emission from Heated Filament |
| 1885 | Heinrich Hertz | Electromagnetic Wave Propagation |
| 1887 | Heinrich Hertz | Spark plug experiment |
| 1888 | Heinrich Hertz | Half-wave dipole antenna |
| 1890 | Ernst Lecher | Lecher wire |
| 1893 | Heinrich Hertz | Spark Gap Generator |
| 1893 | Thomson | Waveguide theory |
| 1894 | Marconi | Wireless Telegraphy |
| 1895 | Jagadish Chandra Bose | 5-6 mm wavelength Signal |
| | Bose | Transmission |
| 1897 | Lord Rayleigh | Boundary values and modes in Metallic cylinders |
| | Jagadish Chandra Bose | Horn antenna and Millimeter wave Source |
| 1898 | Lodge | Tuned Transmitters and Receivers |
| 1900 | Marconi | TransAtlantic Communication |
| 1902 | Weber | Propagation in Hollow Tube1902 |
| | Fleming | Vacuum Tube |
| 1903 | Hulsmeyer | Radar |
| 1906 | Fessenden | Rotating Alternator and audio modulation |
| | Thomas et.al | Crystal Detector |
| | Fessenden | Radio broadcasting |
| | Dunwoody | Crystal detectors |
| 1907 | DeFroest | Triode |
| 1912 | Eccles | Ionospheric propagation |
| 1914 | AT & T | 170 kHz Radio |
| 1915 | Carson | Single side-band transmission |
| 1918 | Watson | Ground wave propagation |
| 1919 | Southworth | Lecher line circuit |
| | Heinrich Barkhausen & Kurz | Triode electron tube at 1.5 GHz |
| 1920 | Hull | Magnetron |
| | Yagi and Uda | Yagi-Uda antenna |
| 1921 | Hull | Smooth bore Magnetron |
| 1922 | Affel | Directional Coupler |
| | Brillouin | Acoustooptic Effect |
| 1923 | HH Beverage | Beverage antenna |
| 1925 | Van Boetzelean | Short wave Radio |
| | Appleton | Ionospheric layer |
| 1927 | Okabe | Split-anode Magnetron |
| 1929 | Clavier | Microwave Communication |
| 1930 | Hansen | Resonant cavity |
| | Karl G Jansky | Bruce Curtain antenna |
| | Barrow L | Waveguides |
| 1931 | Marconi | 600 MHz radio link in Italy |
| | Andre G Clavier | Microwave Radio transmission across English Channel |
| 1932 | Southworth | Circular Waveguide |
| | Marconi | 57 cm Radio telephone and teleprinter service |
| | Claud Cleton | Microwave spectroscopy |
| 1933 | Barrow | Circular Wavegiude Propagation |
| | Armstrong | Frequency modulation |
| 1934 | Schelkunoff | TE01 mode in Circular Waveguide |
| | Watson-Watt | Experimental Radar Station |
| 1935 | Oscar Heil | Velocity modulation |
| | Watson watt | RADAR |
| 1936 | Southworth and Barrow | Microwave propagation in Circular Waveguide |
| | G. H. Brown | Turnstile antenna |
| 1937 | Varian Brothers | Klystron |
| | Janskey | Radio Astronomy |
| | Manson | Waveguide Filter |
| | Russel & Varian Bros | Klystron |
| | A, H. Boot , J T. Randall | |
| | M. L. Oliphant | Magnetron |
| | Pollard Radar aiming anti-aircraft guns | |

SEARCH

Previous Page Next Page

| | | |
|---|---|---|
| 1938 | J. D. Kraus | Corner reflector |
| 1939 | Barrow | Magic Tee |
| | Peterson et.al | Diode Mixer |
| 1939 | P. H. Smith | Smith impedance |
| 1940 | Hansen | Leakywave Antenna |
| | Quakenbush | UHF coaxial Connector |
| | Bowen, Dummer et al | P P I Scope |
| 1942 | Wheeler | Stripline Technology |
| | Neill | N-type connector |
| 1943 | AT&T | 4.5 GHz Multichannel PPM digitally modulated microwave Radio |
| 1944 | Meyers et.al | Reflectometers |
| 1945 | Kompfner | TWT |
| 1946 | Clarke | Forecasts geosynchrous Satellite |
| | J. D. Kraus | Helical antenna |
| | Percy Spencer | Microwave oven |
| 1947 | AT &T | 3.7-4.2 LOS link |
| 1948 | Van der Ziel | Non-linear capacitors |
| 1950 | C. L. Dolph | Dolph-Tchebyscheff array |
| 1953 | Townes | Ammonia Maser |
| | Deschamps | Microstrip antenna |
| 1954 | Towns | Maser |
| 1955 | Page | Monopulse Radar |
| 1956 | Esaki | Tunnel Diode |
| | Bloembergen | Three level Maser |
| 1957 | Kroemer | Hetrojunction Transistor |
| | Bakanowski et.al | Varactor |
| | Hines et.al | Parametric Amplifier |
| | V. H. Rumsey | Frequency independent antenna |
| | Weiss | Parametric amplifier |
| 1958 | Bloembergen | Solid state Maser |
| | John D Dyson | Spiral antenna |
| | Read | Read diode |
| | | Space Communication |
| | Maiman | Ruby Laser |
| 1959 | D. Wigst Isbell | Log periodic antenna |
| 1968 | Victor Veselago | Predicted DNG Materials |
| 1969 | Wen | Coplanar Line |
| 1970 | Silvester | FEM |
| | Byron | Microstrip array |
| 1971 | Itoh and Mittra | Wave Analysis of Microstrip |
| 1975 | Bekati | Relativistic cavity Magnetron |
| 1980 | Mimura | HEMT |
| 1986 | Didenko et. al. | Advance relativistic Magnetron |
| 1988 | S. K. Khamas | High Tc Super conducting dipole |
| 1992 | Victor Trip, Johnson wang | Paste-on Antenna |
| 1993 | Te-Kao Wu et.al | Multiple Diachronic Surface Cassegrain Reflector |
| 1996 | Clorfeine & Delohh | TRAPATT diode |
| 1996 | John W Mc Carkle | Microstrip DC to GHz Field Stacking Balun |
| 2000 | Zhores I Alferov | Fast opto and microelectronic |
| | Herbert Kroemer | Semiconductor heterostructures. |
| 2002 | George V Eleftheriades | Planar Negative LC loaded Refractive media |
| 2004 | Thomas Purr et.al | Miniaturized Directional Antenna |
| 2006 | John C Mather & George F Smoot | Microwave Back ground 2006 (CMB) Cosmic Microwave Background Radiation |
| 2008 | Skin-tenna | Queens University, Belfast |

SEARCH

Previous Page

Next Page

# CONTENTS



SEARCH

Previous Page

Next Page

SEARCH

Previous Page

Next Page

# RESEARCH SESSION 1
# MICROSTRIP ANTENNAS

SEARCH

Previous Page

Next Page

## RESEARCH SESSION 1

## MICROSTRIP ANTENNAS

***Chair: Dr. S.N. Joshi, CEERI, PILANI.***



SEARCH

Previous Page Next Page

# EXPERIMENTAL STUDIES OF CIRCULAR MICROSTRIP RADIATOR BACKED BY A CYLINDRICAL CAVITY

*Manotosh Biswas , Jawad Y. Siddiqui and Debatosh Guha*
Institute of Radio Physics and Electronics, University of Calcutta,
92, A.P.C. Road, Kolkata 700009, India
E-mail: mbiswas@ieee.org, dguha@ieee.org, jysiddiqui@ieee.org

## ABSTRACT:

In this paper we have investigated the effect of cavity diameter and wall height on resonance and radiation characteristics of a circular microstrip patch antenna. Experiments were conducted using a fabricated prototype placed inside a cylindrical cavity. The results were compared and verified with simulated data obtained using an electromagnetic simulator. About 9.6 to 10.5 dBi peak gain was obtained from measured and simulated data.

## INTRODUCTION:

The microstrip antenna is the primary choice for modern wireless and mobile applications due to its lightweight, low volume, thin profile and low fabrication cost. But the miniaturized configurations demand for small or limited ground plane, which causes severe degradation in antenna efficiency and radiation characteristics. Use of a suitable metallic cavity enclosure or cavity backing may help in many cases. As such cavity backed microstrip radiator has gained significant importance over the last decade due to their compact shape, minimum surface wave loss, reduced backward radiation and enhanced gain. Cavity backed patch antenna has been investigated by different researchers [1]–[7] for improving the printed circuit performances. But in those studies, the researchers ignored the effect of cavity diameter and wall height on the performance of the antenna characteristics. Moreover, in all those studies a variable air gap was introduced between the substrate and the ground plane. In our work we considered studying the ignored aspects and thoroughly investigated the effect of cavity wall height and cavity diameter on the antenna performance. Measurements were performed using prototype circular patches fabricated on Taconic substrates and placed in cylindrical cavity of wall height, $e$ and diameter $d$. Experiments were conducted using HP-E8363B vector network analyzer and a standard X band radiation pattern measurement bench. The measured data were compared and verified with simulated data obtained using an electromagnetic simulator [8].

## ANTENNA CONFIGURATION:

The cavity backed circular microstrip patch (CBCMP) antenna is shown schematically in Fig.1 with a circular patch of radius $a$ placed inside a cylindrical cavity of wall height, $e$ and diameter $d$. Fabricated prototype of a circular patch, shown in Fig. 2(a), was etched on a Taconic TLY-3-0620 substrate having dielectric constant ($\epsilon_r$) = 2.33, $\tan\delta$ = 0.001, thickness ($h$) = 1.575 mm and placed on a ground plane without any air gap. The patch was designed to operate around 9.8 GHz using the formulas in [9]. The patch was excited by a SMA (Radiall-R125-462-001), located at a radial distance $r$ = 2.0 mm determined as the matched location as determined from [10].The patch was enclosed in a cylindrical cavity [illegible] 2(b) having inner diameter $d$ = 28.8 mm, wall thickness ($t$) = 1.78 mm and height, $e$.

SEARCH
Previous Page Next Page

## RESULTS AND DISCUSSION:

The performance analysis of the fabricated CBCMP was conducted experimentally on a HP-E8363B vector network analyzer. Simulated results obtained using a commercially available electromagnetic simulator [8] was compared and verified with the measured data. Some representative plots are shown in this section.

Figure 3 depicts the effect of wall height ($e$) on the $S_{11}$ minima characteristic. From the figure it is evident that the variation of $e$ has some effect on the resonance peak as seen from $S_{11}$ minima characteristic. Though, no significant change in the resonant frequency is accounted.

Figure 4 shows the compression studies of simulated and measured peak gain with cavity wall height, $e$. As seen from the plot, the measured and simulated peak gain is obtained at $e$ = 12.0 mm with a gain of 9.6 dBi and 10.0 dBi, respectively.

The effect of cavity diameter on peak gain is shown in Fig. 5. Keeping the cavity wall height optimum i.e. $e$ = 12.0 mm, the peak gain for varying cavity diameter is obtained at $d$ = 32.0 mm and is found to decrease above or below that value of $d$. The peak gain obtained for $d$ = 32 mm is 10.5 dBi.

## CONCLUSION:

The effect of the cavity diameter and wall height on a circular microstrip patch antenna enclosed in a cylindrical cavity without any air gap is investigated in this paper. Extensive experiments on a prototype patch placed inside a fabricated cylindrical cavity were conducted. The measured results were compared and verified with simulated data. Peak gain of 9.6 dBi and 10.5 dBi were obtained from the measured and simulated data, respectively. Optimum cavity diameter and wall height were also revealed from the investigation. The results presented in the paper thus appear to be highly informative particularly for the purpose of design of high gain antenna and practical implementation.

## REFERENCE:


1. J.A. Navarro and K. Chang, "A Ka-band cavity-enclosed aperture-coupled circular patch antenna and array for millimeter-wave circuit integration," in 1992 IEEE AP-S Int. Symp. Dig., pp. 313-316, 1992.
2. J.T. Aberle, "On the use of metallized cavities backing microstrip antennas," in 1993 IEEE AP-S Int. Symp. Dig., pp. 60-63, 1993.
3. N.C. Karmakar and M .Singh, "Investigations into a circular patch antenna in a cylindrical cavity enclosure," ICCS AP-OS, vol. 2, pp. 446-450, Nov. 1994.
4. C. M. Montiel, L. Fan and K. Chang, " A novel active antenna with self-mixing and wideband varactor-tuning capabilities for communication and vehicle identification applications," IEEE Trans Microwave Theory Tech., vol. 44, no. 12, pp. 24 21-2430, Dec.1996.
5. N.C. Karmakar, "Investigations into a cavity-backed circular-patch antenna," IEEE Trans. Antennas Propagat., vol. 50, no. 12, pp. 1706-1715, Dec. 2002.
6. D. Guha and J. Y. Siddiqui, "Effect of a cavity enclosure on the resonant frequency of a inverted microstrip circular patch antenna," IEEE Trans. Antennas and Propagat vol. 52. no.8, pp. 2177- 2180, Aug. 2004.
7. M. Biswas, J. Y. Siddiqui, D. Guha, and Y. M. M. Antar, "Effect of a Cylindrical Cavity on the Resonance of a Circular Microstrip Patch With Variable Air-Gap," IEEE Antennas and Wireless Propagation Letters, vol. 5, pp.418-420, 2006.


SEARCH
Previous Page
Next Page

8. Ansoft's high frequency structure simulator (HFSS) V 9.2.
9. D. Guha, "Resonant frequency of circular microstrip antennas with and without air gaps," IEEE Trans. Antennas and Propagation, vol. 49. no.1, pp.55- 59, Jan. 2001.
10. D. Guha, Y. M. M Antar, J. Y. Siddiqui, and M. Biswas, "Resonant resistance of probe and microstrip line-fed circular microstrip patches," IEE Proceedings Microwaves Antennas Propagat., vol.152, pp. 481-484, Dec.2005.

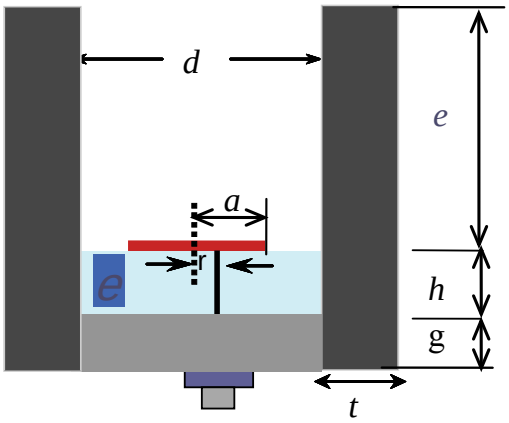


**Fig.1.** Coax-fed circular microstrip patch backed by cavity.

**(a)** **(b)**

**Fig.2.** Photographs of (a) fabricated patch on limited ground plane; (b) cylindrical metallic enclosure to be fitted surrounding the brass-made ground plane.

SEARCH

Previous Page Next Page

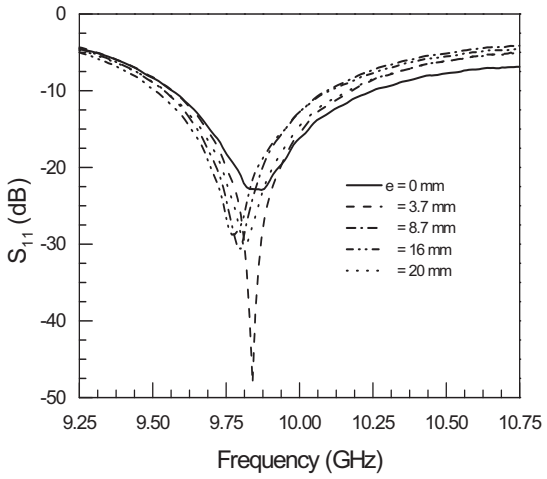


**Fig.3.** Measured Return loss of a coax-fed circular microstrip patch backed by cavity for different *e*. *a* = 5.0 mm, *t* = 1.78 mm, *d* = 28.8 mm, $\varepsilon_r$ = 2.33, *h* = 1.575 mm, *g* = 5.0 mm, $\rho$ = 2.0 mm

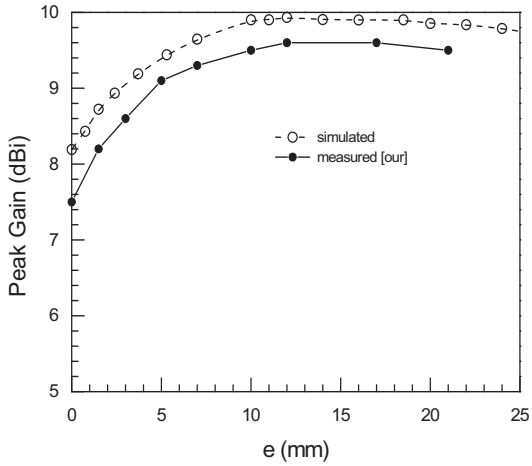


**Fig.4**. Compression of measured and simulated peak gain of a coax -fed circular microstrip patch backed by cavity. $f_r$ =9.98 GHz and other Parameters as in Fig. 3

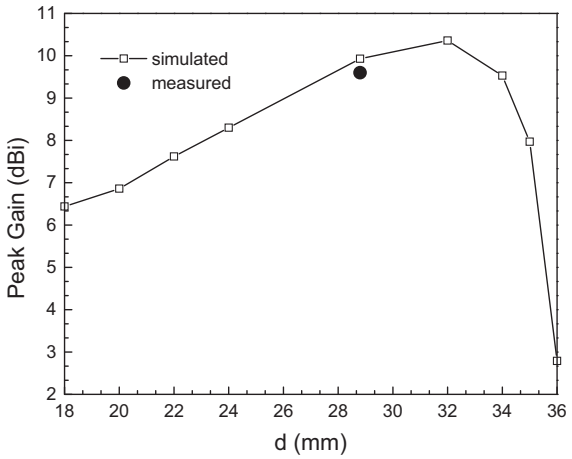


**Fig.5.** Peak gain of a coax-fed circular microstrip patch backed by cavity. *e* = 12.0 mm and other parameters as in Fig.3

SEARCH

Previous Page

Next Page

# DUAL POLARIZED STUB LOADED COMPACT MICROSTRIP ANTENNAS

*A. A. Deshmukh*[*(1)] *and K. P. Ray*[(2)]
(1) IT Department, DJSCOE, Vile-Parle (W), Mumbai – 400 056, India,
**Email:** amitdeshmukh76@yahoo.com
(2) RFMS, SAMEER, I. I. T. Campus, Powai – 400 076, Mumbai, India
**Email:** kpray@rediffmail.com

**Abstract:** The dual polarized stub loaded C-shaped and shorted L-shaped Microstrip antennas for dual and triple frequency and dual polarized response are proposed. The antenna response is verified experimentally and good agreement is obtained between simulated and theoretical results.

## 1. INTRODUCTION

The dual band microstrip antenna (MSA) is realized by placing the open circuit nearly quarter wavelength stub on the edge of the patch or by cutting a resonant quarter wavelength or half wavelength slot on the edges or inside the patch [1, 2]. The stub offers either capacitive or inductive impedance around the resonance frequency of the MSA and realizes dual frequency response. The slot adds another resonant mode near the patch resonance and gives dual frequency response. The compact MSA is realized by cutting a slot at an appropriate position inside the patch [1]. The slot lengthens the length of excited surface current and reduces the resonance frequency. The compact C-shaped MSA is obtained by cutting a slot on the non-radiating edges of the rectangular MSA (RMSA) and the shorted L-shaped MSA is obtained by placing the shorting posts along the zero field line of C-shaped MSA [3]. In this paper, dual band and dual polarized stub loaded C-shaped and shorted L-shaped MSAs are proposed. These MSAs are fabricated on glass epoxy substrate ($\epsilon_r$ = 4.3, h = 0.159 cm, and tan $\delta$ = 0.02) and were first analyzed using IE3D software followed by the experimental verifications [4].

## 2. STUB LOADED C-SHAPED MSA

The stub loaded C-shaped MSA is shown in Fig. 1(a). To ensure the symmetry of the configuration, two stubs are placed on the two edges of the C-shaped MSA as shown in the figure. All the dimensions shown in figure are in cm. The designed guidelines for the given two frequencies for stub loaded RMSAs are reported [5]. Since the C-shaped MSA is derived from the RMSA, therefore the same guidelines are used. The resonance frequency of the C-shaped MSA for the given slot dimensions is calculated using the equations reported in [6]. Using this frequency and the design equations for stub loaded RMSA, the stub dimensions for two frequencies are calculated. For the dimensions shown in figure, the simulated input impedance and VSWR plots are shown in Fig. 1(b). The dual frequencies and BWs are 663 and 1012 MHz and 12, 14 MHz, respectively. However another frequency is seen at 900 MHz with a BW of 13 MHz. To understand the mode distributions at various frequencies this MSA is analyzed using its multi-port network model (MNM) as shown in Fig. 1(c). It was observed from the voltage distributions which is obtained using MNM at all the three frequencies, that the first ($f_1$) and third ($f_3$) frequencies are due to the stub loaded patch modes whereas the second frequency ($f_2$) is due to the orthogonal patch mode. The antenna response is experimentally verified. The measured dual frequencies and BWs are 670, 1110 MHz and respectively. The measured orthogonal frequency and its BW is 911 and MHz, respectively. The radiation pattern at $f_1$ and $f_3$ are in the broadside direction with the

SEARCH
Previous Page
Next Page

cross-polarization levels less than 15 dB as compared to that of the co-polar levels. At $f_1$ and $f_2$, the E and H-planes are aligned along $\Phi = 90^0$ and $0^0$, respectively, whereas at $f_3$, the E and H-plane are aligned along $\Phi = 0^0$ and $90^0$, respectively.

## 3. STUB LOADED L-SHAPED MSA

By placing the shorting post along the zero field line of the C-shaped MSA, a shorted L-shaped MSA is realized. By placing the open circuit nearly quarter wavelength stub on the edges of shorted L-shaped MSA, a dual band and dual polarized MSA is obtained as shown in Fig. 2(a). The shorted L-shaped MSA without the stub has nearly the same resonance frequency as that of the C-shaped MSA therefore for the required dual frequencies the stub dimensions are calculated using the reported design equations for dual band stub loaded MSA. The simulated dual frequencies and BWs are 620, 1154 MHz and 9, 20 MHz, respectively as shown in Fig. 2(b). The measured dual frequencies and BWs are 633, 1182 MHz and 9, 17 MHz, respectively as shown in Fig. 2(c). The MN model of shorted L-shaped MSA is also developed. The orthogonal polarization is due to the reverse direction of surface currents due to the stub at the two frequencies. For the shorted L-shaped MSA, the E and H planes are aligned along $\Phi = 135^0$ and $45^0$, respectively. Similarly for stub loaded shorted L-shaped MSA at $f_1$, the E and H-planes are aligned along $\Phi = 135^0$ and $45^0$, respectively whereas at $f_2$, E and H-planes are aligned along $\Phi = 45^0$ and $135^0$, respectively.

## 4. CONCLUSION

The dual band and dual polarized C-shaped and shorted L-shaped MSAs are proposed. The MN models for these MSAs are also developed. A good agreement is obtained between the simulated, measured and MNM results.

## 5. REFERENCES:


1. G. Kumar and K. P. Ray, *Broadband Microstrip Antennas*, Artech House, USA, 2003
2. K. L. Wong, *Compact and Broadband Microstrip Antennas*, John Wiley & sons, Inc., New York, USA, 2002
3. Amit A. Deshmukh and G. Kumar, "Compact Broadband gap-coupled Shorted L-shaped Microstrip Antennas", Microwave and Optical Technology Letters, Vol. 47, No. 6, 20th Dec. 2005, pg. 599 – 605.
4. IE3D 12, Zeland Software, Freemont, USA
5. A. E. Daniel, *Tunable dual band Rectangular Microstrip antennas and their Arrays*, Ph.D. Thesis, I. I. T. Bombay, 2006
6. Amit A. Deshmukh and G. Kumar, "Formulation of Resonant frequency for Compact Rectangular Microstrip Antennas", Microwave and Optical Technology Letters, Vol. 49, No. 2, Feb. 2007, pg. 498 – 501.

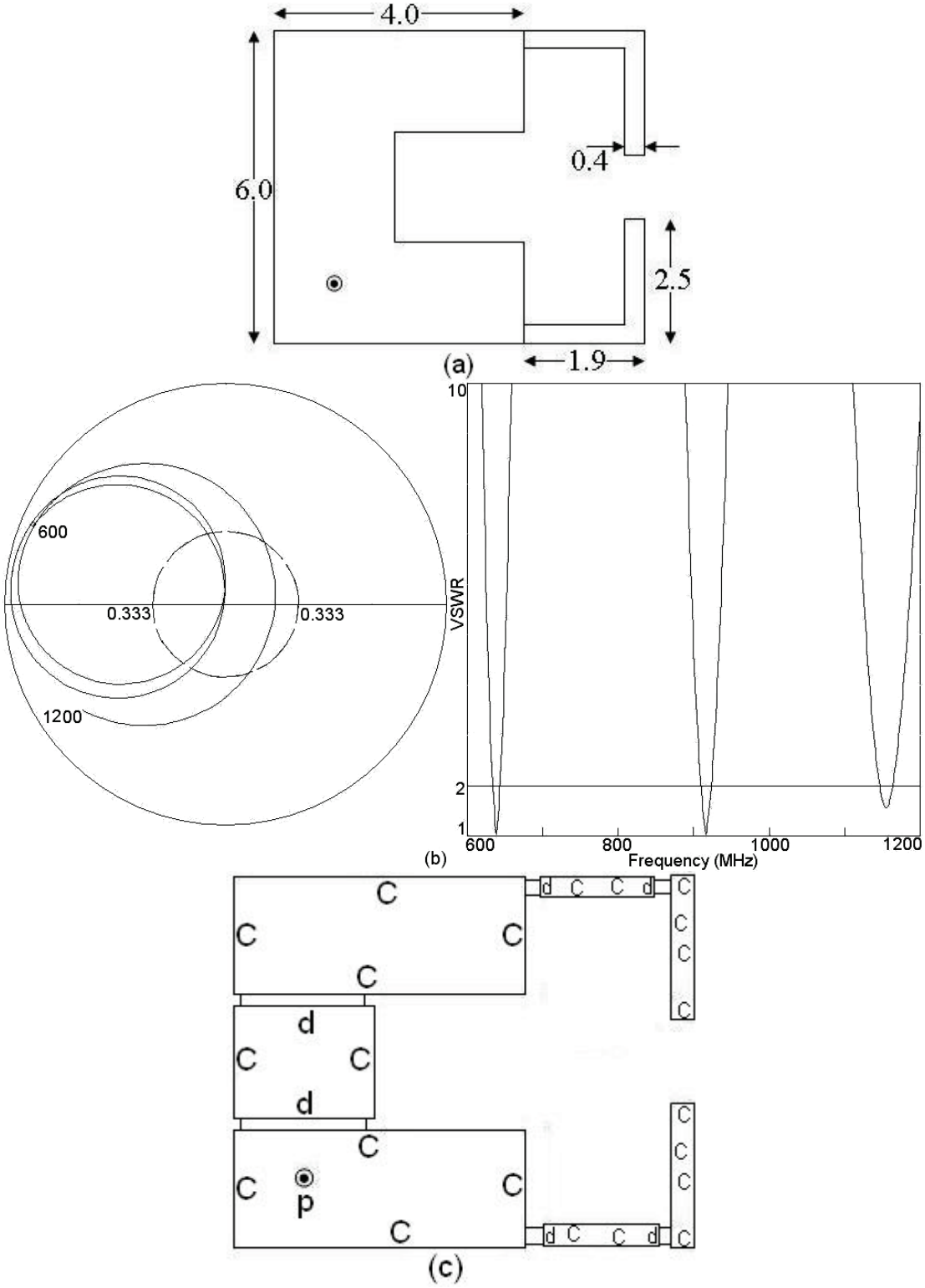


**Fig. 1** (a) Dual band and dual polarized C-shaped MSA, its (b) simulated input impedance and VSWR plots and its (c) MN model

SEARCH

Previous Page

Next Page

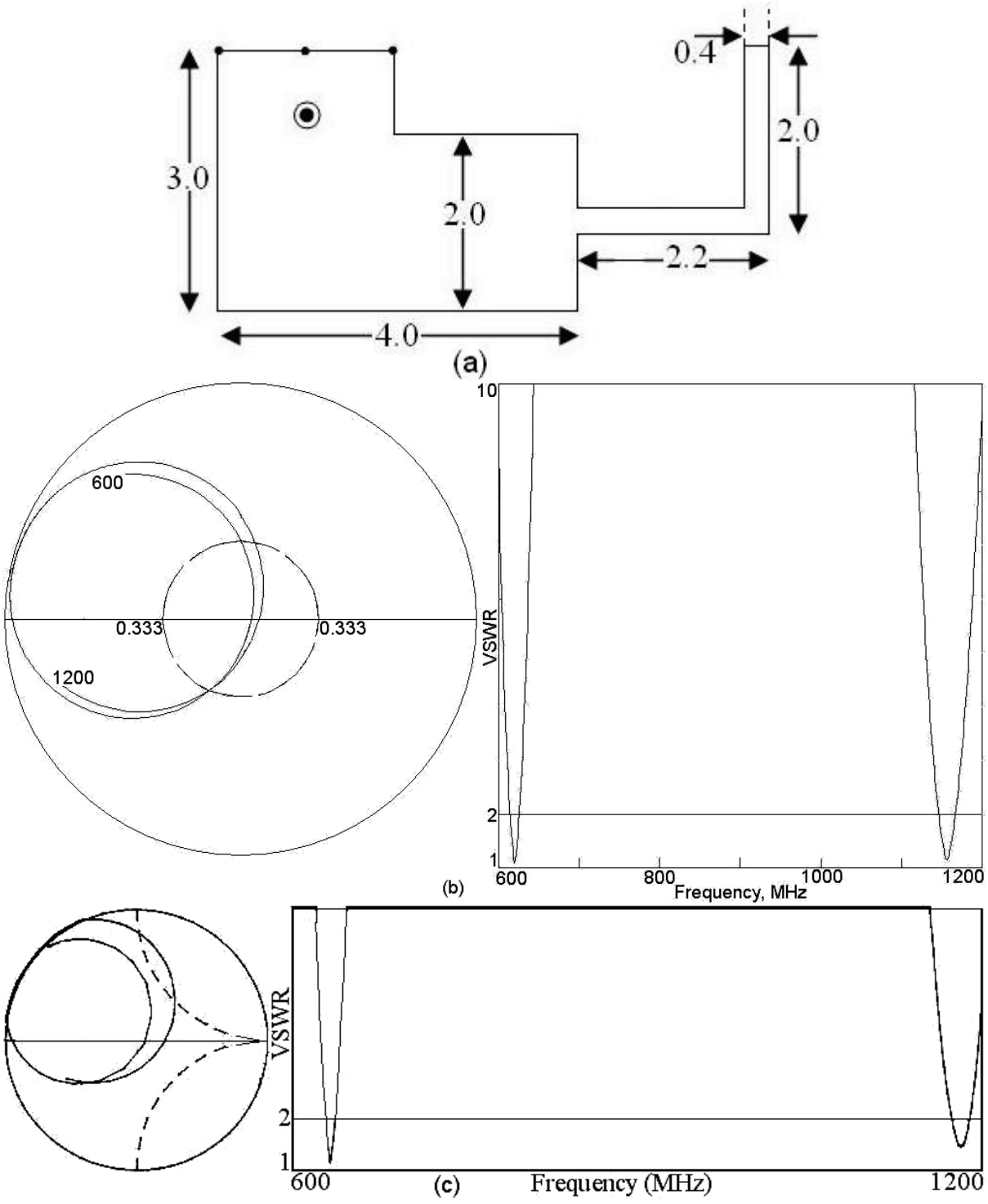


**Fig. 2** (a) Shorted stub loaded L-shaped MSA, its (b) simulated and (c) measured input impedance and VSWR plots

SEARCH

Previous Page

Next Page

# ANALYSIS OF HALF E-SHAPED PATCH FOR WIDE BAND APPLICATION

*[1]J. A. Ansari*, [1]Satya Kesh Dubey, [1]Anurag Mishra, [2]Babau R. Vishvakarma*
[1]Department of electronics and communication, University of Allahabad, Allahabad,
[2]Department of Electronics Engg., IT BHU, Varanasi, India,
E-mail: brvish @bhu.ac.in
*E-mail:jaansari@rediffmail.com

**ABSTRACT :**

In the present paper a half E-shaped patch cut symmetrically from a E-shaped patch [6] has been analysed using equivalent circuit model based on modal expansion cavity model. Proposed analysis is compared to experimental [6] and simulated results using IE3D.

**INTRODUCTION :**

Microstrip antenna have attractive features of low profile and light weight and conformal to mounting structures but two most serious limitations of the microstrip antenna is its low gain and narrow bandwidth. To increase the bandwidth several approaches have been made. U-slot loaded patch [1], V-slot loaded patch [2], W-shaped patch [3] S-shaped antenna [4], and E –shapes patch antenna [5] are very popular wideband operation. Bandwidth enhancement with size reduction is becoming a major design consideration for most practical applications of the microstrip antenna for wireless communications.

In the present paper a half E-shaped patch cut symmetrically from a E-shaped patch [6] has been analysed using equivalent circuit model based on modal expansion cavity model. Proposed analysis is compared to experimental [6] and simulated results using IE3D.

**THEORETICAL CONSIDERATIONS:**

The geometry of proposed half E-shaped patch antenna is shown in Fig.1. A simple patch can be analysed as a parallel combination of $R_1$, $L_1$ and $C_1$ (Fig. 2), where $R_1$, $L_1$ and $C_1$ is given in term of antenna dimension [7].

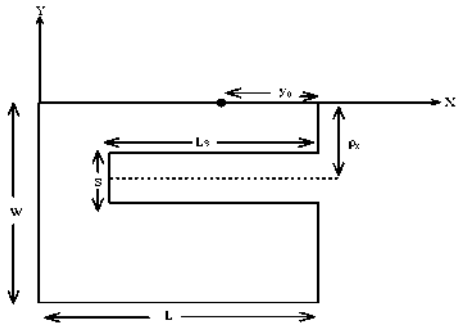


Fig 1 Top view of half E-shaped patch antenna

SEARCH
Previous Page
Next Page

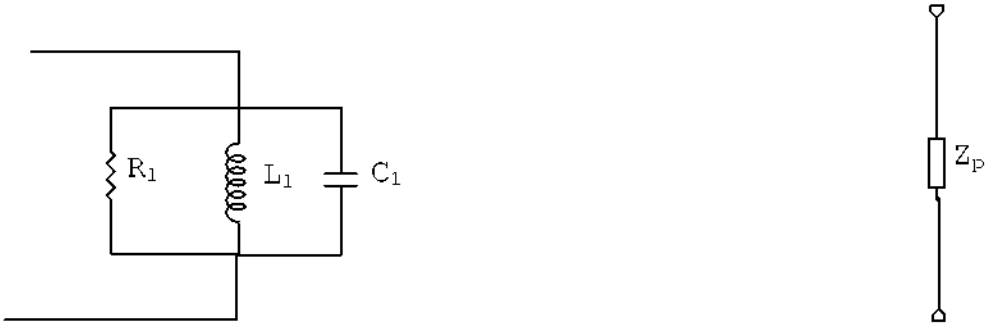


(i) Equivalent circuit of a simple rectangle patch (ii) Equivalent of (i)

Fig 2 Equivalent circuit of a simple rectangle patch

A half-E shaped patch is half of the symmetrically E-shaped patch [6]. This patch can be analysed as a notch ($l_s \times s$) cut on radiating edge which is not equidistant from both ends. With the effect of non-equidistant notch, current length of the patch is increased. Due to this the equivalent circuit of the patch has additional series inductance $\Delta L$ and series capacitance $\Delta C$. Now the modified circuit is shown in Fig. 3.

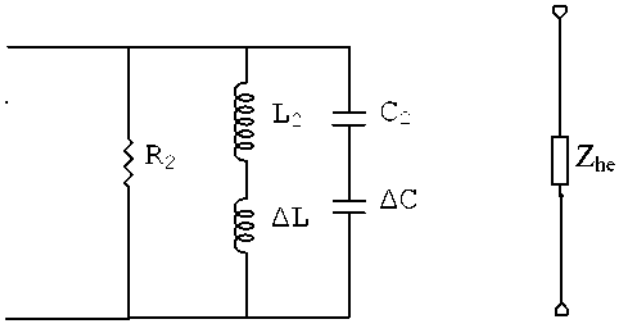


(i) (ii)

Fig 3 Equivalent circuit due to effect of notch

This notch loaded patch has two resonant circuits. These two resonators are coupled through the coupling capacitor resulting into a wideband.

Expression for notch inductance $\Delta L$ is given by [9]. The capacitance $\Delta C$ between upper and lower wing can be calculated by [10] $C_p$ is the coupling factor between the two resonators .

Due to the effect of notch inductance ( $\Delta L$ ), notch capacitance ($\Delta C$ ) and gap capacitance the total impedance of the notch loaded half –E shaped patch can be calculated from Fig. 4.

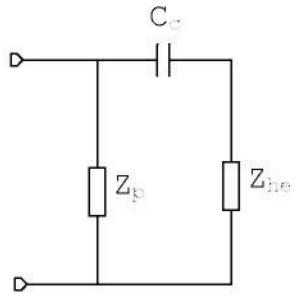

Fig 4 Equivalent circuit of half E-shaped patch

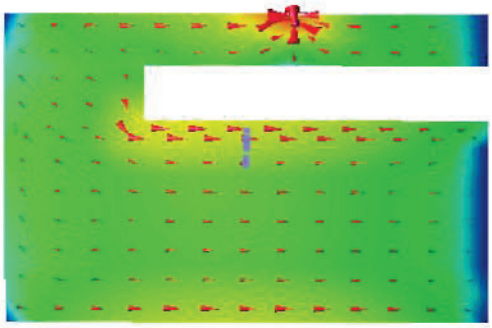

Fig 5 Current distribution of half E-shaped patch (Ls=32 mm, s=6 mm, px=8 mm)

Impedance of simple patch $Z_P = \dfrac{1}{\dfrac{1}{R_1} + \dfrac{1}{j\omega L_1} + j\omega C_1}$

Impedance of patch with gap capacitance $Z_{cp} = \dfrac{1}{j\omega C_c} + \dfrac{1}{\dfrac{1}{R_1} + \dfrac{1}{j\omega L_1} + j\omega C_1}$

Impedance due to effect of notch $Z_{hE} = \dfrac{1}{\dfrac{1}{R'} + \dfrac{1}{j\omega L'} + j\omega C'}$

Now total impedance of the notch loaded patch is given as

$$Z_{in} = \frac{Z_{cp} Z_{hE}}{Z_{cp} + Z_{hE}}$$

## DISCUSSION OF RESULTS

The variations of VSWR as a function of frequency for Half-E shaped patch are shown in Fig. 6 and 7 along with simulated and experimental results.

SEARCH

Previous Page

Next Page

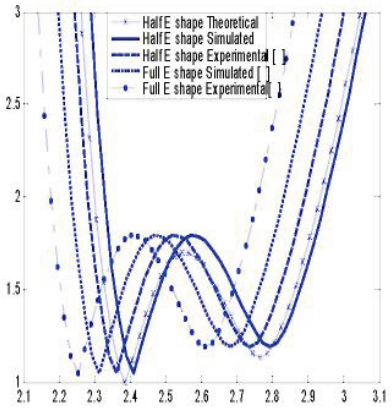


Fig 6 Variation of VSWR with frequency of Half-E-shaped patch and full E-shaped patch

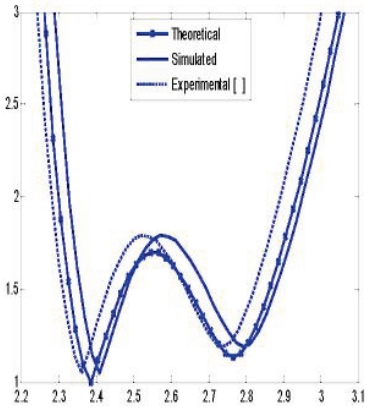


Fig 7 Variation of VSWR with frequency of Half-E-shaped patch

It is observe that the bandwidth of the half-E shaped patch is 24.85 % (Theoretical), 24.3 % simulated, 24.17% experimental compared to full E-shaped patch which is 25.07%. It may be mentioned that the results of the proposed theory is almost in good agreement with the experimental and simulated results (Fig. 7). Further there is a reduction of antenna size by 50%. This result is also corroborated with current distribution figure shown in Fig. 5.

**REFERENCES**

1. T U Huyah and K F Lee, "Single layer single patch wideband microstrip antenna," Electronics Letters, Vol. 31, no. 16, pp 1310-1312, august 1995.
2. G H Rafi and L. safai, "Broadband microstrip patch antenna with V-slot," IEE Proc. Microw. Antenna Propag. Vol 151, no 5, Oct 2004.
3. Abhas Ali Lotfi et. al , "W-shaped enhanced patch antenna for wireless communication," Wireless Pers Commun. Vol. 43, pp 1257-1265,2007.
4. A A Deshmukh and G Kumar, "Compact broadband S-shaped microstrip antennas," Electron. Letters, Vol. 42, no. 5, 2006.
5. Vijay K Pandey and Babau R Vishvakarma, "Analysis of E shaped patch antenna," Microwave and Optical Technology Letters Vol. 49, No. 1, 2007.
6. Rich Chair et al., "Miniature wideband Half U-slot and half E shaped patch antenna," IEEE trans Antenna and Propag. Vol. 53, no. 8, pp 1-1178, 2005.
7. I J Bahal and P Bhartiya, "Microstrip Antennas," Artech house.
8. F E Terman, "Electronics and radio engineering," Kogakusha, Tokyo, pp 15-73,1995.
9. X X Zhang and F Yang, "Study of a slit cut on a microstrip antenna and its application," Microwave and Optical Technology Letters Vol. 18, pp 297-300, 1998.
10. I Bahal, " Lumped elements for RF and microwave circuit," Artech House Boston, 2003, pp 456-459.

SEARCH

Previous Page

Next Page

26

# BROADBAND L-PROBE FED E-SHAPED MICROSTRIP ANTENNAS

*Amit A. Deshmukh*[*(1)], *P. N. Chine* [(2)] *and K. P. Ray*[(3)]
(1) IT Department, D. J. Sanghvi College of Engineering, Vile-Parle (W), Mumbai – 400 056, India,
**Email:** amitdeshmukh76@yahoo.com
(2) ARDL, DRDO, Pashan, Pune,
**Email:** pnchine@hotmail.com
(3) RFMS, SAMEER, I. I. T. Campus, Powai – 400 076, India
**Email:** kpray@rediffmail.com

## ABSTRACT:

Broadband L-probe fed RMSA is discussed and broadband L-probe fed E-shaped Microstrip antenna is proposed. Also the compact and broadband half E-shaped Microstrip antenna is proposed. These broadband antennas give broadside radiation pattern with higher gain.

## 1. INTRODUCTION:

Broadband microstrip antenna (MSA) is realized by using multi-resonator gap-coupled or stacked configurations, in which parasitic patches of slightly different resonant frequencies are coupled to the fed patch [1]. However, use of parasitic patches increases the overall antenna size. When the resonant slot is cut inside the patch, it adds another resonant mode near the patch resonance and increases the bandwidth (BW) by retaining the same patch size [2]. These slotted MSAs require thicker substrates, which can be reduced by using different feeding techniques like L-probe feed [2]. In this paper, the broadband L-probe fed rectangular MSA (RMSA) is discussed and broadband L-probe fed E-shaped MSA is proposed. Also the compact and broadband L-probe fed half E-shaped MSA is proposed. All these MSAs have been fabricated on glass epoxy substrate ($\epsilon_r$ = 4.3, h = 0.159 cm, and tan $\delta$ = 0.02) and they are used in suspended configuration, in which patch fabricated on glass epoxy substrate is suspended above the ground plane with finite air gap. The MSAs have been first analyzed using IE3D software followed by the experimental verifications in some of the cases [3].

## 2. L-PROBE FED RMSA

The broadband L-probe fed RMSA is shown in Fig. 1(a, b). The L-probe fed RMSA is equivalent to the stacked configuration of folded monopole and RMSA and the detailed design analysis of the antenna is reported [4]. The RMSA is fabricated on glass epoxy substrate and it is stacked op top of the L-probe feed. The horizontal portion of the L-probe is fabricated on glass epoxy substrate. For broader BW, the horizontal and vertical lengths of the L-probe feed, air gap between the L-probe and RMSA and the horizontal separation between them are optimized. The simulated BW is 225 MHz (25 %) whereas the measured BW is 180 MHz (20 %) as shown in Fig. 1(c). The difference between the measured and simulated results is due to the fabrication errors. The radiation pattern is in the broadside direction with lower cross polarization levels with the gain of more than 8.5 dBi over the entire BW. This configuration has more BW as compared to that of the stacked RMSA with same total thickness.

SEARCH
Previous Page
Next Page

## 3. L-PROBE FED E-SHAPED MSA

The broadband E-shaped MSA is obtained by cutting a pair of nearly quarter wavelength rectangular slots on one of the radiating edges of the RMSA [2]. This MSA is stacked on top of L-probe MSA to realize the L-probe fed E-shaped MSA as shown in Fig. 2(a, c). In this configuration, total three resonance frequencies are present, which are due to the patch mode, pair of slots mode and the L-probe mode. This broadband MSA is designed using the air substrate and the patches are suspended above the ground plane using the foam spacers. For optimizing this configuration for broader BW, the horizontal and vertical lengths of the L-probe, air gap between the L-probe and E-shaped MSA, the horizontal separation between them and the slot dimensions are optimized. The simulated BW is 194 MHz (22 %) whereas the measured BW is 210 MHz (24 %) as shown in Fig. 3. The radiation pattern is in the broadside direction with cross polar level less than 15 dB as compared to that of the co-polar level in the broadside direction. The MSA has gain of more than 9 dBi over the operating BW. This configuration when designed on suspended glass epoxy substrate for the same total substrate thickness gives more BW as compared to that of the L-probe fed RMSA.

## 4. COMPACT L-PROBE FED HALF E-SHAPED MSA

The half E-shaped MSA is obtained by using the symmetry of E-shaped MSA along the feed point axis [5]. The half E-shaped MSA is stacked on top of L-probe feed as shown in Fig. 4(a, b). The MSA is optimized for the same total substrate thickness as that of the L-probe fed E-shaped MSA. The simulated BW is 170 MHz (18%) as shown in Fig. 4(c). The gain is more than 6 dBi over the operating BW which is less than 3 dB as compared to the E-shaped MSA which is due to the reduced aperture area. The radiation pattern is in the broadside direction with cross-polar level less than 10 dB as compared to that of the co-polar levels. However they increase towards the higher frequencies due to the asymmetrical structure.

## 5. CONCLUSIONS

The broadband L-probe fed RMSA is discussed and broadband L-probe fed E-shaped MSA and half E-shaped MSA are proposed. For the E-shaped MSA, the radiation pattern is in the broadside direction with cross-polar level less than 15 dB as compared to that of the co-polar level.

## 6. REFERENCES:

1. G. Kumar and K. P. Ray, "Broadband Microstrip Antennas", Artech House, USA, 2003
2. K. L. Wong, "Compact and Broadband Microstrip Antennas", John Wiley & sons, Inc., New York, USA
3. IE3D 9.2, Zeland Software, Freemont, USA
4. Amit A. Deshmukh and G. Kumar, "Broadband L-probe fed Rectangular Microstrip Antenna", *Proc. 10th Int. Symp. Microwave and Optical Technology*, Fukuoka, Japan, August 22 – 25, pp. 394 – 397, 2005.
5. Amit A. Deshmukh and G. Kumar, "Compact Broadband E-shaped Microstrip Antennas", Electronics Letters, Vol. 41, No. 18, 1st Sept. 2005, pg. 989 – 990.

SEARCH
Previous Page
Next Page

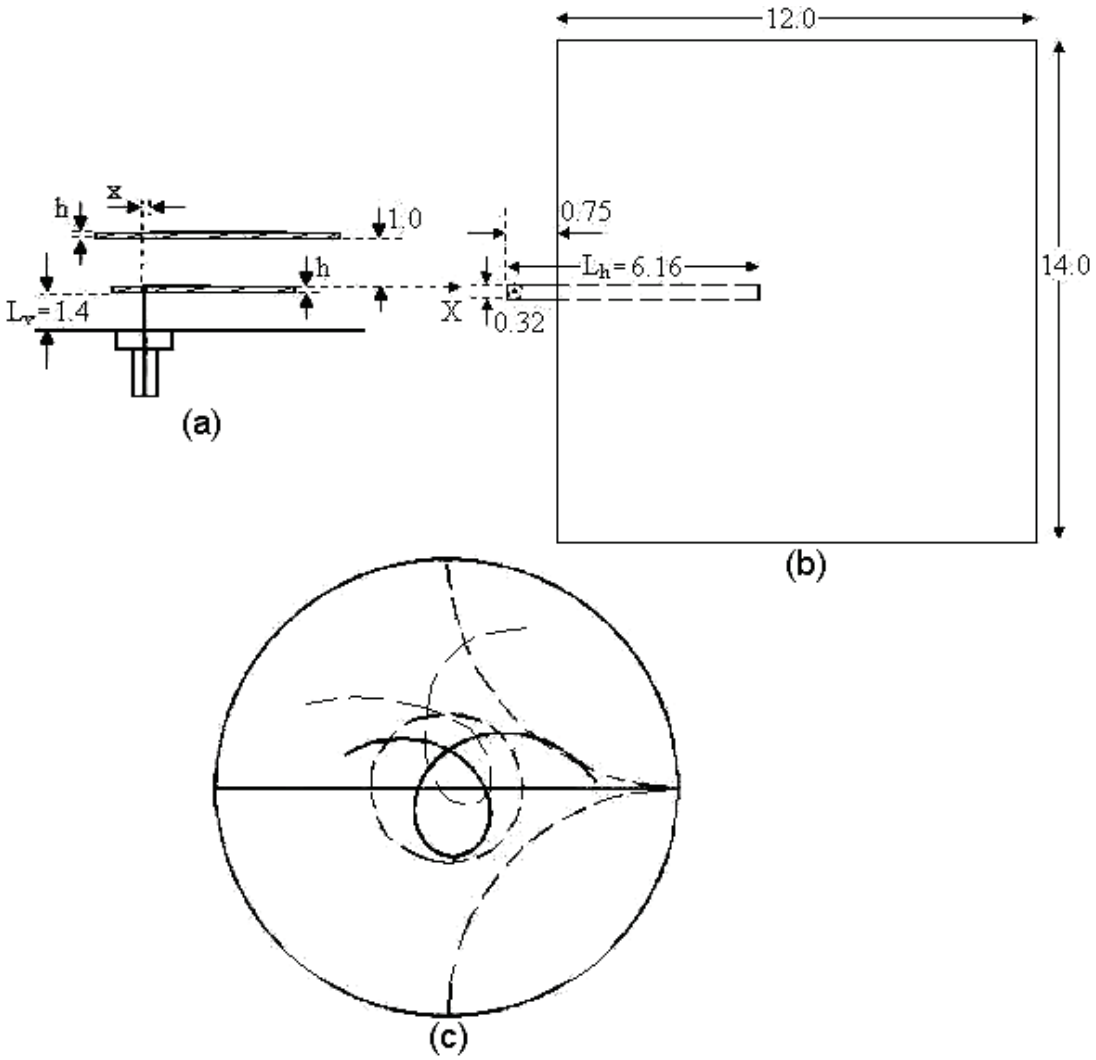


**Fig. 1** (a) Top and (b) side views of L-probe RMSA and its (c) input impedance loci, (——) simulated, (- - - -) measured

SEARCH
Previous Page
Next Page

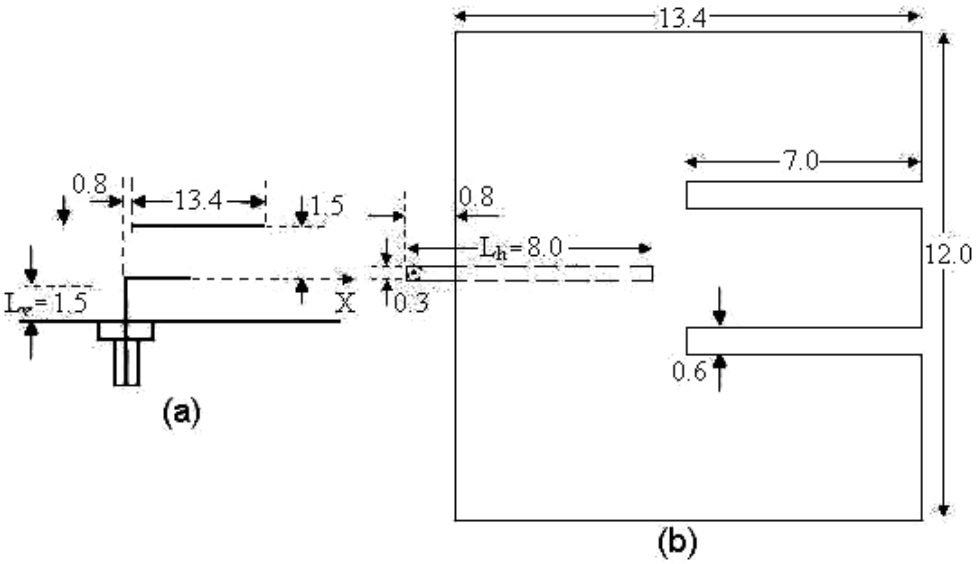


**Fig. 2** (a) Top and (b) side views of L-probe fed E-shaped MSA

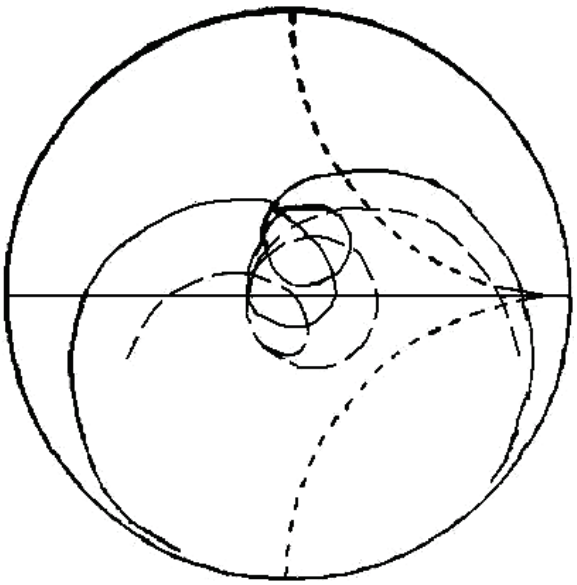

**Fig. 3** Input impedance loci for L-probe fed E-shaped MSA, (——) measured, (----) simulated

SEARCH
Previous Page
Next Page

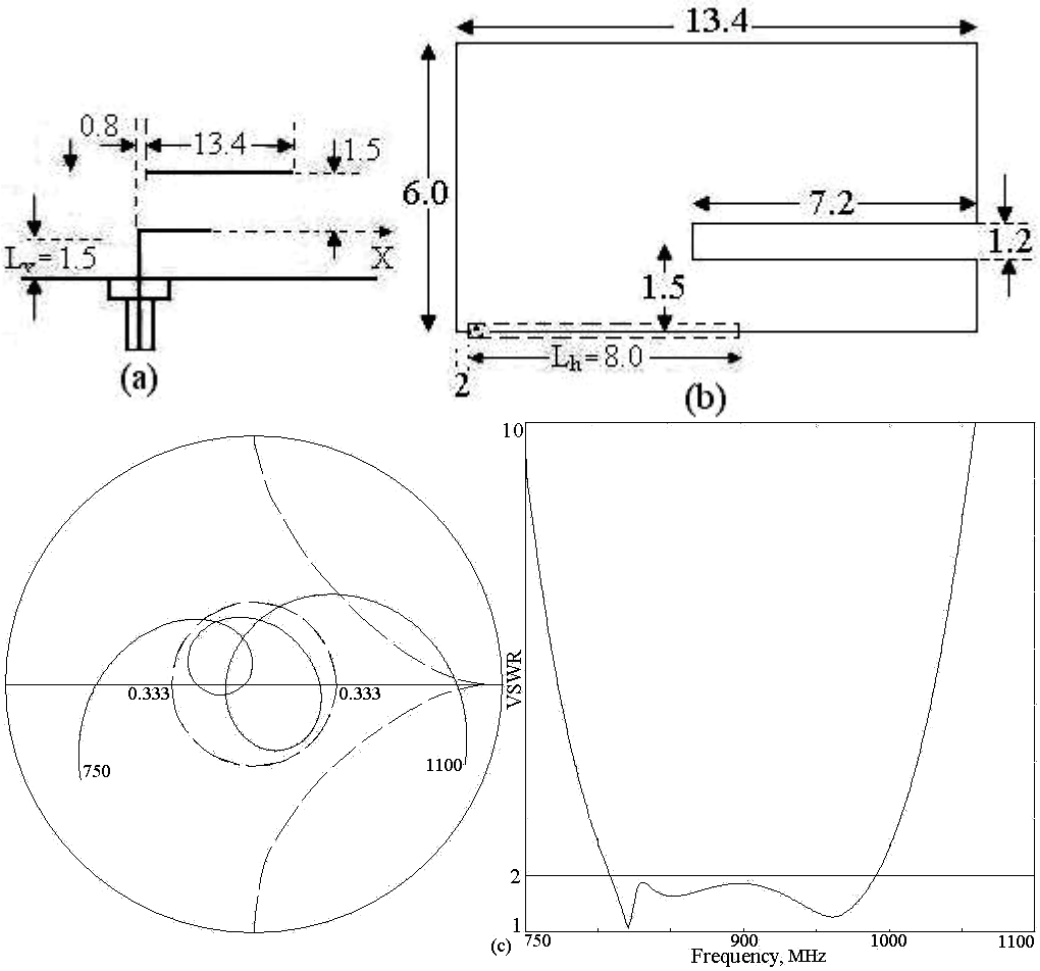


**Fig. 4** (a) Top and (b) side views of L-probe fed half E-shaped MSA and its (c) simulated input impedance and VSWR plots

SEARCH
Previous Page
Next Page

# ENHANCED GAIN TRANSISTOR INTEGRATED ACTIVE MICROSTRIP ANTENNA

*Shweta Srivastava and Anika Chowdhary*
Department of Electronics and Communication Engineering
Birla Institute of Technology, Mesra, Ranchi-835215
E-mail: shwetasri_76@rediffmail.com

**ABSTRACT:**

The results of the analysis match with the simulated results and the testing of the antenna delivered good results too. The gain of the antenna was increased from 4.45 dB without the active device to 10.49 dB with the active device. The bandwidth also increased from 0.1 GHz to 0.2 GHz. The analysis depicted that a high gain antenna was designed using the amplification properties of the transistor.

## 1. INTRODUCTION:

Active integrated antennas are antenna in which the active devices are integrated directly in the antenna structure to obtain active microstrip antenna oscillators, amplifiers, and frequency converters [1,2]. In this endeavor Transistor is integrated with microstrip antenna for amplification. Such types of antennas provide improved gain and bandwidth and also provide improved noise performance as compared to passive antennas.

## 2. THEORETICAL DETAILS:

At low frequency it is assumed that the transistor responds instantly to changes of input voltage or current. But as frequency increases and the associated wavelength of the electromagnetic wavelengths of electromagnetic waves becomes comparable to the dimension of the discrete circuit components such as resistor, capacitor and inductors, these components start to deviate in their electric responses from their ideal from the ideal frequency behavior.

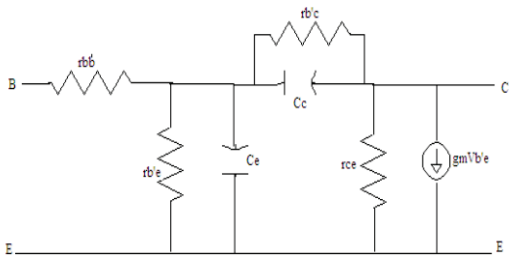


Fig. 1 High frequency equivalent circuit of Transistor

SEARCH
Previous Page
Next Page

## 2.1. DESIGN OF SIMPLE INSET FED MICROSTRIP PATCH ANTENNA:

A microstrip antenna of dimension 43.4mm x 43.4mm is designed using the following equation[3]: $W = \frac{v_0}{2 f_r \sqrt{\frac{2}{e_r + 1}}}$ A notch is realized in one side of the square patch antenna. The feed point is at the border of the notch. The input resonant resistance varies in the same manner as in a full patch antenna fed by an inset feed point. It's given by [4]: $R_{in} = R_{res} \cos^2\left(\frac{\pi X}{L}\right)$

A study with moment method shows that the input resistance depends on the length of the notch X and also its width S. The notch size S=12.8mm is chosen to integrate active components and its feed line, producing as less coupling effects with the patch as possible. The dip size X=16.9 mm is chosen to match the input resistance of the antenna to desired value for the active circuit. The dimension of the microstrip line to feed the antenna at the edge of the notch is also determined. The simple inset fed antenna of the above dimension is designed using the IE3D software which is shown in Fig. 2. below

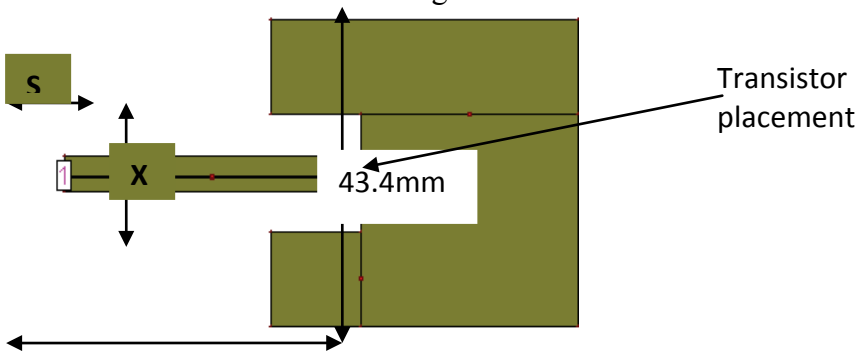


Fig. 2. Simple inset fed microstrip patch antenna

## 2.2. DESIGN OF TRANSISTOR LOADED INSET FED MICROSTRIP ANTENNA

For the antenna to be used as a transmitter the base is soldered to the Microstrip line the collector is soldered to the patch and the emitter leads are soldered to the ground plane through the substrate. The biasing is applied to the transistor externally. For the antenna to be used as a receiver the collector is soldered to the Microstrip line the base is soldered to the patch and the emitter leads are soldered to the ground plane through the substrate. The transistor is chosen such that its input impedance matches the impedance of the transmission line and the output impedance matches the impedance of the antenna.

SEARCH
Previous Page
Next Page

## 2.3. GAIN MEASUREMENT:

Gain of an antenna is given by, $G_r = \left(\frac{4\pi r}{\lambda}\right)\left|S_{21}\right|$

At the time of measurement, the antennas were placed at the far field and the measured value of S21 was -21.83 dB without the active device and with the active device the measured value of S21 was -15.79 dB .

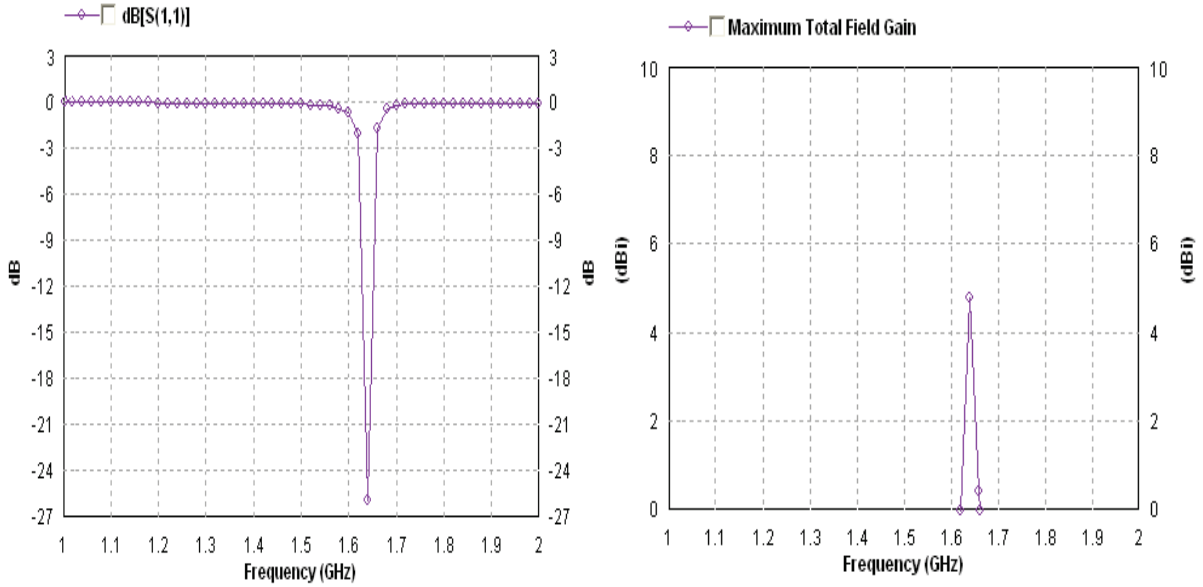


Fig.3 &4 Simulated results for return loss and gain for a simple inset fed microstrip antenna.

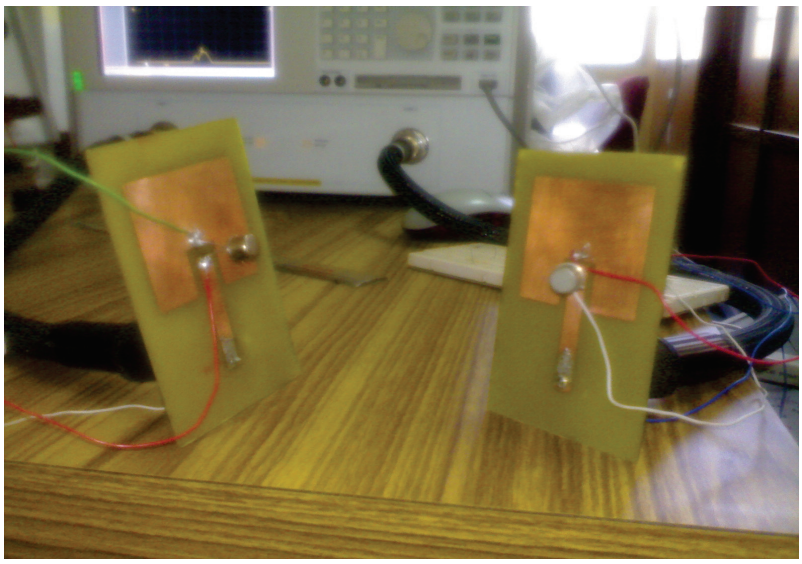

**Fig. 5 Transistor loaded microstrip antenna as a transmitter and receiver for gain measurement**

SEARCH
Previous Page
Next Page

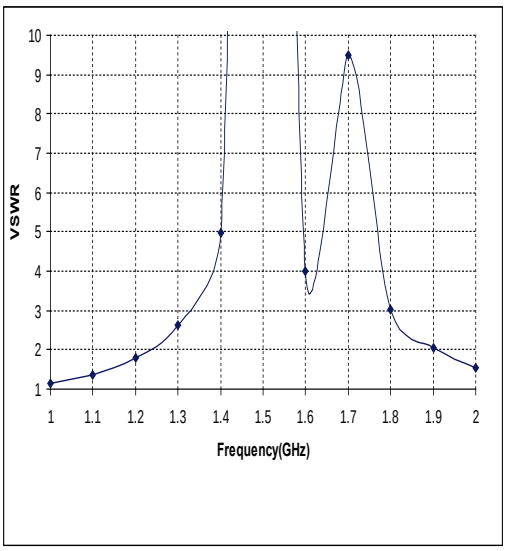


Fig.6 Theoretical results for VSWR for transistor loaded MSA

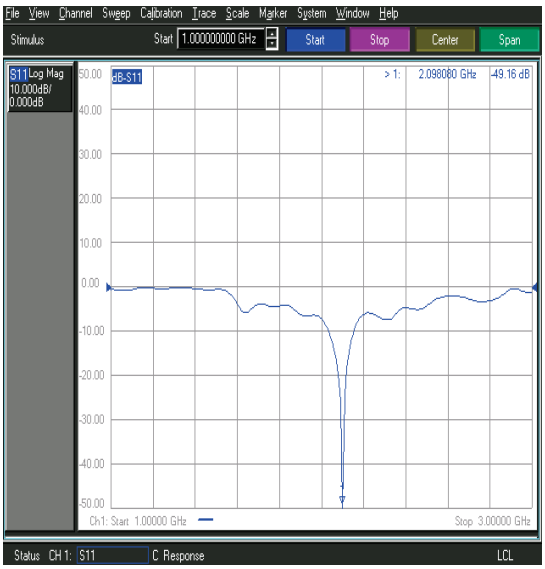


Fig. 7 experimental results for return loss of simple inset fed microstrip antenna

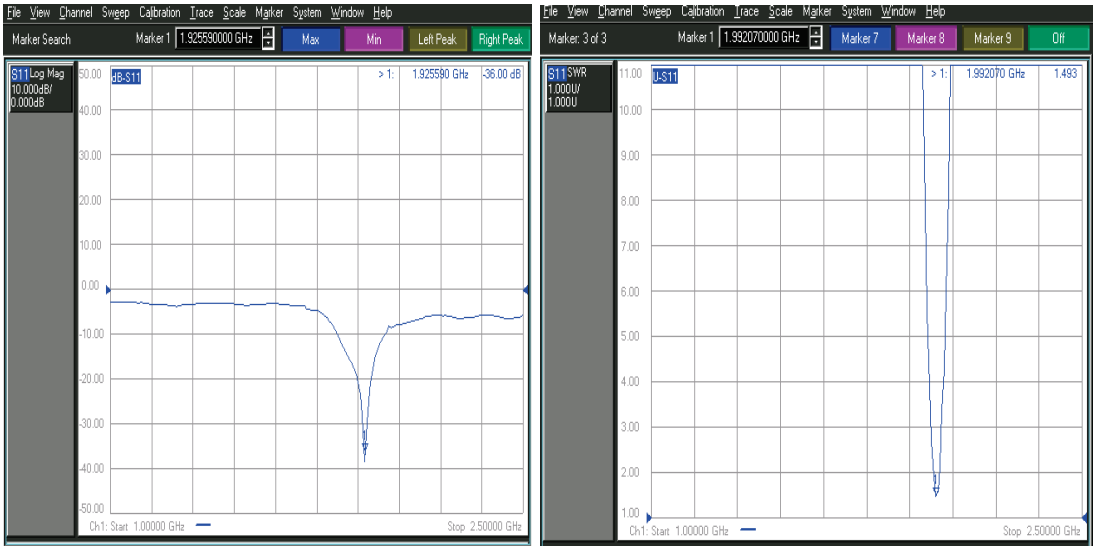


Fig.8&9 Experimental results for return loss and VSWR for transistor loaded microstrip

## 3. DISCUSSION OF RESULTS:

In case of simple microstrip antenna the antenna resonates only at 1.65 GHz (Fig.3) but on loading the antenna with transistor the antenna shows a slight dual band behavior (Fig.6). On testing the simple inset fed antenna without the active device the resonant frequency is shifted to 2.08 GHz and with the active device the frequency is 1.9 GHz (Fig.7 and Fig.8). The simulation results of simple inset fed microstrip antenna in IE3D show a value of -21 dB at the resonant frequency (Fig.1). On testing the antenna on the vector network analyzer without the the value of return loss is -49.16 dB (Fig.7) and the value is reduced slightly to 36 dB when the active device is loaded (Fig.8). Theoretically a VSWR of 1 is achieved at 1.2

SEARCH
Previous Page
Next Page

GHz and 1.9 GHz. But on testing the antenna the value of VSWR almost reaches to 1 at 1.9GHz (Fig.9). The gain of the simple inset fed microstrip antenna is 5 dB at the resonant frequency, but experimentally the value of gain is 4.45 dB. On integrating the antenna with the active device the gain becomes 10.49 dB and on testing the antenna the bandwidth achieved is 0.1 GHz without the active device and is 0.2 GHz with the active device.

## CONCLUSION:

An active antenna was designed, analysed, simulated and tested and results obtained were very good as the gain was enhanced and the bandwidth increased.

## REFERENCES:

1. B N Biswas, A Bhattacharya, D Mondal and P Lahiri, "A novel scheme for reception using an active microstrip antenna", IEEE Trans. Microwave Theory Tech., vol MTT-48, no 10, pp.1765-1768, Oct2000.
2. J. Lin and T. Itoh, "Active integrated antennas," IEEE Trans. MicrowaveTheory Tech., vol. 42, pp. 2186–2194, Dec. 1994.
3. Garg.R, .et.al. "Microstrip Antenna Design Handbook". Artech House 2001.
4. Kai Chang Gellow, Robert A. York, Peter S. Hall and Tatsuo Itoh, "Active Integrated Antennas" IEEE Transactions on microwave theory and Techniques, Vol. 50, No. 3 March 2002.

# ANALYSIS AND DESIGN OF COMPACT DUAL BAND SQUARE PATCH ANTENNA FOR WIRELESS APPLICATIONS

*T.Shanmuganantham[(1)], Dr.S.Raghavan[(1)]*
Department of Electronics and Communication Engineering
National Institute of Technology, Tiruchirappalli, Tamil Nadu-620 015
Email :- eck0601@nitt.edu,raghavan@nitt.edu

**ABSTRACT: -**

In this paper the analysis and design of compact dual band square Microstrip patch antenna for bandwidth improvement and antenna size reduction in a single design is proposed. The fundamental parameters of the antenna such as bandwidth, return loss, gain, radiation pattern and polarization are obtained. This square piece patch antenna has less return loss of -40 dB with bandwidth of 40 MHz and 200 MHz in two bands respectively. The sensitivity of patch antenna towards its patch shape is also discussed. Simulation tool, based on the method of moments (ZELAND IE3D version 12.0) has been used to analyze and optimize the antenna.

## INTRODUCTION:

Recently, the market for Wireless Local Area Network (WLAN) products is booming rapidly with the roll out of IEEE 802.11 b products into the home, public, and office environments. With the increasing consumer demand for wireless multimedia, even higher throughput will be required. In applications where size, weight, cost, performance, ease of installation, and aerodynamic profile are constrains, low profile antennas like Microstrip and printed slot antennas are required. Because Microstrip antennas inherently have narrow bandwidths and, in general, are half-wavelength structures operating at the fundamental resonant mode [1], researchers have made efforts to overcome the problem of narrow bandwidth, and various configurations have been presented to extend the bandwidth [2-6] by introducing slots in the Microstrip patch. In Microstrip antenna research a new trend is found where the researcher try to improve antenna characteristics by introducing different structures within the antenna geometry. Microstrip antennas received considerable attention starting in the 1970's although the idea of a Microstrip antenna can be traced to 1953 and a patent in 1955. Microstrip antennas consist of a very thin metallic strip (patch) placed on small fraction of a wavelength above a ground plane. The Microstrip patch is designed so its pattern maximum is normal to the patch (broadside radiator). This is accomplished by properly choosing the mode (field configuration) of excitation beneath the patch. For a rectangular patch, the length L of the element is usually $\lambda_o/3 < L < \lambda_o/2$. The strip (patch) and the ground plane are separated by a dielectric sheet (referred to as the substrate). The structure of basic Microstrip antenna is simple to understand and fabrication. The Microstrip antenna parameters are very flexible with its patch shape [7]. Even due to small variation in its patch shape, the characteristics of Microstrip antenna will change greatly. These changes may lead sometimes to complete destruction of antenna or sometimes may result in improvement of the parameters of antenna. Here the shape of a simple Microstrip antenna is changed insteps of square pieces and resonate at two different frequencies which applicable for application in Advanced Wireless Services; potentially a spectrum of choice for AWS spectrum holders

(legacy service providers), IEEE 802.16-2004. In this paper the analysis and design of compact dual band square Microstrip patch antenna for bandwidth improvement and antenna size reduction in a single design is proposed. The fundamental parameters of the antenna such as bandwidth, return loss, gain, radiation pattern and polarization are obtained.

## ANTENNA STRUCTURE AND DESIGN:

Microstrip patch of size 40 X 40 mm made on FR4 substrate of thickness 3.2 mm and dielectric constant of 4.2 which is simulated using IE3D simulation tool. When this structure is simulated we had a resonating frequency at 1.7 GHz as shown in Fig. 1.

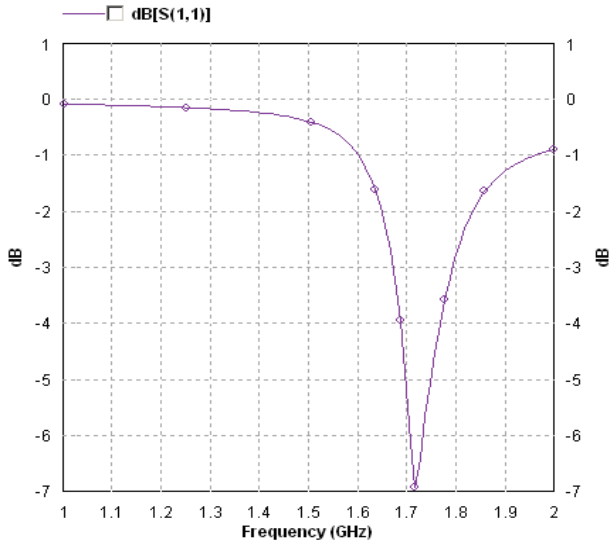


Fig. 1 Fundamental patch antenna return loss

the return loss is very high and it is -7 dB. This square patch is cut into small square pieces and simulated number of times by removing and adding each square piece until good results are obtained. After doing all manipulation same patch antenna started resonating at two different frequencies 1.7 GHz and 5.4 GHz with less return loss around -40 dB. The final structure of this antenna after varying its structure insteps of small square pieces is very much different and shown in next section characteristics simulated using IE3D. Number of changes is made for fundamental patch antenna. The actual antenna is cut into number of square pieces and simulated number of types by changes these square pieces. The proposed structure is shown in Fig. 2. The Microstrip patch in Fig. 2 is of size 40 X 40 mm made on FR 4 substrate of thickness 3.2 mm and dielectric constant of 4.2 .

SEARCH
Previous Page
Next Page

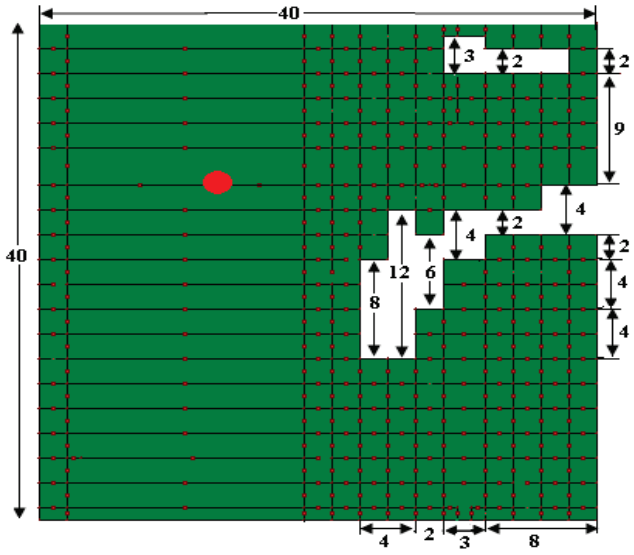


Fig. 2 Proposed square piece Microstrip patch antenna

The feed is coaxial feed. The inner conductor of coaxial cable as diameter 0.6 mm. The feed is at point (12, 28) which is shown as circle on patch.

## RESULTS AND DISCUSSION:

The "Dual Band Square Piece Patch Antenna" is simulated using software tool called IE3D (Ver. 12.0) which works with Methods of Movements numerical technique to simply electromagnetic waves. Figs. 3 & 4 shows the return loss at two frequency bands. In both band antenna is having -40 dB return loss which is more advantageous of this antenna. The radiation characteristics of E-plane polarizations of band I and band II are shown in Figs. 5 and 6.

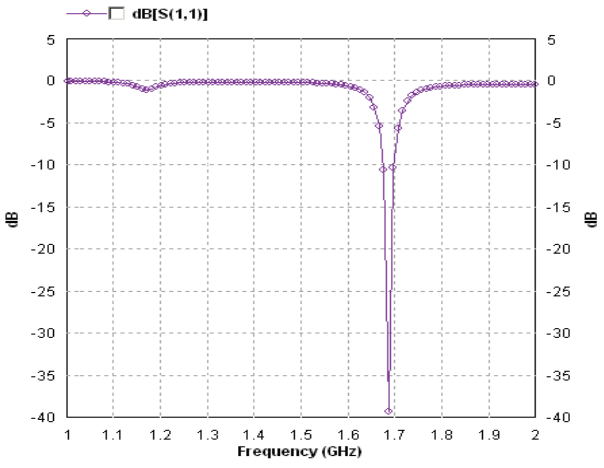


Fig. 3 Return loss at 1st band.

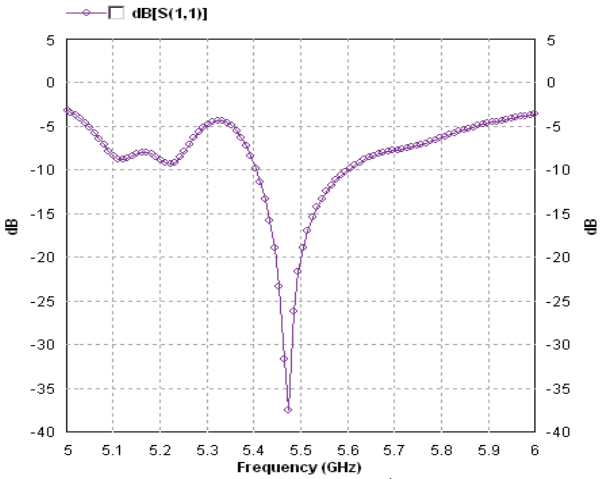


Fig. 4 Return loss at 2nd Band.

SEARCH
Previous Page
Next Page

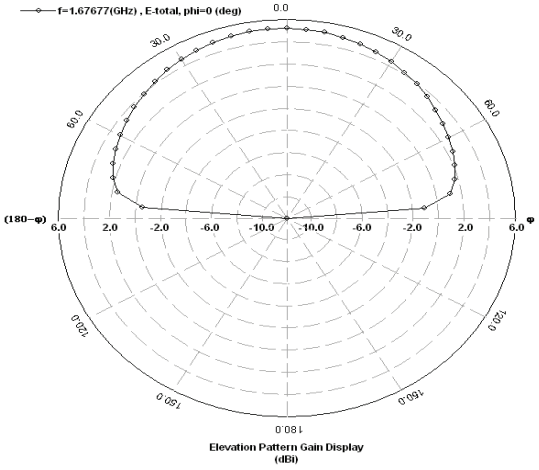


Fig. 5 E-Plane radiation pattern at 1st band

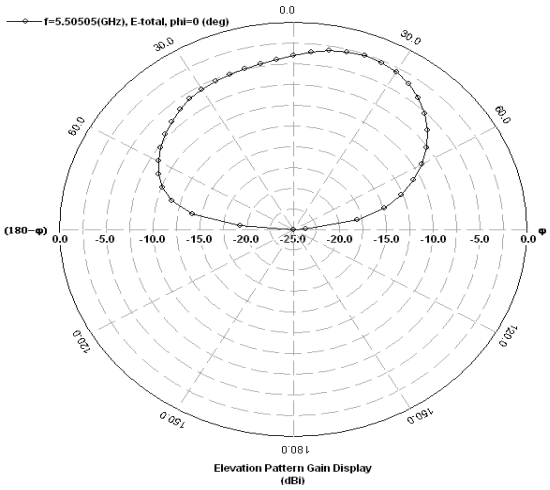


Fig. 6 E- Plane radiation pattern at 2nd band

In first band the antenna is having 5 dBi gain and in second its gain is around 3.5 dBi which are shown in Fig. 7 and 8. The bandwidth of antenna in two bands is 40 MHz and 200 MHz respectively. After seeing all things it is noticed that by changing the shape of antenna in Fig.1 into Fig. 3 a dual band arises and with this we can say that patch antenna is very sensitive towards its patch shape.

## CONCLUSION:

In this paper the analysis and design of compact dual band square Microstrip patch antenna for bandwidth improvement and antenna size reduction in a single design is proposed.

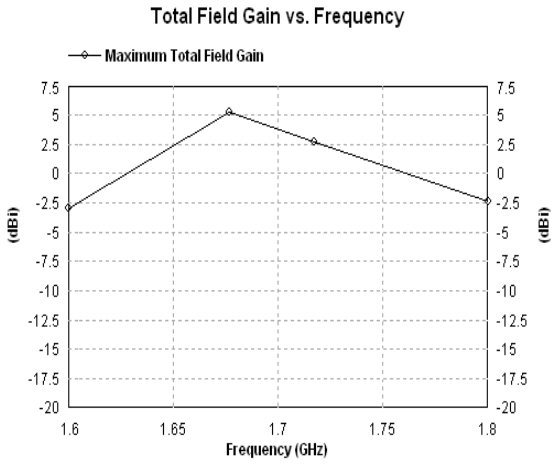


Fig.7 Proposed antenna Gain at 1st band

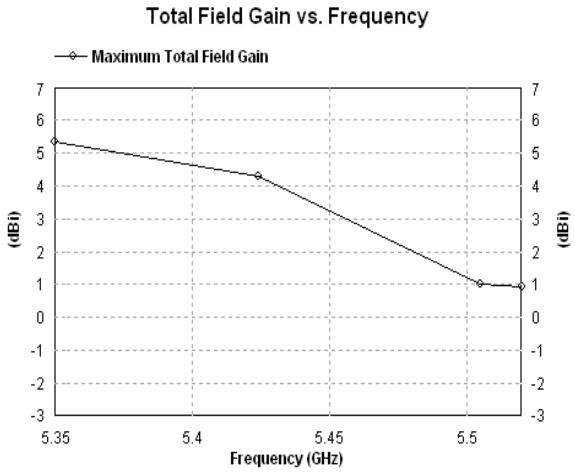


Fig.8 Proposed antenna Gain at 2nd band

SEARCH

The f undamental par ameters of t he ant enna s uch as band width, r eturn l oss, gai n, tern and pol arization ar e obt ained. The s haped of or dinary patch ant e ade t o r esonate at t wo di fferent f requencies. T he ant enna cab be us ed i n

Previous Page
Next Page

applications l ike Wireless Communications, potentially a spectrum of choice for AWS spectrum holders (legacy service providers), IEEE 802.16-2004. Thus the sensitivity of patch antenna towards its patch shape is discussed.

**REFERENCE:**

1. K-L Wong , "*Compact and Broadband Microstrip Antennas*", New York, NY: John Wiley and Sons Inc., 2002.
2. T. Huynh and K. F. Lee, "Single-layer single-patch wideband Microstrip antenna," *Electron. Lett.*, vol. 31, pp. 1310-1312, 1995.
3. K. L. Wong and W. H. Hsu, "Broadband triangular Microstrip antenna with U-shaped slot," *Electron. Lett.*, vol. 33, pp. 2085-2087, 1997.
4. Yong-Xin Guo; Kwai-Man Luk, Kai-Fong Lee, Chair, R., "A quarter wave U-shaped patch antenna with two unequal arms for wideband and dual-frequency operation," *IEEE Trans. On Ant. Prop.*, vol. AP- 50, no. 8, pp. 1082-1087, Aug. 2002.
5. K. F. Tong, K. M. Luk, K. F. Lee, and R. Q. Lee, "A broad-band U-slot rectangular patch antenna on a microwave substrate," *IEEE Trans. On Ant. Prop.*, vol. AP-48, no. 6, pp. 954-960, June 2000.
6. Y. X. Guo, K. M. Luk and K. F. Lee, "L-probe proximity-fed short circuited patch antennas," *Electron Lett.* vol. 35, no. 24, pp. 2069-2070, 1999.
7. S. S. Iqbal, J. Y. Siddiqui, and D. Guha, "Simple design of a compact broadband Microstrip antenna for mobile communication," to be published in the *IEEE Int. Symp. on Antennas and propagation and USNC/CNC/URSI North American Radio Science Meeting*, to be held at Columbus, OH, during June 22- 27, 2003.

# ANN SOLUTION OF PDE FOR REGULAR MICROSTRIP ANTENNAS

*Sridhar Pattanaik*[(1)] *and R.K Mishra** [(1)]
Department of Electronic Science, Berhampur University, Berhampur, India, 760 007,
E.mail: sridhar_pattanaik@yahoo.co.in

**ABSTRACT-**

The microstrip patch antennas are narrow-band resonant antennas. They can be treated as cavities. Therefore, cavity model becomes a natural choice for analysis of patch antennas. This model is suitable for geometries for which the Helhmoltz equation possesses an analytical solution. Trained neural network can be used for high-level design, providing fast and accurate answers to the task it has learned. Neural networks are attractive alternatives to conventional methods such as numerical modeling methods, which could be computationally expensive, or analytical methods, which could be difficult to obtain. We present a method to solve the wave equation in one dimension for the regular (i.e. Rectangular and circular) microstrip antenna for the dominant mode. A trial solution of the differential equation is written by construction the initial/boundary conditions are satisfied then the network is trained to satisfy the differential equation. The method in the treated case proved to be accurate. It is a promising tool for tackling problems of higher dimensions.

## I. INTRODUCTION

The structure of microstrip antenna looks relatively simple. However, the determination of the electromagnetic field components is quite complex due to the presence of different types of inhomogeneities in the structure. For this reason, initially simplified models were developed, based on Transmission line and Cavity model [1]. Later on rigorous methods were derived. Each method has its own merits and drawbacks. ANN can be used for high-level design, providing fast and accurate answers to the task it has learned. The use of neural networks provides good generalization properties; less model parameters are required to other methods, compact solution models, low demand on memory. The method can be realized in hardware, using Neuroprocessors. Hence it has the capacity to tackle differential equations of many engineering problems.

In this paper one-dimensional wave equation for the rectangular patch antenna with two Neumann boundary conditions and wave equation for circular microstrip antenna is solved using ANN. The former is solved using rectangular coordinate system and the later is solved using cylindrical coordinate system. The original constrained optimization problem has been reduced to unconstrained optimization, which is easier to handle due to the choice of the trial solution. In ANN the weights and biases are to be adjusted in order to deal with the minimization problem.

SEARCH

Previous Page

Next Page

## II. PROBLEM FORMULATION

In any antenna problem the wave equation is to be satisfied followed by the boundary conditions. The problem under consideration is a rectangular patch antenna for the dominate mode which can be considered as a one dimensional problem. The one dimensional wave equation for the patch is given by the equation 1 and 2.

$$\nabla\times\nabla\times\vec{E}-k^2\vec{E}=-jw\mu_0\vec{J} \tag{1}$$

$$\frac{\partial^2 E_z}{\partial x^2}+k^2E_z=jw\mu_0 J \tag{2}$$

Where, $k^2=w^2\mu_0\varepsilon_0\varepsilon_r$

Solving the partial differential equation and imposing the boundary condition the electric field mode vector for the patch is found out by using cavity model [1,2]. The eigenfunctions must satisfy the homogeneous wave equation, boundary conditions and normalization condition.

$$\left(\frac{\partial^2}{\partial x^2}+k_m^2\right)\psi_m=0 \tag{3}$$

$$\left.\frac{\partial\psi_m}{\partial x}\right|_{x=0}=0=\left.\frac{\partial\psi_m}{\partial x}\right|_{x=L} \tag{4}$$

$$\int_x\psi_m\psi_m^*dx=1 \tag{5}$$

In this paper the electric field mode vector for the dominant mode of the rectangular Patch antenna is solved using ANN in detailed and in the similar manner the circular antenna is solved. The results are in good agreement with the solution of the analytical counterpart.

## III. IMPLEMENTATION

In order to use ANN [3] we propose the solution of the wave equation to be $F_t$ such that it satisfies the wave equation as well as the boundary condition.

$$\left(\frac{\partial^2}{\partial x^2}+k^2\right)F_t(x)=0 \tag{6}$$

$$\left.\frac{\partial F_t(x)}{\partial x}\right|_{x=0}=0, \tag{7}$$

$$\left.\frac{\partial F_t(x)}{\partial x}\right|_{x=L}=0 \tag{8}$$

The trial solution of the wave equation is written as

$$F_t(x)=LN(x,L,\vec{p})+\left(Lx+\frac{x^2}{2}\right)\frac{\partial N(0,L,\vec{p})}{\partial x}-\frac{x^2}{2}\frac{\partial N(L,L,\vec{p})}{\partial x} \tag{9}$$

SEARCH
Previous Page
Next Page

Where N(x,L,p) is the output of a feed forward network with two inputs x for position coordinate , L length and p is the weight vector of the ANN. By construction the trial solution satisfies the two boundary conditions and the constrained optimization problem is converted to unconstrained optimization problem.

$$N = \sum_{i=1}^{q} w_i \zeta(z_i) \tag{10}$$

where,

$$z_i = v_{1i}x + v_{2i}L + v_{0i} \tag{11}$$

$$\zeta(z\ ) = \tanh(z) \tag{12}$$

The cost function of the network for training is found and given by Error i.e. (13).

$$Error = L\frac{\partial^2 N(x,L,\vec{p})}{\partial x^2} + k^2 LN(x,L,\vec{p}) + \left\{1 - k^2\left(Lx - \frac{x^2}{2}\right)\right\}\frac{\partial N(0,L,\vec{p})}{\partial x} - \left\{1 + k^2\frac{x^2}{2}\right\}\frac{\partial N(L,L,\vec{p})}{\partial x} \tag{13}$$

The square of the error is given by the expression E.

$$E = (Error)^2 \tag{14}$$

The weights of the network are trained according to the normal back propagation algorithms [3,4,5].

In the similar way the wave equation for the circular patch antenna can be solved but here instead of the rectangular coordinate system cylindrical coordinate is used.

Solving the partial differential equation for the circular patch antenna and imposing the boundary condition the electric field mode vector for the patch is found out by using cavity model [1,2]. The eigen-functions must satisfy the homogeneous wave equation, boundary conditions and normalization condition. The boundary condition will ensure the shape where as the normalization condition will give the magnitude.

$$\nabla^2\Phi + k^2\Phi = 0 \tag{15}$$

$$\frac{1}{r}\frac{\partial}{\partial r}\left(r\frac{\partial\Phi}{\partial r}\right) + \frac{1}{r^2}\left(\frac{\partial^2\Phi}{\partial\phi^2}\right) + k^2\Phi = 0 \tag{16}$$

If the variation along the z direction is not taken into account then the equation turns to

$$\frac{1}{r}\frac{\partial}{\partial r}\left(r\frac{\partial\Phi}{\partial r}\right) + k^2\Phi = 0 \tag{17}$$

$$\left(r\frac{\partial^2\Phi}{\partial r^2} + \frac{\partial\Phi}{\partial r}\right) + k^2 r\Phi = 0 \tag{18}$$

$\Phi(r)$ must satisfy $\Phi(0) = 0$ and $\left.\frac{\partial\Phi}{\partial r}\right|_{r=a} = 0$

The trial solution is given by the equation (19).

$$\Psi_t(r) = N(r,a,\vec{P}) - N(0,a,\vec{P}) - r\frac{\partial N(a,a,\vec{P})}{\partial r} \tag{19}$$

The electric field mode vector for the dominant mode of the circular Patch antenna is solved using ANN the results are in good agreement with the solution of the analytical model.

SEARCH
Previous Page
Next Page

## IV. RESULTS AND DISCUSSION

Network structure: The network structure is 2-10-1 and the transfer function for the hidden and output layer are tanh (.) and linear respectively. The network is trained upto $10^{-4}$ tolerance. The values of $a,h$ in this model are same. For the rectangular and circular case it is 0.00078 and 0.00067 respectively.

The results are in good agreement with the analytical model. The error is due to the training error. There is a possibility that the network may be trapped in the local minima.

## V. CONCLUSION

We have presented a novel method appropriate for solving solution of partial differential equation for regular microstrip antenna. The method is new and expected to be used for the analysis of any microstrip antenna structure or in general any electromagnetic problem; there is scope for further research and development.

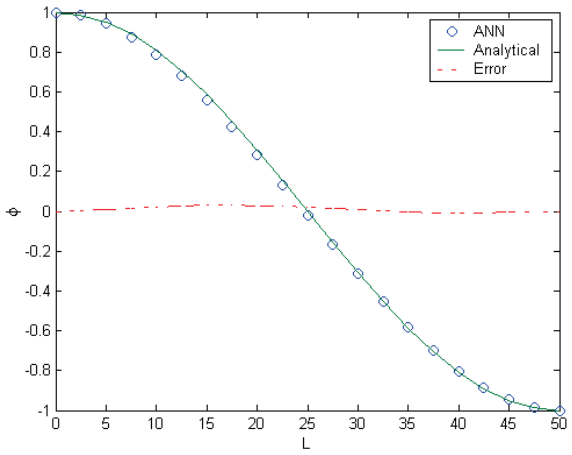


Figure 1Comparison of ANN with analytical model for RMA

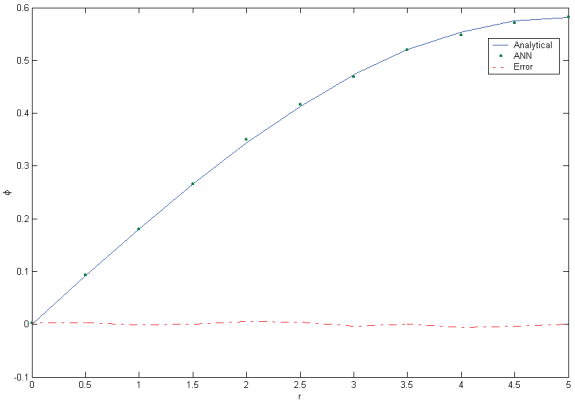


Figure 2 Comparison of ANN with Analytical method for CMA

## VI. REFERENCES:

C arver, J . W . M ink, “M icrostrip A ntenna T echnology,” *IEEE Trans. An and*

*Propagation*, vol. AP-29, no. 1, pp. 2-24, Jan. 1981.

2. K. R. Carver, "A Modal Expansion Theory for the Microstrip Antenna," in *Dig. Int. Symp. Antennas Propagation Soc*., Seattle, WA, pp. 101-104, June 1979.
3. P. K. Simpson, "Foundation of neural network, Artificial Neural Networks *Paradigms, Applications and Hardware Implementations,*" IEEE Press, NJ, 1992.
4. H. Lee and I. Kang, "Neural algorithms for solving differential equations," *J. Comput. Phys.*, vol. 91, pp. 110–117, 1990.
5. A. J. Meade, Jr., and A. A. Fernandez, "The numerical solution of linear ordinary differential equations by feedforward neural networks," *Math. Comput. Modeling*, vol. 19, no. 12, pp. 1–25, 1994.

## RESEARCH SESSION II
## MICROWAVE ANTENNAS

SEARCH

Previous Page

Next Page

## RESEARCH SESSION II

## MICROWAVE ANTENNAS

***Chair: Dr. R.M. Jha, NAL, Bangalore.***



SEARCH

Previous Page

Next Page

SEARCH

Previous Page

Next Page

# UAT ANALYSIS OF THE H-PLANE HORN RADIATION PATTERN

*Maifuz Ali(1) and Subrata Sanyal(2)*
Dept.-Electronics & Electrical Communication Engineering
Indian Institute of Technology Kharagpur
Kharagpur - 721302, INDIA
Email:(1)maifuzali@lycos.com, (2)ssanyal@ece.iitkgp.ernet.in

**ABSTRACT:**

H-plane radiation pattern of pyramidal horn antenna is computed using uniform asymptotic theory (UAT) of diffraction. Theoretical results obtained are compared with experiment to bring out the finer aspects of the UAT.

## INTRODUCTION:

A comprehensive analysis of the E-plane radiation pattern was carried out by Yu, Rudduck and Perers in [1]. Keller's geometrical theory of diffraction (GTD) and parallel plate aveguide mode approximation was used by Yu to obtain the H-plane radiation pattern in [2]. UAT [3] was applied by Menendez and Lee [4] to obtain E-plane horn radiation pattern. Sanyal and Bhattacharyya [5] obtained the E-plane radiation pattern using UAT to obtain superior results in the back lobe region. In the study reported in this paper we use UAT and line sources to obtain the H-plane horn radiation pattern.

## 2 FORMULATION

### 2.1 GO FIELD:

The pyramidal horn is approximated by a dihedral corner reflector formed by two perfectly conducting, inclined, half-planes as shown in Fig. 1, and excited by an anisotropic electric line current source at the vertex SH. Rays from this source are assumed to have electric vector parallel to the corner reflector H-edges (the edges normal to the H-plane [2]). These are incident tangentially on the reflector walls. The ray-optical expansion of this source field is given by

$$E^i(r_1,\theta_x) \sim e^{i(kr_1-\pi/4)}\left(\frac{2}{\pi kr_1}\right)^{1/2}\cos\left(\frac{\pi}{2}\frac{\theta_x}{\theta_H}\right) ----(1)$$

### 2.2 CONTRIBUTIONS OF H-EDGES:

Consider now the corner reflection wall $S_HQ_1$ (Fig. 1) which form a part of the half-plane. In terms of the notations of UAT the field incident on this half-plane may be written as

$$E^i(r_1,\phi_1) \sim e^{i(kr_1-\pi/4)}\left(\frac{2}{\pi kr_1}\right)^{1/2}\cos\left(\frac{\pi}{2}\frac{\pi-\phi_1+\theta_H}{\theta_H}\right) ----(2)$$

SEARCH
Previous Page
Next Page

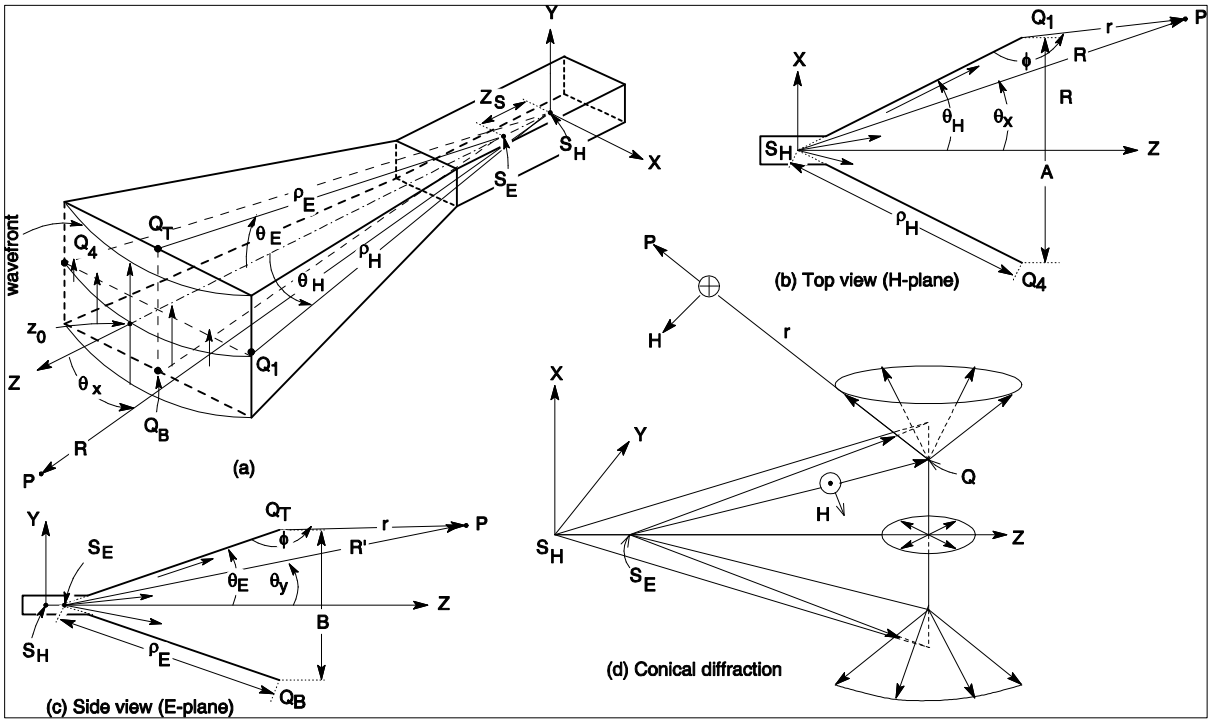


Figure 1: Geometry of horn diffraction.

where $\phi_1 = \pi - \theta_x + \theta_H$. Since this is a case of grazing incidence with E vector parallel to the edge [6], the first order diffraction terms are identically zero. Therefore, considering the next higher order terms we obtain the diffracted field using Eqn. (3.36) of [6]

$$E^d \sim \frac{e^{j(r+\rho_H)}}{4ik^2\rho_H\theta_H}\frac{1}{(r\rho_H)^{1/2}}\frac{\sin\left(\phi/2\right)}{\cos^2\left(\phi/2\right)} + 0\left(k^{-3}\right) ----(3)$$

Then the UAT total diffracted field $E_c^t$ due to diffraction at edge Q1 is obtained as the sum of the GO field and the diffracted field (3), viz

$$E_C^t = E^G + E^d -----(4)$$

At the shadow/reflection boundaries (SB/RB), corresponding to $\phi_1 = \pi$ (refer Fig. 1), the detour parameter vanishes and the singularities present in EG and Ed cancel out. Then the total field reduces to

$$E_c^t(SB/RB) \sim \frac{e^{j(r+\rho_H)}}{\theta_H k(r+\rho_H)}\left(\frac{r}{\rho_H}\right)^{1/2} ----(5)$$

Proceeding as above. the total field $E^t_D$ due to diffraction at the edge $Q_2$ can now be similarly obtained.

The H-plane horn field $E^t$ is then obtained by first summing the contributing $E^t_c$ and $E^t_D$. However, this results in the incident field being computed twice for angles where [illegible]. Thus on subtracting the incident field from this sum we obtain

SEARCH
Previous Page
Next Page

$E^t = E_C^t + E_D^t - E_C^t(r_1, q_x)$ - - - - - (5) where, $E^i(r_1, q_x) = 0$ for $|q_x| < q_H$. Note that for observation points between $f > \frac{3p}{2} - q_H$ and $q_x > p - q_H$ (Fig. 1), the edge $Q_4$ remains invisible and we have $E^t_D$=0.

The practical horn being three dimensional, the contribution due to diffraction at the E-edges (the edges normal to the principal E-plane [2]) are of significance in the back lobe region.

### 2.3 CONTRIBUTIONS OF E-EDGES:

Consider the three-dimensional pyramidal horn; see Fig. 1. The E vectors of the dominant $TE_{10}$ mode in the rectangular waveguide, are oriented at the aperture as shown. Consider now the E-edge, the rays incident off the midpoint, on this edge result in conical diffraction because of the skewed angles of the incidence, see Fig. 1d. These rays contribute significantly to the H-plane radiation pattern in the backlobes region. Fig. 1a shows the intersections of the E-plane and H-plane with pyramidal horn along with the coordinate system. The anisotropic electric line source is assumed to lie along the Y-axis. In the computation of the E-plane pattern a magnetic line source was used in [5]. Here this source is assumed to pass through the point SE and to be parallel to the X-axis. The rays, incident, skewed on the E-edges are assumed to have amplitude variation corresponding to a cylindrical wave. These rays can be viewed as emanating from various inclined line sources located at SE. A method based on Rusch and Sorensen [8] has been used to determine which ray on diffraction from the E-edge contributes to the field at the observation point P.

#### 2.3.1 THE CONICALLY DI_RACTED FIELD AND THE H-PLANE FIELD:

The electric field diffracted by the top E-edge makes an angle $(p - g)$ the Y-axis at P. Taking into account also the bottom E-edge, the contribution of the source $S_E$ to the H-plane field at P is([3], (4.8))

$$E_S^d : \frac{e^{i(kr+p/4)}}{(2pkr)^{1/2}\sin b_0} \frac{2E^i(Q)}{\sin\left(\frac{y^i}{2}\right)} \cos(g) \text{ - - - - (7)}$$

Here $E_i(Q)$ is the value of the incident field at the point Q. On adding $E^d_E$ to the right hand side of Eqn. (6), we have the final form of the H-plane field

$$E^t = E_A^t + E_B^t - E^i(r_1, q_x) + E_S^d \text{ - - - - - (8)}$$

### 3 NUMERICAL RESULTS AND DISCUSSIONS:

H-plane far-field theoretical plots using UAT approach compared with experimental results of Yu [2] are shown in the Fig. 2. Fig. 4 of [2] shows Yu's theoretical and experimental results. The agreement between theory and experiment for the main lobe is about the same in

SEARCH

Previous Page

Next Page

both the figures, so also is the case in those given in [9]. In [2] and [9]

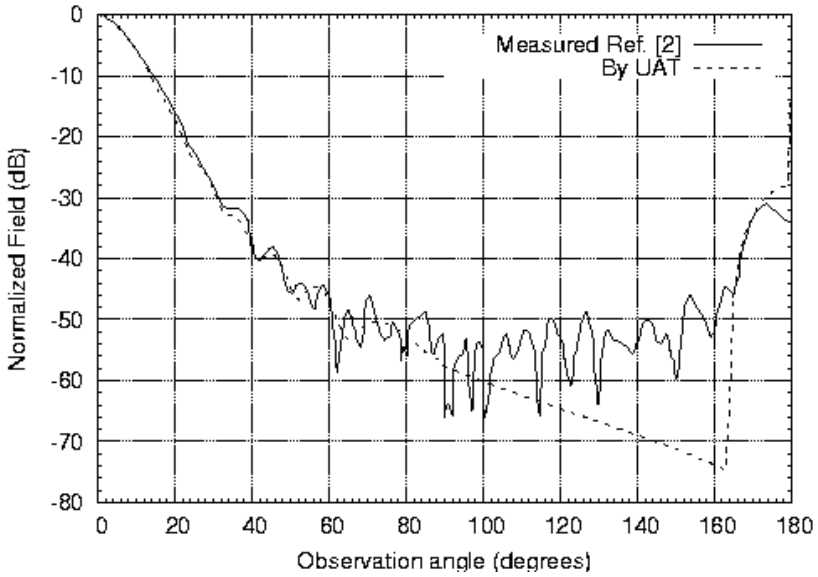


Figure 2: H-plane radiation pattern using UAT.

The results obtained in the backlobe region between $120^0 < \theta_x < 170^0$ by taking in to consideration the finite length of the edges in the H-plane are better than those of Fig. 2. However, the agreement between the present UAT theory and experiment for the backlobe region near $\theta_x = 180^0$ is at least 3 dB better than those of [2] and [9]. Moreover it should be noted that in [2] and [9] methods other than GTD was used in the computation of the effect of finite edges.

**REFERENCE:**

1. J. S. Yu, R. C. Rudduck, and L. Peters Jr., "Comprehensive analysis for E-plane of horn antennas by edge diffraction theory," Antennas and Propagat., IEEE Trans., vol. 14, no. 2, pp. 138-149, Mar. 1966.
2. J. S. Yu and R. C. Rudduck, "H-plane pattern of a pyramidal horn," Antennas and Propagat., IEEE Trans., vol. 17, no. 5, pp. 651-652, Sept. 1969.
3. S. W. Lee and G. A. Deschamps, "A uniform asymptotic theory of electromagnetic diffraction by a curved wedge," Antennas and Propagat., IEEE Trans., vol. 24, no. 1, pp. 25-34, Jan. 1976.
4. R. Menendez and S. W. Lee, "Analysis of rectangular horn antennas via a uniform asymptotic theory," Antennas and Propagat., IEEE Trans., vol. 30, no. 2, pp. 241 - 250, Mar. 1982.
5. S. Sanyal and A. Bhattacharyya, "UAT analysis of E-plane near and far- field patterns of electromagnetic horn antennas," Antennas and Propagat., IEEE Trans., vol. 31, no. 5, pp. 817-819, Sept. 1983.
6. J. Boersma and S. W. Lee, "High-Frequency Diffraction of a Line-Source Field by a Half-Plane: Solutions by Ray Techniques," Antennas and Propagat., IEEE Trans., vol. AP-25, no. 2, pp. 171 - 179, Mar. 1977.
7. R. Menendez and S. W. Lee, "On the role of the geometrical optics field in ape diffraction," Antennas and Propagat., IEEE Trans., vol. 30, no. 2, pp. 241-250, Mar. 1982.
8. W. Rusch and O. Sorenson, "On determining if a specular point exists," Antennas and Propagat., IEEE Trans., vol. 27, no. 1, pp. 99 - 101, Jan. 1979.
9. ntzer, L. Peters Jr., and R. C. Rudduck, "Slope diffraction and its applicat horns," Antennas and Propagat., IEEE Trans., vol. 23, no. 2, pp. 153-159, Mar. 1975.

# MOMENT METHOD ANALYSIS OF TRANSVERSE WALL RECTANGULAR SLOT RADIATOR

*A. Jhansi Rani[1] and P.V. D. Somasekhar Rao[2]*
[1]Asst. Prof., ECE Department, V. R. Siddhartha Engg.College, Vijayawada
jhansi9rani @ gmail.com
[2]Professor of ECE & Director, SIT- School of Information Technology, JNT Univ., Hyderabad

**ABSTRACT:**

Performance characteristics of a radiating slot in the transverse cross-section of a rectangular waveguide are evaluated by the method of moments(MoM) using a conventional approach for free space as well as treating the free space as a big collinear r ectangular w aveguide. T he anal ysis and f ormulation have b een carried out by considering the thick radiating slot as a s tub waveguide.. Three distinct simplification techniques pertaining to free space or infinite half space are pr esented i n t his paper .The var iation of t he per formance char acteristics obtained by these three methods ar e co mpared w ith exper imental r esults. A ll the t hree methods of simplification yield numerical results which have an excellent agreement with one another. These results justify the applicability of the three simplified procedures, with associated computational ease.

## 1. INTRODUCTION

Waveguide f ed s lots ar e w idely us ed i n co mmunications, r adar and var ious ot her microwave s ystems. T he ba sic popul ar r adiating e lement i n al l t hese applications is a rectangular slot, milled in the broad w all or narrow wall, or in the transverse cross-section of the waveguide [1]. Waveguide based antennas are finding potential applications in satellite and mobile communication systems.

Analysis of w aveguide f ed s lot r adiators c an be br oadly di vided i nto two di stinct categories. In one case, the free space into which the waveguide fed slot radiate, is treated as a half-space, and t he convent ional pl ane- wave s pectrum ap proach i s us ed t o det ermine the complex pow er radiated and t he ot her r adiation char acteristics [2]. T wo al ternate methods of reduction of infinite integrals, appearing in the actual half space considerations for waveguide fed slot radiators are proposed in this case - (i) Series Summations M ethod (Method A), and (ii) use of Higher Order Mathematical Functions (Method B) which can be p rogrammed very easily and accurately.

The conventional analysis involving radiation from rectangular slot in an infinite flange into half space is complicated, and it includes good amount of computations. There will be a considerable reduction in the amount of theoretical work and hence the associated computations, if the half space is treated as a collinear large rectangular waveguide filled with a low loss dielectric medium [3]. The second case uses the Waveguide Equivalence of Free Space ( Method C ) [3], in combination with the present MoM analysis, which can be treated as the third simplification method. In this paper, we propose to combine this simple and aveguide equi valence appr oach of f ree s pace with r igorous a nd accur ate analysis [4], thus retaining the advantages of both.

SEARCH
Previous Page
Next Page

## 2. MOM ANALYSIS

Fig. 1 shows the waveguide fed rectangular end slot radiator, and the co-ordinate system adopted for the analysis. The radiating slot is considered to be centrally located in the representation of the radiating slot is shown in Fig. 2, together with the two interfaces.

cross-section of the metallic plate of thickness 't'. An expanded view of the stub

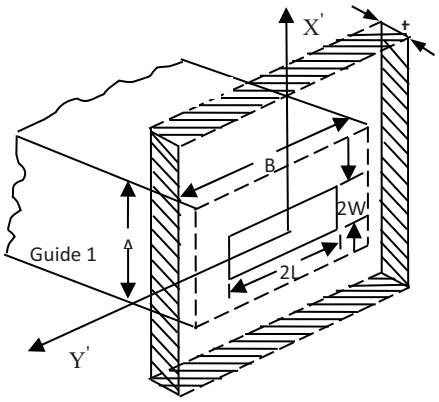


waveguide

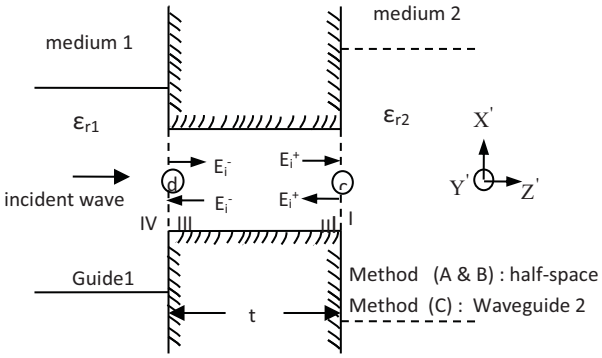


Fig. 1 Waveguide fed rectangular end slot radiator

Fig. 2 Expanded view of the radiating slot

### 2.1 BASIC FORMULATION

The amplitude coefficients for the total tangential electric fields at the two interfaces of the stub waveguide[4], were given by

$$[E^{d,1}] = \{[U]+[B][Y^{cw}]^{-1}[h^{cw}][B]\}[Y^{rw}]^{-1}[h^{rw}][B][Y^{cw}]^{-1}[h^{cw}][B]-[U]\}^{-1}[Y^{rw}]^{-1}2[h^{inc}] \quad (1)$$

$$[E^{c,1}]=\{[B]+[Y^{cw}]^{-1}[h^{cw}][B]\}\{[Y^{rw}]^{-1}[h^{rw}][B][Y^{cw}]^{-1}[h^{cw}][B]-[U]\}^{-1}[Y^{rw}]^{-1}2[h^{inc}] \quad (2)$$

The elements of square matrices [B], $[Y^{rw}]$, $[h^{rw}]$ and $[h^{inc}]$ are given in [4].

## 3. EXPRESSIONS FOR $Y^c_{qs}$ AND $Y^c_{is}$

Two different general procedures are described here for the evaluation of $Y^c_{qs}$ ( $Y^c_{is}$ ). The first procedure is based on the popular "angular spectrum of plane wave approach" [2,5], in which two simplification methods are presented; and the second procedure is based on "Waveguide Equivalence of Free Space".

### 3.1 PLANE-WAVE SPECTRUM APPROACH

The expression for $Y^c_{qs}$ [2] in the case of slot radiating into free space is obtained as

SEARCH
Previous Page
Next Page

The expression for $Y_{qs}^{c}$ [2] in the case of slot radiating into free space is obtained as

$$Y_{qs}^{c} = \frac{qsW^2}{k\eta_0 L^2} \int_{-\infty}^{\infty}\int_{-\infty}^{\infty} \frac{(k^2 - k_y^2)}{k_z} \frac{\mathrm{sinc}^2(k_x W)}{k_y^2 - \left(\frac{s\pi}{2L}\right)^2} \frac{\begin{bmatrix}\cos^2(k_y L)\ q,s\ \text{odd} \\ \sin^2(k_y L)\ q,s\ \text{even}\end{bmatrix}}{k_y^2 - \left(\frac{q\pi}{2L}\right)^2} dk_x dk_y$$ .... for q odd and s odd or q even

and s even

= 0 .... for q odd and s even or q even and s odd.

(3)

### 3.1.1 REDUCTION OF COMPLEX INTEGRALS INTO SERIES SUMMATIONS

The final expression obtained for $Y_{qs}^{c}$ using Series Summations is given by

$$Y_{qs}^{c} = \pi C_1 \sum_{n=0}^{\infty} C_2(n) \int_{\zeta=0}^{1} \left(1 - \zeta^2\right)^{(n+1)} C_3(\zeta)\, d\zeta + j2C_1 \sum_{p=0}^{\infty} C_2(p) \left( \begin{array}{l} \int_{\zeta=0}^{1} (1-\zeta^2)^{(p+1)} C_3(\zeta)\{-\ln(\Lambda W k) - \frac{1}{2}\ln(1-\zeta^2) + C_4(p)\}\, d\zeta \\ + \int_{\zeta=1}^{\infty} (1-\zeta^2)^{(p+1)} C_3(\zeta)\{-\ln(\Lambda W k) - \frac{1}{2}\ln(\zeta^2 - 1) + C_4(p)\}\, d\zeta \end{array} \right)$$

(4)

$$C_1 = \frac{4qs}{\eta_0 L^2},\quad C_2(p) = \frac{(-1)^p (kW)^{(2p+2)}}{(p!)^2 (2p+1)(2p+2)},\quad C_4(p) = \frac{1}{(2p+1)} + \frac{1}{(2p+2)} + \Phi(p);\ \text{and}\ \ln(\Lambda) = 0.5772256$$

$$C_3(\zeta) = \frac{\begin{bmatrix}\cos^2(k\zeta L)\ q,s\ \text{odd} \\ \sin^2(k\zeta L)\ q,s\ \text{even}\end{bmatrix}}{\left[k^2\zeta^2 - \left(\frac{s\pi}{2L}\right)^2\right]\left[k^2\zeta^2 - \left(\frac{q\pi}{2L}\right)^2\right]} \qquad \Phi(p) = \begin{Bmatrix} 1 + \frac{1}{2} + \frac{1}{3} + \ldots\ldots + \frac{1}{p} & \text{for } p > 0 \\ 0 & \text{for } p = 0 \end{Bmatrix}$$

### 3.1.2 REDUCTION OF COMPLEX INTEGRALS INTO HIGHER ORDER MATHEMATICAL FUNCTIONS

The expression for imaginary part of $Y_{qs}^{c}$ is further simplified as

$$Y_{qs}^{c} = \pi C_1 \sum_{n=0}^{\infty} C_2(n) \int_{\zeta=0}^{1} \left(1-\zeta^2\right)^{(n+1)} C_3(\zeta)\, d\zeta + j \left[ \begin{array}{l} C_1 \int_{0}^{1} k^2 W^2 (1-\zeta^2) C_3(\zeta) I_1\left\{2kW\sqrt{1-\zeta^2}\right\} d\zeta \\ + \frac{1}{2} C_1 \int_{1}^{\infty} C_3(\zeta)\ I_2\left\{2kW\sqrt{\zeta^2 - 1}\right\} d\zeta \end{array} \right]$$ (5)

$$I_1(u) = \frac{2}{u^2} + \frac{\pi}{u}\Upsilon_1(u) - \pi\Upsilon_0(u) - \frac{\pi^2}{2}\{I(u)\},\ I(u) = \{H_0(u)\Upsilon_1(u) - H_1(u)\Upsilon_0(u)\},\ I_2(v) = 1 - v\left\{\int_0^v K_0(p)\, dp + K_1(v)\right\}$$

SEARCH

Previous Page Next Page

### 3.2 WAVEGUIDE EQUIVALENCE OF FREESPACE

This is the third proposed method of simplification for expressions involving radiation into free space. In this method, the free space of medium 2 is replaced by an equivalent big collinear rectangular waveguide filled with low loss dielectric[3]. The numerical results from the low loss dielectric cases are used to compute the solution for the actual lossless half-space problem by an extrapolation technique. Expression $Y_{qs}^{c}$ when the medium 2 is considered as a big collinear rectangular waveguide is

$$Y_{qs}^{c} = \sum_{m} \sum_{n} \left[ Y_{mn}^{e,2} V_{mn,q}^{e,2} V_{mn,s}^{e,2} + Y_{mn}^{m,2} V_{mn,q}^{m,2} V_{mn,s}^{m,2} \right] \quad (6)$$

## 4. REFLECTION COEFFICIENT Γ AND ADMITTANCE

The reflection coefficient Γ seen by feed guide is evaluated using the expression

$$\Gamma = -1 + \sum_{\substack{q=1 \\ (odd)}}^{N} E_{q}^{d,1} \sqrt{\frac{2}{AB}}\, 2W \frac{\frac{q\pi}{L}}{\left[\frac{q\pi}{2L}\right]^2 - \left[\frac{\pi}{B}\right]^2} \cos\left(\frac{\pi L}{B}\right). \quad (7)$$

The normalised shunt admittance [4] seen by guide 1 is of the form

$$\frac{Y}{Y_o} = y = g + j\,b = \frac{1 - \Gamma}{1 + \Gamma} \quad (8)$$

## 5. NUMERICAL RESULTS

For the slot radiator structure shown in Fig. 1, the complex amplitude coefficients are evaluated from the three different methods mentioned above. The computations are carried out for number of basis functions N = 5. In the Waveguide Equivalence of Free Space Method, medium 2 is replaced by coaxial rectangular waveguide having cross-sectional dimensions as 30 times that of size of Guide 1. The low loss dielectric have been used for $\varepsilon''$ = 0.1, 0.2 and 0.3. From a knowledge of the amplitude coefficients $E_{q}^{d,1}$ the complex reflection coefficient,and normalised shunt admittance are computed. The value of Γ for the Waveguide Equivalence case is extrapolated for $\varepsilon''$ = 0 [3] using the data for Γ obtained for the three different $\varepsilon''$ values. To facilitate the comparsion with the experimental results presented by Marcuvitz [6] theoretical results are evaluated using the three methods of simplification at f = 9.375 GHz, 2L = 2.286 cm, and t = 0.0794 cm for the slot width range 0.127cm - 1.016cm. The corresponding theoretical results on the variation of magnitude and phase Γ , g and b seen by the feed waveguide are shown in Figs. 3 -4 along with the experimental results.

## 6. CONCLUSIONS

Analysis by moment method using entire sinusoidal basis and testing functions is found to be computationally efficient, as the numerical results for all the three methods of simplification converge very well for number of basis functions N = 5. Interesting conclusions can be drawn from the above results, in the sense that any of the proposed analytical simplification methods can be effectively used for the rigorous and complete analysis of waveguide fed transverse wall slot radiators, retaining the accuraci computational ease associated with the MoM techniques. For the transverse wall slot radiators, verification of the numerical results with experimental results justifies the validity of the three different simplification techniques



Previous Page Next Page

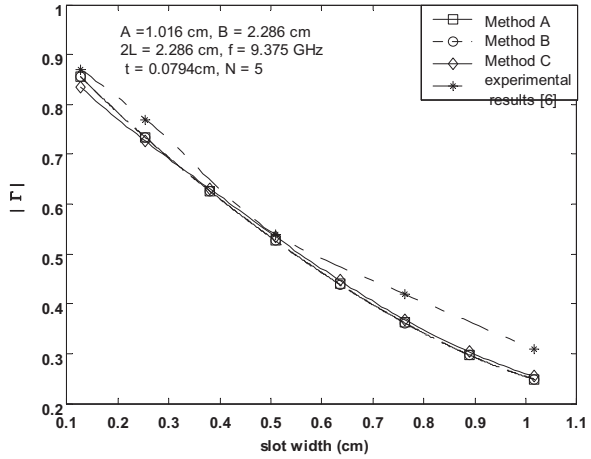


Fig. 3 (a) Variation of $|\Gamma|$ with slot width

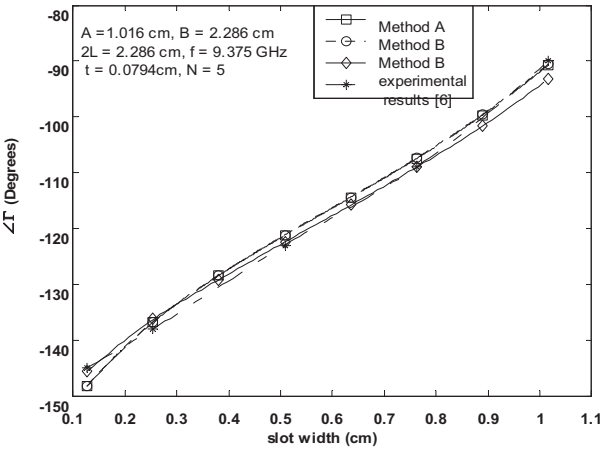


Fig. 3 (b) Variation of phase of $\Gamma$ with slot width

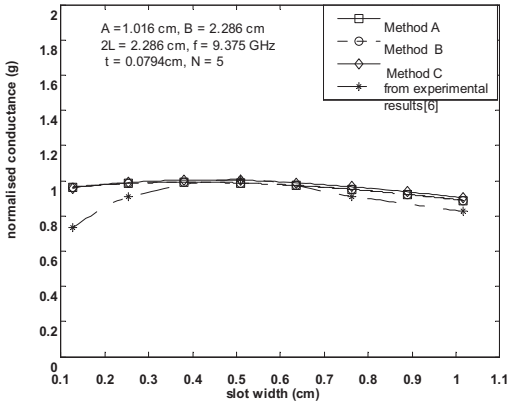


Fig. 4 (a) Variation of g with slot width

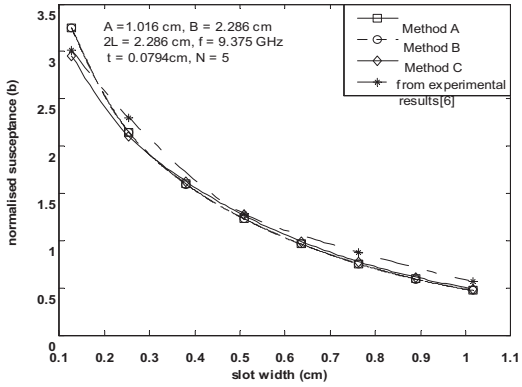


Fig. 4 (b) Variation of b with slot width

## REFERENCES


1. A. Jhansi Rani and P.V. D. Somasekhar Rao "Modeling and Analysis of Round End Slots in Rectangular Waveguides" Special issue of IETE Journal of Research on 'Microwave Circuits and Systems' Vol. 54, No.2, March-April 2008, pp. 129-139.
2. L.G.Josefsson, "Analysis of Longitudinal Slots in Rectangular Waveguides", IEEE Trans. Antennas and Propagat., Vol. AP-35, No.12, pp. 1351-1357, Dec.1987.
3. Shen Zhongxiang and R.H.MacPhie,"A Simple Method for Calculating the Reflection Coefficient of Open-Ended Waveguides", IEEE Trans . MTT, Vol. 45, pp.546-548, April 1997.
4. B.N. Das and P.V.D.Somasekhar Rao, "Moment Method Analysis of a Slot Coupled Junction Between Dissimilar Rectangular Waveguides", IEE Proc., Vo1.137, pt. H, pp.406-410, Dec.l990.
5. D. R. Rhodes, "On a Fundamental Principle in the Theory of Planar Antennas", IEE Proc., Vol. AP-52, pt. H, pp. 1013 – 1021,1964.
6. N. Marcuvitz, Waveguide Handbook, Radiation Laboratory Series, Vol.10, Mc Graw Hill, New York, 1951.

# DIELECTRIC DIAGONAL HORN ANTENNA

*V N Tiwari and T Tiwari*[*]
SMIT, Majitar, Rangpo, East Sikkim – 737132,
E-mail: **drvntiwari@rediffmail.com**
[*]SAMEER, IIT Campus, Powai, Mumbai – 400076

## ABSTRACT

The radiation patterns of solid and hollow dielectric diagonal horn antennas of various dielectric constants and wall thicknesses are studied theoretically and experimentally at spot frequency 9.418 GHz. Theoretical near field distributions at the aperture and at the four side surfaces of a horn under study for TE to x and TE to y modes are obtained by solving the Helmholtz's equation using the separation of variable techniques. The expressions for the near-field components of the horn under study are used to obtain the expression for radiation pattern from Kirchoff's diffraction formula. The theoretical normal and cross-polarized radiation patterns obtained for these antennas are compared with the corresponding experimental ones.

## INTRODUCTION:

Love [1] and Withington & Murphy [2] have investigated the metal diagonal horn antenna and found that this type of antenna possesses some desired properties. Though many types of dielectric horn antennas have been studied, but almost no work has been done on dielectric diagonal horn antennas. Recently efforts have been made by authors [3-6] to study the dielectric diagonal horn antennas both theoretically and experimentally. In the present paper, the authors have attempted to study theoretically and experimentally the radiation patterns of both solid and hollow dielectric diagonal horn antennas in the principal H/E plane at frequency 9.418 GHz. The theoretical near field components at the aperture and at four side surfaces of the antenna for TE to x and TE to y modes are obtained by solving the Helmholtz's equation and using the separation of variables technique. Kirchoff's diffraction formula has been used to obtain the radiation field of the horn from the near field distribution for fundamental $H^x_{11}$ and $H^y_{11}$ modes. The theoretical radiation patterns in H/E and $\pm 45^0$ planes are compared with the corresponding experimental ones. The theoretical radiation patterns of three hollow dielectric wall diagonal horn antennas of wall thicknesses 0.15 cm, 0.15 cm and 0.32 cm and respective dielectric constants of the horn dielectric sheet $\varepsilon^1$ = 2.54, 2.56 and 2.56 in H/E plane are compared with the corresponding experimental ones at spot frequency 9.418 GHz. Similarly the theoretical radiation pattern of a solid dielectric diagonal horn antennas of dielectric constant 2.56 in H/E plane are compared with the corresponding experimental result at spot frequency 9.418 GHz.

## MATHEMATICAL FORMULATION:

The schematic diagram of solid and hollow dielectric diagonal horn antennas, along with the coordinate system used to obtain the radiation patterns are shown in Figs.1 and 2. The radiation from the aperture and four side surfaces of dielectric wall diagonal horn antenna can be obtained by Kirchoff's formula [7], which is given as:

$$E_p = \frac{jk}{4\pi}\left(\frac{\mu_0}{\varepsilon_0}\right)^{1/2} \iint_S \{r_0 \times (n \times H) \times r_0\} - (n \times E) \times r_0 \frac{e^{-jkR}}{R} dS \qquad (1)$$

where, $E_p$, k, R, n, $r_0$, E, and H are, respectively, the radiation field at the far field point P, the free space propagation constant, the distance from the source point to the field point, the unit vector in the z-direction, the unit vector from the origin to the field point, and the electric and the magnetic fields over the surface S. All other terms have their usual meanings. This equation (1) is used for determination of radiation fields of both solid and hollow dielectric diagonal horn antennas from the aperture and all four side surfaces due to TE to x and TE to y modes.

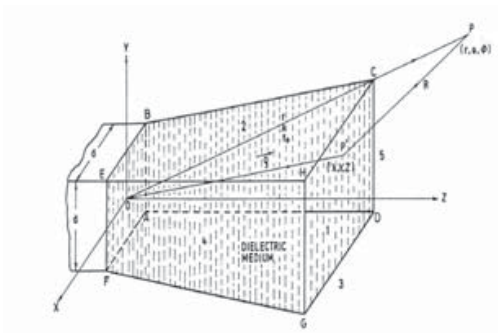


**Fig. 1 Co-ordinate system of solid dielectric diagonal horn antenna**

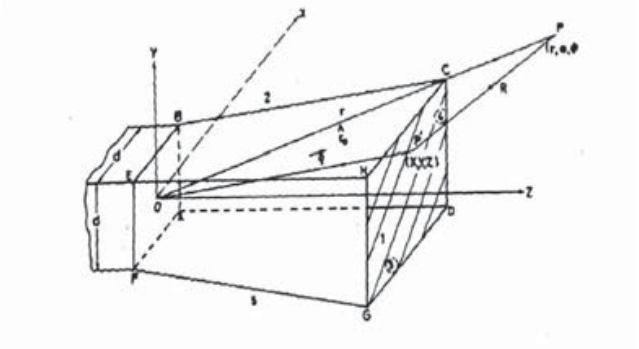

**Fig. 2 Co-ordinate systems of hollow dielectric wall diagonal horn antenna**

**Radiation field due to the aperture and all four side surfaces:** If $E_{px}$ and $E_{py}$ be the sum of the fields due to the aperture and four side surfaces of the horn due to TE to x and TE to y modes, respectively, then

$$E_{px} = E_{px}(GHCD) + E_{px}(ABCD) + E_{px}(EFGH) + E_{px}(BCHE) + E_{px}(ADGF) \quad (2)$$

$$E_{py} = E_{py}(GHCD) + E_{py}(ABCD) + E_{py}(EFGH) + E_{py}(BCHE) + E_{py}(ADGF) \quad (3)$$

After substituting for $E_{px}$(GHCD), $E_{px}$(ABCD), $E_{px}$(EFGH), $E_{px}$(BCHE), and $E_{px}$(ADGF into equation (2) and for $E_{py}$(GHCD), $E_{py}$(ABCD), $E_{py}$(EFGH), $E_{py}$(BCHE), and $E_{py}$(ADGF) into (3), the values of $E_{px}$ and $E_{py}$ are computed. Principal planes are given by $\phi = 45^0$ for the E-plane and $\phi = 135^0$ for H-plane. For $\pm 45^0$ planes, $\phi = 0^0$ and $\phi = 180^0$ can be kept in equations (2) and (3), respectively.

The normal and cross-polarized components in any one of the planes considered are represented as[1]:

$$E_{nor} = \frac{E_{px} + E_{py}}{\sqrt{2}} \quad (4)$$

and $$E_{cros} = \frac{E_{px} - E_{py}}{\sqrt{2}^2} \quad (5)$$

Substituting the values of $E_{px}$ and $E_{py}$ from equations (2) and (3) and choosing the desired value of $\phi$, normal and cross- polarized radiation patterns are computed from equations (4) and (5), respectively, for principal H/E and $\pm 45^0$ planes.

The values of $r_0 \times (n \times H) \times r_0$ and $(n \times E) \times r_0$ are different for all surfaces for TE to x and TE to y modes in case of solid and hollow dielectric diagonal horns. These values are calculated for aperture and all four side surfaces for TE to x and TE to y modes in case of solid and hollow dielectric diagonal horn antennas and are kept in equation (1). In this way for contribution due to all surfaces, i.e., $E_{px}$(GHCD), $E_{px}$(ABCD), $E_{px}$(EFC

SEARCH
Previous Page
Next Page

$E_{px}$(BCHE), $E_{px}$(ADGF), $E_{py}$(GHCD), $E_{py}$(ABCD), $E_{py}$(EFGH), $E_{py}$(BCHE), and $E_{py}$(ADGF) are obtained. These values are substituted into equations (2) & (3) and thus $E_{px}$ & $E_{py}$ are calculated for TE to x and TE to y modes separately for solid and hollow dielectric horns.

## EXPERIMENT AND RESULTS:

One solid dielectric diagonal antenna of dielectric constant 2.56 is constructed. Three hollow dielectric diagonal antennas similar to solid horn with of wall thicknesses 0.15 cm, 0.15 cm and 0.32 cm and respective dielectric constants of the horn dielectric sheet $e^{l}$ = 2.54, 2.56 and 2.56 are also constructed. These horns have square aperture of 4.7 cm. on each side, corresponding to a flare angle of $8.5^0$ and axial length 12.8 cm. The theoretical radiation patterns of these antennas under study in principal H/E plane are shown in Figs. 3-6. The experimental radiation patterns of these antennas are measured with the help of a conventional set-up at the frequency 9.418GHz. The theoretical and experimental radiation patterns of these antennas are plotted in Figs. 3-6. It is found from Figs. 3-5 that both theoretical and experimental HPBW for hollow dielectric diagonal horn antennas in the H/E plane differ from antenna to antenna with differing dielectric constants and wall thickness of the horn dielectrics. With the increase of wall thickness in case of hollow dielectric diagonal horn, the first side lobe level, highest cross-polarization level, and back lobe level are increased. Similarly for such antennas, with increase of dielectric constant, the first side lobe level, highest cross-polarization level, and back lobe level is decreased. HPBW decreases with increase in dielectric constant and/or wall thickness of the material of the horn. It is also observed that the wall thickness has an effect on first side lobe level while the dielectric constant of the material of the antenna plays a minor role in the first side lobe level. It is observed from Fig. 6 that the experimental normal and cross-polarization patterns of solid dielectric diagonal horn antenna in the H/E plane are in agreement with the theoretical result. It is obvious from this figure that the solid dielectric diagonal horn antenna, first side lobe level and highest back lobe level are nil. Further, the solid dielectric diagonal horns under study have reduced beamwidth, no side lobe/back lobe-levels, and acceptable cross-polarized level. In case of hollow dielectric diagonal horn antenna, side lobe levels and highest back lobe level are present while in case of solid dielectric diagonal horn antenna, first side lobe level and highest back lobe level are nil. Beam is sharper in case of solid dielectric diagonal horn antenna in comparison to hollow dielectric horn.

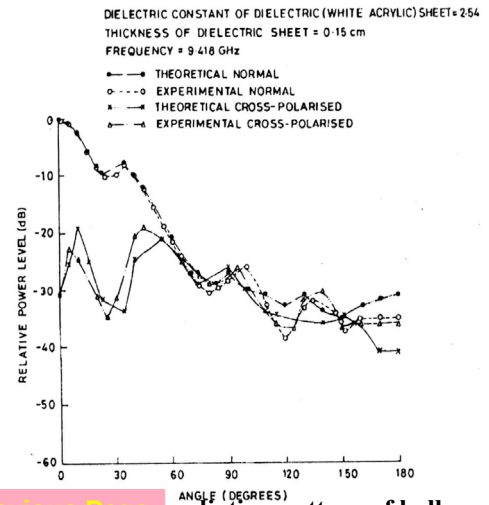


Fig. 3 H/E plane radiation pattern of hollow dielectric wall (acrylic) diagonal horn antenna

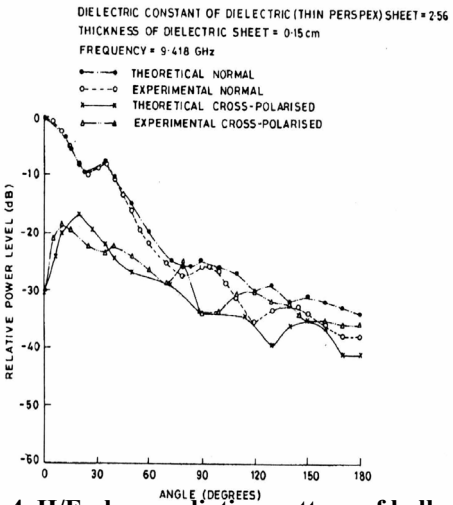


Fig. 4 H/E plane radiation pattern of hollow dielectric wall (Perspex) diagonal horn antenna

SEARCH
Previous Page
Next Page

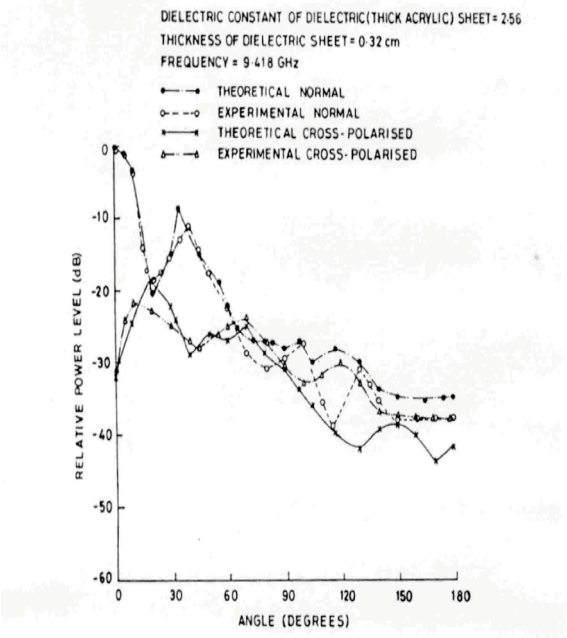


**Fig. 5 H/E plane radiation pattern of hollow dielectric wall (Perspex) diagonal horn antenna**

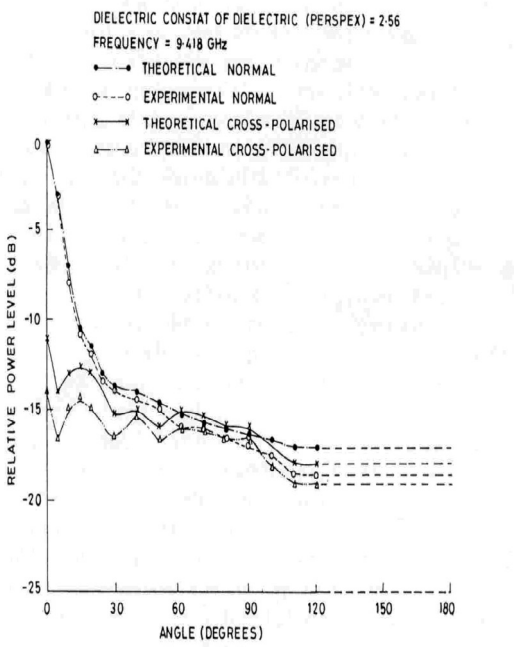


**Fig. 6 H/E plane radiation pattern of solid dielectric (Perspex) diagonal horn antenna**

## CONCLUSION:

The radiation patterns of solid and hollow dielectric diagonal horn antennas have been studied theoretically and experimentally and it is found that the theoretical results are in good agreements w ith t he cor responding exper imental ones . T hese ant ennas have r educed beamwidth an d accept able c ross-polarization l evel. T hese ant ennas ar e us eful in r adio astronomy and satellite communication as a primary antenna.

**Acknowledgement:** One of the authors Dr V N Tiwari is grateful to Director, SMIT for his permission to publish this paper.

## REFERENCE:

1. A W Love, "The diagonal horn antenna", Microwave J., vol. V, pp. 127-122, 1962.
2. Stafford Withington and J Antony Murphy, "Analysis of diagonal horns through Gaussian Hermite modes", IEEE Trans. Antennas Propagat., vol.40, pp. 198-206, 1992.
3. S P Singh, T Tiwari, V N Tiwari, and R K Jha, "Radiation patterns of a metal and dielectric wall diagonal horn antennas", Int. J. Elec., vol.76, pp.1195-1203, 1994.
4. V N Tiwari, T Tiwari, S P Si ngh, and R K Jha, "Near field distribution of solid dielectric diagonal horn antennas", Int. J. Elec., vol.82, pp.167-174, 1997.
5. V N Tiwari, T Tiwari, S P Singh, and R K Jha, "Far field patterns of solid diel diagonal horn antennas", Int. J. Elec., vol.82, pp.175-191, 1997.
6. V N Tiwari, T Tiwari, and R K Jha, "Near field distribution of hollow dielectric wall diagonal horn antennas", IETE Technical Review, vol.16, no.1, pp.9-14, 1999.
7. n, ' Microwave antennas' UK: Pergaman Press, 1961, McGraw Hill Book c 1969.

SEARCH
Previous Page
Next Page

# CALIBRATION OF 320 ELEMENT ACTIVE PHASED ARRAY ANTENNA UNIT

*Virendra Kumar* [(1)], Ashutosh Kedar[(1)], K. S. Beenamole[(1)], Sona O. Kundukulam[(1)], Subhankar Mondal[(1)] and U. S. Pandey[(1)]*
Electronics and Radar Development Establishment, Bangalore, India, 560 093,
E. mail: virendrakumar10@gmail.com; kedar_ashutosh@yahoo.co.in

**ABSTRACT:**

This paper discusses the calibration procedure employed for correcting the non-uniformities observed in the radiation pattern performance of the active phased array antennas. These irregularities occur due to mutual coupling effects, the amplitude and phase variations observed in the associated active electronics and near-field s cattering pheno menon. T he measured r adiation patterns of a 3 20-element act ive phas ed ar ray ant enna taken w ith and without co rrection techniques e mployed as r ecorded i n a near f ield test r ange val idate the calibration procedures.

## INTRODUCTION:

Latest mul ti-functional radars for satellite, ground and airborne platforms are demanding active phas ed array antennas in t he present era owing to their multifunctionality and graceful degradation features. Optimal performance of active phased array antennas is only achievable by employing suitable calibration techniques to mitigate the non-uniformities observed in the radiation pattern of the radiating el ements d ue to the various factors such as mutual coupling, the amplitude and phase sensitivities observed in the as sociated act ive e lectronics and near-field scattering phenomenon [1,3].

## ACTIVE ARRAY ANTENNA UNIT (AAAU) CONFIGURATION:

Active Array Architecture chos en is a l arge size 320 el ement Active Aperture Array. The 320 el ements Active Array Antenna Unit has been r ealized through 2 r adiating s egments of 160 ( 16 x 10 ) elements each, arranged in a lengthy rectangular aperture of size $15\lambda_0$ x $7\lambda_0$, ($\lambda_0$ is free space wavelength in s-band frequency for ease of construction and assembly. Each array col umn of 10 el ements i s d ivided into t wo 5 -element s ubarrays and each of t hese subarrays is driven through an independent T/R module. Thus, Active Array is configured with 64 Transmit/Receive (T/R) Modules to meet with the typical Radar System Requirements, especially for airborne surveillance. A rectangular array grid has been cho sen for location of array el ements, s o as to meet with a maximum s can angl e requirement of >±60° in A zimuth array while pr oviding a l imited s canning o f ±2.5° in Elevation. T he spacings ar e $0.5\lambda_0$ and $0.8\lambda_0$ in Azimuth and in Elevation respectively. Fig. 1 shows the arrangement of T/R modules on one antenna segment feeding 160 (16 x 10) elements. The Elevation Amplitude Taper for realizing a br oad bea m w ith sidelobe levels <-25dB i s bu ilt integral w ith the two 5 e l subarrays of each col umn array. The azimuth beam pattern with low sidelobe levels of –40dB is realised through complex excitations programmed in the T/R Modules.



Previous Page
Next Page

The feed network is integrated with a stripline edge coupler at each subarray level to tap the BITE and signal samples. The BITE samples are then distributed using Wilkinson Power Dividers/Combiners.

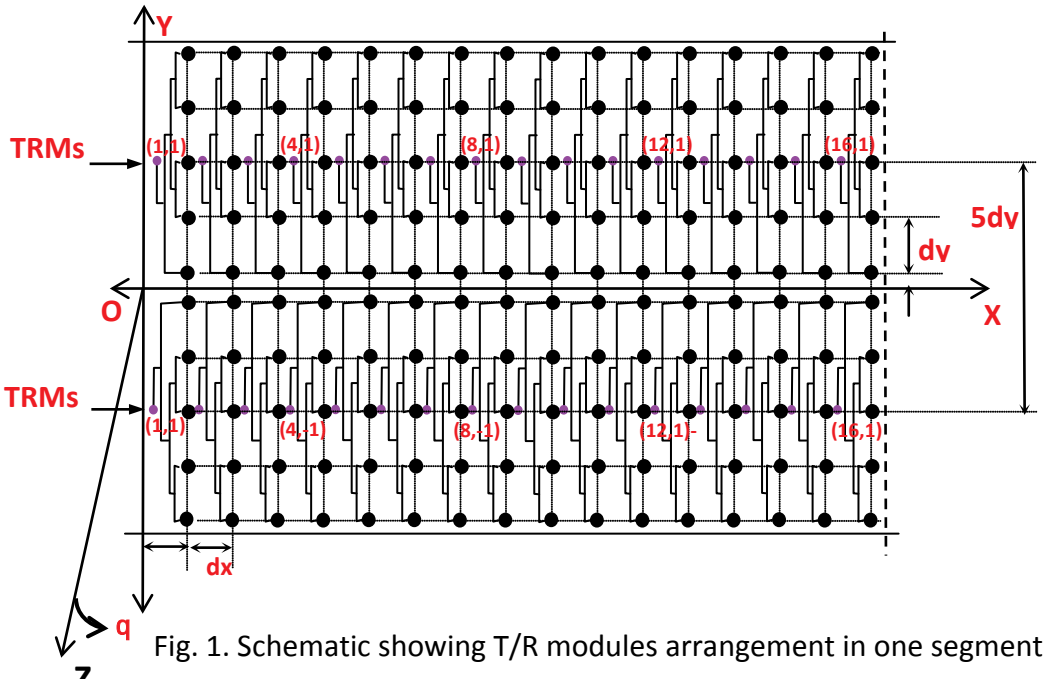


Fig. 1. Schematic showing T/R modules arrangement in one segment

## CALIBRATION:

The Amplitude and phase characteristics of passive circuit viz., pickup element, BITE Feed Network and Cables in the Injection path of each of the T/R module is measured as calibration ratio in the Antenna Chambers (NFTR) during the pattern measurement of the Active array unit. The calibration ratio measurement setup is shown in the Fig. 2. ***Calibration ratio=Probe value-Injection value.*** In NFTR the calibration ratio measurement is carried out at fixed temperature (~22°C) for 41 spot frequencies for both the left and right antenna panels.

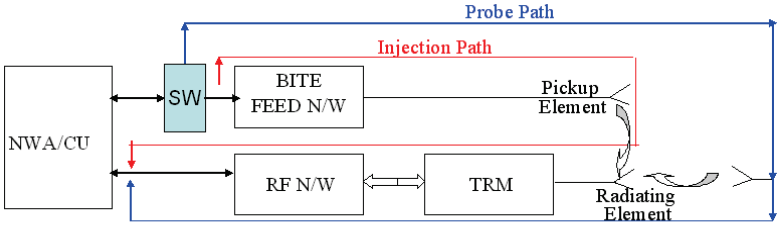


Calibration Ratio= Probe value – Injection Value

Fig. 2: Calibration ratio measurement setup

The basic concept in calibration of T/R Modules is to Switch ON only 1 selected module out of 'N' (64) Modules with rest of N-1 Modules in OFF State. Sample Amplitude and Phase Values of the 'ON' Module through Sum/CAL Receive Channel of Central Unit by injecting the appropriate BITE / CAL RF Signal through BITE / CAL Feed Network.

Previous Page
Next Page
SEARCH

## CALIBRATION PROCEDURE FOR ACTIVE ARRAY:

In order to realize low Side lobe Levels of the order of -30 dB in Receive Mode and good Beam Pointing Accuracies of the order of 0.1°, the Aperture have to be close Phase and Amplitude matched over the operating frequency bandwidth and temperature. The purpose of the calibration is to compensate the phase and amplitude variations of Active T/R Modules over a period of time.

## TRANSMIT PATH CALIBRATION:

During transmit mode calibration as shown in Fig.3, Tx drive signal from the CU is fed as input to all T/R modules through RF feed network. The selected T/R module, whose transmitter is 'ON', amplifies the Tx drive signal and radiates. The other T/R modules are in 'OFF' state (kept in Rx mode with proper isolation). This radiated signal is received by the pickup element of the radiating segment and passes through BITE/CAL feed network. This BITE/CAL signal is switched to the input of Sum/CAL receive channel by the BITE/CAL control network in the CU. The sample of the SUM/CAL receive channel is digitized as base band I and Q data and sent to the RC for computing the amplitude and phase values of the selected T/R module. The Module to be calibrated is set for 0dB attenuation, 0° Phase State during transmit mode at the 1st iteration. The amplitude and phase values are computed by adding this sampled (injection path) value to the respective calibration ratio value. As the transmit amplifiers are saturated, phase calibration only required to co-phase all T/R modules to with in one LSB of 0° phase value.

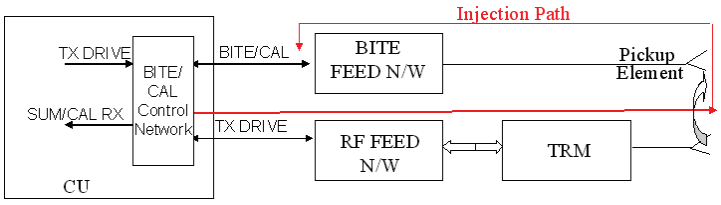


Fig. 3: Transmit Path Calibration

## RECEIVE PATH CALIBRATION:

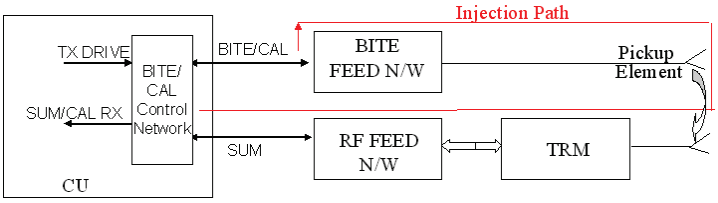


*Fig. 4: Receive Path Calibration*

During receive mode calibration as shown in Fig. 4 below, Tx drive signal from the CU is switched to the BITE/CAL signal in the BITE/CAL control network and fed to the pick up element of the radiating segment through BITE feed network. The selected T/R module, whose receiver is 'ON', amplifies the signal received through its antenna from the pick up element radiation. The other T/R modules are in 'OFF' state (kept in Tx mode with proper isolation). This amplified signal of the T/R module passes through RF feed network. Sum channel of monopusle comparator of the BFU. This Sum signal is fed to the input of

SEARCH
Previous Page
Next Page

Sum/CAL receive channel by the BITE/CAL control network in the CU. The samples of the Sum/CAL receive channel is sent to the RC for computing the amplitude and phase values of the selected T/R module. The Module to be calibrated is set for attenuation state corresponds to distribution value, 0° Phase State at the 1st iteration. The amplitude and phase values required for calibration are computed by adding this sampled (injection path) value to the respective calibration ratio value. As the receive amplifiers are linear, all T/R modules needs to be calibrated to their respective distribution values with in 1 LSB and phase calibration is required to co-phase all T/R modules to with in 1 LSB of 0°phase value.

Signal level received at the input of Sum/CAL receive channel of Central Unit from any one of the T/R module through the pick up element is in the range of -50dBm to -70dBm during in-system calibration for transmit and receive states. A single calibration pulse is sent to each T/R module, to sample its amplitude and phase values both in transmit and receive modes. Pulse modulated CW signal of 20 msec pulse width and 200 msec PRT (10% duty) is used as calibration signal both in transmit and receive modes. Timing unit of the central unit generates a calibration dwell consisting of N (no. of T/R modules) +2 dummy pulses. Two dummy pulses at the start and end of the cal dwell used for sending calibration commands to AAAU.

**RESULTS AND CONCLUSION:**

Transmit bore sight pattern at center frequency is shown in Fig. 5(a). The first side lobe level is –13.51dB and the beam width is 3.38 degree with a beam pointing error of the order of -0.31 degree. Receive bore sight pattern at center frequency is shown in Fig. 5(b). The first side lobe levelis –32.75dB and the beam width is 4.89 degree without any beam pointing error. In this paper, we have presented procedure for transmit path calibration and receive path calibration of 320 Element Active Array Antenna.

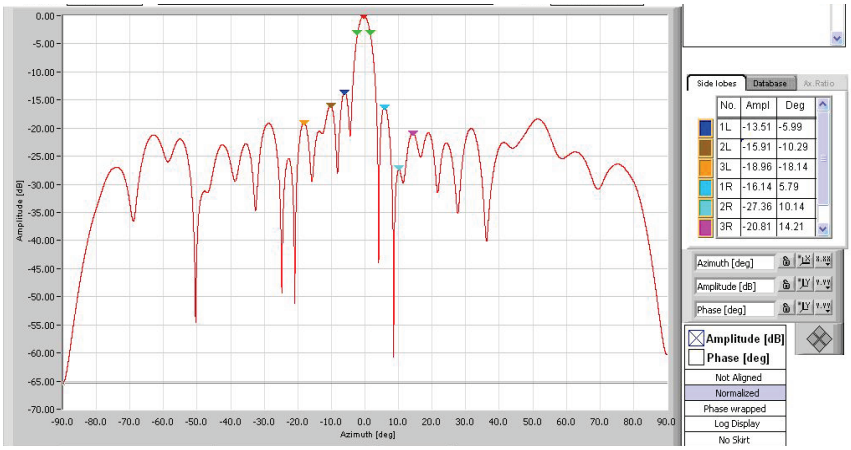


**(a)**

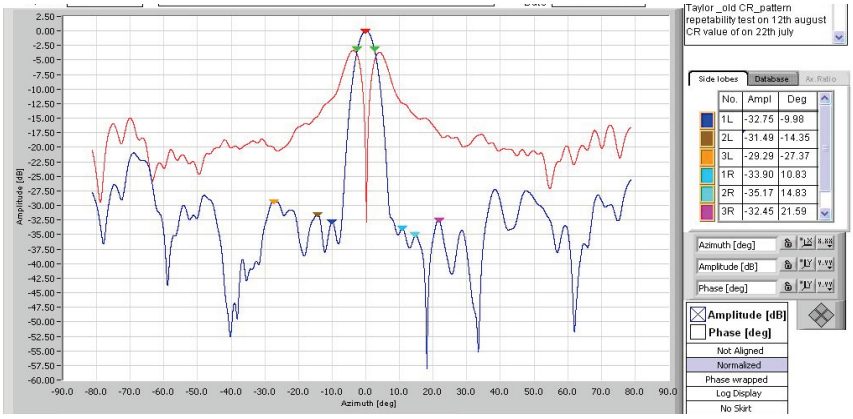


**(b)**

*Fig. 5: Bore sight (a)Transmit and (b)Receive radiation patterns*

**References:**

1. H. Steyskal and J. S. Herd, Mutual coupling compensation in small arrays," *IEEE Trans. on Antennas and Propagation*, vol. AP-38, pp. 1971-1975, December 1990.
2. W. L. Stutzman and G. A. Thiele, *Antenna Theory and Design*. John Wiley & Sons, 2nd ed., 1998.
3. U. S. Pande y, Jeni Anto and Manjushree Tamang, "International Radar Symposium India, 2005, pp.686-690.

# BROADBAND BLADE DIPOLE ANTENNA FOR AIRBORNE PLATFORMS

*S.D. Ahirwar, C.Sairam, T. Khumanthem, Ashwani kumar*
Defence Electronics Research Laboratory
Chandrayangutta Lines, Hyderabad-500005.
Fax No. 91-040-24440525
*E-mail :- sdahirwar@rediffmail.com*

**ABSTRACT :**

In this paper, design and development of electrically small, broadband blade dipole antenna is presented with measured results. The antenna covers a frequency band of 20-500 MHz. Here, a narrow band resonant dipole antenna is transformed into a broadband dipole antenna. This broadband transformation is accomplished with specially designed and developed impedance matching circuit. The impedance matching circuit transforms the frequency dependent antenna impedance to 50Ω system impedance to achieve the VSWR less than 3.5:1 over wide band with minimum insertion loss. Antenna elements are realized in printed form so that it can fit in the aerodynamically designed radome for airborne platform.

## INTRODUCTION:

Dipole and monopole antenna elements are preferred antenna structures for airborne platform as these antennas can be realized in compact form with less weight. Apart from size and weight, air drag on the antenna structures is an important factor for airborne applications. Hence, they are required to be shaped aerodynamically. Printed radiating elements in the form of blade are best suited for such applications. Blade antennas in monopole configuration are used on airborne platforms where the metallic skin of the aircraft provides a ground plane as part of the antenna. Problem related to this ground plane dependency of the antenna can be solved by use of dipole antenna in blade form. Such type of dipole antennas becomes very essential in airborne platforms such as UAV (Unmanned Aerial Vehicle) and aerostat where there is no metallic ground plane available to support monopole antenna electrically. On platform like aerostat the system is generally suspended under the balloon in a wind screen. Also, the antennas must be installed lower than the equipment to have a clear view without any obstruction. A dipole antenna is the most suitable candidate in such type of applications. Conventional broadband biconical antennas cannot be used at such platforms because they require full size (λ/2) for their operation [1]. This requirement increases the size and weight of the antenna which are considered as the critical factors in such platforms. Moreover, it is difficult to shape these structures aerodynamically for reduced air drag. Considering the above facts, a light weight, compact, low profile, electrically small, omni directional antenna has been designed and developed. This printed circuit antenna can be easily encapsulated in aerodynamically shaped blade form for low air drag on airborne platforms.



Previous Page
Next Page

## DESIGN APPROACH AND REALIZATION:

The schematic diagram of the developed antenna is shown in Fig. 1. It consists of two radiating elements printed on one side of an FR4 substrate of thickness 1.6mm.The width of these elements were kept λ/150 only to reduce antenna size and weight, while keeping it sufficient for aerodynamic shape. Antenna dimensions are 0.05λx0.007λx0.00009λ at lowest frequency of operation. Antenna is fed coaxially using a 0.141" diameter coaxial cable. The unbalance current on the outer surface of the coaxial cable is suppressed by use of ferrite beads over it.

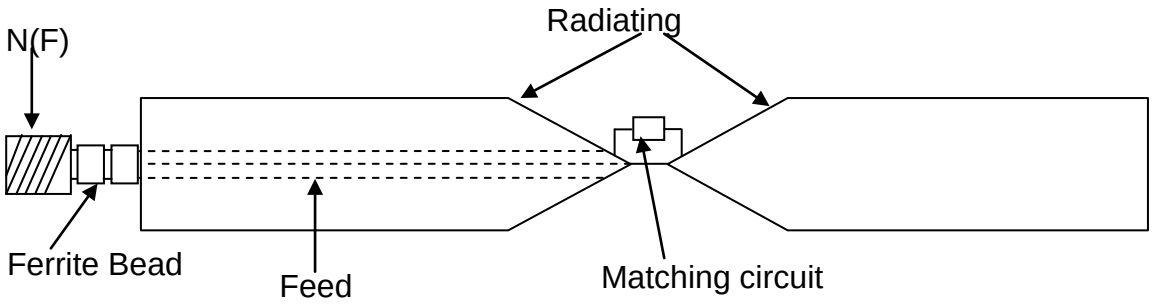


Fig.1. Sketch of the Antenna

In order to achieve the pattern bandwidth in 25:1 ratio (20-500 MHz) total length of antenna elements is restricted to 1λ at highest frequency of operation [2]. The length of this antenna is only λ/25 at lowest frequency of operation. Fat planar elements are used to get improvement in impedance bandwidth up to a limited extent [3].Hence, a matching circuits has been incorporated with this antenna for covering large frequency bandwidth of 20-500MHz.

For impedance matching circuit, a π- transformation circuit topology has been used [4]. This type of circuit topology is shown in Fig. 2. In this circuit both the components $B_1$ ( L or C ) and $X_2$ ( C or L ) acts as the impedance transforming elements while the third component $B_3$ ( L or C ) is the compensation element that tunes out the excess reactance for the first two elements. If R' and R'' are the first level and second level transformed resistances and X' and X'' are the first level and second level transformed reactances; $Q_1$ and $Q_2$ are the quality factors of corresponding levels then these parameters are related as follows: -

$R' = R / 1+Q_1^2$ .....(1)  $X' = - R'Q_1$ .....(2)

$R'' = R' (1+Q_2^2)$ .....(3)  $X'' = - R'' / Q_2$ .....(4)

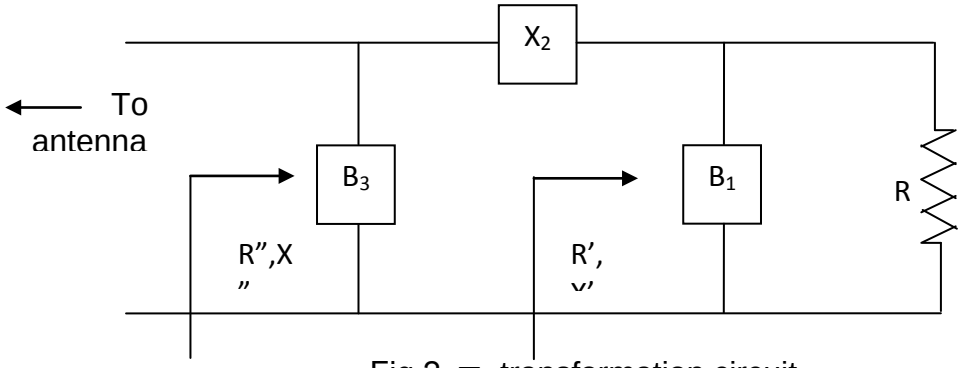


Fig.2. π- transformation circuit

SEARCH
Previous Page
Next Page

In order to maintain Q values constant, custom built toroidal inductors were used to match the antenna over the frequency band of interest.

## MEASURED RESULTS AND DISCUSSIONS:

The antenna was evaluated for its VSWR using M/s Agilent E5071C Network Analyzer. The measured VSWR plots without impedance matching circuit and after integrating the impedance matching circuit are shown in Fig.3 and 4 respectively. It is observed from the measurements that the VSWR of the antenna has improved very significantly, specially at lower end of the frequency band, by use of impedance matching circuit. The maximum VSWR is $\leq$ 3.4:1 throughout the required band. The antenna was evaluated for its radiation characteristics in ground reflection test range. Measured elevation and azimuth plane patterns at 20MHz, 200MHz, 250MHz and 500MHz are shown in Fig.5. Achieved omni deviation is within ± 2.5dB and 3dB elevation beam width is more than 40º. At 20MHz the electrical length of the antenna is very small due to which the elevation pattern at this frequency is circular. Measured gain varies from -35 dBi at 20MHz to + 2 dBi at 500MHz. The antenna weight without radome is less than 250 grams.

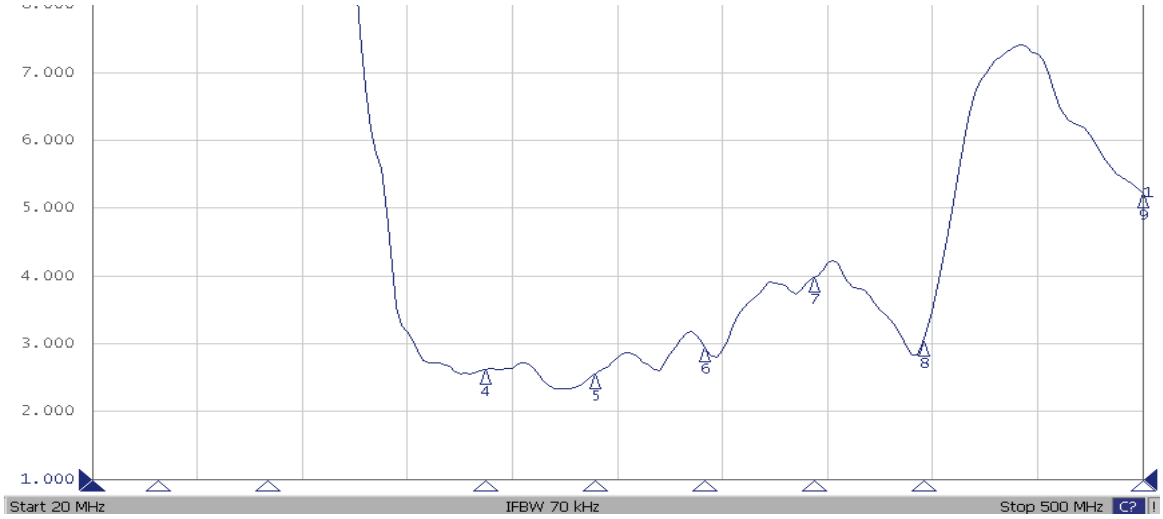


Fig.3. Measured VSWR plot without matching network

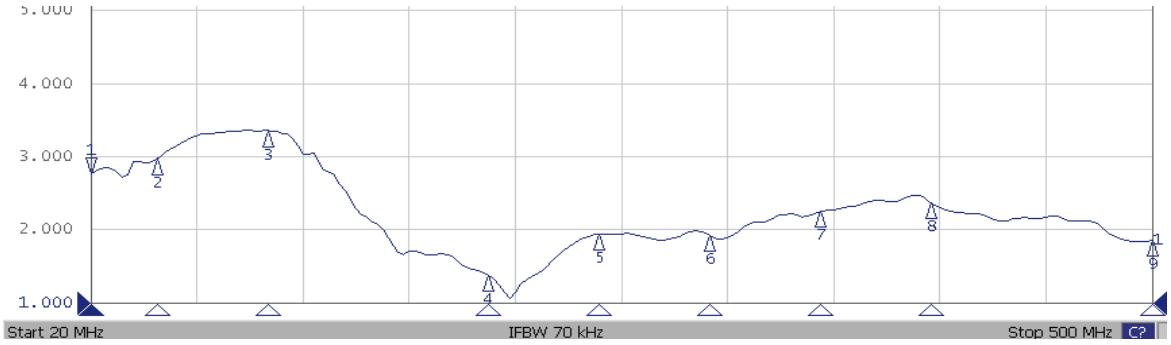


Fig.4. Measured VSWR plot with matching network

SEARCH
Previous Page
Next Page

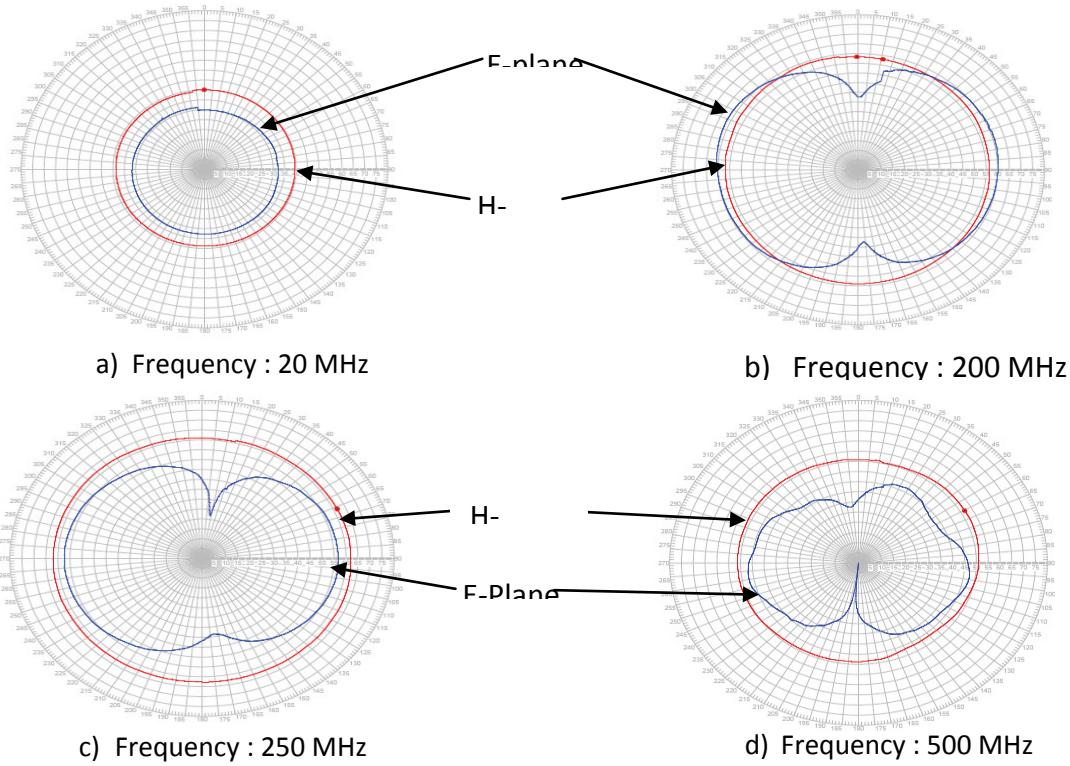


Fig.5. Measured E and H plane radiation

## CONCLUSIONS:

An electrically small, light weight, compact pr inted circuit dipole antenna has been designed and devel oped. T he ant enna s hows w ide bandw idth and can be easily encl osed i n aerodynamically shaped radome. It is linearly polarized and exhibits omni directional coverage in one plane and directional in other plane with sufficient elevation coverage. Antenna finds use i n U AV, Aerostat and ot her s imilar ai rborne pl atforms for di rection f inding, s pectrum monitoring and in communication systems.

## REFERENCES

1. John D . K raus, R onald J . Marhefka, "A ntennas f or al l appl ication" 3rd ed., T ata McGraw-Hill Pub. New Delhi, pp 380-385,2003.
2. Richard C. Johnson, "Antenna Engineering Handbook", 3rd ed., McGraw- Hill, Inc. Pub. New York, pp 4-10 to 4-12, 1995.
3. Y.T. Lo/ S.W. Lee, "Antenna handbook", Volume-I, Van Nostrand Reinhold Pub. New York, pp 3-27 to 3-30,1994.
4. W. Alan Davis, K. Agarwal, "Radio frequency circuit design" 1st ed. John Wiley & Inc. Pub.,pp 33-35, 2001.

SEARCH
Previous Page
Next Page

# DUAL PORT FREQUENCY RECONFIGURABLE RADIATOR FOR ACTIVE ANTENNA APPLICATION

*Madhur Deo Upadhayay, M. P. Abegaonkar and A. Basu*
Center for Applied Research in Electronics, Indian Institute of Technology Delhi, Hauz-Khas, New Delhi-110016, INDIA.
madhur_deo@yahoo.com, mpjosh@yahoo.com, ananjan_b@yahoo.com

**ABSTRACT:**

This paper presents a design for T- shaped coupled patch antenna with two U shape elements for achieving antenna radiate and transmit transmits equal amount of power, keeping return loss higher for oscillator type active antenna operations at two frequencies using switches. Ideal ON condition has T coupled patch with coupled U structures which gives 8.5GHz and ideal OFF condition has T coupled patch with U shape coupling which gives 6.25GHz.

## INTRODUCTION:

An oscillator type active antenna required a two port antenna as a feedback network with amplifier to behave as an oscillator. This two port antenna works as load and as a resonator also for amplifier. For this kind of application two port antennas should be capable in both, to radiate in free space and transmit to second port the same amount of power [1]. T-shaped coupled patch antenna is useful in oscillator type active antenna operation because, it eliminates the use of DC block. This antenna was designed using conventional design equations. The return loss and coupling can be control by changing width of gap and the thickness of the coupling element [2]. The frequency of resonance is function of length. Both resonant frequencies of the patch antenna are decided by the length (L) and width (W) of the antenna. Hence it was considered that by using switching diode, one could vary the dimensions and get required frequencies. Two U shapes structures were used that increase physical dimension of antenna in switch on condition. The design of proposed antenna is described. The transmission line matrix based simulation software Microstrip 7.0 was used. The results of the simulation and experiment are presented and discussed .The radiation pattern was measured in H plane and E plane using UWB Pyramidal horn antenna.

## DUAL - PORT FREQUENCY RECONFIGURABLE ANTENNA DESIGN:

The designed antenna was a T- shaped coupled Patch antenna. The first step in the design was to specify the dimensions of a microstrip patch antenna i.e. *L*, *W*. The patch conductor can be assumed at any shape, but generally simple geometries are used, and this simplifies the analysis. Here, the half-wavelength rectangular patch element is chosen as element (as commonly used in microstrip antennas). Its characteristic parameters are the length *L*, the width *W*, and the thickness *h*, as shown in Figure 1. To meet the initial design requirements ( operating frequencies = 6.25 and 8.5 GHz) various analytical approximate approaches may be used. Here, the calculations were based on the transmission line model. Although not critical, the width *W* of the radiating edge is specified first. The rectangular-patch geometry was chosen. In practice, the length *L* is slightly less than a half wavelength (in the dielectric) [3].

Previous Page
Next Page
SEARCH

Resonance frequency of antenna can be chan ge by varying length of antenna. For this purpose PIN diode can be used to switch between two frequencies. For simulation purpose two states of ideal diodes was considered.

a)When an ideal diode is forward biased it behaves as a conduct ing strip which offers path for RF and DC also. This state refers to ON state.

b)When an ideal diode is reverse biased it behaves as infinite impedance which blocks RF. This state refers to OFF state

The pr oposed antenna i n i deal O FF s tate o f di ode w as realized by non connect ion between T shaped coupl ed an tenna and two U shape structure, as shown in figure (2a), and radiates at $f_1$ frequency. T he pr oposed ant enna i n ideal O N s tate of d iode w as r ealized by conducting s trips of w idth 0.5m m be tween T s haped co upled ant enna and t wo U s hape structure, as shown in figure (2b), and radiates at $f_2$ frequency. The U shape structure, coupling gap and strip width was optimized for required frequencies. The proposed antenna is printed on a GML substrate with dielectric constant of $\varepsilon_r$=3.2 and a thickness of h=0.762mm. The ground plane dimensions are 25.4 X 25.4 $mm^2$. The dimensions of antenna are L=18.79 mm, W=14.5 mm, G= 0.1mm, $W_1$=0.25 mm, $L_1$ =20 mm, $W_2$=18 mm.

**RESULTS AND DISCUSSION:**

Measured and simulated return loss and coupling in OFF state and ON state are shown in figure 3 (a) and 3( b) respectively. T he comparison of measured and s imulated, return loss and coupling shown in Table1. The frequency of measured result shift 5.4%, 9.6% more than simulated result for ON state and OFF state respectively. There is slight shift in frequency but measured r eturn l oss and cou pling ar e much bet ter than s imulated r esults. C omparison of HPBW is shown in Table 2. OFF state has same HPBW in both plane, while ON state has narrow beamwidth in H plane, means antenna become directional in ON state. The radiation pattern in H plane and E plane for OFF state and O N state are shown in figure 4(a) and 4(b) respectively. In ON state antenna is directional, while OFF state antenna is omni directional. For better results and miniaturization of this circuit, it can be fabricated Monolithic Microwave Integrated Circuits (MMIC) and using micromachining process for RF (MEMS).This scheme shows the satisfactory results and good agreement with theoretical result.

Table1. Measured and simulated return loss and coupling

| | Measure d | Simulated | Measured | Simulate d |
|---|---|---|---|---|
| | ON State | | OFF State | |
| Frequency (GHz) | 8.56 | 8.12 | 6.25 | 5.7 |
| Coupling(dB) | 3.03 | 2.38 | 2.85 | 4.48 |
| Return Loss (dB) | 27.24 | 12.33 | 20.9 | 14.48 |

Table2. Half power beamwidth of proposed antenna

| Frequency (GHz) | Beamwidth in H Plane | Beamwidth in E Plane |
|---|---|---|
| 8.5 (ON state) | 60° | 160° |
| 6.25 (OFF state) | 165° | 165° |

SEARCH

Previous Page

Next Page

## CONCLUSION:

The design, simulation and experimentation of microstrip patch with frequency switching capabilities are discussed. This is designed with approximately 160° beamwidth and useful in active antenna design. The switching between two frequencies is obtained successfully in this proposed antenna. This proposed antenna is never reported in the literature as far as my knowledge. People reported T- coupled antenna without reconfigurable features. But this proposed structure include the reconfigurable features and shows good results.

## REFERENCES:

1. K Chang, K A Hummar,G Gopalkrishnan, "Active Radiating Element using FET source integrated with Microstrip patch antenna", Electronics Letter, vol.24, No. 21, pp. 1347-1348,Oct 1988.
2. Dong-Hyuk Choi and Seong-Ook Park, "Active Integrated Antenna using a T- shaped microstrip coupled patch antenna", Microwave and Optical Technology letters, vol.44, No. 5,March 2005
3. Constantine A Balanis, Antenna Theory-Analysis and Design, 2nd edition, John Wiley & Sons, pp.249-328, 1997.

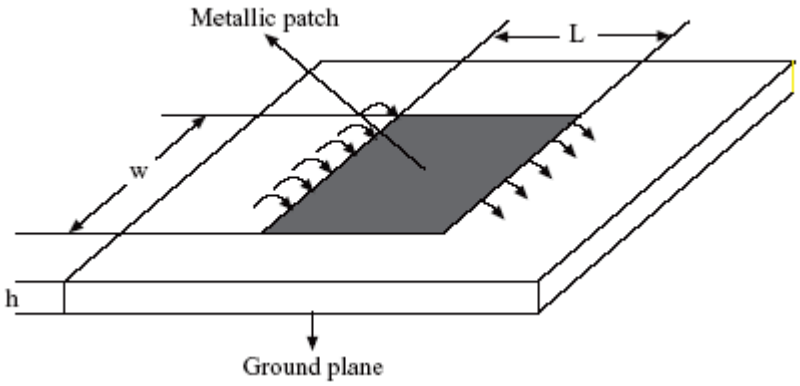


Figure1. Rectangular Patch Antenna

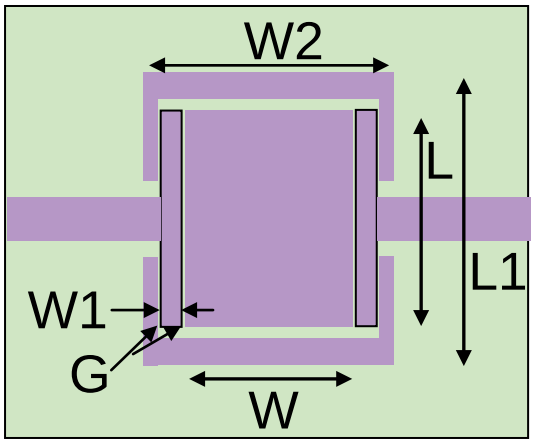


Figure 2(a) Antenna in ideal OFF state

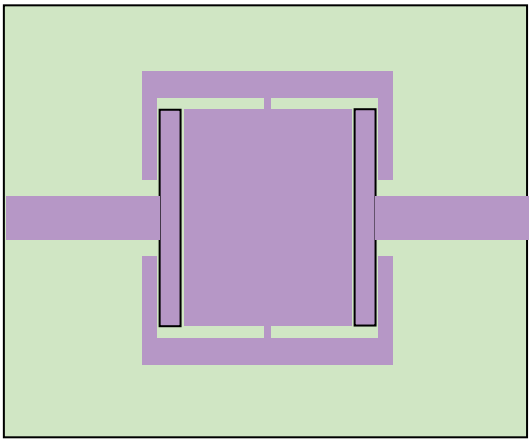

Figure 2(b) Antenna in ideal ON state

SEARCH
Previous Page
Next Page

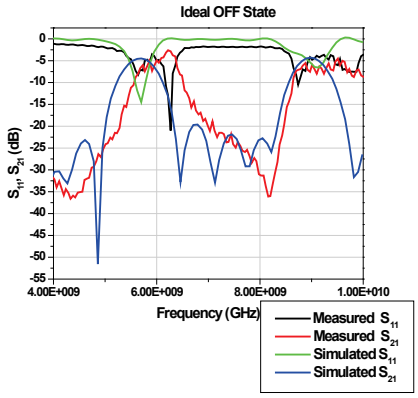


Figure 3(a) Return Loss and Coupling in ideal OFF state

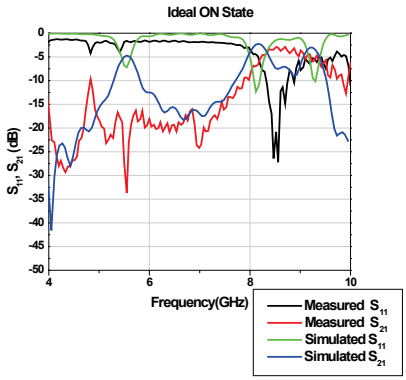


Figure 3(b) Return Loss and Coupling in ideal ON state

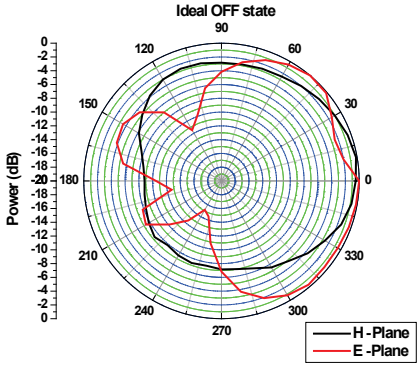


Figure 4(a) Radiation Pattern in ideal OFF state

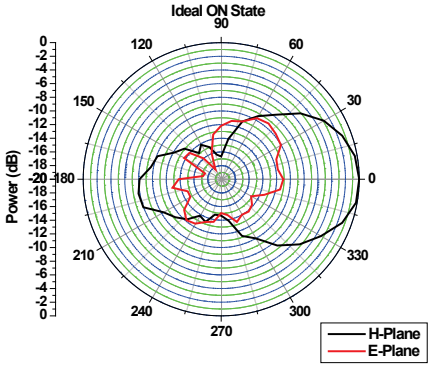


Figure 4(b) Radiation Pattern in ideal ON state

SEARCH
Previous Page
Next Page

# ON DESIGN AND CHARACTERISATION OF A LOOP ANTENNA FOR APPLICATION IN LUNAR RADIO DETECTION

*Kalpana Roy Sinha*[(1)], *Pranayee Datta*[(2)], *Pranjal Borah*[(2)]
[(1)] Assam Engineering Institute, Guwahati, India, Pin-781003, E.mail:kroysinha@yahoo.co.in
[(2)]Deptt of Electronics Science, Gauhati University, Guwahati, India, Pin-781014,
E.mail:pranayee_d@yahoo.com

**ABSTRACT:**

High energy neutrino interactions in the lunar regolith produce VHF radio emission (RE). Along with VHF emission VLF-LF RE are also emitted from the lunar regolith-vacuum interface due to excess charge mechanism. Many experiments are underway for detecting these VHF RE from lunar surface. We have proposed a detecting system to detect VLF-LF lunar pulses. A LF loop antenna is designed for this detecting system for investigating the lunar radio environment.

## INTRODUCTION:

The ultra high energy neutrino interactions in the lunar regolith can initiate electromagnetic shower. The theory of radio emission from showers in dense materials due to negative excess charge mechanism was formulated by Askaryan[1].Radio frequency detection of high energy cascades in solid media can be applied for the investigation of UHE neutrinos and their interactions. The search for the UHE neutrinos requires enormous detector volume, because their flux is extremely low and their interaction cross sections are very small. The moon offers a surface area of $10^7$ $km^2$ and a volume of $10^{14}$ $m^3$. Dagkesamansky and Zheleznykh [2] proposed to detect showers initiated by neutrinos by measuring coherent radio Cherenkov radiation (RCR) emitted from just below the surface of the moon. Recent analysis has led to a number of experimental searches for high energy neutrinos by exploiting the effect at energies up to $10^{20}$ eV or more in lunar regolith, using large ground based radio telescopes. RCR pulses have been studied theoretically and experimentally for many years by different groups all over the world [3] [4].

Recently LORD(Lunar orbital Radio Detector) experimental project has been proposed, where an array of antennas at VHF band is installed on board of a satellite orbiting the moon with orbit altitude of 100-1000km [5]. The ELVIS [6] (Electromagnetic Vector Information Sensor) instrument was also recently proposed for the Indian Chandrayaan-1 mission to the moon and is presently under consideration by the Indian Space Research Organisation (ISRO). The scientific objective of ELVIS is to explore the electromagnetic environment of the moon. Antennas would navigate the lunar surface and detect short radiopulses of nanosecond duration. Along with the VHF RE, VLF-LF RE is also emitted from the lunar-vacuum interface due to excess charge of the cascades [7].



It is quite evident that simultaneous investigation of VLF-LF RE and VHF RE could be more useful for getting confirmed information of the original event characteristics as well as of the lunar environment. We have proposed a method for investigating the VLF-LF pulses to be

Previous Page the lunar orbiting satellite borne detectors [ 8]. In this paper, the design Next Page

characterization of a L F loop antenna is discussed which is an important component of the proposed experimental set up.

**METHOD:**

Block diagram of the proposed experimental set up for receiving lunar radiopulse and then transmitting the same to satellite borne or earth based radio telescope is shown in the figure 1.

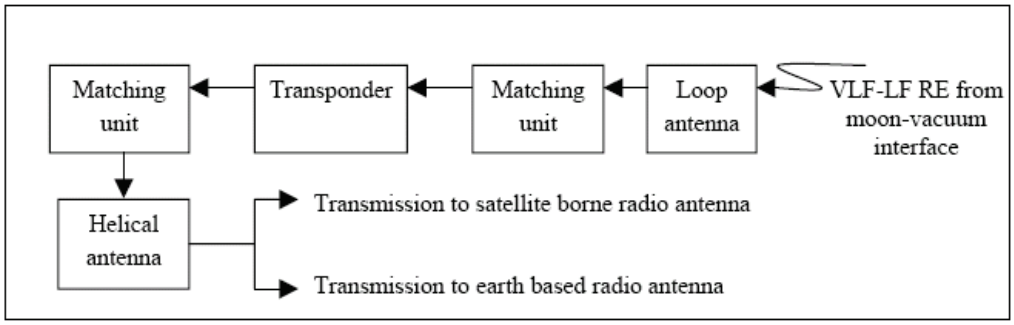


Fig 1. Block diagram of the proposed Experimental set-up.

**DESIGN OF THE LOOP ANTENNA AT 2MHZ:**

The shape of the loop antenna is made hexagonal to get a larger loop area than its equivalent area with the same perimeter in case of a square loop. The circular shape of the loop is not preferred because of practical difficulty in constructing an exact circular shape. The number of turns we took is 17 where the copper wire used is of SWG 14 (i.e. almost 2.14mm) the winding pitch is maintained at 4-5 mm. Larger the diameter of the wire more will be the sensitivity of the loop. The design of the antenna is done using the software rjeloop3, which describes efficiently about the parameters needed for the matching of the loop at its desired frequency. Corresponding to the data given in table 1, a self resonance frequency of 2.6 MHz approximately, which is near to the desired frequency by our antenna i.e. 2MHz, is obtained.

**DESIGNED PARAMETERS:**

Table 1.

| | |
|---|---|
| 1. Desired working frequency of our antenna | 2 MHz |
| 2. Wavelength | λ=150m |
| 3. Shape of the antenna | Regular hexagon each side with 0.5m |
| 4. Wire in SWG | 14 (b=2.14mm) |
| 5. number of turns | N=17 |
| 6. Spacing between windings | c=4mm |
| 7. Wire material | copper |
| 8. Conductivity | $\sigma = 5.7' 10^{7} \Omega^{-1} m^{-1}$ |

The inductance measured with LCR bridge was found to be 506.5mH. For proper resonance we need a capacitance of 12pf. We used a variable capacitor in the range of 5-30 pf to tune the antenna to 2 MHz. Some parameters estimated for the loop antenna are as follows:

=27Ω

Q factor =235.7

From this we can find out the fieldstrength if we have the output voltage from our loop. We designed our transmitting antenna which transmits the source frequency i.e.1.99999 (≈2MHz). The wire diameter is 0.04mm, it consists of total 19 turns where we had the feed point at six and half turns which exactly matched the transmitting frequency of ≈2MHz. It has a standing wave ratio of ≤ 1.5.

## TUNING OF THE RECEIVING ANTENNA:

We kept the receiving antenna at a distance of 5-8m from the transmitting antenna. For resonance a capacitor of the desired value is connected across the loop. Then changing the transmitting frequency from the transmitter the output voltage of our receiving loop is studied from the CRO which is coupled directly. From the variation of received voltage with frequency, graph given in fig 2 is obtained.

The bandwidth is found to be almost 500 KHz, the resonance portion with magnification is shown in fig 2. Thus we found that our antenna is tuned to our desired frequency ≈2MHz. Here we have not used the preamplifier as the distance between the transmitter and the receiver is less. For larger distance we need a preamplifier which we designed with a transistor 2N918.

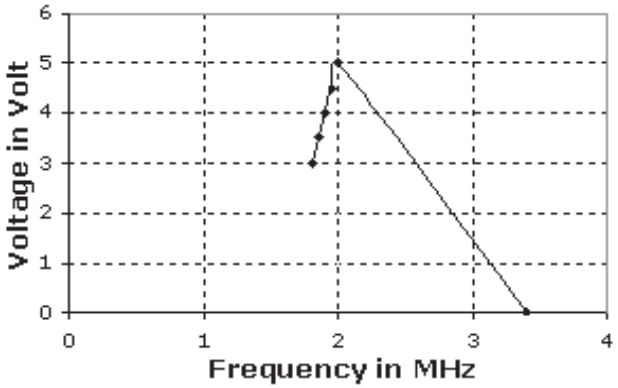


FIG. 2. Tuning of the receiving antenna

## POWER AND FIELD STRENGTH CALIBRATION:

The set up is same as that of the tuning section , only the distance is increased up to 8m. Then by changing the transmitted power from the transmitter through the transmitting antenna we observed the data (voltage peak) from the CRO. This calibration curve helps us in determining an unknown source of power by observing the voltage response at the output.

The fieldstrength received by the antenna is calculated from the loop sensitivity equation. The calibration curve is obtained by plotting the receiving voltage vs the transmitting power as well as the fieldstrength. The calibration curve is as shown in fig 3 and fig 4.

SEARCH

Previous Page

Next Page

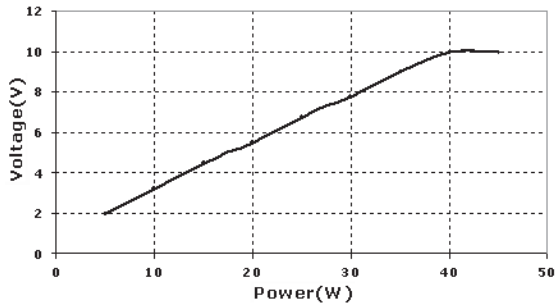


Fig.3. Power Calibration curve

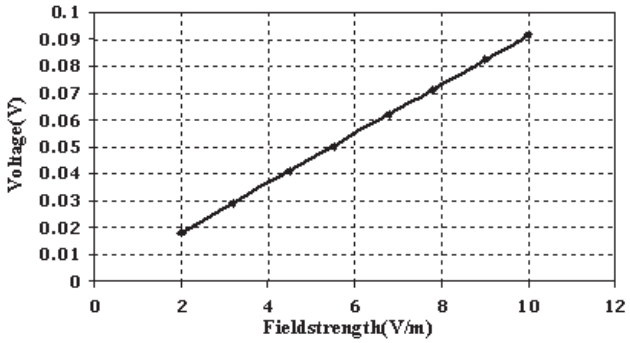


Fig. 4. Field strength Calibration

**ANTENNA ALIGNMENT OBSERVATION:**

We checked our antenna for the directional pattern by keeping the receiving loop antenna at a distance of 30m from the transmitting antenna in a ground plane.

The directional pattern for different angles shows a good variation in the receiving voltage by our loop (fig5). This property of the loop antenna is used for direction finding application. From power received by the VHF satellite borne antenna orbiting the moon, several important characteristics of the neutrino event can be determined. Fieldstrength of VLF-LF RE from moon-vacuum interface due to excess charge can be calculated theoretically [9].

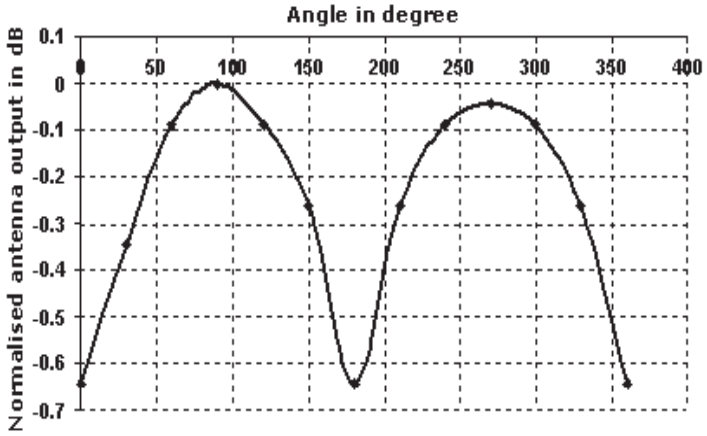


Fig: 5. Directional pattern of the receiving loop antenna

The proposed experimental investigation described above is conceptualization of the Transition Radiation (TR) model developed [7].

SEARCH

Previous Page

Next Page

Voltage induced in the loop antenna will be, $V_{RMS} = \frac{2\pi E_{RMS} AN \cos f}{l}$ (1)

Power absorbed by the loop antenna is $P_{ML} = \frac{V_{RMS}^2}{4R_r}$ (2)

where $R_r$ = radiation resistance of the antenna [8].

Knowing the characteristics of the coaxial cable and different units of the frequency converter and helical antenna, power radiated by the helical antenna can be determined, i.e. power gain of the experimental set up can be estimated. Hence from the power received by the satellite borne VHF antenna, $V_{RMS}$ can be estimated from eqn (2) and then $E_{RMS}$ from eqn (1). Knowing $E_{RMS}$, several characteristics of the original particle events in the lunar regolith can be estimated.

**DISCUSSION AND CONCLUSION:**

Observed characteristics of the designed loop matches with its desired working condition. After designing and fabricating other units of the proposed set up, its overall efficiency can be tested. Results obtained with such set up erected on the lunar surface can be compared with those from LORD experiment (HF detection). Such comparison would give valuable information on lunar electromagnetic environment.

**REFERENCE:**


1. G. A. Askaryan, Sov.Phys. JETP 14, p 441 (!962).
2. R.D. Dagkesamansky and I.M. Zheleznykh, JETP letters 50, p 233 (1989).
3. I. Zheleznykh et al., Proc13th Int Conf on Neutrino Physics and Astrophysics. p 528, (1988).
4. P.W. Gorham et al., Proc. 26th Int Cosmic Ray Conf. Vol 2 p 479, (1999).
5. http://theor.jinr.ru/riastro05/Reports/18oct/07_Tsarev_LORD.pdf
6. arXiv: astro-ph/0509864
7. K.R.Sinha et al., *Proc.29 ICRC*, Pune, vol HE 9, p 131, (2005).
8. K.R.Sinha et al., *Proc.* GNSS-2007,Hyderabad, p 98-100, (2007).
9. K.R.Sinha et al., *Proc.* APSYM 2004, Kochi, p 81-85, (2004).

# A COMPACT CPW FED ANTENNA FOR ULTRA WIDE BAND APPLICATIONS

*Shameena.V.A* and P. Mohanan*
Centre for Research in Electromagnetics and Antennas, Department of Electronics, CUSAT
Email: shameenashine@gmail.com

**ABSTRACT:**

A new compact coplanar waveguide fed slot antenna is proposed.The antenna has a small size of 26x26 mm$^2$ and provides ultra wide band width. The antenna consists of a triangular aperture on a printed circuit board ground plane and a T-shaped exciting stub. The proposed planar coplanar waveguide fed antenna is easy to be integrated with radio-frequency/microwave circuitry.

## INTRODUCTION:

Recent years have witnessed an increased interest in ultra wide band antenna since the adoption of UWB technology by FCC in 2002. One of the most important issues in a UWB system is to develop compact and wide band antennas. In contrast to the patch antennas, antennas with slot configurations exhibit improved characteristics including wide bandwidth, less conductor loss and better isolation etc. The coplanar feeding mechanism can easily accommodate passive and active components without any via hole. In this paper,a novel UWB slot antenna fed by a grounded CPW is proposed. A 2:1 VSWR band width from 3.4 to 10GHz is observed. Antenna gain and radiation patterns are also presented.

## DESCRIPTION OF ANTENNA GEOMETRY:

Fig 1 shows the geometry and configuration of the proposed antenna. The antenna consists of a triangular slot etched on a single sided substrate and a CPW fed T shaped antenna for excitation.. Design of the triangular aperture is determined by minimizing the aperture area while satisfying the input impedance matched for the UWB band. The excitation of the antenna is formed by a simple T-shaped structure as shown in Fig. 1. The width of the CPW line is fixed at 3 mm and the width of the gap G between the line and symmetric ground plane is fixed at 0.5 mm to achieve 50Ω characteristic impedance.

## EXPERIMENTAL RESULTS:

The commercial simulation tool Ansoft HFSS is employed to perform the design and optimization process. The optimized antenna is implemented on a low cost FR4 substrate with dielectric constant 4.4 and thickness 1.6mm. The measurement of return loss is carried out with an HP8510C network analyzer. Fig 2 shows the measured return loss of the antenna along with simulation. A good agreement between simulation and measurement is achieved. The first resonance is produced due to ground and second resonance is due to the T structure.

SEARCH

Previous Page

Next Page

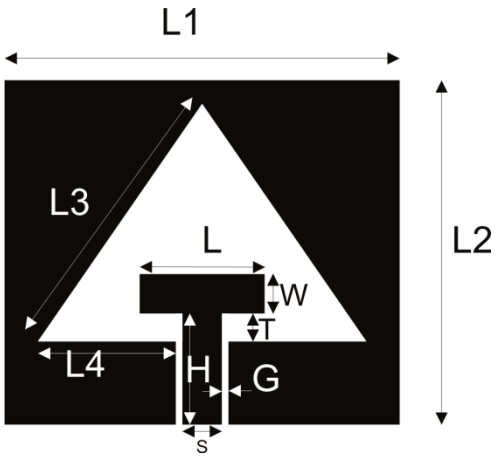


Figure 1: geometry of the proposed antenna
L1=26,L2=26,L3=22,L4=10.5,L=12,W=3.5,H=9,T=2,G=0.5,S=3(unit:mm)

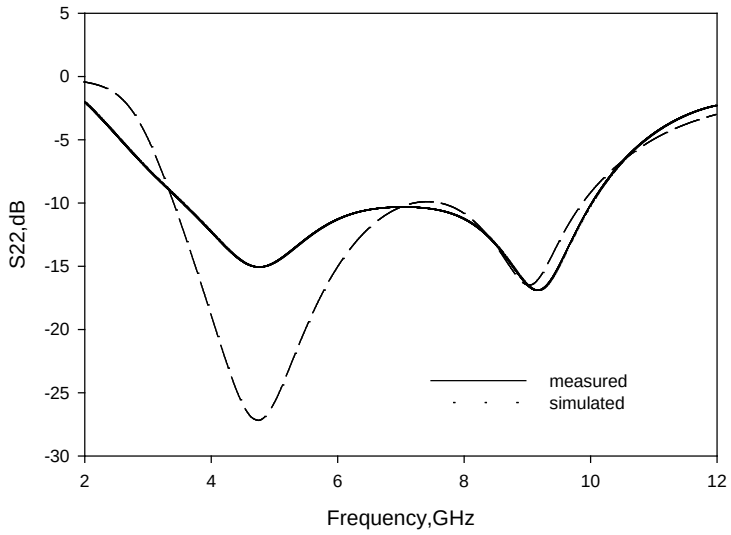


Figure (2) Measured and simulated Return loss of the proposed antenna

Fig 3 shows the measured radiation patterns of the antenna at 4.5 and 9 GHz respectively. The patterns are nearly omnidirectional as required for UWB applications. Gain of the antenna for the entire band is also measured and plotted in Fig 4. As shown in the figure, gain is almost constant in the entire frequency band.

**CONCLUSION:**

In this paper a compact UWB slot antenna is proposed. The antenna structure is simple and the aperture size compact.Broad impedance band width, stable radiation patterns and constant gain are also observed.

SEARCH

Previous Page

Next Page


(a) (b)

Figure (3) Measured Radiation patterns of the antenna at (a)4.5GHz and (b) 9GHz

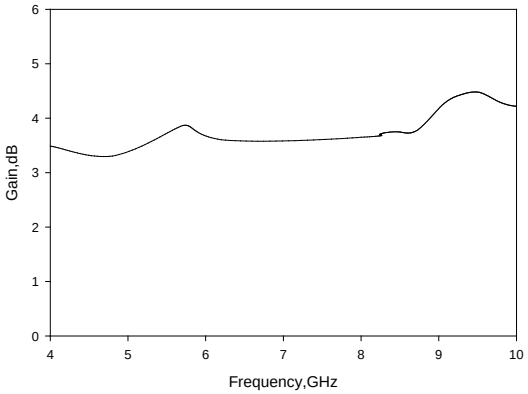


Figure (4) Measured gain of the antenna

**ACKNOWLEDGEMENT:**

The authors would like to acknowledge UGC,DST and DRDO for providing financial assistance.

**REFERENCES:**

1. Yi-Cheng Lin and Kuan-Jung Hung, "Compact Ultrawideband Rectangular Aperture Antenna and band notched designs", *IEEE Trans Antennas and Propag*, Vol. 54,No.11, , pp. 3075-3081, November 2006.
2. S.Sorbello,m.Pavone,and l .Russello,"Numerical and experimental study of a rectangular slot antenna for uwb communications",*Microwave Optical technol.Lett.*,vol.46,no.4,pp.315-319,Aug.2005.

SEARCH

Previous Page Next Page

# INFLUENCE OF PERMITTIVITY CONTRAST ON THE PROPERTIES OF MICROSTRIP PATCH ANTENNA MADE OF A DUAL SUBSTRATE

*Thomas Sebastian[1], Sherin Thomas[1], G. Subodh[1], V. Deepu[2], P. Mohanan [2], and M. T. Sebastian [1]*

[1]Materials and Minerlas Division
National Institute for Interdisciplinary science and Technology
Trivandrum-695019
[2]Dept. Electronics
Cochin University of Science and technology
Cochin

## ABSTRACT

Dual substrates based on $Sr_2Ce_2Ti_5O_{16}$ and $Sm_2Si_2O_7$ ceramic loaded polystyrene were prepared using melt mixing and hot moulding technique. A very thin layer Cu was electroplated on both surface of the composites. Then micro strip patch antennas were made on the substrates and their properties were investigated.

## 1. INTRODUCTION

Ceramic dielectric resonator antennas are becoming popular in microwave and millimetre-wave applications because of the advantages such as no conductor loss, frequency stability at various temperatures associated with their low temperature coefficient and radiation patterns that vary with the excited mode[1]. They are simple to integrate into existing fabrication technology and have flexible design process with numerous design parameters such as shape, size, aspect ratios and permittivity. The substrates carrying the antenna should possess certain important characteristics such as (i) low dielectric constant $\epsilon_r < 10$ (to increase the signal speed), (ii) low dielectric loss or high quality factor (to increase selectivity), (iii) high thermal conductivity (to dissipate the heat generated), (iv) low or matching coefficient of thermal expansion to that of the materials attached to it, (v) low temperature coefficient of resonant frequency $\tau_f$[1,2,3,4] Ceramic-polymer composites consisting of ceramic particles filled in a polymer matrix are now widely used in the electronics industry as substrates for high frequency uses, since they combine the electrical properties of ceramics and the mechanical flexibility, chemical stability and processing possibility of polymers[1,2].

The radiation from microstrip antennas occurs from the fringing fields between the edge of the antenna conductor and the ground plane. The factors affecting the overall Q factor of the microstrip antenna are resonator dimensions, operating frequency, relative permittivity and the thickness of the substrate. The theoretical and experimental results show that at high frequencies the radiation loss is much larger than the conductor and dielectric losses. Also an open-circuit microstrip radiate more power when fabricated on thick low dielectric constant substrates. In the present study we focus on the applicability of a dual substrate for antenna applications. This dual substrate consists of two dissimilar materials with different relative permittivities. The relative permittivities are chosen such that the ratio is nearly 2, which provides maximum radiation.

## 2. EXPERIMENTAL

The two dissimilar materials, $Sr_2Ce_2Ti_5O_{15}$ (SCT) and $Sm_2Si_2O_7$ ceramics used [illegible] investigation were prepared by conventional solid state ceramic route. [illegible]

purity $SrCO_3$, $TiO_2$ and $SiO_2$ (99.9+%, Aldrich Chemical Company, Inc, Milwaukee, WI, USA) and $CeO_2$ and $Sm_2O_3$ (99.99%, Indian Rare Earth Ltd, Udyogamandal, India) were used as the starting materials. Stoichiometric amount of powder mixtures were ball-milled in distilled water medium using yttria-stabilized zirconia balls in a plastic container for 24h. The slurry was dried, ground, and calcined at 1250 °C for 4h. The calcined powders were fine grained and sieved using 45-µm sieves. Polystyrene (PS) (Nikunj Industries, Mumbai, India) was used to make the composites The polystyrene - $Sm_2Si_2O_7$ and polyethylene - SCT were mixed separately in a kneading machine. The kneading machine consists of variable speed mixer having two counter rotating sigma blades and heating facility up to 350 °C. Different volume fractions, 0 to 0.5 of SCT and $Sm_2Si_2O_7$ ceramics were added to the melted polystyrene and blended at 150 °C for 30 minutes to obtain the desired permittivity ratio of 2. Thus obtained composite were hot pressed under a pressure of 50 MPa and 150 °C for 15 min. After the hot pressing, the composites with desired shapes were polished. The microwave dielectric properties of the sample were measured by the cavity perturbation technique using HP 8510 C Network Analyzer (Agilent Technologies).

It was observed that PS/$Sm_2Si_2O_7$ composites obtained a relative permittivity value of 4.2 for filler content of 0.2 vf whereas PS/SCT composites exhibited a value of 7.5 for a filler content of 0.3 vf. The dual substrate for antenna fabrication was implemented with these particular compositions. The dual substrate was made by hot pressing these composites in a square die of dimension 50x50 mm with half the area filled with PS/SCT composites and the other half filled with PS/$Sm_2Si_2O_7$ composites. A schematic representation of the dual substrate is shown in Fig. 1.The dual substrate thus obtained is properly cladded with copper. The microstrip antenna design obtained from simulation is transferred onto the substrate by the process of etching.

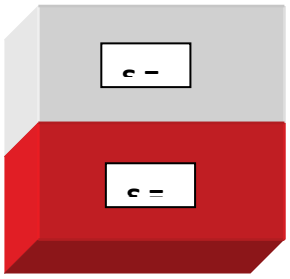

Fig. 1 Schematic representation of the dual substrate.

## 3. RESULTS AND DISCUSSION

Ceramic loaded polystyrene composite were prepared in desired shape by melt mixing and hot moulding technique. Both sides of the (5x5 $cm^2$) substrates were electroplated with Cu. Then patch antennas of desired dimensions simulated using HFSS were fabricated on these substrates. The filling ratio of the dual substrates is varied step by step process and the change in resonant frequency, gain and return loss is noted. Table 1 shows the variation in resonant frequency, power and return loss with respect to width of the SCT loaded substrates. It can be noted from the table that as the width of SCT decreases the resonant frequency increases.

In order to confirm the variation in resonant frequency with respect to the width of the SCT loaded polystyrene the variation in resonant frequencies of another FR4 epoxy loaded with split ring resonators is investigated. Here, FR-4 substrate is taken as one material and air as the other, which is resonated using a split ring resonator (SRR). The position of the SRR on the patch determines the effective filling ratio of FR-4 to air. An arbitrary position on the coordinates is taken as the reference point (0,0). The position of SRR is changed to different

SEARCH
Previous Page
Next Page

points on the rectangular coordinate and the change in resonant frequency, gain and return loss is noted as shown in table 2. The resonant frequency varies with the changing positions of the SRR on the patch, i.e. the effective filling ratio is changed with the position. Hence the phenomenon observed with the Strontium Cerium Titanate and Samarium Silicate ceramic filled polystyrene dual substrate is empirically verified

Table 1 Variation in resonant frequency, power and return loss with respect to width of the SCT loaded substrates.

| Width of SCT (mm) | Resonant frequency (GHz) | Power (dBm) | Return loss (dBm) |
|---|---|---|---|
| 10 | 2.25 | -17 | -25 |
| 7.5 | 2.325 | -17 | -17 |
| 5 | 2.375 | -18 | -12 |
| 2 | 2.45 | -18 | -10 |
| 0 | 2.55 | -19 | -7 |

.

Table 2. variation of resonant frequency of SRR loaded FR 4 Substrate.

| Position of split ring resonator over the substrate (x,y) | Resonant Frequency (GHz) | Power (dBm) | Return loss (dBm) |
|---|---|---|---|
| (0,0) | 2.42 | -17 | -11.5 |
| (0,1) | 2.50 | -17 | -10.0 |
| (-3,1) | 2.50 | -17 | -11.0 |
| (-3,0) (optimum) | 2.45 | -17 | -11.0 |

The radiation pattern obtained for dual substrates is shown in Fig. 1. The principle E and H patterns of dual substrate antenna was taken at 2.25 GHz.

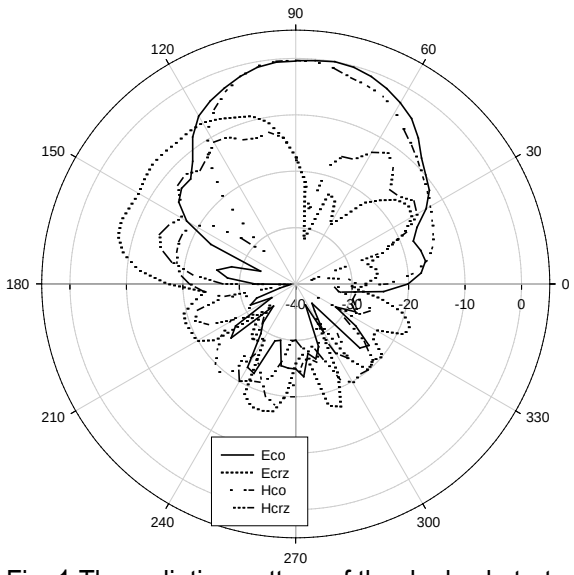


Fig. 1 The radiation pattern of the dual substrate.

SEARCH
Previous Page
Next Page

## 4. CONCLUSIONS

A novel dual substrate made of ceramic loaded polystyrene is configured as a microstrip patch antenna. The resonant frequency of the patch antenna can be varied by changing the width ratio of the constituent materials in the dual substrate. This was verified by using a reference substrate loaded with split ring resonator and analyzing the resonant frequency changes with the position of the split ring resonator. An inverse relation exists between the resonant frequency and the width ratio. Using the dual substrate configuration it's been showed that an arbitrarily low resonant frequency is achieved for a fixed dimension. Enhanced performance characteristics can be achieved by configuring it as array of patches.

## REFERENCE


1. M. W. Meallister, S. A. Long and G. L. Lonway, *Electron. Lett.* 19 (1983) 218-219.
2. R. R. Tummala, *J. Am. Ceram. Soc.* 74 [5] 895-08 (1991).
3. D. D. L. Chung, Materials for Electronic Packaging, Butterworth-Heinemann, Boston, (1995) pp. 19-27.
4. Y. Guo, H. Oshato K. Kakimoto, *J. Eur. Ceram. Soc.* 26 1827-1830 (2006).
5. M. Kono, H. Takagi, T. Tatekawa, H. Tamura, *J. Eur. Ceram. Soc.* 26 1909-1912 (2006).
6. S. K oulouridis, "Polymer-Ceramic Composites for Microwave Applications: Fabrication and Performance Assessment," *IEEE Trans. Micro. Theory Techniques.*, **54**, 4202-4208 (2006).
7. S. Che, I. Kanada and N. Sakamoto, "Dielectric properties of Spherical Dielectric Oxide Powder and its Ceramic-Polymer Composite," *Jpn. J. Appl. Phys.* **44**, 7107-7110 (2005).

## RESEARCH SESSION III

## MICROWAVE DEVICES, MATERIALS etc.

SEARCH

Previous Page

Next Page

SEARCH

Previous Page

Next Page

## RESEARCH SESSION III

## MICROWAVE DEVICES, MATERIALS etc.

***Chair: Dr. C.S. Sridhar, Bangalore Institute of Technology, Bangalore***



SEARCH

Previous Page Next Page

# A NEW DGS BASED MICROSTRIP RESONATOR WITH QUASI-ELLIPTIC BANDPASS FILTERING CHARACTERISTICS

*Tamosi Moyra[1], Susanta Kumar Parui[2] and Santanu Das[2]*
[1]College of Engineering and Management, Kolaghat, and
[2]Department of Electronics and Telecommunication Engineering, Bengal Engineering and Science University, Shibpur, Howrah – 711 103, INDIA
E-mail: arkapv@yahoo.com & santanumdas@yahoo.com

**ABSTRACT:**

In the proposed resonator, a new asymmetric defected ground structure (DGS) is etched in the ground plane under a pair of end-coupled microstrip line. The DGS consists of two square headed slots connected transversely with a rectangular slot. The DGS-microstrip resonator provides a band-accept filtering characteristics. The presented equivalent circuit shows both resonant and anti-resonant properties. The circuit parameters are extracted. A better selectivity in lower transition band in comparison to upper transition band is observed in the frequency response. The prototype is fabricated on Arlon substrate and measured with a vector network analyzer. The simulation and measurement results show good agreement.

## INTRODUCTION:

A defected structure etched in the metallic ground plane of a microstrip line effectively disturbs the shield current distribution in the ground plane and thus, introduces high line inductance and capacitance of the microstrip line. Dumb-bell shaped DGS element explored by D. Ahn offers the lowpass characteristic with one finite transmission zero [1-2]. Using the element, lowpass filter and bandpass filter are implemented in recent time [3-4]. A filter with high selectivity would be preferable owing to the demand for currently expanding communication systems within finite spectrum resources. It is well known that a filter with attenuation zero and transmission zero at finite frequencies shows high selectivity. Few novel DGSs with quasi-elliptical response was proposed [5-7].

The proposed asymmetric DGS pattern consists of two square headed thin slots connected with a rectangular slot under microstrip line transversely. The equivalent circuit is modeled as a L C resonant circuit in series with the characteristic impedance of the transmission line along with parallel capacitances. Higher value of parallel capacitances provide sharper transition band. A DGS based resonator has been realized by a coupling gap between microstrip lines over a proposed DGS unit. The coupled gap between microstrip lines over proposed DGS unit creates both series R C resonant circuit and parallel R C resonant circuit in parallel to the capacitance connected in series connected with a transmission line of characteristic impedance $Z_0$. The DGS resonator shows a band-accept filtering characteristics.

## FREQUENCY CHARACTERISTICS:

Along a microstrip line, a DGS can be achieved by etching an area in the metallic ground plane. In the proposed DGS pattern, two square headed (of side length e) transverse slots ( of length c and width g) connect a rectangular slot ( of length a and breath b)



Previous Page Next Page

transversely. The DGS microstrip resonator is constructed by the proposed DGS unit under a pair of end-coupled microstrip line as shown in Fig. 1.

In order to investigate the frequency characteristics of the DGS resonator circuit, it is simulated by the MoM based IE3D EM-simulator. The different dimensions of the DGS unit are considered as b=10 mm, a=e=4 mm, d= c= 2 mm, and g=0.4 mm. The coupled gap (s) between microstrip resonators is taken as 0.4 mm. The substrate with a dielectric constant of 3.2, loss tangent 0.0025 and thickness 0.79 mm is considered. The width (w) of the conductor strip of the coupled line is taken as 1.92 mm, corresponding to 50Ω. The length of each resonator line is taken as 8 mm.

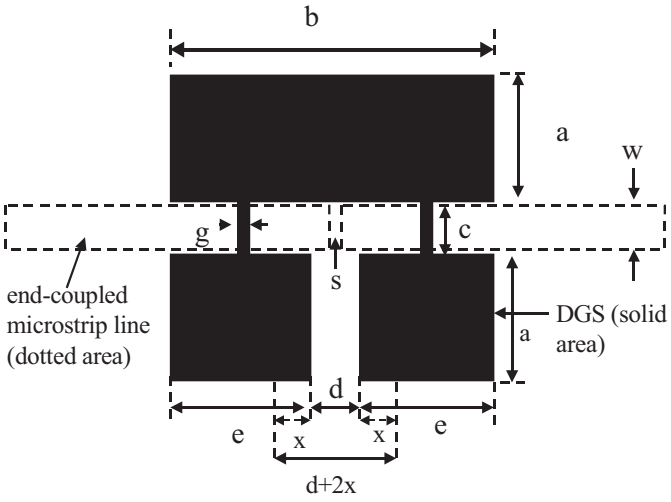


Fig. 1. Schematic diagram of the proposed DGS resonator ( dotted area are microstrip lines on signal plane and solid area are slots in the ground plane)

The simulated magnitude of the S-parameters of the DGS resonator is shown in Fig. 2(a). The attenuation minima's are obtained at 3.3 GHz and 4.5 GHz. The center frequency, bandwidth and insertion loss are observed as 3.8 GHz, 55% and 0.8 dB respectively. The rejection of the lower stop band is better than 40 dB, whereas it is only 12 dB for the upper stop band.

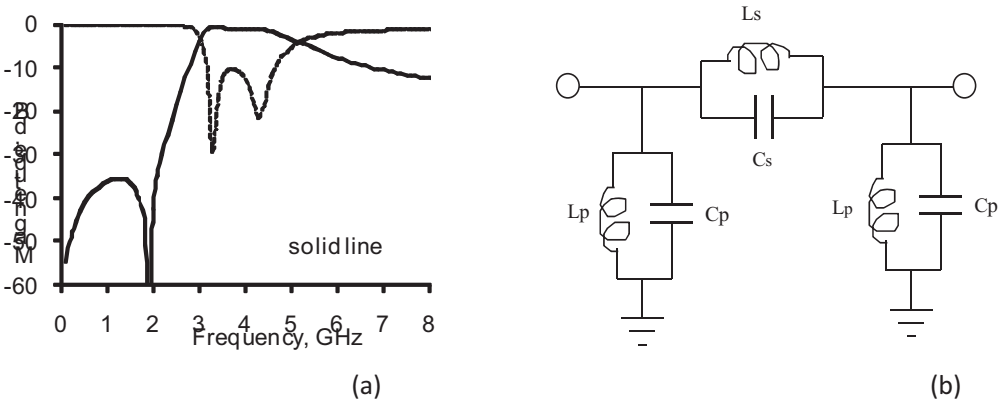


**Fig. 2. DGS resonator: (a) IE3D simulated S-parameters and (b) proposed equivalent circuit**

SEARCH
Previous Page
Next Page

## MODELING AND PARAMETER EXTRACTION:

The equivalent circuit of a DGS under uniform microstrip line is generally modeled as a LC resonant circuit in series with the characteristic impedance of the transmission line alongwith parallel capacitances. The equivalent circuit of the investigated DGS microstrip resonator is represented by series resonant and parallel resonant circuit connected with a transmission line of characteristic impedance $Z_0$ as shown in Fig. 2(b). The series resonant circuit composed of $L_s$ and $C_s$ gives attenuation pole at 2 GHz and parallel resonant circuit composed of $L_p$ and $C_p$ give zero attenuation frequency at 4 GHz. The attenuation zero frequency is located higher than pole frequency. The extracted LC values are given by $L_s$=4.8nH, $C_s$=1.5pF, $C_p$=1.17pF, and $L_p$=0.9nH for above dimensions.

## FABRICATION OF PROTOTYPE:

The DGS resonator circuit is fabricated by ARLON make PTFE substrate and measurement has been carried out by Agilent make vector network analyzer of model N5230A. The measured center frequency, bandwidth and insertion loss are obtained as 4.5 GHz, 45% and 1.2 dB respectively. The measured S-parameter results are compared with simulated and circuit model values in Fig. 3 and good agreement are observed among them.

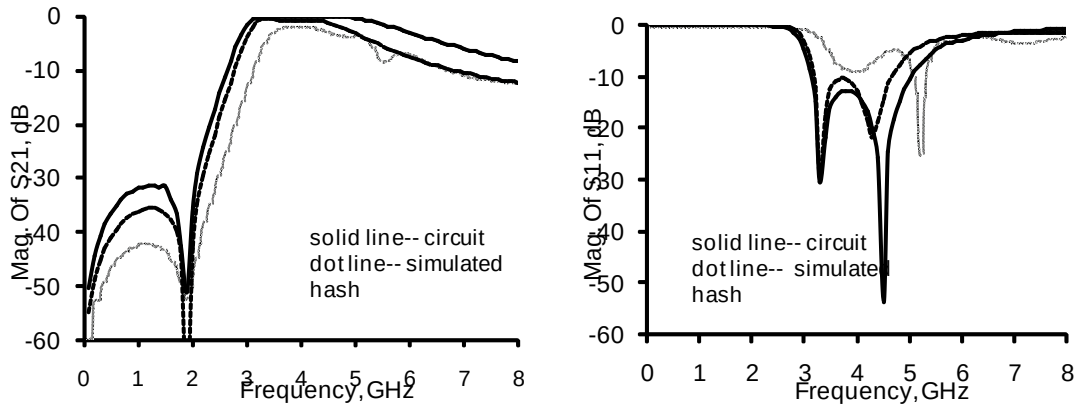


Fig. 3. S-parameters of the DGS resonator :circuit ,simulated, and measured: (a) S21 (b) S11

## INFLUENCE OF PASSBAND CENTER FREQUENCY ON OVERALL DIMENSION OF DGS UNIT:

Varying the over all dimension of DGS unit, keeping relative ratios between different dimensions (except g) fixed, we can change the over all pass band performance of the filter. The S-parameters are plotted for different distance b= 5 mm, 7.5 mm, 10 mm, and 12.5 mm as illustrated in Fig. 4. The center frequency of the passband is reduced for increased dimension of the DGS unit.

SEARCH

Previous Page

Next Page

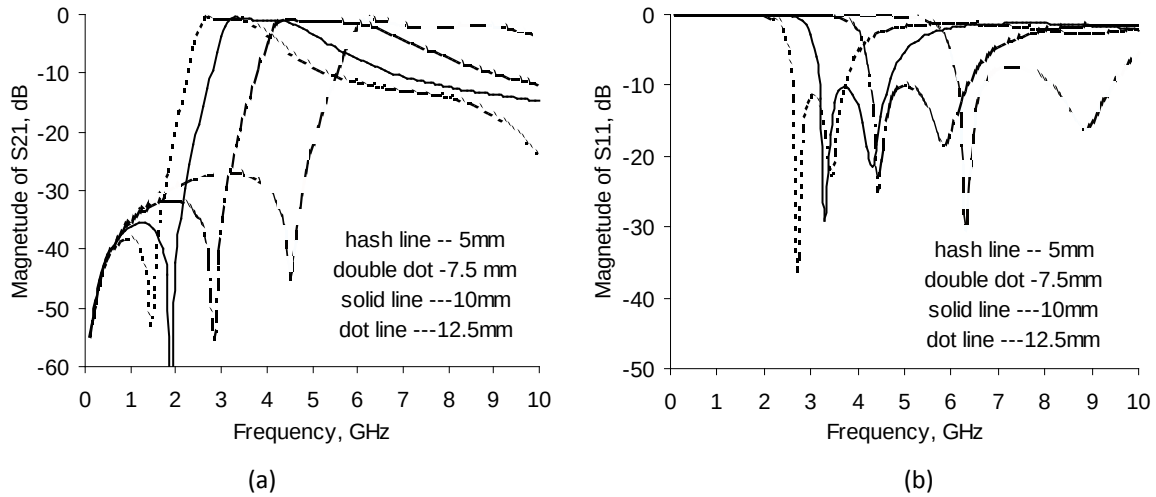


(a) (b)

Fig. 4. S-parameters of the DGS resonator for different value of b (a) S21 (b) S11

## INFLUENCE OF PASSBAND INSERTION-LOSS ON DISTANCE BETWEEN THE SLOT-HEADS:

Varying the dimension of slot heads, we can change the passband of the filter. The width (e) of the square slot is reduced by x, keeping the total length (b) of the DGS fixed; it became rectangular in shape and distance between the slot increases to d+2x. We have plotted the S-parameters for different distance between slots as illustrated in Fig. 5.

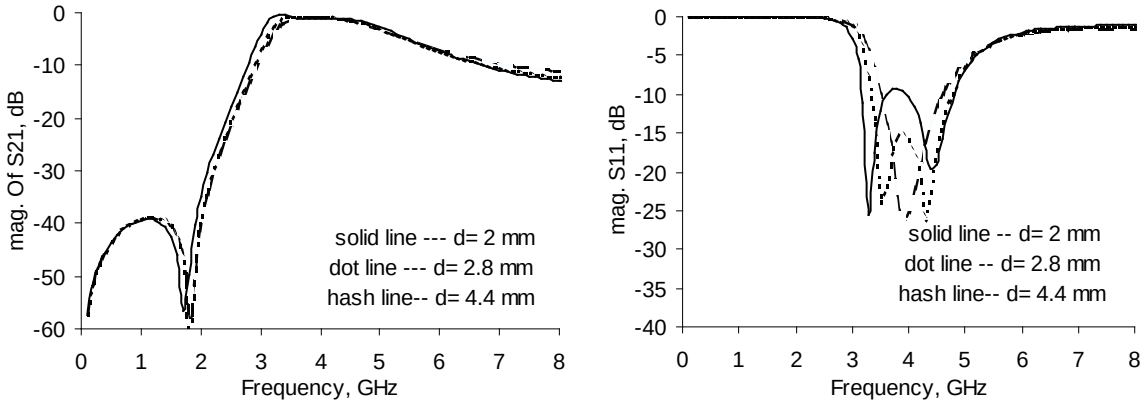


(a) (b)

Fig. 5. Simulated S-parameters of DGS resonator for different value of d : (a) S21 (b) S11

The frequency response in Fig. 2(a), shows two attenuation minima's at 3.3 GHz and 4.5 GHz in the return loss characteristics for d = 2 mm. The passband insertion loss of 0.8 and 3-dB bandwidth of 2.1 GHz are obtained. Now, we choose the slot heads of width 3.6 mm and the distance between heads (d) becomes 2.8 mm. The attenuation minima's are obtained at 3.5 GHz and 4.3 GHz and observed insertion loss of 0.5 and 3dB bandwidth of 1.8 GHz as shown in Fig. 5. Both the minima's came closer and passband insertion loss improved. By adjusting the length of slot-head further, the two minima's are made overlapped at 3.9 GHz. As a result, an extremely low insertion loss (below 0.05 dB) and 3-dB bandwidth of 1.4 GHz are observed in Fig. 5. Here, the width of the slot heads is 2.8 mm and



Previous Page een slot-heads is 4.4 mm. For all three cases the length of the slot head has Next Page

taken fixed as 4 mm. Thus, the passband insertion loss is improved by varying the slot-head dimension.

**CONCLUSION:**

Along a microstrip line, a microstrip DGS can be achieved by etching an area in the metallic ground plane. In the proposed DGS pattern, two square headed (of side length e) transverse slots (of length c and width g) connect a rectangular slot (of length a and breath b) transversely. The DGS microstrip resonator has been constructed by the proposed DGS unit and a pair of end-coupled microstrip lines. The equivalent circuit is represented by series and parallel resonant circuits. The resonant frequency is located higher than anti-resonant frequency. The passband of the filter can be tuned by varying the dimension of slot heads. The passband insertion loss can be improved by varying the slot-head dimension. An uneven stopband transition edge is observed in both side of the passband.

**REFERENCES:**


1. D. Ahn, J.S.Park, C.S.Kim, J.Kim, Y Qian and T. Itoh. "A design of the lowpass filter using the novel microstrip defected ground structure", IEEE Trans. on Microwave Theory and Techniques.Vol. 49, No. 1, pp.86-93, 2001.
2. Lim J., Kim C., Lee Y., Ahn D., and Nam S. "Design of lowpass filters using defected ground structure and compensated microstrip line", Electronics Letter, Vol. 38, No. 25, pp.1357-1358, 2002.
3. A. Abdel-Rahman, A.K. Verma, A. Boutejdar, and A.S. Omar, "Control of bandstop response of Hi-Lo microstrip lowpass filter using slot in ground plane", IEEE Trans. On Microwave Theory Tech., Vol. 52, No. 3, pp.1008-1013, 2004.
4. Abdel-Rahman., A., Verma, A.K., Boutejdar, A., and Omar, A.S. "Compact Stub type microstrip bandpass filter using defected ground plane", IEEE Microwave and Wireless Comp. Letters, Vol.14, No. 4, pp.136-138, 2004.
5. Chen J.-X., Li J.-L., Wan K.-C. and Xue Q. "Compact quasi-elliptic function filter based on defected ground structure", IEE Proc.-Microwave and Antenna propagation Vol.153 No. 4, pp.320-324, 2006.
6. Susanta Kumar Parui and Santanu Das, "A novel asymmetric defected ground structure for implementation of Elliptic filters," Proc. of IEEE-MTTS International Microwave and Opto-electronics conf. (IMOC-2007), Brazil, pp.946-949, 2007.
7. [Susanta Kumar Parui and Santanu Das, "Design of Planar Filters Suitable for Satellite System Using Asymmetric Defected Ground Structure Technology," Proc. of National Conference on Global Navigation Satellite System (GNSS-2007), Hydrabad, India, pp.157-160, Oct 25-26, 2007


SEARCH

Previous Page Next Page

# DESIGN AND DEVELOPMENT OF SPST MEMS SWITCHES

*Usha Kiran K., Sripadaraja K., Mubassira Banu S.N. and K. J. Vinoy*
Microwave Laboratory, ECE Dept., Indian Institute of Science, Bangalore, India, 560 012
Email: usha.kirank123@gmail.com

**ABSTRACT:**

The micromachining technique offers potential for bulk fabrication of miniature components at microwave and millimeter wave frequencies. Critical components of integrated RF front ends are RF switches. In this paper, we present the design and modeling studies of the RF MEMS switches for C, X and Ku band applications. The proposed switches have good isolation, low insertion loss and a low pull-in voltage. Both electromagnetic (EM) and electromechanical modeling of the proposed switch designs is studied. The electromagnetic modeling is done using electromagnetic solver HFSS while the electromechanical modeling is carried out using FEA solver (IntelliSuite).

## INTRODUCTION:

Micromachined components are poised to form a significant share of telecommunications equipment in the very near future. RF MEMS devices including switches promise to endow wireless handsets, with key properties of low-power consumption and reconfigurability, which in turn will enable superior functionality and performance. RF MEMS switches combine the advantages of both mechanical and semiconductor switches and at the same time avoid the drawbacks of conventional switches [1]. A comprehensive model of RF MEMS switch was reported by Rebeiz [2-3] which analyzed the RF switch through the lumped parameter model. An overview of switches and RF circuits built with these is available in [4].

Common RF MEMS switch designs consist of a thin metal cantilever, air bridge, diaphragm, or some other structure electrically configured in series or parallel with an short-circuit RF transmission line and are designed to open the line or short-circuit the structure to ground upon actuation. Electrostatic actuation has a special significance in the context of MEMS due to the advantages offered by scaling, and is widely preferred. MEMS devices are usually fabricated using silicon, GaAs, quartz, glass and alumina which has the required mechanical and electrical properties required to fabricate high precision mechanical components. Surface and bulk micromachining and RIE are used for the fabrication of RF MEMS switches.

In this paper, we present the design and modeling studies of RF MEMS SPST (single-pole and single-throw) series and shunt switches which are actuated electrostatically. These switches are designed on 50Ω CPW on a quartz substrate. The series switch is primarily useful for frequencies up to C-band. For higher frequency applications a shunt switch is designed. The simulations are carried out over C, X and Ku bands to meet the requirements. The EM, pull-in, dynamic response are done and presented. Fabrication is to be taken up by BEL, Bangalore and the experimental results will be presented at symposium available by then.



Previous Page Next Page

## 2. Design and simulations of SPST Series Switch:

Schematic of a series RF MEMS switch is given in Fig. 1. The series switch design consists of CPW on a quartz substrate. Here, the switch beam is a cantilever strip fixed at one end of the t-line. An electrically isolated dc electrode is used to pull down the cantilever beam. A thin dielectric layer is placed on this electrode to avoid the stiction. Two interconnects are provided across the cantilever strips to maintain mechanical integrity for the moving structure. The air bridges are placed above the DC-line to provide good RF characteristics.

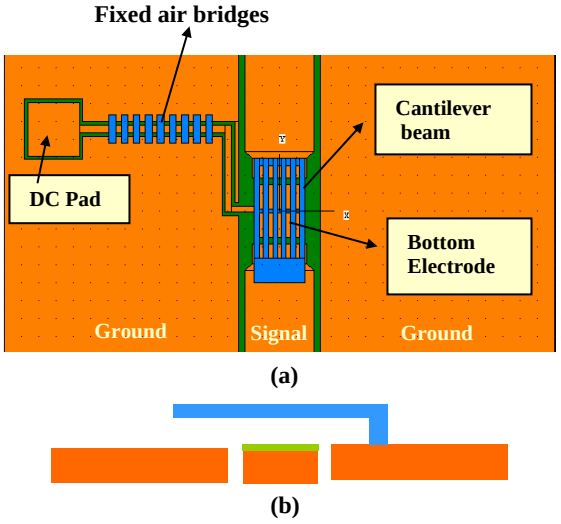


**Fig. 1: Schematics of Series Switch, (a) Top view (b) Side view.**

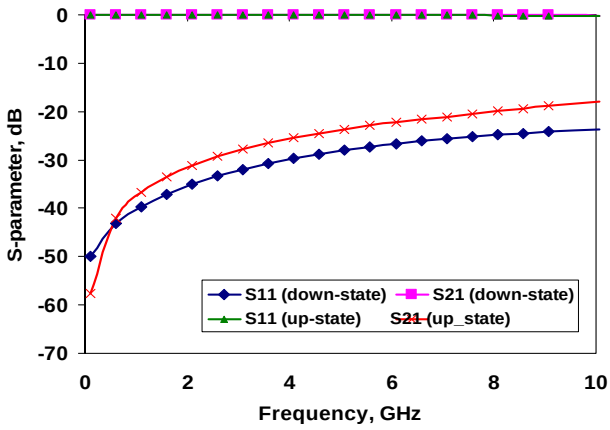


**Fig. 2: Simulated S-Parameters for the series switch.**

The EM simulations are done using Ansoft HFSS. In downstate (ON) the cantilever beam is assumed to be in contact partially with the actuation electrode and fully with the RF electrode. S-parameters for this configuration are measured over frequencies from up to 10 GHz and are as shown in the Fig. 2. It is seen from the figure that the device meets 20 dB isolation with an low insertion loss less than 0.1 dB up to 8 GHz.

Later, the electromechanical simulations are done using FEA solver (IntelliSuite). As per the design topology given earlier, the Pull-in Voltage, Switching, and Hysteresis responses were found. The pull-in voltage for switch is found to be 4 V. Fig. 3 shows the hysteresis response of the switch. Analyses using 2D and 3D analyses in IntelliSuite are compared Fig. 4.

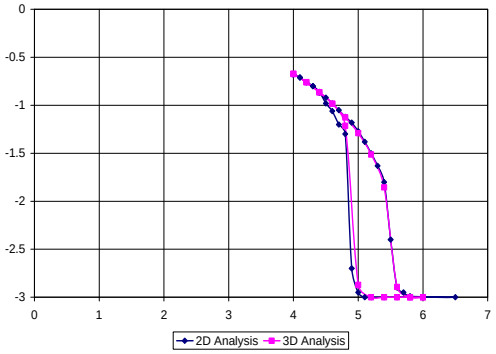


**Fig. 3: Hysteresis response of Series switch.**

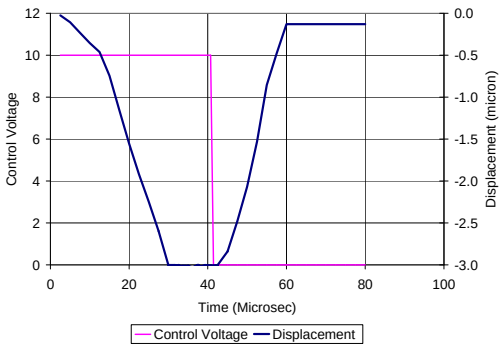


**Fig. 4: Dynamic response of Series switch.**

SEARCH
Previous Page
Next Page

The dynamic response from the simulation ON-Time (downward transition) was

found to be ~ 18 µSec and the OFF-Time (upward transition) was found to be ~12µSec. For the transition to turn on the device, 10 V is applied.

## 3. DESIGN AND SIMULATION OF SPST SHUNT SWITCH:

In the design of shunt switch a shunt beam is studied. The shunt switch is designed on 50Ω CPW on quartz substrate. The moving structure is a fixed-fixed beam. The schematic diagram for this model is as shown Fig. 5. Here, the switch beam is suspended at a height above the t-line. The anchors of the beam are connected to the CPW ground planes. The electrostatic actuation of the beam is done through two dc electrodes under the beam placed between the t-line and ground planes.

A single DC Pad is used with the DC line passing through the transmission line for the shunt switch. The beam strips have one interconnecting strip across them, in the middle. Air bridges are provided for better RF performance.

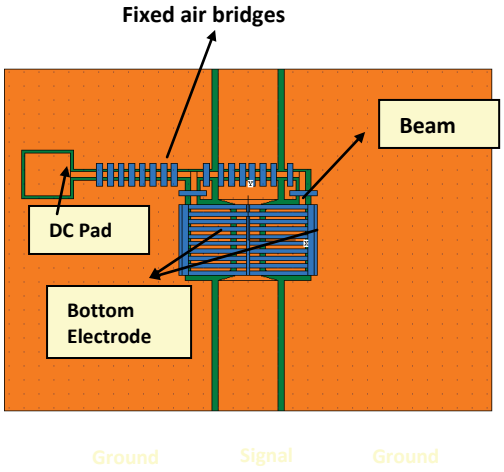


(a)

(b)

Fig. 5: Schematics of Shunt Switch.
(a) Top view (b) Side view.

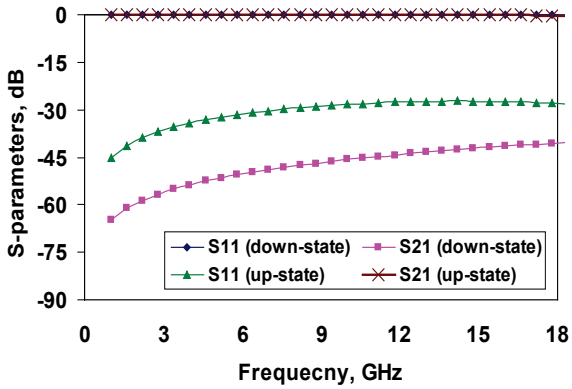


Fig. 6: Simulated S-Parameters for the shunt switch.

The shunt switch is simulated using HFSS. As the beam is placed in shunt between the transmission line and ground, in downstate (OFF) the beam is assumed to be in contact partially with the actuation electrode, fully with the RF electrode and ground. S-parameters measured for upstate (ON) and downstate (OFF) over frequency range 1 to 18 GHz and are as shown in the Fig 6. The switch gives good isolation of more than 40 dB over the entire frequency range.

Using electromechanical simulations, Pull-in Voltage, Switching and hysteresis response of the switch were found. The Pull-in voltage for switch is found to be ~8V DC. The full contact occurs at 9 V. Fig. 7 shows the hysteresis response of the shunt switch. The dynamic response was also found using the macromodel extraction of shunt switch (Fig. 8). Another point to be noted is the difference in the mechanical behavior of the beam cantilever based switches. Series switch appears faster as this uses cantilever geometry.



Previous Page Next Page

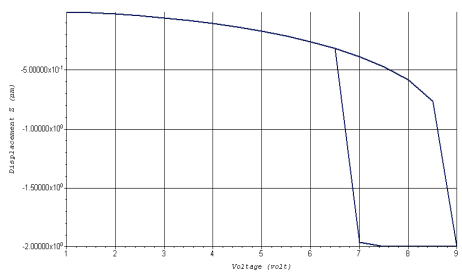

Fig. 7: Hysteresis response of Shunt switch.

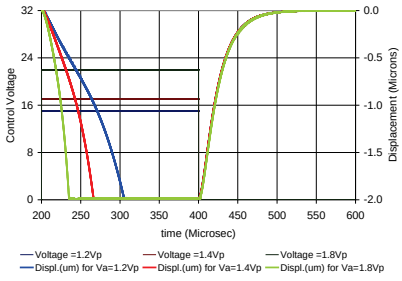


Fig. 8: Dynamic response of Shunt switch.

## 4. CONCLUSIONS:

The RF MEMS SPST series and shunt switches are designed and the performance was studied over a frequecny range 4-20 GHz for various parameters. The series switch is studied for the lower frequency bands and shunt switch is studied for higher frequency bands. Both series and shunt switches show high isolation and with low insertion loss. These designs have low actuation voltage. The dynamic analysis presented here show that these designs are comparable to the state of art. The devices are being fabricated by BEL, Bangalore.

## ACKNOWLEDGEMENT:

The authors acknowledge financial support from DRDO-RCI, Hyderabad and process related inputs from Dr. Natarajan and his team from BEL, Bangalore.

## REFERENCE:

1. K. J. Vinoy and V. K. Varadan, "Design of reconfigurable fractal antennas and RF-MEMS for space-based systems", Smart Materials and Structures, Vol. 10, pp. 1211-1223, 2001.
2. J. B. Muldavin and G. M. Rebeiz, "High isolation CPW MEMS shunt switches, part I: modeling", *IEEE Trans. Microwave Theory and Techniques*, Vol. 48, No. 6, pp.1045–1052, 2000.
3. J.B. Muldavin, G.M. Rebeiz, "All-metal series and series/shunt MEMS switches", *IEEE Microwave Wireless Comp. Lett.*, Vol. 11, pp. 373-375, 2001.
4. J.B. Muldavin, G.M. Rebeiz, "RF MEMS switches and switch circuits", *IEEE Microwave Magazine*, pp. 59-71, Dec 2001.

SEARCH

Previous Page Next Page

# ACCURATE MODELLING OF THE RESONANT FREQUENCY OF SQUARE SPLIT RING RESONATORS

*Chinmoy Saha[1], Jawad Y. Siddiqui[2], Debatosh Guha[2] and Y.M.M. Antar[3]*

[1]Heritage Institute of Technology, Chowbaga Road, Anandapur, Kolkata-700107, India.

chinmoy_rpe@yahoo.com

[2]Institute of Radio Physics and Electronics, University of Calcutta, 92, A.P.C. Road, Kolkata-700009,India.

ysiddiqui@ieee.org, dgirpe@yahoo.co.in

[3]Royal Military College of Canada, Kingston, Ontario K7K 7B4, Canada

antar-y@rmc.ca

**ABSTRACT:**

In this paper, we propose a new theoretical model for accurate estimation of resonance frequency of the Square Split Ring Resonators (S-SRR) using a new equivalent circuit. The effect on resonance frequency due to different parametric variation like the effective side length, width, split gap within the rings and dielectric constant of the substrate are thoroughly studied. Several simulations were performed using an electromagnetic simulator and the results were compared with the proposed theory showing good agreement.

## INTRODUCTION:

The split ring resonator (SRR) is a fundamental component for design and realization of metamaterials. The prime inherent characteristic of this structure is that it exhibits negative effective permeability [1], for a narrow band of frequency, which is one of the constitutive parameter for realizing metamaterials. They have been extensively studied in [1] and [2]. Another variant of the SRR is the Square SRR (S-SRR) which has more degrees of freedom from the design aspect [3]. The SRRs possess large magnetic polarizability and exhibit negative effective permeability for frequencies close to their resonance frequency [2]. They also show a large magnetic dipole moment when excited by a magnetic field directed along its axis. This was shown by measurements performed by [2] using circular SRR. Fig. 1 shows a schematic view of a S-SRR having strip width $c$ and spacing $d$ between the rings. $g_1$ and $g_2$ are split gaps within the inner ring and outer ring, respectively. $a_{ext}$ is the half the side-length of the outer ring of the SRR. $a_0$ is the average length of the S-SRR calculated from the center of the structure It is printed on a dielectric substrate with dielectric constant, $\epsilon_r$ and thickness $h$. We have used a commercially available electromagnetic simulator [4] to simulate our S-SRR structures and have analytically modeled the resonant frequency for varying width of the rings, spacing between the rings and split gap width within the rings. Most of the previous models neglected the split gap width within the rings. We propose a new equivalent circuit which accounts for the split gap widths and their capacitive contribution is incorporated in the theoretical model. The computed results are verified with the simulations showing good agreement with the proposed model.

## THEORY:

To determine the simulated resonant frequency, the S-SRR shown in Fig. 1 is placed are iris having length $L$ of a metallic screen located inside a rectang

waveguide similar to the setup used for characterization in [2]. The schematic view of the setup is shown in Fig. 2. When a magnetic field is applied along the z-axis, an electromotive force will appear around the SRR inducing currents which would pass from one ring to the other through the gaps, $g_1$ and $g_2$ and the structure behaves as an $LC$ circuit having resonance frequency $\omega_0$ given by

$$\omega_0 = \sqrt{\frac{1}{LC_{eq}}} \qquad (1)$$

Here $L$ is the total inductance of the structure $C_{eq}$ is the total equivalent capacitance of the structure. Fig. 3 shows the equivalent circuit of the SRR. Here $L$, $R$ are the equivalent inductance and resistance respectively. $C_1$ and $C_2$ are the capacitances of the upper and lower half portions between the rings about an imaginary line AB passing through the centers of the split gaps $g_1$ and $g_2$. The split gaps are incorporated in the model as gap capacitances $C_{g1}$ and $C_{g2}$. The gaps also effect the total inductance $L$ of the structure and has been accounted for in our model.

The capacitances $C_1$ and $C_2$ for the upper and lower half portions of the rings is given as

$$C_1 = C_2 = (4a_0 - g)C_{pul} \qquad (2)$$

$C_{g_1}$ and $C_{g_2}$ are calculated by using the parallel plate capacitance formula. Because of identical gap dimensions,

$$C_{g_1} = C_{g_2} = C_g = \frac{\varepsilon_0 A}{g_1} = \frac{\varepsilon_0 ch}{g_1} \qquad (3)$$

Since here $C_{g_1} = C_{g_2}$ and $C_1 = C_2$, from the circuit of Fig. 3 the equivalent capacitance $C_{eq}$ is modified as,

$$C_{eq} = \frac{\left(C_1 + C_{g_1}\right)}{2} \qquad (4)$$

Substituting the values of $C_1$ and $C_{g_1}$ from equation (2) and (3) we get,

$$C_{eq} = \left(2a_0 - \frac{g}{2}\right)C_{pul} + \frac{\varepsilon_0 ch}{2g_1} \qquad (5)$$

*where as in [5]*

$$C_{pul} = \sqrt{\varepsilon_r}/c_0 Z_0 \qquad (6)$$

$Z_0$ is the characteristic impedance $c_0$ is the velocity of light in free space. The total inductance $L$ of the S-SRR is and is calculated from [2].

**RESULTS:**

To verify the proposed theoretical model a set of square SRR having different $a_0$, strip width c , and gap $g_1$ and $g_2$ printed on a substrate with dielectric constant, $\varepsilon_r$ = 2.43, and thickness $h$ = 0.49 mm was simulated using an electromagnetic simulator, HFSS. Figure 4 shows the variation of the resonant frequency as a function of $a_0$. As seen from the figure, increase in $a_0$ decreases the resonance frequency of the structure which can be attributed to the increase in total inductance $L$ for same strip width $c$, per unit length capacitance $C_{pul}$ remaining unaltered. Similar work is performed for different strip width, $c$ keeping the outer dimension of the S-SRR $a_{ext}$ fixed. The plot of the resonance frequency against the variation of $c$ is shown in Fig. 5. With increasing $c$, per unit length capacitance $C_{pul}$ increases, but

SEARCH
Previous Page
Next Page

$a_0$ and $L$ decreases resulting in increase in the resonance frequency. The plot of the resonant frequency against the variation of split gap $g = g_1 = g_2$ is shown in Fig. 6. In tune to our proposed new equivalent circuit, with increasing split gap $g$ the gap capacitance $C_g$ as well as the ring capacitances $C_1 = C_2$ decreases the cumulative effect of which increases the resonant frequency as seen from the figure. The computed results show excellent agreement with the simulation.

## CONCLUSIONS:

A new theoretical model to estimate the resonant frequency of an edge coupled S-SRR is proposed. The proposed model incorporates the effect of gap capacitance due to presence of the gap splits with the rings which was neglected in earlier models. Proper prediction of the resonant frequency is important since the SRRs exhibit negative effective permeability for frequencies close to their resonance frequency. A single element structure is modeled and simulated using an electromagnetic simulator. The simulated results obtained are compared with the theory showing excellent agreement for a wide range of parametric variation of the rings.

## REFERENCES:

1. J.B. Pendry, A.J. Holden, D.J. Ribbins, and W.J. Stewart, "Magnetism from conductors and enhanced nonlinear phenomenon" *IEEE Trans. Microwave Theory Tech.,* vol. 47, pp. 2075-2084, Nov. 1999.
2. R.Marquez, F. Mesa, J. Martel, F. Medina, "Comparative analysis of edge- and broadside- coupled split ring resonators for metamaterial design-theory and experiments," *IEEE Trans. Antennas Propagat.,* vol. 51, pp. 2572-2581, Oct. 2003.
3. C. Saha, J.Y. Siddiqui, D. Guha,Y.M.M. Antar ,"Square Split Ring Resonators: Modelling of Resonance Frequency and Polarizability" *Proc. IEEE AEMC,India, Dec. 2007.*
4. HFSS: *High Frequency Structure Simulator*, Ansoft.
5. I.Bahl and P. Bhartia, *Microwave Solid State Circuit Design*, Ch.2,Wiley, New York, 1998.

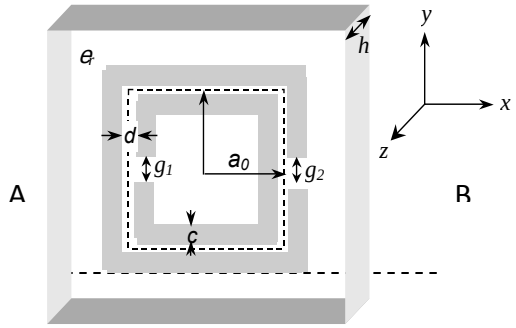


Fig. 1. Edge coupled square split ring resonator

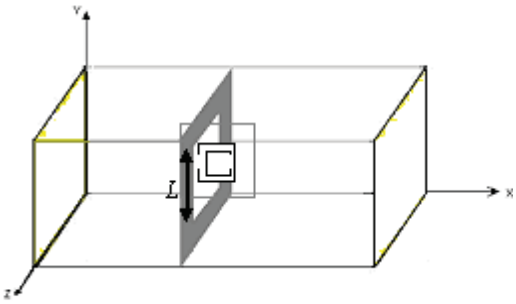


Fig. 2. A S-SRR placed inside a square iris of length, *L* within a waveguide

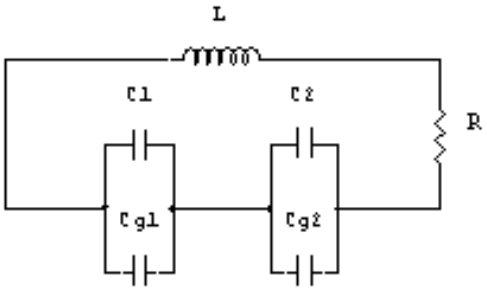


Fig. 3. New equivalent circuit considering the gap capacitance

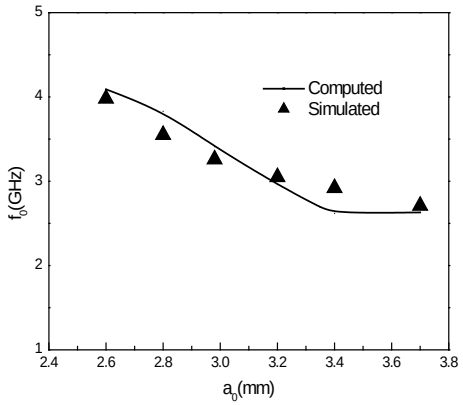


Fig. 4. Computed and simulated resonant frequency of an edge coupled SRR as a function of $a_0$. $\epsilon_r$ = 2.43, *c* = 0.94 mm, *d* = 0.36mm, *h* = 0.49 mm.

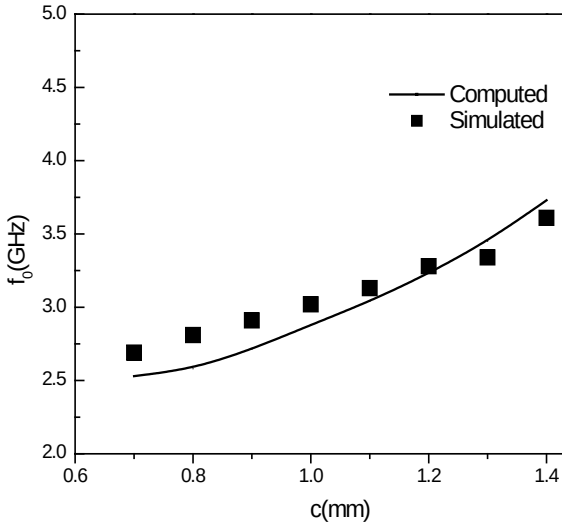


Fig. 5. Computed and simulated resonant frequency of an edge coupled SRR as a function of *c*. $a_{ext}$ = 4.47 mm, $\epsilon_r$ = 2.43, *d* = 0.36mm. *h* = 0.49 mm.

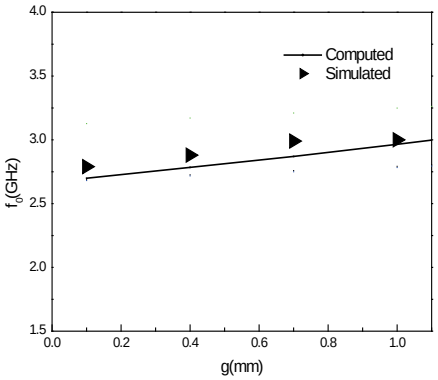


Fig. 6. Computed and simulated resonant frequency of an edge coupled SRR as a function of gap $g_1$=$g_2$=$g$.
$a_{ext}$ = 4.47 mm, $\epsilon_r$ = 2.43, c=0.94mm, *d* = 0.36mm,
*h* = 0.49 mm.

SEARCH
Previous Page
Next Page

# DESIGN OF DOUBLE NEGATIVE METAMATERIAL USING HEXAGONAL OMEGA STRUCTURE

*[1]Sudhakar Sahu, [2] R.K.Mishra, [3] D.R.Poddar*

[1]Department of Electronics &Telecommunication Engineering, KIIT University, Bhubaneswar 751024,India,
sudhakarsahu@yahoo.co.uk

[2] Electronic Science Department, Berhampur University, Bhanja Bihar, Berhampur 760 007, Orissa, India
r.k.mishra@ieee.org

[3] Dept. of Electronics &Telecommunication Engineering, Jadavpur Uiversity, Kolkata 700032, India,
drp_ju@yahoo.com

## ABSTRACT

This paper proposes a new structure for double Negative Metamaterial using Hexagonal Omega structures. It investigates the effect of geometrical parameters, like gap width, length and width of each side, length and width of feed, on magnetic resonant frequency behavior. The Double Negative ($-\mu_{eff}$ & $-\varepsilon_{eff}$) character of the hexagonal Omega structure is verified by numerical retrieval of parameters obtained from simulated results.

## I. INTRODUCTION

The credit for theoretical prediction of Double Negative Material in 1967 goes to Russian Physicist V. Veselago [1]. Metamaterials (MTMs) denote artificially constructed materials [3–4] exhibiting uncommon natural electromagnetic properties. Example includes double negative media i.e. MTMs exhibit negative value of effective permittivity and permeability in a certain frequency range. In1999, Pendry *et al.* proposed artificial system made only of nonmagnetic conducting materials that could exhibit a large response to the magnetic field of electromagnetic radiation. They proposed a combination of split ring structure with rods for MTMs [2]. Engheta [5–6] proposed the omega structure as an alternative to Pendry'd structure. The present work proposes a unit cell of single hexagonal Omega Structure for realization of MTM. The superiority of Omega structure over split ring type resonator lies in the fact that the double negative (DNG) characteristic is obtained on a planner structure. The advantage of using hexagonal shape is that it has a better packing capability than the circular structure and hence can result in controlled 2-D anisotropy when necessary. The magnetic resonance frequency with gap width, metal width, side length, feed length and width is investigated. The Double Negative Metamaterial behavior is also observed in a certain range of frequency.

## II. HEXAGONAL OMEGA DOUBLE NEGATIVE METAMATERIAL

### Design and Simulation

The substrate used for the structure has $\varepsilon_r = 2.4$, h (thickness) = 1.6 m.m. with a copper layer of thickness 0.03 m m. The geometrical parameters of hexagonal Omega Structure shown in figure 1 are: gap width (d) = 0.2 mm, strip width (w) = 0.9 mm, each side length of hexagon = 2.7 mm. The dimension of a unit cell containing a single hexagonal omega structure are $a_y$=5.6 mm and $a_z$ = 6.5 mm. For the electromagnetic simulation setup HFSS (a full wave finite element method based EM simulator) the follo

procedures have been adopted. The top and bottom face of the vacuum wave guide box containing the hexagonal omega structure has been taken as perfect electric. The front and back face of the vacuum box acting as a wave guide has been taken as perfect magnetic walls. The wave is propagating in the positive Y-direction. The left side and right side faces are taken as wave ports 1 & 2 to calculate the transmission spectrum (S-parameters). Using the above, a unit cell of hexagonal omega structure is simulated.

## III. RESULTS AND DISCUSSION:

The simulated result for a single unit cell of hexagonal omega structure is shown in figure 2. The structure has a dip at 4.75 GHz which is magnetic resonance frequency of the hexagonal omega structure. From the figure 2, it is observed that the band gap occurs in the range 4.6 to 4.65 GHz. Also, the simulation results shown in figure 2 demonstrate that the hex- omega structure is low pass and it could achieve a quite flat pass band upto 4.5 GHz. Other simulation results for various gap widths which are not shown in this paper, also indicate that the pass band could be well controlled by adjusting the resonance frequencies of the hex-omega structure. It can be observed that a band gap is present in the transmission spectrum of hexagonal omega medium corresponding to $\mu < 0$. The double negative character ($\mu_{eff}$ and $\varepsilon_{eff}$) is retrieved from the S-parameter and is shown in figure 3. Further, we observe negative refraction retrieved from the S-parameters of hex-omega structure which are well-known metamaterial particles with magnetic response to incident waves. The negative refractive index is found from 3.25GHz to 5.4GHz

## V. CONCLUSION

The characteristics of unit cell MTM has been studied employing Ansoft HFSS and the retrieval procedure using MAT LAB 7.0. The simulated results show that the metamaterial sample has double negative property at the microwave frequency range from 3.25GHz to 5.4GHz. Some unique characteristics have been demonstrated by full-wave analysis. This hexagonal omega structure will be highly beneficial in the design of microwave devices, e.g. filters and in antenna to suppress surface waves. Further, it is also easy to integrate with microstrip components and its electric dimension is quite small.

## REFERENCES

1. V. Veselago, "The Electrodynamics of substances with simultaneously negative values of μ & ε ", Soviet Physics USPEKHI Vol. 10, No. 4, pp. 509 – 514, 1968.
2. J.B. Pendry, A.J. Holden, D.J. Robbins & W.J. Stewart, "Magnetism from conductors and enhanced nonlinear phenomena", IEEE Trans. Microwave theory and Technique, vol 47, no. 11, pp. 2075-2081, Nov. 1999.
3. R. W. Ziolkowski, "Design, Fabrication & Testing of Double Negative Metamaterials", IEEE Transaction on Antenna and propagation, vol. 51, no. 7, pp. 1516-1529, 2003.
4. Nader Engheta, R. W. Ziolkowski "A positive future of Double Negative Metamaterials", IEEE Trans. Microwave theory and Technique, vol 53, no. 4, pp.1535-1556, April 2005.
5. M.M.I Saadown & N. Engheta, "Theoretical study of Electromagnetic properties of Non local omega media", Progress in Electromagnetic Research, PIER, vol. 9, pp 351-397, 1994.
6. Nader Engheta, Metamatrial Physics and Engineering Explorations, 2005, John Willey Publication.



Previous Page Next Page

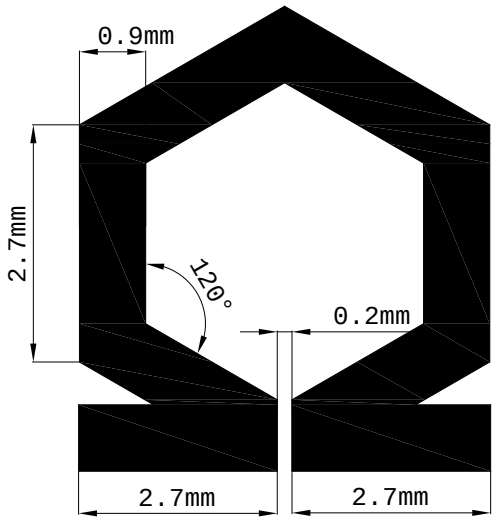


*Fig.1. schematic of finalized hexagonal omega structure design from Ansoft HFSS*

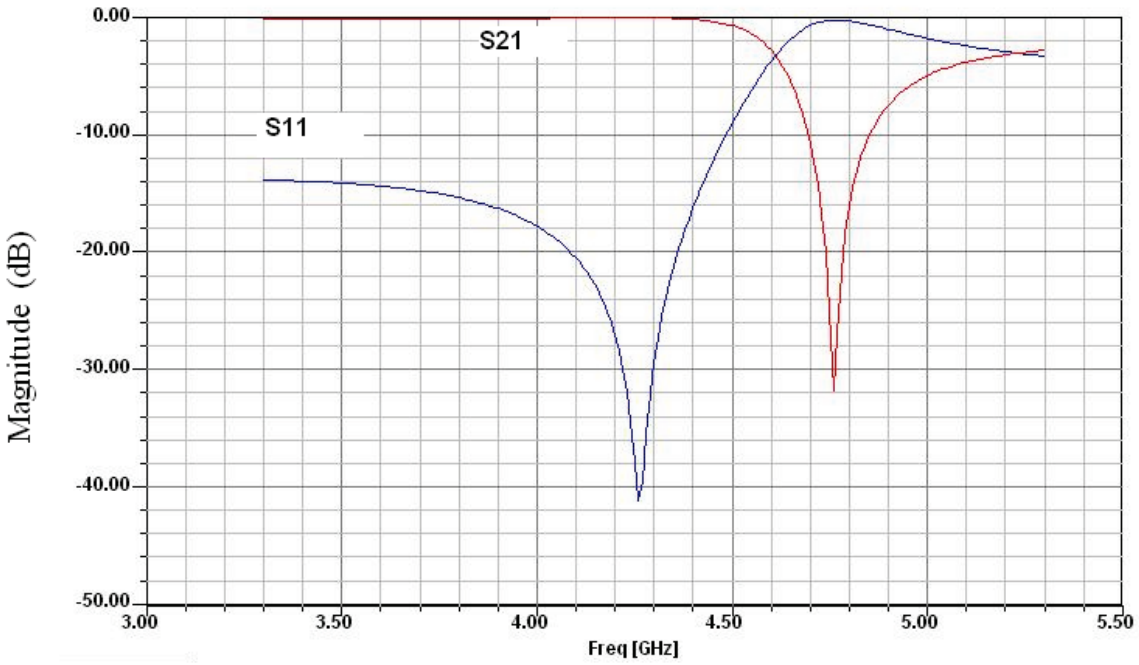


*Fig.2. HFSS- predicted S-parameter for the Hex-Omega*

SEARCH

Previous Page

Next Page

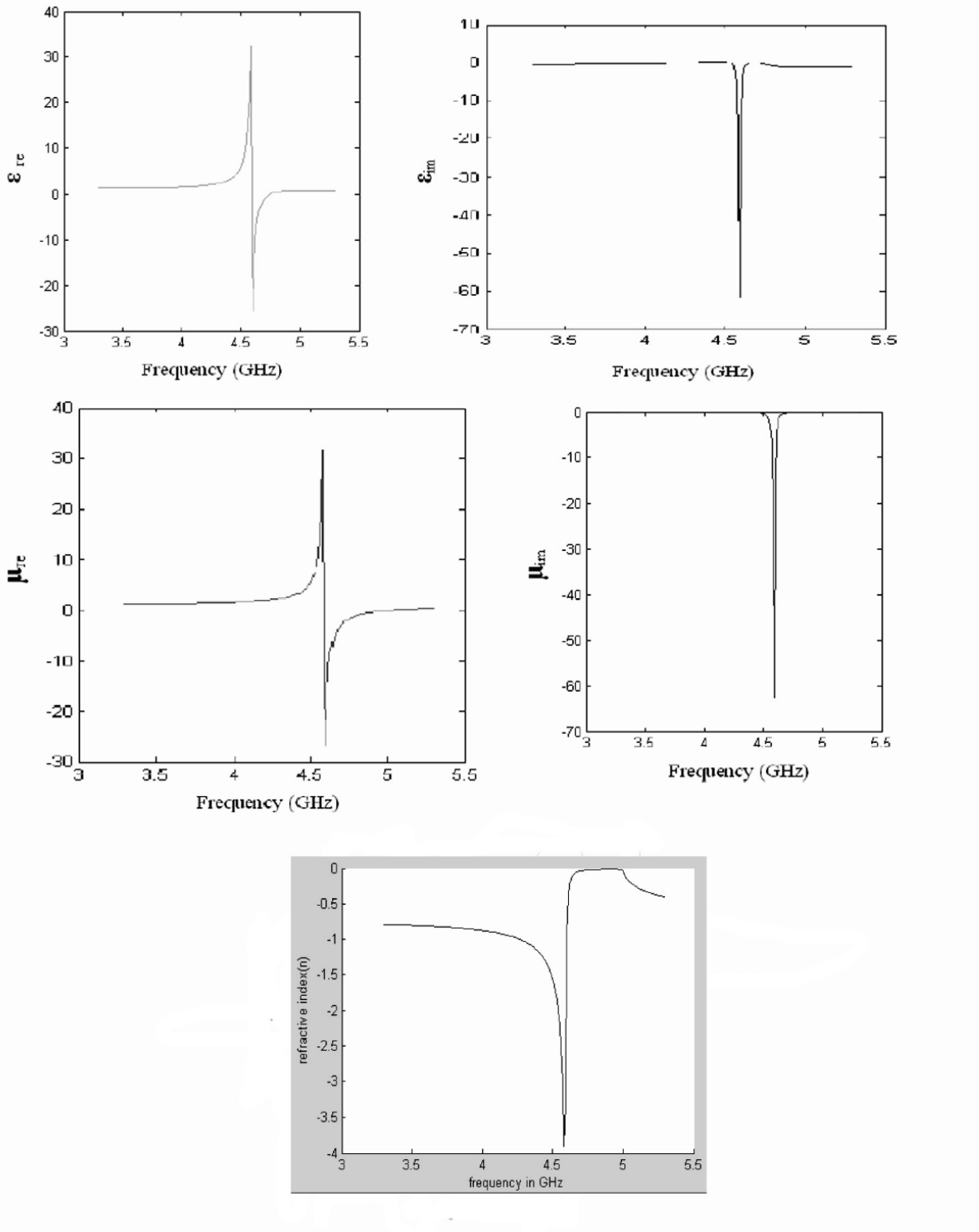


Fig.3. Retrieved material properties from the HFSS-predicted S-parameter for the Hex-Omega structure

SEARCH

Previous Page

Next Page

# A NOVEL SCHEME FOR UWB SIGNAL GENERATION USING MESFET

*Mithilesh Kumar, Member, IEEE, Ananjan Basu, Member, IEEE and Shiban K. Koul, Senior Member, IEEE*

Center for Applied Research in Electronics Indian Institute of Technology Delhi, Hauz-Khas, New Delhi-110016, INDIA

mith_kr@yahoo.co.in, ananjan_b@yahoo.com, shiban_koul@hotmail.com

## ABSTRACT

A new scheme for generation of UWB signal using MESFET is proposed in this paper. The novel scheme was simulated using Agilent ADS software and experimentally verified by fabricating the circuit using GML 1000 substrate and testing on Agilent Infiniium DSO 9000A oscilloscope in time domain and on spectrum analyzer in frequency domain. The simulated and experimental results show good agreement for the proposed scheme to generate UWB pulses of pico-second order that conform to most of the FCC's laid regulation for UWB system.

## I. INTRODUCTION

**UWB** technology for consumer electronics and communications has received considerable attention recently. Ideal targets for UWB systems are: low power, low cost, high data rates, precise positioning capability and extremely low interference. UWB communication differs significantly from other wireless communication standards. In the UWB system a series of pulse are sent instead of using a carrier wave. The pulse can be seen as an intense burst of RF energy where each pulse carries one symbol of information. The benefits and possibilities of UWB can be best summarized by examining Shannon's famous capacity equation [C=B log(1+S/N)]. Increasing the bandwidth, increasing the signal power or decreasing the noise can increase the channel capacity. We can see that capacity of channel grows linearly with increasing bandwidth *B*, but only logarithmically with signal power *S*. Thus, from Shannon's equation we can see that UWB systems have a great potential for high capacity wireless communications. UWB transmitters and receivers do not require expensive components such as modulators, demodulators and IF stages [1]. Therefore, UWB is one of the most promising technologies for future high-data-rate wireless communications, high-accuracy radars, and imaging systems. Compared with conventional broadband wireless communication systems, the UWB system operates within an extremely broad bandwidth in the microwave frequency band and at a very low emission limit.

Generally speaking, the extremely short pulses with fast rise and fall times have a very broad spectrum and very small energy content. Ultra wideband systems cover a large spectrum and interfere with existing users. In order to keep this interference to the minimum, the FCC and other regulatory groups specify spectral masks for different application that show the allowed power output for specific frequencies [1]. Furthermore, according to the FCC, a large contiguous bandwidth of 7.5 GHz is available between 3.1 GHz and 10.6 GHz at a maximum power output of -41.3dBm/MHz [2].

## II. GENERATION OF UWB PULSE

Single short pulse (or impulse) generation is the traditional and fundamental approach for generating UWB waveforms. By varying the pulse characteristics, the characteristics of the energy in the frequency spectrum may be defined based on the design criteria. Pulse duration in the time domain determines the bandwidth in the frequency domain. As a rule of thumb we may write, 1/duration≈ bandwidth. UWB pulses are typically of nanosecond or picoseconds order. One pulse by itself does not communicate a lot of information. Information or data needs to be modulated onto a sequence of pulses called pulse train. When pulses are sent at regular interval, which are sometimes called the pulse repetition rate or duty cycles, the resulting spectrum will contain peaks of power at certain frequencies.

While many applications and procesing of UWB signals are known, very few practical circuits have been described which can conveniently generates UWB pulses. In the literature circuit are proposed by base band-pulse-antenna techniques [3], ultra-wideband technology for short- or medium-range wireless communications, novel low-cost ultra-wideband, ultra-short-pulse transmitter with MESFET impulse-shaping circuitry for reduced distortion and improved pulse repetition rate [4], recent system applications of short-pulse ultra-wideband (UWB) technology [5], and UWB pulse generation techniques with RF pulse compression to generate high instantaneous RF power by compressing the energy distributed over a long duration into short period using the basic theory of switched resonators[6].

## III. GENERATION OF UWB PULSE USING MESFET

A novel scheme proposed for the generation of short pulse is shown in Fig.1. To generate the short pulse, first the forced step pulse is applied to the gate of MESFET transistor. The circuit gives the short pulse of the duration of few *nsec* at the output. One pulse by itself does not communicate a lot of information. Information or data needs to be modulated onto a sequence of pulses called pulse train. Thus we have applied the pulse train shown in Fig.2 of rate=10MHz, $V_{low}$=0.2V, $V_{high}$=2.5V, rise time=1nsec, fall time=1nsec to the gate of the MESFET. Other parameters of the circuit are: $V_{dc}$=2.0V for biasing, the value of inductor L=1nH, capacitor C=1pF and load impedance R=50 ohm. With this arrangement, we got the repetitive short pulse in the form of pulse train shown in Fig.3 required for UWB communication. The spectrum of the train of UWB pulses is shown in the Fig.4.

## IV. PRACTICAL IMPLEMENTATION

The practical UWB pulse generator was implemented using MIC fabrication technique. The lumped components were converted into the distributed components. Finally the circuit was integrated with the RF MESFET NE32S01 on GML 1000 substrate shown in Fig.5 (a). The circuit was tested in the frequency domain. The spectrum of UWB pulse was measured using the spectrum analyzer and result shows the spectrum up to 12 GHz as shown in Fig.5 (b). Using Agilent Infiniium DSO 9000A oscilloscope, the results in time domain were observed as shown in Figs. 6(a)-(b). The input and output waveforms observed on DSO 9000A in time domain and frequency spectrum observed on the spectrum analyzer show encouraging results for generation of UWB signal using MESFETS.

SEARCH

Previous Page Next Page

## V. CONCLUSION

A novel method proposed for generation of UWB pulse using the MESFET was simulated and practically verified and the initial results obtained are encouraging. This circuit can be easily converted realized using monolithic microwave IC technology.

## REFERENCES


1. M.Ghavami, L.B.Michael, R .Kohno, "Ultra wideband signals and systems in communication engineering", John Wiley & Sons, Ltd, England, 2004.
2. Federal Communications Commission, First Report and order, February 14, 2002.
3. David L amensdorf and L eon Sus man , "B aseband-pulse-antenna techniques", I EEE Antennas and Propagation Magazine, Vol.36, No.1, February 1994. pp 20-30.
4. Jeong Soo L ee and C am N guyen, "N ovel low-cost ultra-wideband, ultra-short-pulse transmitter with M ESFET impulse-shaping ci rcuitry f or r educed di stortion an d improved pulse repetition rate", IEEE Microwave and Wireless Components Letters, Vol. 11, No. 5, May 2001, pp 208-210.
5. Robert J. Fontana, "Recent system applications of short-pulse ultra-wideband (UWB) technology", I EEE T ransactions on M icrowave T heory and T echniques, V ol.52, No.9, September 2004, pp2087-2104.
6. Shinho K im and Yuanxun Ethan W ang, "UWB pulse generation techniques with switched resonators", IEEE International Conference on UWB, Sept 2006, pp 91-95.


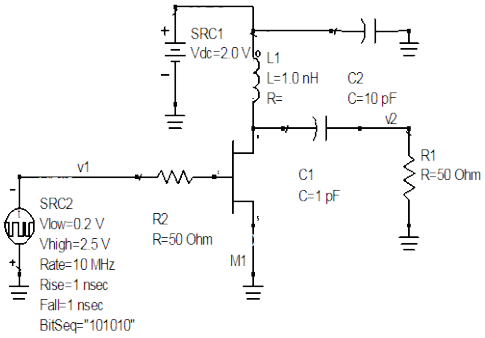


Fig 1: The generation of short pulse using MESFET.

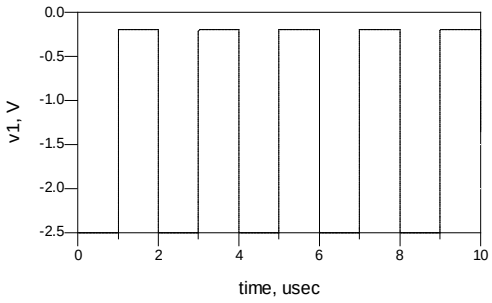


Fig. 2: The input waveform given to gate of MESFET.

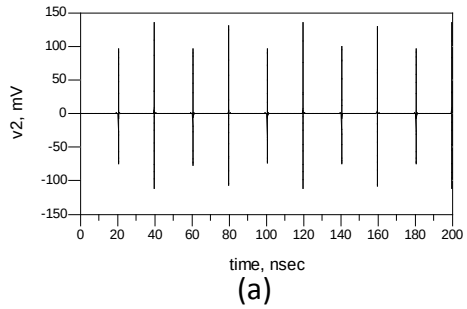


(a)

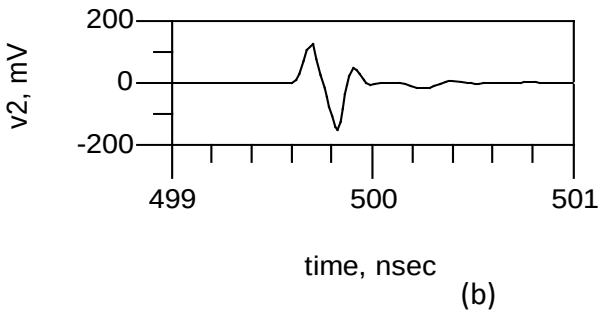


(b)

Fig. 3: (a) The output wave form of short pulse train using MESFET in time-domain. (b) The zoomed view of the output waveform

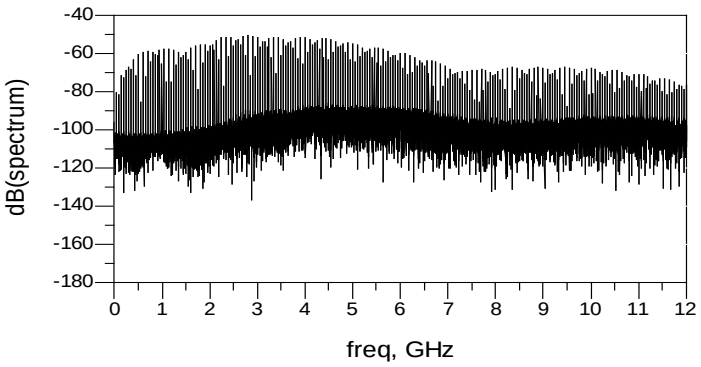


Fig. 4: The spectrum of short pulse using MESFET

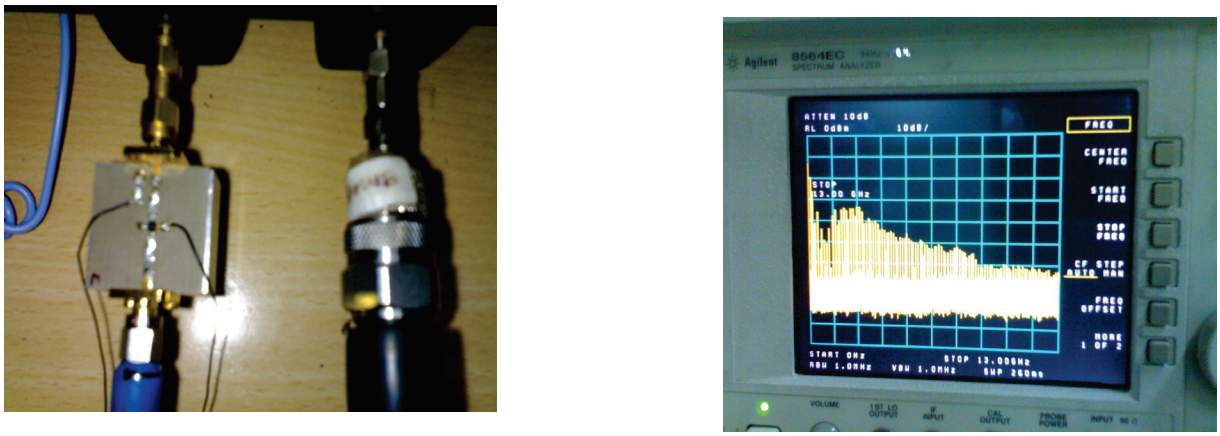

(a) (b)

Fig. 5. (a) Practical circuit for UWB pulse generation. (b) Frequency spectrum of UWB pulse.

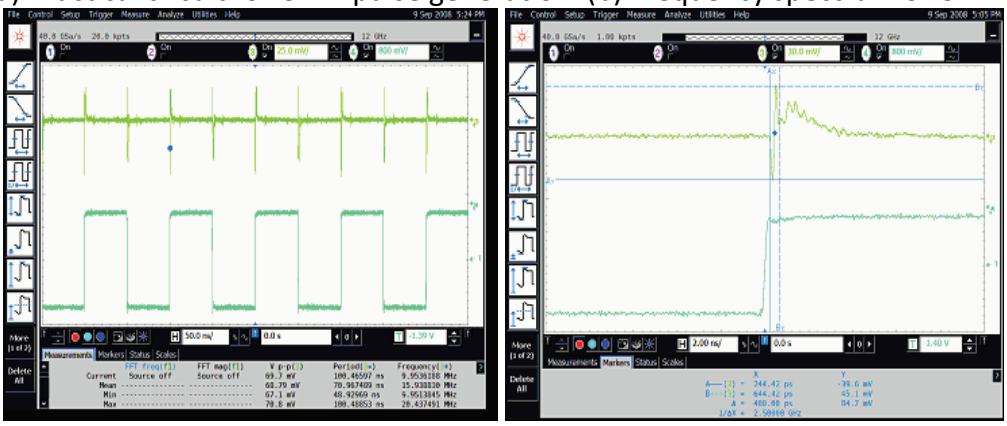

(a) (b)

Fig. 6.(a) The output and input wave forms of short pulse train using MESFET in time-domain.
(b) The zoomed view of the output waveform.

SEARCH

Previous Page Next Page

# DUAL RING SRR FREQUENCY ESTIMATOR

*Anju Pradeep, S.Mridula , P. Mohanan , C.K. Aanandan and K. Vasudevan*
Centre for Research in Electromagnetics and Antennas (CREMA)
Department of Electronics, Cochin University of Science and Technology
Kochi 682 022, Kerala, INDIA
Ph: +91 484 2576418 Fax: +91 484 2575800
e-mail: anjupradeep@cusat.ac.in

**ABSTRACT:**

The paper reports the frequency determination of a non magnetic dual ring Split Ring Resonator (SRR). An expression for the resonant frequency of the SRR is developed from exhaustive experimental and simulation studies. The study is conducted on an edge coupled dual ring SRR placed on a Microstrip transmission line working in the frequency band 1-8 GHz. A front end using Matlab™ (GUI) is also developed for calculating the resonant frequency of the dual ring SRR.

## 1. INTRODUCTION

Development of artificial materials has been a subject of growing interest in recent years. Electromagnetic waves interact with the atoms and molecules that compose naturally occurring materials. Materials can therefore be used to guide or manipulate electromagnetic waves, in the way a glass lens can focus light. But the available electromagnetic response from naturally occurring materials is limited. Artificially constructed materials, however, are not subject to the same limitations as real materials, and can be used to extend material response. Basically a metamaterial is an artificially engineered material that has highly desirable properties that do not occur in nature. In electromagnetism, a metamaterial is an object that gains its (electromagnetic) material properties from its structure rather than inheriting them directly from the materials it is composed of. Metamaterials are often a collection of small objects whose dimensions and separation are much less than the wavelength, behaving like a continuous material exhibiting exotic electromagnetic properties at microwave frequencies.

Two important parameters, electric permittivity and magnetic permeability determine the response of the materials to the electromagnetic propagation. Metamaterial media include artificial plasmas (which exhibit negative electric permittivity below their plasma frequency), negative magnetic permeability media (NMPM) and left-handed media (LHM- these are media with simultaneously negative electric permittivity and magnetic permeability). Negative permittivity can be obtained by arranging thin metallic wires periodically. These wires simulate plasma behavior at microwave frequencies. Since free magnetic charges are not present in nature, such approach does not provide negative permeability. However, NMPM can be built up by using small resonant metallic particles with very high magnetic polarisability. An artificial medium consisting of an aggregate of Split ring resonator (SRR) particles shows a negative permeability region near and above the resonant frequency. LHM can be fabricated by combining a periodic array of metal p with an array of SRR's. The continuous medium parameters describing the aforementioned SRR arrays can be predicted from their individual electromagnetic behavior near the resonances. The application of an axial, uniform, and time varying magnetic field to the rings nt loops at resonance. These current loops are closed through the distrib



Previous Page Next Page

edge capacitance between concentric rings; which can be potentially very high due to the presence of the splits and the particle behaves as an externally driven LC resonator. On account of the current circulation between rings and the relatively large value of the edge capacitance achievable, the electrical size of the particle can be made small at resonance. SRR's can thus be considered as lumped or quasi lumped elements. Current loops can also be induced by an axial, uniform time varying electric field. The arrangement shown in Fig.1(a) is used to evaluate the SRR resonances. Fig.1(b) illustrates the SRR parameters.

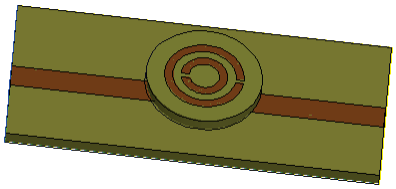

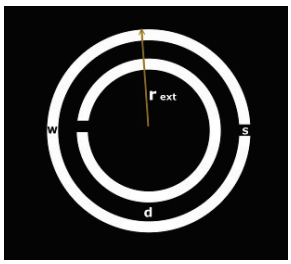


Fig.1(a). SRR coupled to a Microstrip transmission line
(b) SRR Parameters

The parameters considered are the external radius ($R_{ext.}$), width of ring(w), gap between rings(d), height(thickness) of substrate (h),r permittivity of substrate ($\varepsilon_r$). The width of the slit in ring(s) is optimised at 0.3mm.

## 2. DEVELOPMENT OF THE DESIGN EQUATION.

The parameter extraction of a 50 Ω Microstrip transmission line of length 25mm fabricated on a substrate of εr =4.4 and h=1.6mm was performed for a frequency range of 1 to 8GHz. The process was repeated after placing the SRR on the transmission line. Using curve fitting, equations for inductance and capacitance are found as follows.

$$L = 2.57e^{\frac{-w_3}{\sqrt{2}}}(\pi r - 2.2d_1 - \frac{\pi}{2}) \quad \text{..... ..(1)}$$

$$C = 0.217 + \left[\left(0.059(2r + er - 5)\right)(0.437w_1 - 0.317{w_2}^2 + 0.07{w_2}^3)\left(3.3367e^{-3.2d_1} - 0.1955e^{-0.47h}\right)\right] + (0.05er - 0.218) + \left(\frac{0.599h}{0.0248 + h} - 0.599\right) \quad \text{..... (2)}$$

where $w_1=w$; $w_2=w$; $w_3=w$; for d<1;
$w_1=w/3$; $w_2=1.414w$; $w_3=w/1.414$; for d>1
$d_1=d$; for d<1

The resonant frequency for SRR is calculated using the standard relation

$$F = \frac{1}{2\pi\sqrt{LC}} \quad \text{f or r >5.2; ..... (3)}$$

$$F = \frac{1}{2\pi\sqrt{LC}} + \frac{5.2-r}{2} \quad \text{for r<5.2; ..... .(4)}$$

SEARCH
Previous Page
Next Page

The validity of this relation is confirmed through experiment and simulation as detailed in Table.1.The graphical user interface for the SRR frequency estimator designed using Matlab$^{TM}$ is shown in figure.2.

| $R_{ext}$ mm | w mm | d mm | F(eqn) GHz | F(sim) GHz | %error |
|---|---|---|---|---|---|
| 8 | .3 | .2 | 1.19 | 1.2 | .83 |
| 5.8 | 1.3 | 1 | 2.57 | 2.59 | .7 |
| 5.4 | 1.4 | .5 | 2.60 | 2.63 | 1.1 |
| 5.7 | 1.7 | 1 | 2.91 | 2.88 | .6 |
| 4 | .2 | 1.5 | 3.4 | 3.05 | 1.7 |
| 3 | .3 | .9 | 4.22 | 4.11 | 2.6 |
| 2.6 | .4 | 1 | 5.3 | 5.21 | 1.7 |
| 2.2 | .3 | 1 | 6.4 | 6.27 | 2 |
| 2 | .3 | 1 | 7.4 | 7.45 | 0.6 |
| 1.9 | .3 | 1 | 8.15 | 7.97 | 2.2 |

Table.1. Validation of equation

## 3. CONCLUSION

The exhaustive experimental and simulation conducted on SRR clearly indicate the properties inherent to SRR and the external factors affecting it. It is observed that the resonant frequency is directly proportional to width of ring (w), gap between rings (d) and the height of substrate (h) and inversely proportional to the radius of SRR ($R_{ext}$) and the dielectric constant of the substrate. The validation of the equation is done through experiment and simulation. The intriguing physical properties of metamaterials can be made use in many important technological applications. Reduction of radiation hazards in mobile phones and reduction of radar cross section are few of them.

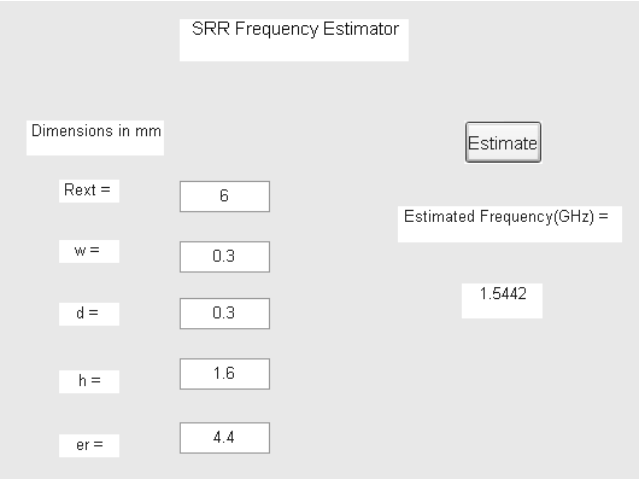


Fig.2. GUI – Frequency Estimator

SEARCH
Previous Page
Next Page

## 4. REFERENCES


1. K.Aydin, I.Bulu, K.Guven, M.Kafesaki, C.M.Soukoulis and E.Ozbay, "Investigation of magnetic resonances for different split ring resonator parameters and designs," New Journal of Physics, 168, 7, 2005
2. J.Garcia-Garcia and F.Martin, "On the resonances and polarizabilities of split ring resonators," Journal of applied Physics, 98, pp. 033103.1-9, 2005.

# COMPACT WIDEBAND BANDSTOP FILTER BY USING STEPPED IMPEDANCE RESONATOR

*Ajay Babu Gunutpalli*[(1)], *Subrata Sanyal* [(2)]

Department of Electronics and Electrical Communication Engineering
Indian Institute of Technology, Kharagpur,Kharagpur-721302, West Bengal.
ajaymicrowave@gmail.com[(1)]ssanyal@ece.iitkgp.ernet.in[(2)]

**ABSTRACT:**

In this study, a novel transmission line configuration consists of PI network using the Stepped impedance resonator (SIR) has been proposed to design a sharp-rejecting, compact wideband bandstop filter (WBBSF) with wide rejection-bandwidth. Stepped impedance Resonator (SIR) technique is used to obtain transmission zeros, and which provide the wide rejection characteristic. The 3dB , 20dB fractional Bandwidth (FBW) and Rejection bandwidth are controlled by the choosing the characteristic impedances of transmission lines. The WBBSF Filter is analyzed using transmission line model. Theoretical predictions have been verified by the Full Wave Electromagnetic Simulator (IE3D).Good agreements are obtained among theoretical prediction, Circuit Simulation and full-wave simulation.

## INTRODUCTION

Bandstop filter ( BSF) is an important component in microwave circuit applications and is often required to suppress unwanted frequency bands .In planar technology, conventional method of designing wide-stopband BSF uses different form of shunt/series stubs. The procedures to design BSFs in printed circuit technology may be divided into two broad categories. One is the so-called exact design consisting of shunt open-circuited stubs separated by transmission lines of appropriate length this method is applicable for design of narrow band as well as wide band BSFs. In the second method, a transmission line is coupled to resonators, either by capacitive gaps or by parallel-line couplings and the method is suitable for design of narrow band BSFs. Recently, another procedure Based on the signal interference technique [4] was reported for the design of a wideband BSF with sharp Rejection characteristics. The basic filter structure consists of PI network containing two open ended stubs. Bandstop behavior is obtained because of open ended stubs. . Wide-stopband characteristics also can be obtained by using defected ground planes structures (DGS). But, the problem with DGSs is the Backside radiation loss, which increases with frequency. Recently, another method based on signal interference technique has been reported for designing a wide stopband BSF having sharp rejection characteristics but it occupies larger size when compared to the proposed design

In recent years uniplanar transmission lines such as coplanar waveguides (CPW), coplanar strip (CPS), and slot line (SL) have become preferable over conventional microstrip lines with an increasing use in monolithic or hybrid integrated circuit applications at microwave frequencies, owing to their small dispersion, low radiation, easy integration with lumped elements or active devices, high circuit density, and no need for via holes. Many [illegible]mponents using uniplanar structures have been developed. However, uniplanar wideband bandstop filters to reject out-of-band frequencies have not been sufficiently

considered in microwave literature, whereas bandstop circuits are one of the most important parts of many passive and active microwave and millimeter-wave devices employed to suppress the harmonics. Some frequency bands in microwave applications can be filtered using quarter-wave open-end or short-end stubs along a transmission line or stepped-impedance structures [4].In [4] SIR has been used to achieve the dual band charecterstics.In this work stepped impedance resonator (SIR) is used to obtain the desired characteristics, simple transmission line approach has been used to analyze the circuit.

**FILTER DESIGN**

The basic BSF configuration has been shown in Figure 1(a). The conventional band stop filter is shown in the figure1(a)is designed @1.4Ghz.For Wide band BSF signal interference technique has been proposed in [8]. The Standard PI network with open ended stubs produces a single stop band BSF response is shown in the figure1(a). Here all the impedances Za, Zb are selected as $50\,\Omega$, and of electrical length $90^{O}$ .The rejection level can be varied by changing the impedances of the open ended stubs. The circuit simulated and full wave simulated results are compared and shown in the figure2.For the same operating frequency DBBSF is designed and simulated results shows that dual band is achieved around the operating frequency @1.4Ghz.[Fig1]

**STEPPED IMPEDANCE RESONATOR:**

The basic SIR responses were shown in fig1.The impedances were chosen according to the design graphs given in Fig1. Transmission line approach was used to derive the equivalent for the given impedance, electrical length. The electrical length $\theta_2$ and impedance $Z_2$ are set as $26^{O}$ and $76.4\,\Omega$ respectively. With $100\,\Omega$ and $15.75^{O}$ being assigned to $Z_{2B}$ and $\theta_{2B}$ respectively, the transformed impedance [from equations (1) and (2)] $Z_{2A}$ and the electrical length $\theta_{2A}$ can be derived as $57\,\Omega$ and $6.85^{O}$ respectively. Here the proposed circuit was designed at the operating frequency of (f1=)2 GHz, such that all the electrical lengths were multiplied by a factor of 3.So The Electrical lengths for the present circuit become $47.25^{O}$ , $20.55^{O}$ .The impedance for the middle open stub were chosen by optimization in the ansoft designer student version.

**PROPOSED DESIGN:**

The proposed design for wide band bandstop Filter is shown in the figure 3(a). The PI network which is shown in figure2 (a) possess dual band bandstop (DBBSF) charecterstics.The Circuit Full wave simulated response shown in fig 2(b), here the operating frequency was chosen as 1.4@Ghz.The proposed design is obtained by the cascade connection of the two such PI networks, here all the open ended stubs were replaced by the SIR, the middle stub having uniform characteristic impedance obtained by the taking the equivalent for the two parallel open stubs. The stubs at the input and output ports were replaced by the SIR. The impedances for the SIR were obtained from the equation 1 and 2.The set of values for the proposed design are obtained as

$Z_1$=$100\,\Omega$ , $\theta_1=90^{O}$ , $Z$ =$35.5\,\Omega$ , $\theta=47.25^{O}$ , $Z_{2A}$=$57\,\Omega$ , $\theta_{2A}=20.55^{O}$ , $Z_{2B}$=$100\,\Omega$ , $\theta_{2B}=47.25^{O}$ .He re $Z$ , $\theta$ , were chosen by the optimization in the ansoft designer student version. The Circuit simulated and full wave simulated results were compared and shown in Fig 3(b).

## 3. FULLWAVE SIMULATION AND FABRICATION

Theoretical circuit which is designed at operating frequency of 2Ghz is simulated by using Full simulation and optimization engine (IE3D).The lay out of WBBSF is shown in the figure 5, The lengths and widths obtained by line gauge were given in the lay out. The simulation result shows that the 3 dB, 20dB rejection bandwidth of the filter are 109%, 70% respectively. The rejection level in the stop bands is 30dB; the return loss in the pass bands is almost below 10dB.The two transmission zeroes were created in the stop band by using the SIR technique. The lay out which is given in the Fig5 can be fabricated on RT Duriod Substrate with dielectric constant $\varepsilon_R$ =2.2, thickness of substrate=.381mm.

## 4. CONCLUSION

A compact Wideband bandstop (WBBSF) is designed by using the stepped impedance resonators. The main advantage of the proposed design is that it can be meandered so that it occupies a very compact in size of $28.3 \times 14.2\, mm^2$ [3,6],The rejection 3dB rejection bandwidth of the filter was 109%, the 20dB rejection bandwidth of the filter was 70%.The filter was analyzed by using the simple transmission line approach. The proposed circuit was very compact, wide bandstop with high rejection level, and excellent out of band performance when compared to the designed proposed designs in the literature. The simulated results were excellent in comparison with circuit simulated results.

## ACKNOWLEDGMENT

The authors wish to deeply acknowledge Mr. Vamsi Krishna velidi for giving the valuable suggestions in preparing this work.

## REFERENCES

1. Matthaei g.l., Young l., Jones E.m.t.: 'Microwave filters, impedance-matching network, and coupling structures' (Artech House, Norwood, MA, 1980)
2. Hong j.s.,Lancaster M.J'Microstrip filters for RF/microwave application'(Wiley,New York, 2001)
3. Mandal M.K., Sanyal S.: 'Compact bandstop filter using signal interference technique', IET Electron. Lett., 2007, 43, (2), pp. 110–111
4. Kuo-sheng chin, Member, IEEE, jun-hong yeh, and shuh-han chao," Compact Dual-Band Bandstop Filters Using Stepped-Impedance Resonators" IEEE Microwave and Wireless Components Letters, vol. 17, no. 12, december 2007.
5. M.K.Mandal,P.Mondal, "Design of sharp-rejection, compact, wideband bandstop filters" IET Microw. Antennas Propag, 2008, Vol. 2, No. 4, pp. 389–393, 2008.
6. Mrinal kanti mandal,K divyabramham, and Subrata sanyal" design of compact, wide-band Bandstop filters with sharp rejection characteristics", MOTL, vol. 50, no. 5, may 2008.

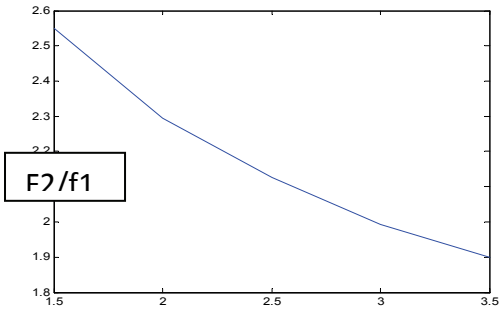


Fig1 (a) f2/f1 variation Vs Z2B/Z2A ratio.

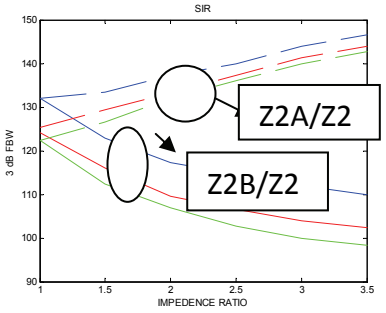


(b) FBW variation Vs Impedance ratio.

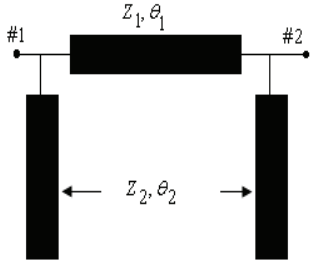


Fig1 (a) Conventional BSF

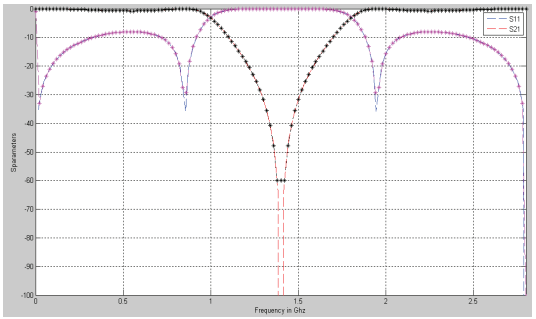

(b) Circuit Computed and Full wave Simulated Responses

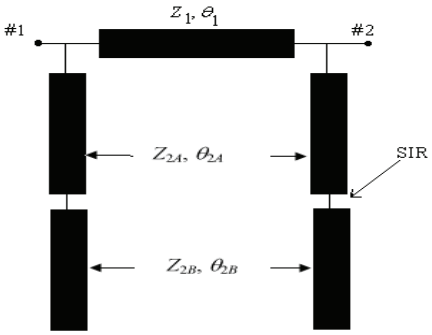


Fig2 (a) DBBSF Using SIR

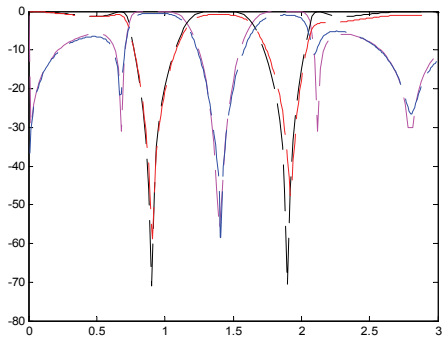

(b) Circuit Computed and Full wave Simulated Responses

SEARCH

Previous Page

Next Page

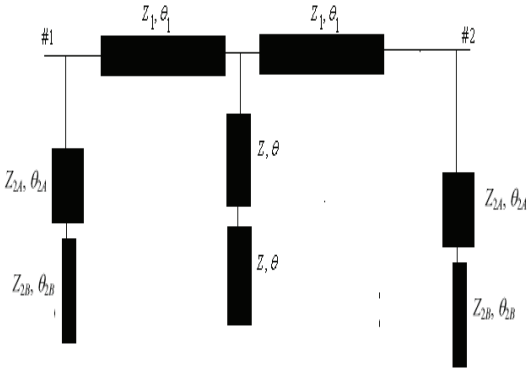


Fig3 (a) Proposed WBSF.

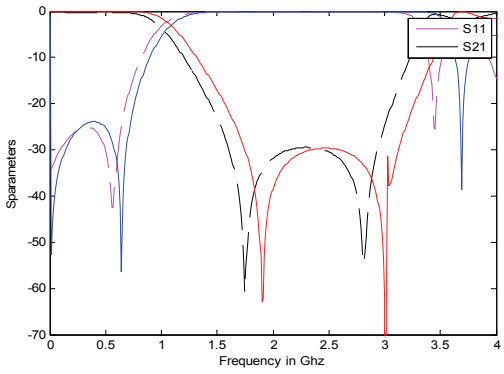


(b) Circuit and Full wave Simulated Responses Comparison

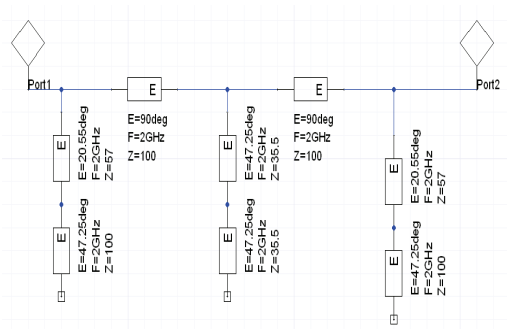


Fig4: Circuit Schematic for proposed filter

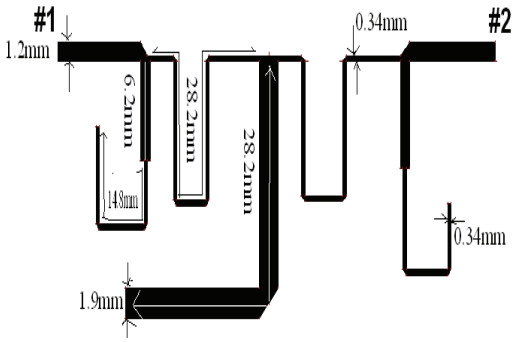


Fig5: Microstrip Layout of the filter.

SEARCH

Previous Page

Next Page

# FINITE ELEMENT ANALYSIS OF SEMICYLINDRICAL DIELECTRIC RESONATOR BASED FILTER

*Jaimon Yohannan, K. Vasudevan and K. T. Mathew*
Department of Electronics, Cochin University of Science and Technology,
Cochin, 682022, Kerala, India,
E.mail: jaimonyohannan@yahoo.com

## ABSTRACT:

Microwave dielectric resonator loaded multiple cavity filter is designed and fabricated. A 3-D finite element technique is used for the simulation of electric and magnetic field distribution and current density. Microwave band pass filter characteristics are studied by measuring the return loss and transmission characteristics of the multiple cavity resonators. The measured transmission characteristics show that it has 8.5 MHz bandwidth at the resonant frequency at 1752.2 MHz. By using Ansoft's HFSS for numerical simulations, electric field, magnetic field and vector $J_{vol}$ field distribution are simulated. The numerical results of the semicylindrical DR loaded multiple cavity filter is in good agreement with experimental measurements.

## INTRODUCTION:

Dielectric resonator (DR) loaded cavity filters are widely used in ground and satellite based communication systems. They exhibit excellent in-band performance over a wide temperature range as well as less volume and mass compared to conventional metal cavity filters [1, 2, 3]. $HE_{11\delta}$ mode DR, often used in dual degenerate mode [4], gives further size and mass reduction with slightly lower Q, reduced spurious performance and even smaller tuning range. The objective of the study is to avoid intensive experimental work and allow the use of arbitrarily shaped elements. This article presents a FEM analysis of a microwave dielectric resonator filter. The Ansoft' high frequency structure simulator (HFSS) is used to design and simulate the 3D structure of the DR filter.

## DESIGN AND IMPLEMENTATION:

Dielectric resonator bandpass filters can be realized by axially spaced semi-cylindrical dielectric resonators of relatively high permittivity. The resonators are placed in a circular waveguide section operating below cutoff, and the entire filter component is embedded in a rectangular metallic structure. Since microwave materials with high $\varepsilon_r$, low tanδ and good temperature characteristics are available, these types of filters become increasingly attractive when short filter components are required. The photograph of the multiple cavity filter are shown in figure 1 (a). The filter consists of a rectangular metallic enclosure, comprising four cylindrical cavities, coupling windows, co-axial probes. The enclosure main body is provided with input/output terminals. The frequency response such as pass band and attenuation characteristics of the cavity filter are generally determined by the resonant frequency and Q factor of each of the resonators, and the amount of coupling between the individual dielectric resonators. Therefore the configuration and the dimensions of each of the resonators are calculated at the design stage. The height and diameter of the cylindrical cavity are 29 mm respectively and the width and height of the coupling windows are 4 mm, 29

respectively. Four semi cylindrical dielectric resonator of dimension 12.5 mm radius and 15 mm height having dielectric constant 83, are prepared. These semicylindrical dielectric resonators are loaded inside the cylindrical cavities. The s-parameters, electric field, magnetic field and current field distributions are simulated. The return loss and transmission characteristics measurements are done using Agilent 8714 ET Network Analyzer, in the frequency range 1000 MHz to 3000 MHz.

**RESULTS AND DISCUSSIONS:**

A typical dielectric resonator filter consists of a number of DRs mounted inside cavities machined in a metallic housing. Figure 1 (a) illustrates a four-pole version of a semicylindrical dielectric resonator filter. The probes are used to couple the input and output RF energy, while the irises are used to provide the necessary coupling between resonators. By using Ansoft's HFSS for numerical simulations, the device's electric vector field, magnetic vector field and vector $J_{vol}$ field distribution can be visualized in the computer model which simplifies design process. The FEM analysis permits accurate parameter design and predictions of field that are difficult to measure. The resonant frequency of each semi cylindrical dielectric resonator depends on the height, radius and dielectric constant. In this filter, all the four semi cylindrical DR operate in the cut off frequency range of the cavities.

Figure 1 (b) shows simulated $S_{22}$ and $S_{12}$ characteristics of the design. Figure 1(c & d) show the measured return loss ($S_{22}$) and transmission characteristics ($S_{12}$) of the filter. The first resonant frequency is at 1752.2 MHz with a 10 dB bandwidth of 8.5 MHz. The numerical results of the co-axial fed multiple cavity filter are in good agreement with the experimental results.

Figure 2 (a) shows HFSS design of multiple cavity filter loaded with semi cylindrical dielectric resonators, showing triangular meshing. Figure 2 (b & c) shows the top and side view of electric field distribution inside the multiple cavity filter loaded with dielectric resonators. Figure 3 (a) shows the top view of magnetic field distribution whereas fig. 3 b shows the side view of the multiple cavity filter, loaded with dielectric resonators. Figure 3c shows the simulated surface current distribution over the semicylindrical DR. From the electric field and magnetic field distributions it is evident that the field is very strong in the first input cavity. The field strength decreases significantly as it passes through the 2nd, 3rd and 4th cavities. Thus only the resonant frequency is transmitted, whereas the other frequency bands are attenuated. The cavity along with the DR serves as a resonant band pass filter operating in the L-band. The pass band frequency can be tuned by varying the dimensions of the DR.

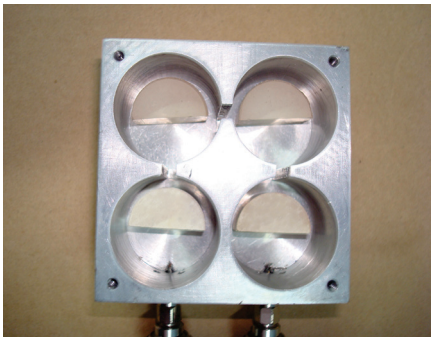

a

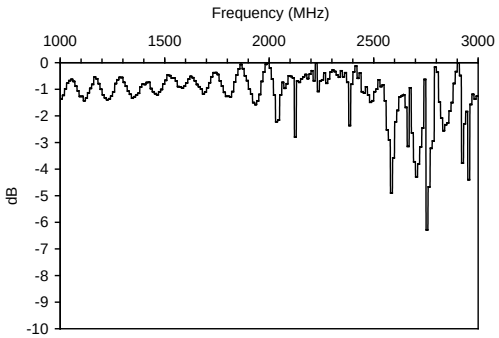


c

SEARCH
Previous Page
Next Page

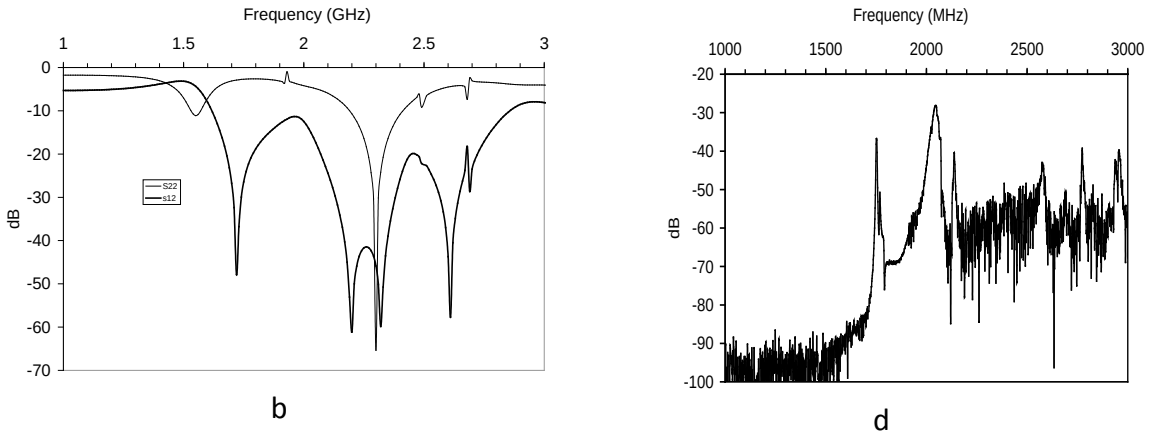


Figure 1. (a) Photograph of semicylindrical DRs mounted inside cavities machined in a metallic housing, (b) Simulated $S_{22}$ and $S_{12}$ characteristics, (c) return loss measured and (d) measured transmission characteristics.

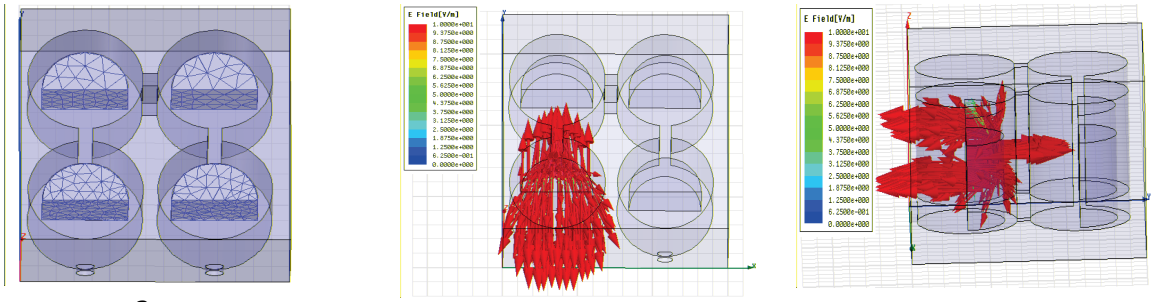


Figure 2 (a) Design of multiple cavity filter loaded with semicylindrical DRs, showing triangular meshing, simulated using Ansoft HFSS software, and (b & c) shows the top and side view of electric field distribution of the multiple cavity filter loaded with dielectric resonators.

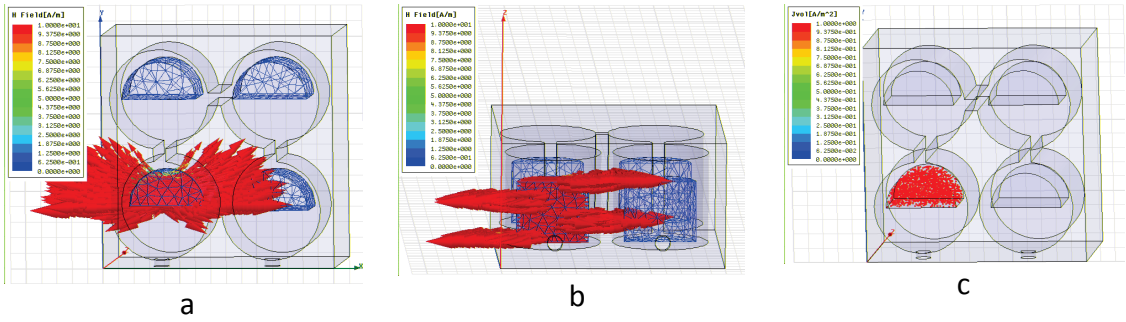


Figure 3 (a & b ) shows the top and side view of magnetic field distribution of the multiple cavity filter loaded with dielectric resonators and (c) shows the surface current distribution.

SEARCH

## CONCLUSIONS:

A class of dielectric resonator filters in waveguide sections below cut off has been designed. In comparison with conventional evanescent-mode reso

Previous Page Next Page

coupling, the proposed resonator coupling via a triple rectangular waveguide section features a better pass band separation and improved stop band attenuation. Furthermore, the filter component can be reduced by up to 50% or more. Microwave band pass filter characteristics are studied by measuring the reflection and transmission characteristics of the multiple cavity resonator filters. The measured transmission characteristics show that it has a resonant transmission frequency at 1752.2 MHz with 8.5 MHz bandwidth. By using Ansoft's HFSS for numerical simulations, electric field, magnetic field and vector $J_{vol}$ field distributions are simulated. The numerical results of the DR loaded multiple cavity filter is in good agreement with experimental measurements.

**ACKNOWLEDGMENTS:**

The research was supported by DST, Ministry of Science and Technology, New Delhi, India. The authors thankfully acknowledge the financial support extended through DST SERC Fast Track Project.

**REFERENCES:**

1. FEM analysis of semicylindrical dielectric resonator loaded multiple cavity filter., Jaimon Yohannan, K. Vasudevan and K. T. Mathew, *IEEE AP-S/URSI Int. Symp., San Diego, CA, USA, July 5-12, 2006.*
2. S. J. Fiedziuszko, I. C. Hunter, T. Itoh, Y. Kobayashi, T. Nishikawa, S. N. Stitzer, K. Wakino, "Dielectric Materials, Devices, and Circuits", IEEE Trans. Microwave Theory and Tech., Vol. MTT-50, pp706-720, Mar. 2002.
3. C. Kudsia, R. Cameron, W. Tang, "Innovations in Microwave filters and Multiplexing Networks for Communication Satellite Systems", IEEE Trans. on Microwave Theory and Techniques, Vol. 40, June 1992, pp 1133-1149.
4. S. J. Fiedziusko, "Dual-mode Dielectric Resonator Loaded Cavity Filters", IEEE Trans. Microwave Theory and Tech., Vol. MTT-30, pp1311-1316, Sept. 1982.

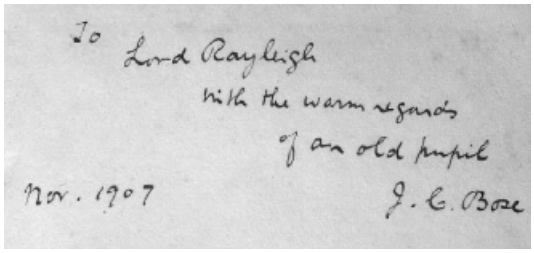


## RESEARCH SESSION IV
## MICROWAVE PROPAGATION I

SEARCH

Previous Page

Next Page

SEARCH

Previous Page

Next Page

## RESEARCH SESSION IV

## MICROWAVE PROPAGATION I

***Chairs : Prof. T.K. Sarkar, Syracuse University, USA***



SEARCH

Previous Page Next Page

# REDUCTION OF CO-CHANNEL INTERFERENCE IN CELLULAR SYSTEMS

*Dr MC Chandra Mouly, Dr K Srinivasa Rao, Dr D Srinivasa Rao*, L Rangaiah*
Department of Electronics and Communication Engg, TRR College of Engg.,
Hyderabad - 502 319, INDIA,
rleburu@gmail.com
*JNTU College of Engineering, Hyderabad - 500 072

**ABSTRACT :**

In this paper, a method to reduce the co-channel interference in cellular systems employing Directional Antennas developed by the authors has been presented.

## INTRODUCTION :

While the frequency reuse method enhances the spectrum utility, it obviously results in co-channel interference since the same frequency band is used repeatedly in different channel cells by different users.

In most mobile radio environments, use of a seven cell reuse pattern is not sufficient to avoid co-channel interference. Increasing frequency-reuse pattern ie., making K > 7 would reduce the number of channels per cell and spectrum efficiency. Therefore, it might be advisable to retain the same number of radios as in the seven cell system but to sector the cell radially. This technique would reduce the interference, resulting in the use of channel sharing and channel borrowing schemes to increase the spectrum efficiency.

## 2. DETERMINATION OF CO-CHANNEL INTERFERENCE AREA

Two tests are available for this purpose.

### 2.1 TEST 1 : FROM A MOBILE RECEIVER :

When Co-channel interference occurs in one channel, it will equally occur in all other channels. The co-channel interference can be measured by selecting any one channel and transmitting on that channel, at all co-channel sites, at night while the mobile receiver is traveling in one of the co-channel cells. While performing this test, .any change detected by a field strength recorder in the mobile unit and comparing the data with the condition of no channel sites being transmitted. This test has to be repeated as the mobile unit travels in every co-channel cell. To facilitate this test, install a channel scanning receiver in moving vehicle. One channel ( $f_1$) records the signal level (no co-channel condition), second channel ( $f_2$) records the interference level (six channel condition is the maximum), third channel receives $f_3$, recorded only in $f_3$, which is not in use. Therefore, the noise level is recorded only in $f_3$. The carrier to interference ratio C / I can be obtained by subtracting the result obtained from $f_2$ and the result obtained from $f_1$ (Carrier minus Interference C – I). Carrier to Noise ratio C / N can be obtained by subtracting the result obtained from $f_3$ from the result obtained from $f_2$ (Carrier minus Noise C – N).

Four conditions are used to compare these results.

I. If C / I is greater than 18 dB throughout most of the cells, the system is properly designed.

SEARCH
Previous Page
Next Page

II. If C / I is less than 18 dB and C / N is greater than 18 dB in some areas, there is co-channel interference.

III. If both C / N and C / I are less than 18 dB and C / N ≈ C / I in a specific area, there is a coverage problem.

IV. If both C / N and C / I are less than 18 dB and C / N > C / I in a specific area, there is a coverage problem and co-channel interference.

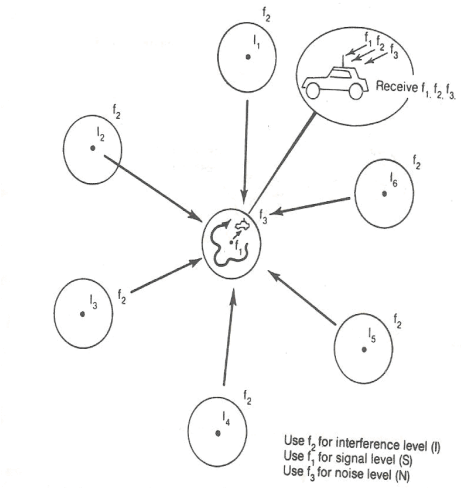


Fig1 Test 1: Co-Channel Interference at the Mobile Unit

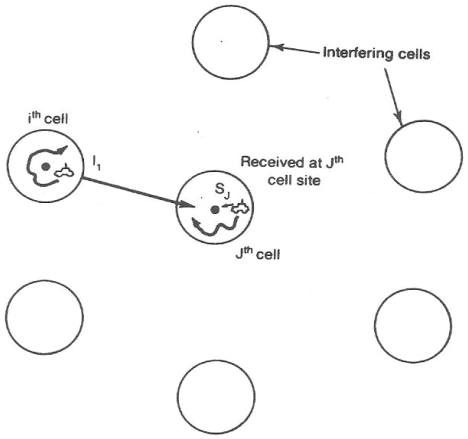


Fig2 Test 2: Co-Channel Interference at the Cell Site

## 2.2 TEST 2 : FROM A CELL SITE :

The areas in an interfering cell in which the top 10 per cent level of the signal transmitted from the mobile unit in those areas is received at the desired site. This top 10 per cent level can be distributed in different areas in a cell. The average value of the top 10 per cent level signal strength is used as the interference level from that particular interfering cell. The mobile unit also travels in different interfering cells. Up to six interference levels are obtained from a mobile unit running in six interfering cells. Then calculate the average of the bottom 10 per cent level of the signal strength which is transmitted from a mobile unit in the desired $j_{th}$ cell and received at the desired cell site as a carrier reception level. The carrier to interference ratio received in the $j_{th}$ cell site will be as follows.

$$C_j / I = C_j / \sum_{i=I,\, i \neq j}^{6} I_i \qquad \text{----------(1)}$$

The number of co-channel cells in the system can be less than six. Therefore a translation from decibels to linear is needed before summing all the interfering sources. The test can be carried out repeatedly for any specified cell. Compare $C_j / I$ and $C_j / N_j$ and determined the co-channel interference condition. $N_j$ is the noise level in the $J_{th}$ cell assuming that no interference exists.

## 3. DESIGN OF A DIRECTIONAL ANTENNA SYSTEM

When the call traffic begins to increase, use the frequency spectrum efficiently to avoid increasing the number of cells K in a seven cell frequency-reuse pattern. When K increases the number of frequency channels assigned in a cell may become less and the frequency-reuse scheme decreases.

SEARCH
Previous Page
Next Page

Instead of increasing the number K in a set of cells, Directional antenna arrangement is K = 7 is choosen. The co-channel interference can be reduced by using directional antennas. This means that, each cell is divided into three or six sectors and use three or six directional antennas at a base station. Each sector is assigned a set of frequencies.

### 3.1 DIRECTIONAL ANTENNA IN K = 7 CELL PATTERN

**Three Sector Case :** To illustrate the worst case situation, two channel cell scheme shown in Fig(3.a). The mobile unit at position E will experience greater interference in the lower shaded cell sector than upper shaded cell-sector site. This is because the mobile receiver receives the weakest signal from its own cell but fairly strong interference from the interfering cell. In a three-sector case, the interference has affected in only one direction because the front to back ratio at a cell site directional antenna is at least 10dB or more in a mobile radio environment. Because of the use of directional antennas, the number of principal interferences is reduced from six to two. The worst case of C / I occurs when the mobile unit is at position E, at which point the distance between the mobile unit and the two interfering antennas is roughly (D+R/2). However, C / I can be calculated more precisely as follows :

$$(C / I)_{\text{worst case}} = R^{-4} / [(D+0.7R)^{-4}+D^{-4}] = 1 / [(q+0.7R)^{-4}+q^{-4}] \quad \text{-------- (2)}$$

q=4.6, then Eq(2) becomes

$$(C / I)_{\text{worst case}} = 285 = 24.5 \text{ dB} \quad \text{---------- (3)}$$

The C / I received by a mobile unit from the 120° directional antenna sector system expressed in Eq.(3) highly exceeds 18 dB in the worst case. Eq.(3) shows that using directional antenna sectors can improve the Signal to Interference ratio, i.e., the co-channel interference gets reduced. In reality the C / I could be 6 dB weaker than Eq.(3). In heavy traffic area, as a result of irregular terrain and imperfect site locations. The remaining 18.5 dB of C / I is adequate.

**Six Sector Case :** The cell can be divided into six sectors by using six 60° beam directional antennas shown in Fig(3.b). In this case only one instance of the interference can occur in each sector. The C / I is

$$(C / I) = R^{-4} / (D+0.7R)^{-4} = (q+0.7)^{4} \quad \text{---------- (4)}$$

For q=4.6, the above equation becomes C / I = 29 dB, results in a further reduction of co-channel interference. When heavy traffic occurs, the $60^0$ sector configuration can be used to reduce co-channel interference.

### 3.2 DIRECTIONAL ANTENNA IN K = 4 CELL PATTERN

**Three Sector Case :** To obtain the C / I as in Sec 3.1. The 120° directional antennas used in the sectors reduce the interferers to 2 as in the K=7 system.

$$(C / I)_{\text{worst case}} = R^{-4} / [(q+0.7)^{-4}+q^{-4}] = 20 \text{ dB} \quad \text{---------- (5)}$$

If 6 dB is subtracted from the result , the remaining 14 dB is unacceptable.

**Six Sector Case :** There is only one interferer at a distance D+R shown in Fig(3.b) with q = 3.46

$$(C / I)_{\text{worst case}} = R^{-4} / (D+R)^{-4} = 1 / (q+1)^{-4} \quad \text{-------- (6)}$$

If 6 dB is subtracted from the result, the remaining 21dB becomes inadequate. Under heavy traffic conditions, there is still a great deal of concern over using a K = 4 cell pattern in 60° sector.

SEARCH

Previous Page Next Page

## 4. COMPARING K = 7 AND K = 4

A K = 7 cell pattern system is a logical way to begin the design of an omni-cell system. The co-channel reuse distance is more or less adequate, according to the designed criterion. When the traffic increase a three sector system should be implemented, i.e. with three 120° directional antennas in place. In certain hot spots 60° sectors can be used locally to increase the channel utilization. If a given area is covered by both K=7 and K=4 cell patterns and both patterns have a six sector configuration, then the K=7 system has a total of 42 sectors, but K = 4 system has a total of 26 sectors. One advantage of 60° sectors with K=4 is that they require fewer cell sites than 120° Sectors with K = 7. Two disadvantages of 60° (1) They require more antennas to be mounted on the antenna mast. (2) They often require more frequent handoffs because of the increased chance of that the mobile units will travel across the six sectors of the cell.

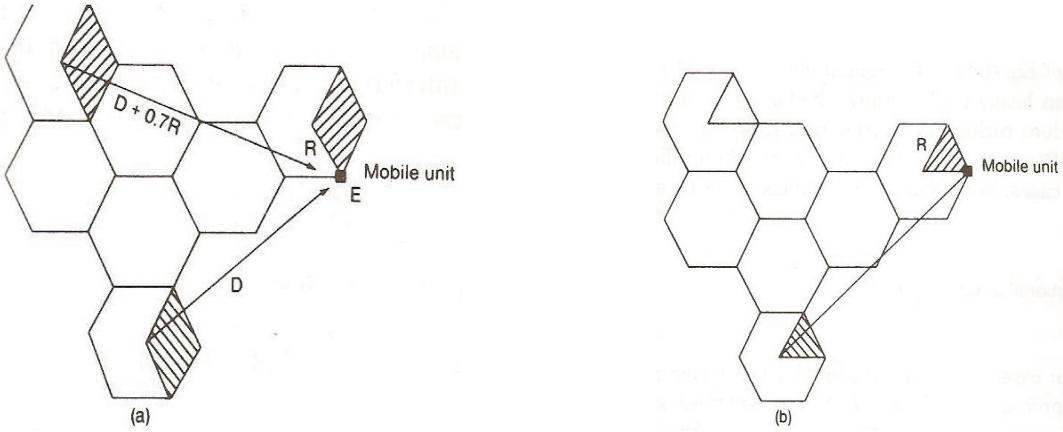


Fig 3 Determination of Carrier-to-Noise ratio C / I in a directional antenna system (a) Worst case in a 120° directional antenna system (N = 7), (b) Worst case in a 60° directional antenna system (N = 7)

**ACKNOWLEDGEMENT :**

The authors remain beholden and grateful to the scientists of the CUSAT and organizers of the **APSYM – 2008** for the encouragement given by them to present this paper at this august forum.

## CONCLUSION:

In mobile environment, use of a seven cell reuse pattern is not sufficient to reduce co-channel interference. Increasing frequency-reuse pattern with K > 7 would reduce the number of channels per cell and spectrum utility. Therefore, it might be advisable to retain the same number of radios as in the seven cell system but to sector the cell radially. This technique would reduce the interference optimally. The co-channel interference can be reduced by using directional antennas. This means, division of each cell into three or six sectors and the use of three or six directional antennas at a base station.

SEARCH

Previous Page Next Page

**REFERENCES :**


1. W C Y Lee, Statistical Analysis of the Level Crossings and Duration of Fades of the Signal from an Energy Density Mobile Radio Antenna, Bell System Technical Journal, vol 46, Feb 1967, pp 417 - 448.
2. Theodore S. Rappaport, Wireless Communications -- Principles And Practice, 2nd Ed, PHI, 2002.
3. William C Y Lee, Mobile Cellular Telecommunications – Analog And Digital Systems, 2nd Ed, Tata McGraw-Hill, 2006.
4. S. Kozono and M. Sakamoto, Channel Interference Measurement in Mobile Radio Systems, Procedings of the 35th IEEE Vehicular Technology Conference, Boulder, Colorado, May 21-23, 1985, pp. 60 - 66.
5. V. H. MacDonald, The Cellular Concept, Bell System Technical Journal, vol.58, January 1979, pp. 15-42.
6. S.N. Ahmed and P.C Constantinon, A Mobile Intereference Model into UHF Television Receivers, IEEE Transactions on Vehicular Technology, vol.VT – 32, May 1983, pp.206-208.

# ELECTROMAGNETIC MODELING OF POWERLINE CHANNEL

*Syed Samser Ali (1) and Amithabha Bhattacharya (2)*
(1) Department of Electronics and Communication Engineering
Durgapur Institute of Advanced Technology and Management,
Durgapur,West Bengal-713212, India,
Email: samserali@rediffmail.com
(2) Department of Electronics and Electrical Communication Engineering
Indian Institute of Technology, Kharagpur
West Bengal-721302, India.
Email: amitabha@ece.iitkgp.ernet.in

## ABSTRACT

A new technique for modeling three conductor transmission line based powerline channel has been introduced in this paper. Parameters of three conductor line are varied to incorporate the effects of multipath and impedance mismatches. Finally frequency response of the channel is calculated. The model could be gainfully used to study the effects of Electromagnetic Compatibility, Performance Analysis and so on. The paper also suggests some ways to improve the precision of the said method.

## INTRODUCTION:

The electric power network is an important medium for internet connectivity and home networking [1, 2]. The major reason behind such an importance lies in the fact that they are already installed and cost effective. Since the systems connected to powerline network encounters hostile channel properties like multipaths and impedance mismatches, the task of modeling the channel still remains a challenging one. There have been efforts in the past by employing both bottom-up and top-down strategies to mitigate such challenges. There have been also methods based on scattering matrix [3] and four-pole impedance and admittance values [4 - 6], derived from the components property. The above models are valid below the frequency range of 150 KHz. Therefore the analysis of electromagnetic compatibility cannot be carried out using such models. Another model based on the top-down approach has been reported in [7] where the relevant parameters are not derived from component properties and it requires an idea about the overall network topology. Also the above model is validated only up to a frequency of 20 MHz. In this paper, a novel method of modeling is proposed based on the top-down approach [7]. It uses the measured frequency response of the channel, along with the length, attenuation constant and characteristic impedance of the main distribution line. It requires no knowledge about either the network topology or the multi-paths and impedance mismatches involved.

## METHODOLOGY:

A typical three conductor transmission line modeled using distributed parameter SEARCH shown in Figure 1. The three conductor line is similar to a two conductor line except for the existence of crosstalk. The effect of crosstalk is included by the mutual components ($l_m$, $C_m$, $g_m$). The two conductor transmission line model can be readily extended to analyze the

Previous Page Next Page

radiated emissions and susceptibility of the line. Computational techniques such as Finite Difference Time Domain (FDTD) is used to study the radiated susceptibility of the line.

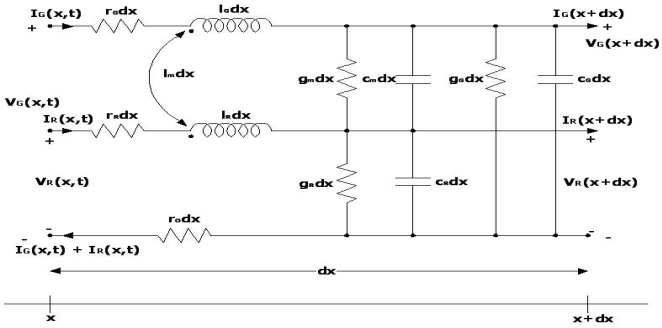


**Fig 1**. The parameters of a typical Three Conductor Transmission Line

Powerline Channel is finally modeled as a three conductor transmission line using the measured frequency response. The procedure begins with identifying the main distribution line of the network. Then using the characteristic impedance and attenuation factor of the main line, corresponding distributed parameters are calculated at some frequency higher than that of our interest. These values are then substituted for the line parameters of the three conductor transmission line model. Here it is assumed that the model is immersed in a homogenous medium whose parameters are fixed to particular predefined values. The three conductor transmission line is assumed to be of same length as that of the main distribution line of the network. This helps in the analysis of electromagnetic compatibility problems with ease. The main fact that attributes to the hostility of the Powerline Channel is the numerous impedance mismatches and multipaths that exist in the network topology. The proposed method includes the effects of such factors in the values of the mutual components, keeping other parameters constant. Then using an one dimensional search algorithm, the value of the mutual inductance is varied until the frequency response of the model matches with that of the measured one. The variation in the mutual inductance automatically leads to the variation in the other mutual component values through the basic relation between them [8]. The important feature of the proposed method lies in the fact that the channel is modeled using very few parameters and by varying only one of them. Hence a simple one dimensional search algorithm can be used for the purpose.

**RESULTS:**

For verification of the method through simulation, frequency response of the channel given in [7] is used. The aforementioned frequency response is claimed to be valid from 500 KHz to 20 MHz. The main distribution line in that topology is identified as type NAVY 150 cable with characteristic impedance (Z) of 45 Ω with a length of 200 m. Using the above values along with its attenuation profile ($\alpha = 7.8 \times 10^{-10} \times f$) and a zero conductance per unit length, as given in [7], inductance (L) per unit length is calculated using the relation shown below as in [9], at a frequency of 35 MHz.

$$L = Z / V. \quad (1)$$

$$C = L / Z^2. \quad (2)$$

$$r = ((2\alpha^2 + \omega^2 LC)^2 - \omega^4 L^2 C^2) \; / \; \omega^2 C^2)^{1/2}.$$

In the above relations, V is the phase velocity, C is the capacitance per unit length, r is the resistance per unit length and ω is the angular frequency. The same values of per unit length parameters are used for each of the corresponding elements in the lines of the model as in (4) and (5). These values are tabulated in Table 1.

SEARCH
Previous Page
Next Page

$$r_0 = r_g = r_r = r. \quad (4)$$
$$L_g = L_r = L. \quad (5)$$

| Parameters (Ref Fig. 1.) | Value |
|---|---|
| Conductivity of the Medium | 1 X $10^{-6}$ siemens |
| Relative Permeability | 1 |
| Relative Permittivity | 1 |
| Lg | 0.150 micro henries |
| Lr | 0.150 micro henries |
| $r_g$ | 1.3491 X $10^{-20}$ ohms |
| $r_r$ | 1.3491 X $10^{-20}$ ohms |
| $r_0$ | 1.3491 X $10^{-20}$ ohms |

**Table 1**. Parameters for the Proposed Model

The three conductor line model is 200m in length. The basic one dimensional linear search was used and the final frequency response obtained is as shown in Figure 2. The model closely follows the frequency response from a frequency of 5.537 MHz upto the higher limit of 20 MHz. The mutual inductance per unit length for the proposed model was found to be 1.3604 micro henries.

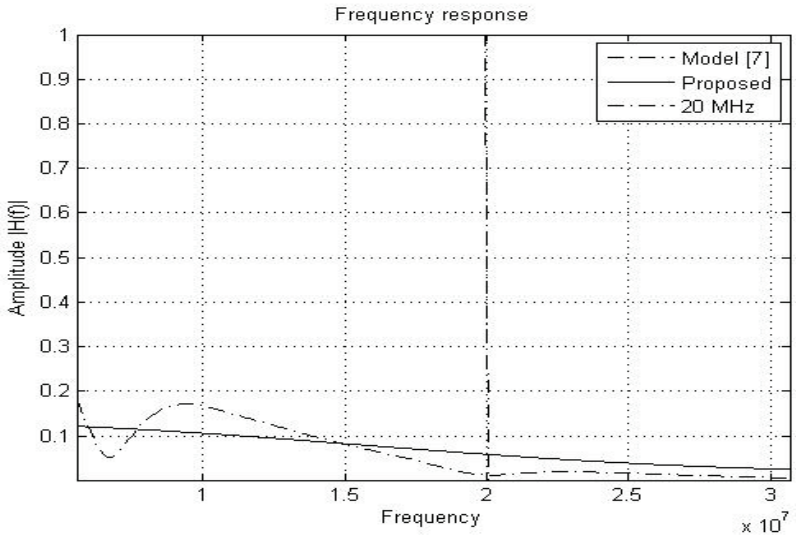


**Fig 2**. Comparison of the Frequency Responses of the Proposed Model 5.537 MHz. with that of in [7].

**FUTURE SCOPE:**

A lot of variables can be used for optimizing the model leading to a better precision. These parameters are the values of distributed elements and medium properties of the model. One can use advanced multidimensional search algorithms [10], with the initially obtained values from the main distribution line as a starting point, to achieve a more precise model. One can extend the idea of three conductor line model to four or more conductor line model for a higher precision.

Previous Page Next Page

## CONCLUSION:

A novel method of modeling Powerline channel is proposed here. The development of the model requires only the measured frequency response of the channel along with some details about the main distribution line of the network. The versatility of the model lies in the fact that it can be readily deployed for Electromagnetic Compatibility as well as Performance Analysis. The paper also points out further ways of improving the precision of the model using multidimensional search algorithms.

## REFERENCES:


1. P. Langfield and K. Dostert, "OFDM System Synchronization for Powerline Communications", Proc. 4th Int, Symp. on Powerline Communications and its Applications, pp. 15–22, Limerick, Ireland, 2000.
2. Majumder and J. Caffery, "Powerline Communications", IEEE Potentials, Vol. 23, Issue 4, pp. 4-8, Oct-Nov 2004.
3. G. Threin, Datenübertragung über Niederspannungsnetze mitn Bandspreizverfahren, Fortschrittberichte VDI, Reihe 10, VDI-Verlag, Düsseldorf, 156, 1991.
4. J. Barnes, "A Physical Multipath Model for Power Distribution Network Propagation ", Proc.1998 Int. Symp. Powerline Communications and its Applications, pp. 76-89, Tokyo, Japan, Mar. 1998.
5. Dalby, "Signal Transmission on Powerlines-Analysis of Power Line Circuits", Proc. 1997 Int. Symp. Powerline Communications and its Applications, pp. 37-44, Essen, Germany, Apr. 1998.
6. M. Karl, Möglichkeiten der Nachrichtenübertragung über elektrische Energieverteilnetze auf der Grundlage Europäischer Normen, Fortschrittsberichte VDI, Reihe 10, VDI-Verlag, Düsseldorf, 500, 1997.
7. Manerd Zimmermann and Klaus Dostert, "A Multipath Model for the Powerline Channel", IEEE Trans. on Communications, pp. 553-559, Vol. 50, No. 4, April 2002.
8. Clayton R. Paul, "Introduction to Electromagnetic Compatibility", John Wiley & Sons Inc, New York, 1992.
9. John D. Ryder, "Networks, Lines and Fields", 2nd ed. PHI, India, 2003, ch. 6.
10. K. C. Gupta, Ramesh Garg and Rakesh Chadha, "Computer Aided Design of Microwave Circuits", 1st ed. Artech House Publishers, New York, 1981.

# LINE, SURFACE AND VOLUME INTEGRATION USING ANN TECHNIQUE EXTENDABLE TO ELECTROMAGNETIC PROBLEMS

*Sridhar Pattanaik* [(1)] *and R.K Mishra** [(1)]
Department of Electronic Science, Berhampur University, India, 760 007
sridhar_pattanaik@yahoo.co.in

**ABSTRACT:**

Line, surface and volume integrations are the integral part of electronics, particular for the Electromagnetic problems. Neural network is capable of solving the ODE and partial differential equations. Here trials have been made to use the ANN techniques for integration from the deferential equation point of view. Some line, surface and volume integrations are used to test the accuracy of the method and are in good agreement with the established numerical methods used for the engineering problems.

## INTRODUCTION:

Integration plays a major role in electronics problem. Analytical and Numerical methods are the most common to find the value of integration. Numerical method is gaining importance to its analytical counter part due to its capability to implement in the computer.

The Maxwell's equation can be in integral or differential form. The line, surface and volume integration is very frequently used in electromagnetics particularly in antenna problems. The radiation field produced by a transmitting antenna system having any known arbitrary current distribution can be found by adding the separate fields produced by elementary lengths of thin conductors with each elementary length treated as a very small radiating doublet antenna. In adding the contributions to the total field that are made by the individual doublets that can be considered as making up the actual current distribution of an antenna it is necessary to take into account the phase and the plane of polarization of each contributing component field. Those field strength summations can be done by either graphical or mathematical integration. The moment method of far field radiation calculation is a mathematical integration method based in principle upon the fundamental concept of summing fields from many small elemental sections of thin antenna conductors that compose an antenna system. In this paper some fundamental work is done for the line, surface and volume integration using neural network.

Solution of ODE and partial differential equations can be computed using ANN [1-2]. Artificial Neural Network [3-4] is being used for high-level design, providing fast and accurate solutions to the task it has learned. The use of neural networks provides advantages like good generalization properties, less model parameters than other methods, compact solution models and low demand on memory. Hence it has the capability to tackle differential equations of many engineering problems. Here for the first time the value of integration is calculated using ANN from the differential equation point of view.

In this paper line, surface and volume integration is calculated using ANN compared with the established numerical methods. The results are encouraging and in good agreement with each other.



Previous Page Next Page

## PROBLEM FORMULATION

The total numbers of treated problems are six, two from each category.

1-6 gives the treated problems; the RHS shows the results using established Analytical/Numerical methods.

$$\int_0^{\pi/2} \sin(x)dx = 1 \tag{1}$$

$$\int_0^2 1/(x^3 - 2x - 5)dx = -0.4605 \tag{2}$$

$$\int_{\pi}^{2\pi}\int_0^{\pi/2} y\sin(x) + x\cos(y)dxdy = -9.8696 \tag{3}$$

$$\int_{\pi}^{2\pi}\int_0^{\pi/2} e^y \sin(x) + x\cos(y)dxdy = -44.2814 \tag{4}$$

$$\int_1^3\int_2^5\int_0^{\pi/2} xe^y \sin(z)dxdydz = 3.6945 \tag{5}$$

$$\int_1^2\int_1^{1.2}\int_1^{1.3} x^2 ye^{yz}dxdydz = 8.8556 \tag{6}$$

## III. PROPOSED ANN TECHNIQUE FOR INTEGRATION

The general method for computing the line, surface and volume integration using ANN is illustrated below.

For Line integration using ANN we propose an ANN network with input x and P is the weight vector of the network.

$$\int_{x_1}^{x_2} f(x)dx = N(x,P) \tag{7}$$

The network is to be trained to minimize and the cost function is given by (8).

$$\frac{d}{dx}N(x,P) - f(x) = 0 \tag{8}$$

Surface and volume integral is calculated in the similar manner with a network with two and three inputs respectively. The cost function for the surface and volume integrals is given by (10) and (12) respectively.

$$\int_{x_1}^{x_2}\int_{y_1}^{y_2} f(x,y)dxdy = N(x,y,P) \tag{9}$$

$$\frac{\partial}{\partial x}\frac{\partial}{\partial y}N(x,y,P) - f(x,y) = 0 \tag{10}$$

$$\int_{x_1}^{x_2}\int_{y_1}^{y_2}\int_{z_1}^{z_2} f(x,y,z)dxdydz = N(x,y,z,P) \tag{11}$$

SEARCH
Previous Page
Next Page

$$\frac{\partial}{\partial x}\frac{\partial}{\partial y}\frac{\partial}{\partial z}N(x,y,z,P) - f(x,y,z) = 0 \quad (12)$$

## IV. TRAINING THE NETWORK

The net work used for training is a normal feed-forward neural network [5-7] with number of inputs equal to the number of variables (i.e. for double integration the number of inputs are two). Linear transfer function is used for the output layer and the transfer function for the hidden layer is tanh (.) The network is trained upto $10^{-3}$ tolerance. Number of hidden neurons are 8.

The network is trained according to the normal back-propagation algorithm [7].

For the double integration the equation for the ANN is given below.

$$N = \sum_{i=1}^{g} w_i z(r_i) \quad (13)$$

$$r_i = v_{1i}x + v_{2i}y + v_{0i} \quad (14)$$

$$z(r) = \tanh(r) \quad (15)$$

The error is calculated from the cost function for the surface integration and it is given in equation (10).

$$Error = \frac{\partial}{\partial x}\frac{\partial}{\partial y}N(x,y,P) - f(x,y) \quad (16)$$

$$E = (Error)^2 \quad (17)$$

$$w_i^{k+1} = w_i^k - \eta\frac{\partial E^k}{\partial w_i} + \alpha\left(w_i^k - w_i^{k-1}\right) \quad (18)$$

$$v_{1j}^{k+1} = v_{1j}^k - \eta\frac{\partial E^k}{\partial v_{1j}} + \alpha\left(v_{1j}^k - v_{1j}^{k-1}\right) \quad (19)$$

$$v_{2j}^{k+1} = v_{2j}^k - \eta\frac{\partial E^k}{\partial v_{2j}} + \alpha\left(v_{2j}^k - v_{2j}^{k-1}\right) \quad (20)$$

$$v_{0j}^{k+1} = v_{0j}^k - \eta\frac{\partial E^k}{\partial v_{0j}} + \alpha\left(v_{0j}^k - v_{0j}^{k-1}\right) \quad (21)$$

Where, k is the iteration number, $v_{ij}$ are the weights from the input to hidden neuron (except for i = 0); $w_i$ are the weights from hidden to output and $v_{0j}$ is the threshold. $\eta$, $\alpha$ are the learning rate and momentum respectively. Selection of a value for the *learning rate parameter*, $\eta$, has a significant effect on the network performance. Usually, $\eta$ must be a small to ensure that the network will settle to a s olution. A small value of $\eta$ means a l arge number of iterations. It is often possible to increase the size of $\eta$ as learning proceeds. The value of alpha should be positive but less than 1 and represent the momentum term. Similarly the updated equations can be found for the line and volume integration.

## V. RESULTS

Table I: compares the ANN results with the Analytical\Numerical result.

The error is calculated using the formula (22).

$$C = ( A - B ) \times 100 / A \quad (22)$$

The results for the line, surface and volume integration in the treated case is found to be in good agreement with established methods used in engineering calculations.

SEARCH
Previous Page
Next Page

**TABLE I:**

| Problem defined in the equation | Analytical Or Numerical (A) | ANN Result (B) | Percentage of error (C) |
|---|---|---|---|
| Equation 1 | 1 | 0.995 | 0.50 |
| Equation 2 | -0.4605 | -0.473 | -2.7144 |
| Equation 3 | -9.8696 | -9.640 | 2.3263 |
| Equation 4 | -44.2814 | -45.104 | -1.8577 |
| Equation 5 | 3.6945 | 3.751 | -1.5293 |
| Equation 6 | 8.8556 | 8.521 | 3.7784 |

## VI. CONCLUSION

In this paper for the first time ANN is used for integration from differential equation point of view. The results are encouraging in the treated cases and can be used for the applications of electromagnetics and antenna problems. Training the ANN for a low tolerance value can reduce the error.

## VII. REFERENCES


1. H. Lee and I. Kang,, "Neural algorithms for solving differential equations," *J. Comput. Phys.*, vol. 91, pp. 110–117, 1990.
2. A. J. Meade, Jr., and A. A. Fernandez, "The numerical solution of linear ordinary differential equat ions by f eedforward neur al net works," *Math. Comput. Modeling*, vol. 19, no.12, pp. 1–25, 1994.
3. Silvia Fer rari and Robert F. Stengel, J an. 2005 ,"Sm ooth Function A pproximation Using Neural Networks", *IEEE Trans. Neural Networks,* Vol. 16, No. 1, pp. 24–28,
4. R. Y entis and M . E . Z aghoul,, "V LSI i mplementation of l ocally connect ed neur al network for s olving par tial di fferential equat ions," *IEEE Trans. Circuits Syst. I*, vol. 43, no, 8, pp. 687–690, 1996.
5. A. Patnaik and R. K. Mishra, "ANN Techniques in Microwave Engineering," *IEEE Microwave Magazine*, vol. 1, no. 1, pp. 55 – 60, ,March 2000.
6. K. C . Gupta a nd P. M . Watson,, "A pplication of A NN c omputing t o microwave design," *1996 Asia-Pacific Microwave Conference Proceedings,* vol. 3, pp. 825- 828, 1996.
7. A. Patnaik, "Some Studies on use of Artificial Neural Network for Analysis of Microstrip Antenna," Ph.D. dissertation, 2000


SEARCH

Previous Page Next Page

# DIELECTRIC RELAXATION MEASUREMENTS OF FMD AND PLG BINARY MIXTURE USING TDR & FDR TECHNIQUES

*A. M K Bhanarkar[(1)], B. C M Bhanarkar[(2)], C. R R Mudholkar[(1)], D. S R Sawant[(1)], E. V V Navarkhele[(3)]*

(1)Department of Electronics, Shivaji University, Kolhapur-416004, INDIA

(2)Kendriya Vidyalaya, Cantonment Area, Aurangabad-431002, INDIA

(3)Dept. of Physics, Dr. Babasaheb Ambedkar Marathwada University, Aurangabad-431004, INDIA

Email: mk_bhanarkar@rediffmail.com

**ABSTRACT:**

The di electric relaxation s tudies of F MD ( formamide) and PLG ( propylene glycol) binary m ixture ar e car ried out by us ing T DR & F DR m ethod. T he static dielectric permittivity ($\varepsilon_0$) and r elaxation t ime (t ) with exces s parameters a re r eported t hrough T DR t echnique f or 20º C, 30ºC, 40º C. T he dielectric par ameters have been obtained by fitting experimental data with Harviliak-Negami equat ion. Observation s hows t hat t he s tatic di electric permittivity and relaxation time decreases with increasing temperature as well as the dielectric permittivity decreases and relaxation time increases with increasing percentage volume of PLG in FMD. The permittivity (ε') and loss (ε") with tan δ are reported through FDR technique for 9-12GHz frequency ranges us ing X-band s et up. I t gi ves t he di electric per mittivity decr eases an d dielectric loss increases for increasing concentration as well as the dielectric permittivity and dielectric loss decreases for increasing frequencies.

**INTRODUCTION:**

A gr eat i nterest has been evinced i n t he s tudy of di electric r elaxation be havior i n FMD with a v iew of understanding the role of hydrogen bonding and rotation of $NH_2$ group in t he PL G. T he FM D i s an interesting cl ass of s olvents. A gr eat var iation i n l iquid state properties and di electric r elaxation i s f ound bet ween uns ubstituted FM D. I n t he pr esent paper, a co mparative di electric s tudy of FM D w ith increasing per cent vol ume of PL G ha s been made.

Dielectric techniques have b een used to observe the well-known a or s tructural relaxation process over a broad frequency and temperature range. Recently, special interest in the dynamic at high frequencies, in the microwaves and sub millimeter range has risen due to the prediction of some theoretical and scaling approaches elaborated in the past. The static permittivity of bipolar liquid is closely related to its molecular structure. In former theories this relation finds an obvious expression in the orientation correlation factor which has regard to t he f act t hat, under ce rtain condi tion, the di pole or ientation an en semble of ne ighbored molecules is not randomly distributed but may be object to molecular order.

Dielectric relaxation of l iquid mixture gives information about molecular interaction. T he FM D i s an a ssociative liquid w ith C = O group. T he FM D r epresent an important characteristic of amides of organic solvents due t o high pol arity, strong solva power. FMD is the excellent proton donors as well as proton acceptor and hence i s strongly associated through intermolecular H-bonds.

The association pattern and level of hydrogen bonding in liquids like monoalcohols ixture of these has been a s ubject of intense research. These studies have bee n

SEARCH
Previous Page
Next Page

extended to dialcohol ( diol), which have the possibility to form both intra and inter - molecular hydrogen bonds. The interest in diol is further emphasized by the fact that these molecules play an important role in many chemical and biological processes.

**MEASUREMENTS TECHNIQUES:**

The experimental techniques used to measure dielectric parameters are as follows, TDR and FDR are the two method which are used in this paper to study the dielectrics parameters,

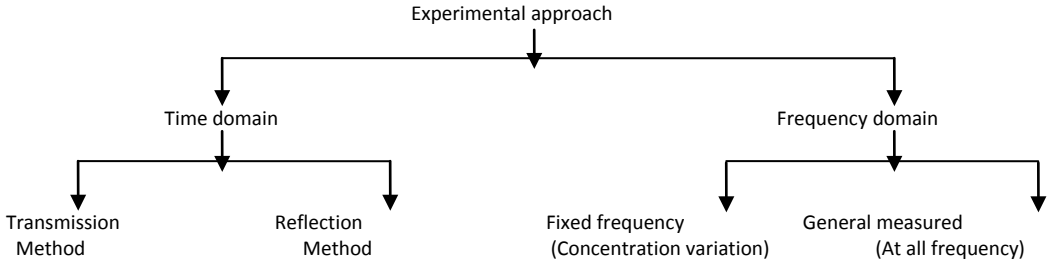


The time dependent data was processed to obtain a complex reflection coefficient spectra $r^*(w)$ over the frequency range from 10 MHz to 20 GHz. Using Fourier transformation as

$$r^*(w) = (c/jwd)\,[p(w)/q(w)]$$

Where $p(w)$ and $q(w)$ are Fourier transforms of $R_1(t) - Rx(t)$ and $R_1(t) + Rx(t)$ respectively, C is the speed of light, w is the angular velocity, d is the effective pin length and $j = \sqrt{-1}$. The complex permittivity spectra $e^*(w)$ were obtained from reflection coefficient spectra $r^*(w)$ by applying calibration method. The experimental values of $e^*$ are fitted with Debye equation

$$e^*(w) = e_\infty + (e_0 - e_\infty) / (1+jwt)$$

where $e_0$, $e_\infty$ and t as fitting parameters. A non-linear least squares fit method was used to determine the values dielectric parameters.

An alternating electric field of appropriate frequency gives rise to dielectric dispersion. When the direction of the field changes sufficiently fast, the molecular force impending the dipole orientation dominates and dipoles becomes unable to flow the charges; at these frequencies the orientation of the permanent dipoles no longer contributes to the dielectric constant. In a certain frequency band a phase lag between the field and the dipole orientation develops and energy is drawn from the electric source is dissipated as heat. This phenomena is described by a complex representation of dielectric constant, $e^*(w)$ gives as,

$$e^*(w) = e' - j\,e''$$

The imaginary part $e''$, is known as dielectric loss and the real part $e'$ is constant of the medium that measure the efficiency of transfer of electric charge and it is called as dielectric constant of the medium. The expressions are useful for evaluating $e'$ and $e''$ are,

$$e' = \lambda_o^2\{1/\lambda_c^2 + (b_1^2 - a_1^2) / 4p^2\} \quad \text{and} \quad e'' = \{\lambda_o^2 b_1 a_1\} / 2p^2$$

where $\lambda_c$ is the cutoff wavelength given by,

$\lambda_c = 2 X a$, a is the border side of the rectangular waveguide.

SEARCH

Previous Page Next Page

## RESULTS AND DISCUSSION:

### For TDR;

**Table1:** Static permittivity ($e_0$) and relaxation time (t) of FMD + PLG mixture

| % Volume of | T=20°C | | T=30°C | | T=40°C | |
|---|---|---|---|---|---|---|
| PLG in FMD | ($e_0$) | (t) | ($e_0$) | (t) | ($e_0$) | (t) |
| 00 | 110.08 | 44.24 | 101.08 | 37.52 | 97.52 | 29.45 |
| 10 | 101.12 | 64.34 | 90.31 | 50.53 | 83.02 | 41.23 |
| 20 | 86.22 | 81.65 | 82.24 | 73.62 | 72.17 | 63.54 |
| 30 | 80.42 | 94.61 | 75.30 | 89.85 | 64.29 | 83.39 |
| 40 | 43.80 | 101.13 | 38.48 | 96.59 | 34.71 | 90.41 |
| 50 | 35.77 | 120.73 | 31.95 | 103.45 | 28.96 | 95.56 |
| 60 | 33.02 | 191.45 | 29.64 | 175.84 | 26.80 | 133.39 |
| 70 | 32.92 | 239.63 | 28.56 | 219.36 | 25.63 | 200.26 |
| 80 | 32.52 | 269.54 | 27.32 | 239.56 | 24.52 | 225.85 |
| 90 | 31.32 | 312.02 | 27.21 | 268.97 | 24.39 | 262.97 |
| 100 | 31.10 | 335.74 | 27.00 | 298.67 | 23.39 | 285.95 |

**Graph 1:** Static dielectric permittivity of FMD + PLG mixture

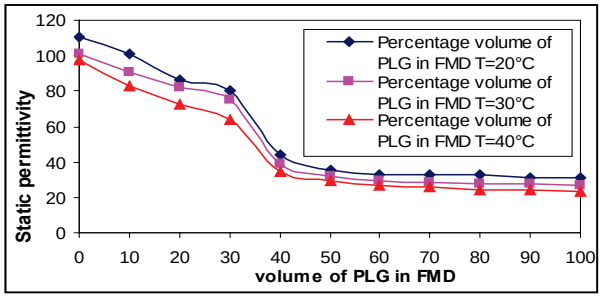


**Graph 2:** Relaxation time of FMD + PLG mixture

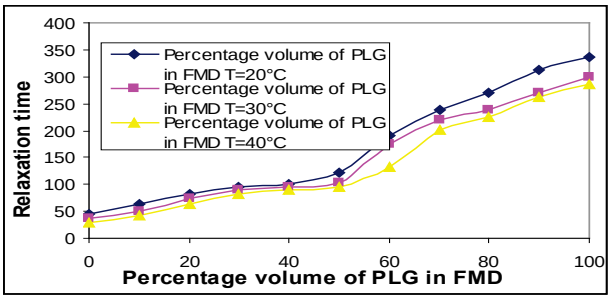


SEARCH

Previous Page

Next Page

**Table 2**: Excess permittivity ($e^E$) and excess inverse relaxation time $(1/t)^E$ of FMD + PLG mixture

| X2 | T=20°C | | T=30°C | | T=40°C | |
|---|---|---|---|---|---|---|
| | $(e^E)$ | $(1/t)^E$ | $(e^E)$ | $(1/t)^E$ | $(e^E)$ | $(1/t)^E$ |
| 0 | 0 | 0 | 0 | 0 | 0 | 0 |
| 0.0577 | -51.94 | -13.88 | -48.38 | -14.85 | -48.65 | -21.76 |
| 0.1212 | -74.07 | -18.48 | -69.48 | -21.2 | -68.99 | -28.72 |
| 0.1912 | -73.78 | -16.66 | -69.68 | -20.7 | -68.28 | -25.76 |
| 0.2688 | -59.5 | -11.63 | -56.35 | -15.6 | -54.76 | -18.3 |
| 0.3555 | -39.3 | -6.477 | -36.74 | -8.667 | -36.35 | -11.29 |
| 0.4527 | -18.55 | -3.166 | -16 | -2.878 | -18.3 | -7.543 |
| 0.5627 | 2.8639 | -1.34 | 5.1247 | -0.584 | -0.377 | -5.558 |
| 0.6881 | 30.446 | 2.2948 | 30.288 | 2.159 | 23.407 | 1.2683 |
| 0.8323 | 59.342 | 9.9117 | 54.25 | 12.124 | 50.448 | 16.75 |
| 1 | 0 | 0 | 0 | 0 | 0 | 0 |

**Graph 3:** Excess dielectric constant of FMD + PLG mixture

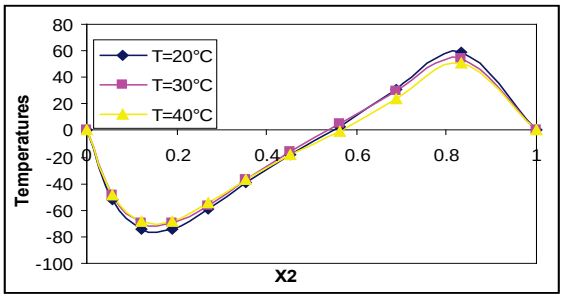


**Graph 4:** Excess inverse relaxation time of FMD + PLG mixture

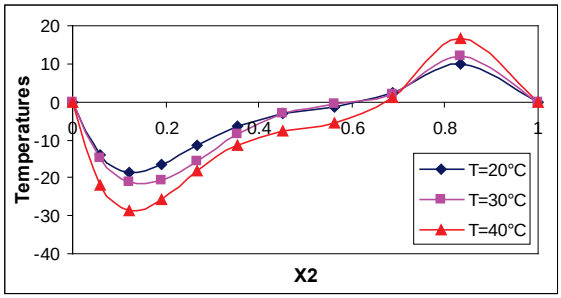


**Note:** X2 is mole fraction of PLG in FMD binary mixture

The results are recorded in above tables, show that the static permittivity is going to decrease for increasing range of temperature and per centage volume of PLG in FMD. The relaxation time is going increasing for increasing range of volume of PLG in FMD but relaxation time decreases for increasing temperature ranges. Information related to solute–solvent interaction might be obtained by excess properties related to the permittivity and relaxation time in the mixture. The excess permittivity $e^E$ is defined as,

$$e^E = (e_0 - e_\infty)_m - [(e_0 - e_\infty)_A X_A + (e_0 - e_\infty)_B X_B]$$

Where X is mole fraction and, A, B represents mixture, solvent and solute respectively. The excess permittivity may provide qualitative information about multimer formation in the mixture as fallows:

1. $e^E = 0$: Indicates the solute and solvent do not interact.
2. $e^E < 0$: Indicates the solute-solvent interaction is in such a way that the effective dipole moment gets reduced. May form multimers leading to the less effective dipoles
3. $e^E > 0$: Indicates the solute-solvent interact in such a way that the effective dipole moment increases.

The excess inverse relaxation time is defined as,

$$(1/t)^E = (1/t)_m - [(1/t)_A X_A + (1/t)_B X_B]$$

Where $(1/t)^E$ is the excess inverse relaxation time which represents the average broadening of dielectric spectra.

The excess inverse relaxation time gives information regarding the dynamics of mixture interaction is as fallows:

1. $(1/t)^E = 0$: There is no change in solute – solvent interaction.
2. $(1/t)^E < 0$: The interaction produces a field such that the effective dipoles rotate slowly.
3. $(1/t)^E > 0$: The solute–solvent interaction produces a field such that the effective dipoles i.e. the field will co-operate in rotation of dipoles.

SEARCH
Previous Page
Next Page

The experimental values of both the excess parameters were fitted to the Redlich-Kister equation

$$Y^E = (X_A X_B) \sum B_K (X_A - X_B)^K$$

Where $Y^E$ is either $e^E$ or $(1/t)^E$. The coefficient $B_K$ was then calculated. The excess permittivity of FMD+PLG and their excess inverse relaxation time values are given in table respectively, following conclusion can be drawn from the tables:

1. The excess permittivity values of mixture are negative for 0.05 to 0.45 mole fractions. This indicates the antiparallel alignment of the dipoles in FMD rich region. This also indicates that the solute and solvent may form multimers leading to the less effective dipoles in FMD rich region for the systems. The excess permittivity values are positive in PLG rich region. This indicates the parallel alignment of the dipoles and increase in effective dipole moment in PLG rich region.

2. The excess inverse relaxation time values of mixture are negative for 0.05 to 0.56 mole fractions. This indicates the slower rotation of the dipoles of the system in FMD rich region. The excess inverse relaxation time value of mixture is positive in PLG rich region. This indicates the faster rotation of the dipoles of the system and the field will co-operate in rotation of dipoles in PLG rich region. This may be due to the higher dipole moment of FMD (3.8) than of PLG (2.4)

**For FDR;**

**Table 3:** Dielectric permittivity (e') and Dielectric loss (e'')

| % Volume of | 9GHz | | 10GHz | | 11GHz | | 12GHz | |
|---|---|---|---|---|---|---|---|---|
| PLG in FMD | (e') | (e'') | (e') | (e'') | (e') | (e'') | (e') | (e'') |
| 0.0 | 2.4314 | 0.0610 | 2.4131 | 0.0451 | 2.3112 | 0.0334 | 2.2136 | 0.0237 |
| 0.2 | 2.3978 | 0.0902 | 2.3646 | 0.0598 | 2.2456 | 0.0414 | 2.1784 | 0.0341 |
| 0.4 | 2.2345 | 0.1024 | 2.3045 | 0.0894 | 2.1464 | 0.0623 | 2.1132 | 0.0536 |
| 0.6 | 1.9456 | 0.1232 | 1.9025 | 0.0996 | 1.8932 | 0.0845 | 1.8435 | 0.0799 |
| 0.8 | 1.6635 | 0.1325 | 1.4365 | 0.1006 | 1.3214 | 0.0998 | 1.2304 | 0.0974 |
| 1.0 | 1.1001 | 0.1423 | 1.0964 | 0.1212 | 1.0745 | 0.1121 | 1.0654 | 0.1025 |

SEARCH

Previous Page Next Page

**Graph 5:** Dielectric permittivity of FMD and PLG mixture

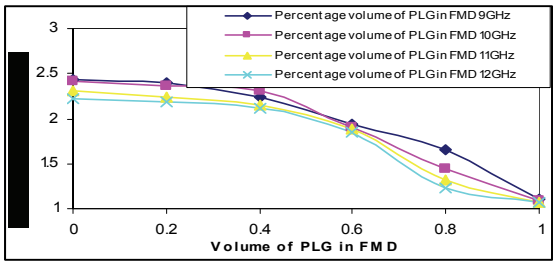


**Graph 6:** Dielectric loss of FMD and PLG mixture

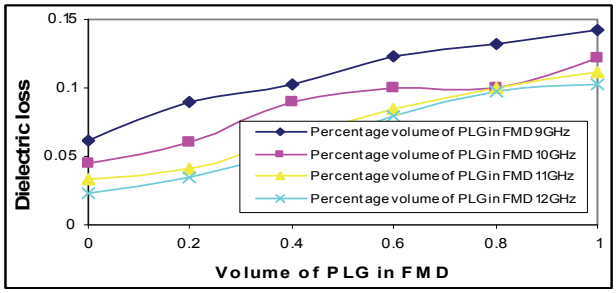


**Graph 7:** Tan δ of FMD and PLG binary mixture

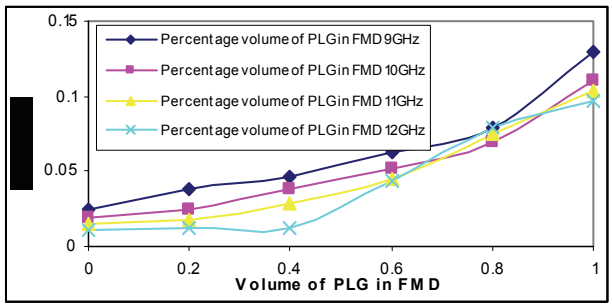


**Table 4:** Tan δ of FMD and PLG binary mixture

| % volume of PLG in FMD | 9GHz | 10GHz | 11GHz | 12GHz |
|---|---|---|---|---|
| 0.0 | 0.0250 | 0.0186 | 0.0144 | 0.0107 |
| 0.2 | 0.0378 | 0.0252 | 0.0184 | 0.0125 |
| 0.4 | 0.0458 | 0.0387 | 0.0290 | 0.0125 |
| 0.6 | 0.0633 | 0.0523 | 0.0446 | 0.0433 |
| 0.8 | 0.0796 | 0.0700 | 0.0755 | 0.0791 |
| 1.0 | 0.1293 | 0.1105 | 0.1043 | 0.0962 |

Dielectric permittivity, dielectric loss and tanδ for the interaction between FMD with PLG are given in above tables.

It is observed that the dielectric permittivity decreases and dielectric loss increases for increasing concentration. It is also observed that the dielectric permittivity and dielectric loss decreases for increasing frequencies. Such type of investigation and similar behavior of dielectric constant has been reported by S.M Puranik and M Malathi.

The dielectric permittivity of this binary solutions decreases with increasing volume percent of PLG in FMD. The decrease in dielectric permittivity of the FMD with increasing volume percent of PLG in FMD indicates the formation of hydrogen bonding with oxygen's of neighboring molecules, the molecules are under the influence of ions resulting in lowering of the values of dielectric permittivity of the binary mixture. Also the rotation of molecules due to dynamics of hydrogen bonds formed between carboxyl oxygen's of an acceptor molecules and formal proton of donor hindered intermolecular rotation around C-N bond. This would be another region for faster relaxation and decrease in dielectric permittivity in FMD with increasing volume of PLG.

Another reason in decrease in dielectric permittivity of this binary mixture due to the bigger molecular dimensions of PLG are greater than FMD, when these higher dimension PLG are added to FMD the resultant dipole moment of the binary mixture get increases which will reduce its mobility in the mixture and hence decrease in permittivity.

SEARCH

Previous Page

Next Page

Dielectric spectrum of FMD

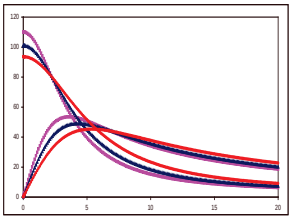

Dielectric spectrum of PLG

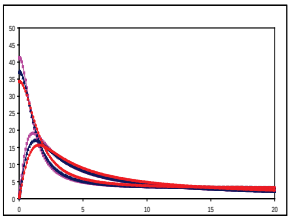

Cole-Cole model of FMD

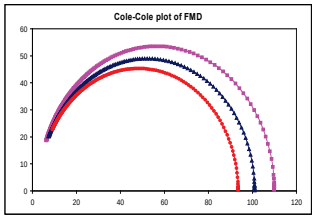


Cole-Cole model of PLG

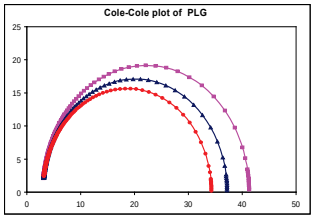


**ACKNOWLEDGEMENTS:**

Authors are very much thankful to Dr. P. W. Khirade, Reader, Department of Physics, Dr. Babasaheb Ambedkar Marathwada University, Aurangabad-431004 (MS) for providing facilities of TDR lab. Also thankful to Prof. S.C. Mehrotra, Head of Department computer, Dr. Babasaheb Ambedkar Marathwada University, Aurangabad-431004 (MS) INDIA for their guidance.

**REFERENCES:**

1. V V Navarkhele and M K Bhanarkar; "Dielectric relaxation study of N-methyl formamide with glycol using time domain reflectometry technique", Physics and Chemistry of liquids, Taylor and Francis group, 1-6, 2007
2. M K Bhanarkar and V V Navarkhele; "Dielectric relaxation study of formamide with glycols using time domain reflectometry technique", Frontiers of Microwaves and Optoelectronics, Anamaya publishers, New Delhi, India, 662-669, 2007
3. S C Mehrotra; "Dielectric relaxation study through time domain technique", NCMMT-2001, Aurangabad (India), 13-17, 2007
4. H Frohlich; "Theory of dielectrics", Oxford University Press, Oxford, 1949.
5. P Debye; "Polar molecules", Chemical catalog, Dover publications, New York 1929.
6. M Weissermal, H J Arpe; "Industrial Organic Chemistry". 2nd Edn, VCH, Weinheim, 1993
7. M. Malathi, R. Sabesan and S. Krishnan, "Dielectric relaxation studies of dilute Solutions of amides", Material science and Engineering, Vol. B104, 529, 2003
8. J.B. Hasted, "Aqueous Dielectrics", Chapmann and Hall Ltd. London, 1973.

SEARCH

Previous Page

Next Page

# NEW APPROACH FOR SPACE DIVISION MULTIPLE ACCESS RECEIVER -THE MOST SOPHISTICATED UTILIZATION OF SMART ANTENNA TECHNOLOGY

*Md. Bakhar[1], Vani.R.M[2] and P.V.Hunagund[2].*
Department of E&CE, Guru Nanak Dev Engineering College, Bidar-585403, Karnataka.
Email: mohammed.bakhar@gmail.com.
2 Department of Applied Electronics, Gulbarga University, Gulbarga-585106, Karnataka.
Email: vanirm123@rediffmail.com

**ABSTRACT:**

Smart antenna system attracts a lot attention now and believably more in the future. The system of antennas include a large number of technique that attempt to enhance the received signal, and suppress all interfering signals, and increase capacity in general. The final phase in the development of cellular radio systems will be space division multiple access (SDMA). It's advanced spatial-processing capability enables it to locate many users, creating a different sector for each user.

This new approach is based upon a recent patent by Carl Elam. In this new method adaptation is not necessary and tracking is not performed, while excellent results are achieved. This technique essentially works by designing the array weights to be time-varying random phase functions. The weights act to modulate each array element output. The receiver is superior in performance because contiguous beams can be formed in any regions of interest without the need for hardware phase shifters. The beams are created by correlation. The main purpose of this article is to provide a concept of a novel digital beam former (DBF) receiver.

## INTRODUCTION:

Many research and development activities have been poured into developing smart antennas for wireless communications systems. Interest in this technology is increasing since spatial processing is considered as a 'last frontier' in the battle of cellular system capacity with a limited amount of the radio spectrum. SDMA means that more than one user can be allocated simultaneously to the some physical communications channel in the same cell with only an angular separation. This technology dramatically improves the interference-suppression capability while it greatly increases frequency reuse, resulting in increased capacity and reduced infrastructure cost [1].

This new DBF receiver is based upon a recent paten by Carl Elam [2] and a radical shift in traditional DBF methods. This approach blends the virtues of switched beam and adaptive array technologies while avoiding many of their respective weaknesses. This falls under the general topic of waveform diversity. This works by designing the array weights to be time-varying random phase functions. The weights act to modulate each array element output. Specifically, the array outputs are weighted or modulated with a set of statistically independent pol y phase chipping sequences. A different and independent waveform is used for each antenna output. The phase modulation waveform purposely shifted the phase of each antenna output by chipping at rates much higher than the

SEARCH
Previous Page
Next Page

base band frequency of the message signal. This shredding process breaks up the phase relationship between all array elements and thus purposely eliminates array phase coherence (opposite of the traditional goal). The receiver then can see all incoming signals simultaneously without the necessity of steering or adapting because the array elements, for the moment, become statistically independent from one another. The chipped incoming waveforms are processed in a quadrature receiver and are subsequently compared to similar chipped waveforms stored in memory. The memory waveforms are created based upon expected angles of arrival. The theoretical spatial capacity is simply the angular space of interest divided by the antenna beam solid angle [3].

**DESCRIPTION OF THE NEW SDMA RECEIVER:**

The novel digital beamformer is depicted in fig. 1. This new SDMA DBF can be used with any arbitrary N-element antenna array. It can be linear array but should preferably be a two dimensional random array such that the antenna geometry and element phasing is a unique for each incoming angle-of-arrival.

For purpose of illustration, consider N-element linear array. The incoming signals arrive at angles $\theta_l$ where l=1, 2…L. Each different angle of arrival produces a unique array element output with a unique phase relationship between each element. These phase relationship will be used in conjunction with the modulations $\beta_n(t)$ to produce a unique summed signal $y^r(t)$.

Corresponding to the actual N-element antenna array is a second virtual array modeled in memory. The virtual array is modeled after the actual physical array used. The memory array has K possible virtual outputs for each expected directions $\theta_k$ (k= 1, 2, …, K). The total number of expected directions K should be less than or equal to the number of antenna of antenna elements N. These memory signals are generated based upon knowledge of the antenna array geometry and the calculated phase delays for each specific direction of interest. The expected directions are generally chosen by the user to be no closer than the angular resolution allowed by the array.

The N-element array outputs and the N-antenna array memory outputs are both phase modulated (PM) by the same set of N pseudo-noise (pn) phase modulating sequences. The $n^{th}$ phase modulating sequence will be designated as $\beta_n(t)$. $\beta_n(t)$ is composed of M polyphase chips. Each chip is of length $\tau_c$ and the entire sequence is of length $T=M\tau_c$. The chip rate is chosen to be much greater than the Nyquist rate of the incoming baseband signal modulation. The purpose for this over sampling is so that the phase modulation of the incoming signal is nearly constant over the entire group of M chips. In general, the goal should be such that $T \leq 1/(4B_m)$ where $B_m$ is the message signal bandwidth.

Each phase modulating waveform $\beta_n(t)$ is used to modulate or tag each array output with a unique marking or identifying waveform- $\beta_n(t)$ deliberately shreds or scrambles the phase of the signal at array element n. This shredding process temporarily scrambles the phase relationship between all other array elements. The desired element phasing is restored in the correlator if the incoming signal correlates with one of the memory signals.

SEARCH

Previous Page Next Page

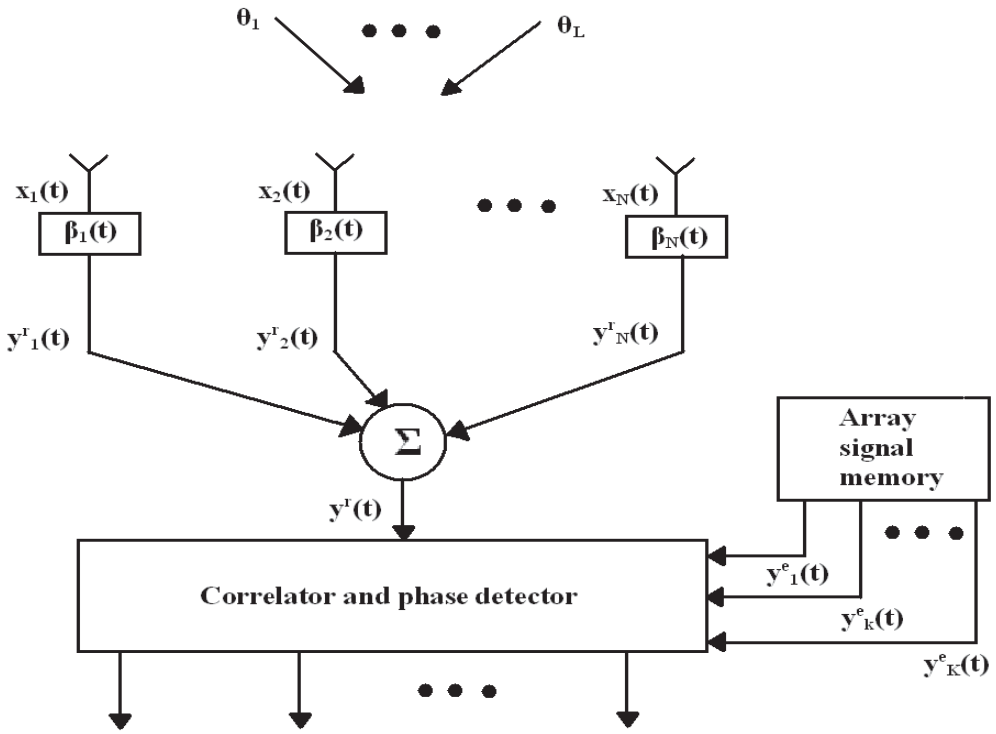


Fig. 1. SDMA quadrature receiver.

**MATHEMATICAL DESCRIPTION:**

Each baseband output of the receive array will have a complex voltage waveform whose phase will consists of each emitter's message signal $m_l(t)$ and the unique receive antenna element phase contributions. Ignoring the space loss and polarization mismatches, the received baseband array output is given in vector form as

$$\bar{x}^r(t) = \begin{bmatrix} 1 & \cdots & 1 \\ e^{jkd\sin(\theta_1)} & \cdots & e^{jkd\sin(\theta_L)} \\ \cdot & \cdots & \cdot \\ \cdot & \cdots & \cdot \\ e^{j(n-1)kd\sin(\theta 1)} & \cdots & e^{j(n-1)kd\sin(\theta_L)} \end{bmatrix} \begin{bmatrix} e^{jm_1(t)} \\ \cdot \\ \cdot \\ \cdot \\ e^{jm_L(t)} \end{bmatrix} = A^r . s^r(t)$$

where $m_l(t)$=lth emitter's phase modulation, d= array element spacing

k= wave number, $\theta_l$= angle of arrival of the lth incoming signal

$\bar{a}_l^r = \left[1, e^{jkd\sin(\theta_L)}, \ldots . e^{j(n-1)kd\sin(\theta_l)}\right]^T$ = steering vector for direction $\theta_l$

$\bar{A}^r$ = matrix of steering vectors for all angles of arrival $\theta_l$

$S^r$ = vector of arriving signal baseband phasors

The received signals, for each array output, are phase modulated with th chipping sequences. the chipping waveforms can be viewed as phase-only array weights. These array weights can be depicted as the vector $\beta(t)$. The total weighted or chipped array o e received signal vector and is given by

SEARCH
Previous Page
Next Page

These array weights can be depicted as the vector $\beta(t)$. The total weighted or chipped array output is called the received signal vector and is given by

$$y^r(t) = \bar{\beta}(t)^T . \bar{x}^r(t)$$

In a similar way, the array signal memory steering vectors are created based upon M expected angles-arrival $\theta_m$.

$$\bar{A}^e = \begin{bmatrix} 1 & . & . & . & 1 \\ e^{jkd\sin(\theta_1)} & . & . & . & e^{jkd\sin(\theta_K)} \\ . & . & . & . & . \\ . & . & . & . & . \\ e^{j(n-1)kd\sin(\theta_1)} & . & . & . & e^{j(n-1)kd\sin(\theta_K)} \end{bmatrix} = \left[\bar{a}^e \ldots \bar{a}^e_K\right]$$

where $\bar{a}^e_k$ is the steering vector for expected direction $\theta_k$ and $\bar{A}^e$ is the matrix of steering vectors for expected direction $\theta_k$.

The memory has k outputs, one for each expected direction $\theta_k$. Each memory output, for the expected angle $\theta_k$ is given by

$$y^e_k(t) = \bar{\beta}(t)^T . \bar{a}^e_k$$

The signal correlator is designed to correlate the actual received signal with the conjugate of the various expected direction memory signals. The best correlation occurs when the actual AOA matches the expected AOA. The correlation can be used as a discriminant for detection. Since the arriving signals have a random arrival phase delay, a quadrature correlation receiver should be employed such that the random carrier phase does not affect the detection. The general complex correlation output, for the kth expected direction, is given as

$$R_k = \int^{t+T} y^r(t).y^e_k{}^*(t)dt = |R_k|e^{j\phi k}$$

where $R_k$ is the correlation magnitude at expected angle $\theta_k$ and $\phi_k$ is the correlation phase at expected angle $\theta_k$.

The new SDMA receiver doesnot process the incoming signals with phase shifters or beam steering. The correlation magnitude $|R_k|$ is used as the discriminant to determine if a signal is present at the expected angle $\theta_k$. If the discriminant exceeds a predetermined threshold, a signal is deemed present and the phase is calculated. Since it is assumed that the emitter PM is nearly constant over the code length $M\tau_c$, the correlator outpt phase is approximately the average of the emitter PM. Thus

$$\phi_k = \arg(R_k) \approx \tilde{m}_k$$

where $\tilde{m}_k = \frac{1}{T}\int^{t+T} m_k(t)dt$ = average of emitter's modulation at angle $\theta_k$

The average phase $\tilde{m}_k$ retrieved for each quarter cycle of the m(t) can be used to reconstruct the user's phase modulation using an FIR filter.

**ADVANTAGES:**

1. It can process multiple angles of arrival simultaneously.
2. It is not limited by acquisition or tracking speeds.
3. Interfering signals are minimized because the shredded waveforms at interferer angles do not correlate well with expected direction waveforms stored in memory.
4. Any arbitrary and/or random antenna array geometry can be incorporated into this as long as the expected memory signals are based upon the array geometry.

## CONCLUSION:

In this article we discussed the concept of a SDMA and a new approach for SDMA receiver with a mathematical description. Advantages of this approach are also discussed.

## REFERENCES:

1. S. Bellofiore, C.A.Balanis, J.Fouz and A.s spanias, "Smart Antenna System for Mobile Communication Networks Part1: Overview and Antenna Design", IEEE antenna and Propagation Magazine, Vol.44, No.3, June2002.
2. Elam,C., "Method and Apparatus for Space Division multiple access Receiver", patent No. 6, 82,021, rights assigned to Greenwich Technology Associates, One Soundview way, Darien, CT.
3. Frank Gross,"Smart Antennas for Wireless Communications with matlab", McGraw Hill Publication 2005.

# IONOPSHERIC TIME DELAY STATISTICS OF GPS SIGNALS AT LOW LATITUDE STATIONS

*V. Satya Srinivas, A.D. Sarma and K. Ravichandra*
Research and Training Unit for Navigational Electronics, Osmania University, Hyderabad.
Email:ad_sarma@yahoo.com

## ABSTRACT:

The most prominent parameter affecting the accuracy of GPS Aided Geo Augmented Navigation (GAGAN) is ionospheric delay which is a function of Total Electron Content (TEC). The ionospheric time delay of the propagating radio wave is subjected to geographical, seasonal, diurnal and solar activity variations. Prediction of this time delay is particularly difficult in equatorial and low latitude regions. In these regions the ionosphere often causes more problems for navigation, surveying and communication systems. In this paper analysis is carried out by investigating data from several TEC stations of GAGAN network comprising dual frequency Global Positioning System (GPS) receiver. The observations of measured TEC values over Indian region due to GAGAN TEC stations show large variations, which can adversely affect the Required Navigation Parameters (RNP) requirements. The hourly and seasonal time delay statistics of ionospheic region over india gives interesting features.

## INTRODUCTION:

Navigation is a process of directing a vehicle from one known position to another, which can be done by several systems. GPS is one such satellite based navigation system designed and developed by Department of Defense (DOD), USA. It provides reasonably accurate, all weather three dimensional position of user on or near the surface of the earth. But, the reliability of system is not guaranteed due to various sources of errors such as satellite based errors, atmospheric errors and receiver based errors. The most predominant error among these is the ionospheric time delay. Because of the errors, the standalone GPS cannot provide the positional accuracy required for civil aviation applications i.e., CAT I precision approach. Therefore, various satellite based augmentation system are being developed all over the world (Hofmann et al, 2008). GAGAN is one such system in India. Several near real time grid based ionospheric models are investigated for GAGAN applications (Sarma et al, 2006). However, significant work has not been reported as far as statistical behavior of the ionosphere is concerned. Therefore, an attempt has been made to investigate the ionosphere time delay statistics for GAGAN application using GPS data.

## DATA ACQUISITION AND PROCESSING:

The data from various TEC stations of GAGAN network is obtained from Space Applications Center (SAC), ISRO, Ahmedabad, India. In the GAGAN network 20 TEC stations are installed to monitor the ionospheric behavior. The processed GPS data contains 23 parameters. Out of these only seven parameters, namely user position, PRN number of satellite, GPS week number, GPS seconds of the week, elevation angle, azimuth angle and in the analysis.

SEARCH
Previous Page
Next Page

## HOURLY VARIATIONS OF THE VERTICAL DELAY AT IPPS:

For better understanding of the ionospheric delay variations, the TEC data of storm (6<Kp<9) day (27th July 2004) is considered. Vertical delays are calculated at IPPs for all the visible Satellite Vehicles (SVs). However, SVs visible for more than 3 hours in each time slot are only preferred for analyzing the hourly TEC variations. The analysis is carried out by dividing the day into four slots, that is 0000-0600 hours, 0600-1200 hours, 1200-1800 and 1800-2400 hours. In a particular time slot, an SV which is visible in more number of stations is only considered for the analysis.

## DATA DURATION 0000-0600 HRS:

**(i) During this time slot**, the PRN 24 data is available for 4 to 6 Hrs from 9 TEC stations. Maximum delays of 1.86 m (Bagdogra), 1.172 m (Bangalore), 4.92 m (Bhopal), 2.23 m (Delhi), 3.9 m (Hyderabad), 2.22 m (Jodhpur), 3.68 m (Mumbai), 1.42 m (Raipur) and 1.97 m (Visakhapatnam) are observed at these stations. Elevations at these points are observed to be above $53^0$. All stations experienced maximum delay during early hours of the pass between 0000 to 0130 Hrs. These delays are observed when satellite is in between $180^0$ to $270^0$ azimuthally. Even though the elevation angles are decreasing during 0130 Hrs to 0500 Hrs, the ionospheric delays at each station found to be gradually decreasing instead of increase correspond to this period. During this time period azimuths are observed to be in between $320^0$ to $60^0$. The least delay (0.3 m) was experienced at Bangalore at an elevation of $15.5^0$. In some of the stations where the satellites pass is more than 5 hours (Bagdogra, Raipur and Visakhapatnam), the delays are observed to be increasing with time (after 0005Hrs).

**(ii) Data duration 0600-1200-1800 hours:** The significance of this time slot is that, due to gradual increase of solar ultraviolet light with time the ionosphere is heated and its electron content changes gradually. As a result more delay is expected. Since sufficient number of satellites are visible for more than 6 Hrs, complete 0600 to 1800 Hrs timeslot is considered instead of 0600 – 1200 Hrs and 1200 – 1800 Hrs. During this time slot the PRN14 data is available for 6 to 8 hours from 11 TEC stations. Maximum delays of 9.7 m (Aizwal), 9.93 m (Bagdogra), 6.21 m (Bangalore), 8.59 m (Bhopal), 7.28 m (Delhi), 9.2 m (Guwahathi), 8.3 m (Hyderabad), 6.3 m (Jodhpur), 7.18 m (Lucknow), 6.74 m (Mumbai), 7.7 m (Raipur), and 7.7 m (Visakhapatnam) are observed at these stations. Elevations at these points are observed to be less than $26^0$. All stations experienced maximum delay during the pass between 1400 to 1500 Hrs. During this time period azimuths are observed to be in between $70^0$ to $120^0$. As expected, the delays reached to peak values and gracefully decreased. On storm day Bagdogra (9.9 m) and Aizwal (9.7 m) experienced maximum delays.

**(iii) Data duration 1800-2400 hours:** During this time slot, the PRN 31 data is available for 4 to 5 hours from 11 TEC stations. Maximum delays of 7.85 m (Aizwal), 6.64 m (Bagdogra), 5.57 m (Bangalore), 9.32m (Bhopal), 7.73 m (Delhi), 5.61 (Guwahathi), 7.80 m (Hyderabad), 7.79 m (Jodhpur), 8 m (Mumbai), 6 m (Raipur), and 6.47 m (Visakhapatnam) are observed at these stations. Elevations at these points is observed to be varying from a minimum of $15.36^0$ (Jodhpur) to a maximum of $55.99^0$ (Mumbai). During this time period azimuths are observed to be between $70^0$ to $120^0$.

## CUMULATIVE PROBABILITY OF RANGE DELAY:

For studying the effect of seasons on ionosphere, the calendar year is divided into [illegible] depending on the ionospheric conditions. They are winter (Nov-Feb), ve[illegible]

SEARCH
Previous Page
Next Page

Equinox (Mar-Apr), summer (May-Aug) and autumn equinox (Sept-Oct). The delay statistics are based on satellite elevation angle. The delays that fall within ± 0.5 of each integer degree of elevation angle are grouped together. The delay values at $10^0$, $20^0$, $30^0$, $40^0$, $50^0$, $60^0$, $70^0$, $80^0$ and $90^0$ are considered. Using statistical probability (Bendat et al, 1986), the cumulative distribution of ionospheric time delay at these elevations is studied for four stations of GAGAN network namely Ahmedabad, Hyderabad, Kolkata and Trivandrum.

**AUTUMN EQUINOX:**

The TEC data for the year 2004 is processed and analyzed. As the mask angle has been set at $15^0$, the investigation of elevation angles beyond $10^0$ are considered and presented in Table 1. From Table 1, it is clear that, maximum vertical delay (17.48m) for an elevation of $60^0$ is occurred at Hyderabad station. It is interesting to know that the delay at Trivandrum is lower among all the stations considered. This could be due to equatorial anomaly effect. However at crest regions the delay is expected to be more. Further, it is also observed the slant and vertical delay values are nearly same at $80^0$ and $90^0$ elevations for the stations in consideration indicating the minimum effect of the mapping function. Among the stations considered the delay is large at higher elevations for Kolkata station. The maximum vertical delay is same for all elevations at Ahmedabad and Trivandrum that is around 13 m and 9 m respectively. The cumulative probability (in percentage) of slant delay at these stations is shown in Table 2. The delay observations at all elevations for each station are considered in calculating percentage of cumulative probability. The cumulative distribution of delays for elevations ($20^0$ – $50^0$) at kolkatta station is shown in Fig.1.

**CONCLUSIONS:**

Worldwide Satellite Based Augmentation Systems for precision approach are being considered for deployment. Ionopsheric statistics will help in optimizing the locations of ionospheric reference stations. Large TEC variations can be observed at all stations for storm day during 1800 to 2400 Hrs. Seasonal variations of TEC with respect to elevation angle for four stations for autumn equinox shows that maximum vertical delay (17.48 m) was found at Hyderabad for an elevation of $50^0$. This preliminary analysis can be further extended to various stations as well as seasons, which help in characterizing Indian ionosphere. This type of statistics would be useful for developing and modifying the proposed algorithms for GPS applications at low latitude stations. And also useful in developing an ionospheric time delay model for low latitude regions such as India.

**ACKNOWLEDGMENTS:**

The research work presented in this paper has been carried out under the project entitled "Analysis and modeling of Indian Ionospheric Electron Content for GPS Applications" funded by ISRO, Bangalore, Vide Order No: CAWSES:05, Dated: 28th December 2005.

**REFERENCE**

1. Bendat S Julius and Piersol G Allan, "Random Data: Analysis and Measurement Procedures", 2nd edition, Wiley Interscience Publication, 1986.
2. Hofmann-Wellenhof, B., Lichtenegger, and Wasle, "Global Navigation Satellite Systems – GPS, GLONASS, GALILEO and More", Springer-Verlag Wien New York, 2008.

SEARCH
Previous Page
Next Page

3. Sarma, A.D., Prasad, N. and Madhu, T.: 'Investigation of suitability of grid-based ionospheric models for GAGAN', Electronics Letters, 42, ( 8), pp.478-479, 13th April 2006.

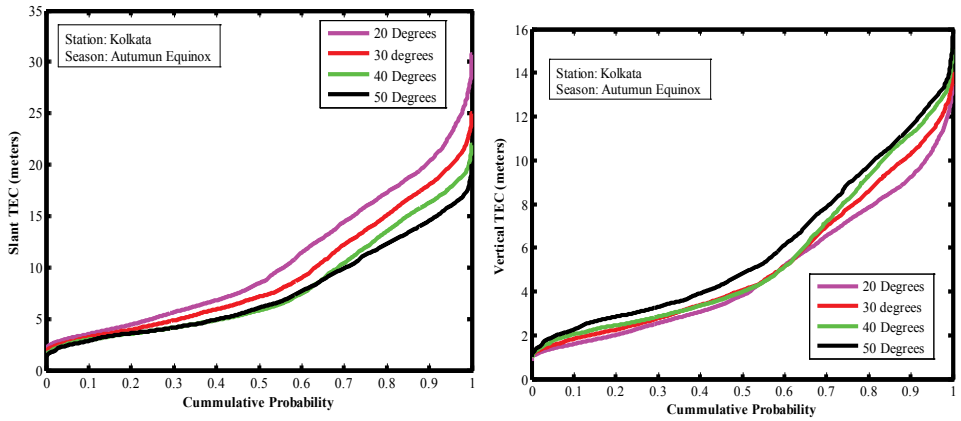


(a) (b)

Fig.1 (a, b) Delay Vs Cumulative distribution for various elevation angles in autumn equinox

**Table 1. Maximum slant and vertical delay for autumn equinox (Sept. - Oct., 2004) (Elevations $20^0$ to$60^0$)**

| *Station* Name | Elevation ( in Degrees) / VTEC/STEC (meters) | | | | |
|---|---|---|---|---|---|
| | *$20^0$* | *$30^0$* | *$40^0$* | *$50^0$* | *$60^0$* |
| *Ahmedabad* | *13.5m / 30.93m* | *13.49 m/23.88 m* | *13.26m/19.62 m* | *13.03m/16.53m* | *13.22m/15m* |
| *Hyderabad* | *15.43m/34m* | *16.19m/27.95m* | *16.41m/23.81m* | *16.73m/21.18m* | *17.48m/20.08m* |
| *Kolkata* | *13.51m/30.77m* | *14.07 m/25.02m* | *15.08 m/21.98m* | *15.66 m/19.86m* | *15.4 m/17.62m* |
| *Trivandrum* | *9.49m/21.52 m* | *9.46m/16.59m* | *9.55m/14.15 m* | *9.55m/12.19 m* | *9.71/11.01 m* |

**Table 2. Cumulative probability of slant delay at all elevations (autumn equinox)**

| Probability of slant delay exceeds (%) | *Station Name/ Delay (meters)* | | | |
|---|---|---|---|---|
| | Ahmedabad | Hyderabad | Kolkata | Trivandrum |
| *50%* | 5 m | 8 m | 8 m | 8 m |
| *40%* | 7 m | 10 m | 11 m | 9 m |
| *20%* | 13 m | 16 m | 17 m | 13 m |
| *10%* | 17 m | 19 m | 20 m | 15 m |

SEARCH

Previous Page Next Page

## RESEARCH SESSION V
## MICROWAVE PROPAGATION II

SEARCH

Previous Page

Next Page

# RESEARCH SESSION V

## MICROWAVE PROPAGATION II

***Chair : Prof. Subrata Sanyal, IIT, Khragpur***



SEARCH

Previous Page Next Page

# RATE ADAPTIVE RESOURCE ALLOCATION FOR OFDM SYSTEMS

*M Padmaja [1] and Dr MC Chandra mouly[2]*
(1)Assistant Professor in ECE, VR Siddhartha Engineering College, VIJAYAWADA-520 007
Padmaja19_m@yahoo.co.in
(2) Professor and HOD,ECE & EIE, Dean Engineering, TRR Engineering College,
*Patancheru,HYDERABAD-502319*
mcchandramouly@yahoo.com

**ABSTRACT:**

Orthogonal Frequency Division Multiple Access (OFDMA) basestations allow multiple users to transmit simultaneously on different subcarriers during the same symbol period. This paper considers basestation allocation of subcarriers and power to each user to maximize the sum of user data rates, subject to constraints on total power, bit error rate, and proportionality among user data rates. Previous allocation methods have been iterative nonlinear methods suitable for offline optimization. A non-iterative method is proposed by relaxing user rate proportionality constraints. Compared to the previous methods, the proposed method waives the restriction of high subchannel SNR, has significantly lower complexity, and yields higher user data rates.

## 1. INTRODUCTION

OFDMA is an extension of Orthogonal Frequency Division Multiplexing (OFDM), which is currently the modulation of choice for high speed data access systems, also referred to as Multiuser OFDM. In the current OFDM systems, only a single user can transmit on all of the subcarriers at any given time, and time division or frequency division multiple access is employed to support multiple users. OFDMA allows multiple users to transmit simultaneously on the different subcarriers per OFDM symbol. Since the probability that all users experience a deep fade in a particular subcarrier is very low, it can be assured that subcarriers are assigned to the users who see good channel gains on them.

The problem of assigning subcarriers and power to the different users in an OFDMA system has recently been an area of active research. In [1], the margin-adaptive resource allocation problem was tackled, wherein an iterative subcarrier and power allocation algorithm was proposed to minimize the total transmit power given a set of fixed user data rates and Bit Error Rate (BER) requirements. In [2], the rate-adaptive problem was investigated, wherein the objective was to maximize the total data rate over all the users subject to power and BER constraints. This problem was partially addressed in [3] by ensuring that each user would be able to transmit at a minimum rate, and also in [4] by incorporating a notion of fairness in the resource allocation through maximizing the minimum user's data rate. In [5], the fairness was extended to incorporate varying priorities. Instead of maximizing the minimum user's capacity, the total capacity was maximized subject to user rate proportionality constraints.

A subcarrier allocation scheme is developed that linearizes the power allocation problem while achieving approximate rate proportionality. The resulting power allocation problem is thus reduced to a solution of simultaneous linear equations. In simulation, the proposed algorithm achieves a total capacity that is consistently higher than the previous [illegible]res significantly less computation, while achieving acceptable proportionality.

## 2. SYSTEM MODEL

The block diagram for the downlink of a typical OFDMA system is shown in Fig.1. At the base station transmitter, the bits for each of the different K users are allocated to the N subcarriers, and each subcarrier n ($1 \le n \le N$) of user k ($1 \le k \le K$) is assigned a power $p_{k,n}$. It is assumed that subcarriers are not shared by different users. Each of the user's bits are then modulated into N M-level QAM symbols, which are subsequently combined using the IFFT into an OFDMA symbol. This is then transmitted through a slowly time-varying, frequency-selective Rayleigh channel with a bandwidth B. The subcarrier allocation is made known to all the users through a control channel beforehand; therefore, each user needs only to decode the bits on their respective assigned subcarriers.

Fig.1 OFDMA system block diagram for K users

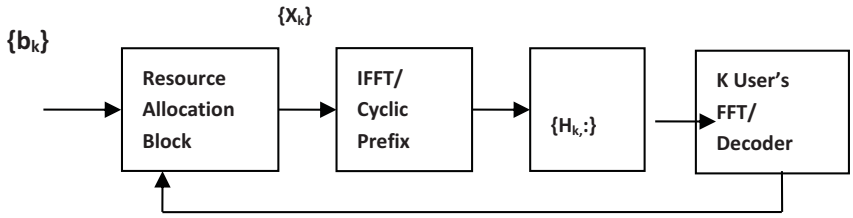


It is assumed that each user experiences independent fading and the channel gain of user k in subcarrier n is denoted as $g_{k,n}$, with Additive White Gaussian Noise (AWGN) $\sigma^2 =$ No(B/N) where No is the noise power spectral density. The corresponding subchannel-to-noise ratio is thus denoted as $H_{k,n} = g^2_{k;n}/\sigma^2$ and the $k^{th}$ user's received Signal-to-Noise Ratio (SNR) on subcarrier n is $\gamma_{k,n} = p_{k,n} H_{k,n}$. In order that the BER constraints be met, the effective SNR has to be adjusted accordingly. The BER of a square M-level QAM with Gray bit mapping as a function of received SNR $\gamma_{k,n}$ and number of bits $r_{k,n}$ can be approximated to within 1 dB for $r_{k,n} \ge 4$ and BER$\le 10^{-3}$ ,

$$\overline{\mathrm{BER}}_{\mathrm{MQAM}}\left(\gamma_{k,n}\right) \approx 0.2 \exp\left[\frac{-1.6\gamma_{k,n}}{2^{\gamma_{k,n}}-1}\right] \qquad (1)$$

Solving for $\gamma_{k,n}$

$$\left(\gamma_{k,n}\right) = \log_2\left(1+\frac{\gamma_{k,n}}{\Gamma}\right) \qquad (2)$$

where $\Gamma = -\ln(5BER)/1.6$. The objective of the resource allocation is formulated as

$$\max_{c_{k,n},p_{k,n}} \frac{B}{N} \sum_{k=1}^{K} \sum_{n=1}^{N} c_{k,n} \log_2\left(1+p_{k,n}\frac{H_{k,n}}{\Gamma}\right) \qquad (3)$$

Subjected to

$$C1: c_{k,n} \in \{0,1\}\ \forall\, k,n, \qquad C2: p_{k,n} \ge 0\ \forall\, k,n, \qquad C3: \sum_{k=0}^{K} c_{k,n} = 1\ \forall\, k,n,$$

$$C4: \sum_{k=0}^{K}\sum_{n=0}^{N} c_{k,n}\, p_{k,n} \le P_{tot}, \qquad C5 = R_i : R_j = \phi_i : \phi_j\ \forall i,j \in \{1,\ldots K\}, i \ne j$$

where $c_{k,n}$ is the subcarrier allocation indicator such that $c_{k,n} = 1$ if and only if subcarrier n is assigned to user k, and $P_{tot}$ is the transmit power constraint.

Previous Page Next Page

is the total data rate for user k and $f_1, f_2, \ldots f_k$ are the normalized proportionality constants where $\sum_{k=1}^{K} f_k = 1$. It ensures the correct values for the subcarrier allocation indicator and the power.

## 3. RELATED METHODS

The approach in [5] was to first determine the subcarrier allocation, followed by the power allocation. The subcarrier allocation was determined by allowing each user to take turns choosing the best subcarrier for him. In each turn, the user with the least proportional capacity gets the priority to choose his best subcarrier. After the subcarrier allocation, the maximization over continuous variables $p_{k,n}$ given by

$$\max_{p_{k,n}} \frac{B}{N} \sum_{k=1}^{K} \sum_{n \in \Omega_k} \log_2 \left( 1 + p_{k,n} \frac{H_{k,n}}{\Gamma} \right) \quad (5)$$

where $\Omega_k$ refers to the set of subcarriers assigned to user k and $R_k = \frac{B}{N} \sum_{n \in \Omega_k}^{N} r_{k,n}$ is the total data rate for user k. The set of total power assigned for each user k, denoted as $P_k$ for $1 \le k \le K$, can be solved using Lagrangian multiplier techniques. Although these can be solved with less computation, iterative methods are still needed.

## 4. PROPOSED METHOD

*Step1:* Determination of the number of subcarriers $N_k$ to be initially m assigned to each user; This initial step is based on the reasonable assumption that the proportion of subcarriers assigned to each user is approximately the same as their eventual rates after power allocation.

*Step2:* Assigning the subcarriers to each user in a way that ensures rough proportionality; This step allocates the per user allotment of subcarriers $N_k$ and then the remaining $N^*$ subcarriers in a way that maximizes the overall capacity while maintaining rough proportionality. The first step of the algorithm initializes all the variables. $R_k$ keeps track of the capacity for each user. The second step assigns to each user the unallocated subcarrier that has the maximum gain for that user. The third step proceeds to assign subcarriers to each user according to the greedy policy that the user that needs a subcarrier in each iteration gets to choose the best subcarrier for it. The fourth step assigns the remaining $N^*$ subcarriers to the best users for them, wherein each user can get at most one unassigned subcarrier.

*Step3:* The total power $P_k$ is assigned for user k to maximize the capacity while enforcing the proportionality; The output of the first two steps is a subcarrier allocation for each user, which reduces the resource allocation problem to an optimal power allocation as in (5).

$$P_k = \begin{cases} \left( P_{tot} - \sum_{k=2}^{K} \frac{b_k}{a_{kk}} \right) \Big/ \left( 1 - \sum_{k=2}^{K} \frac{1}{a_{kk}} \right) & , \text{for } k = 1 \\ \left( b_k - P_1 \right) / a_{kk} & , \text{for } k = 2, \ldots K \end{cases} \quad (6)$$

SEARCH

Previous Page Next Page

*Step4:* Assigning the powers $p_{k,;n}$ for each user's subcarriers subject to the total power constraint $P_{k.}$ Step 3 gives the total power $P_k$ for each user k, which are then used in this final step to perform waterfilling across the subcarriers for each user as

$$p_{k,n} = p_{k,1} + \frac{H_{k,n} - H_{k,1}}{H_{k,n} H_{k,1}}, \qquad \text{where} \qquad p_{k,1} = \frac{P_k - V_k}{N_k} \qquad (7)$$

The under lying pr emise be hind t hese s teps i s t hat i n pr actical s ystems, adherence to the proportionality constraints need not be strictly enforced. The proportionality constraints ar e us ed t o di fferentiate var ious s ervices, w herein t he s ervice pr ovider may choose t o pr ioritize t heir cu stomers bas ed on di fferent billing mechanisms. Si nce the proportion of rates is more of a soft guarantee than a hard one, a rough proportionality is acceptable as long as the capacity is maximized and the algorithm complexity is low.

## 5. RESULTS

In this section, the performance of the proposed subcarrier and power allocation for proposed method *is* compared to the approach of [5].

The f requency selective multipath channel is modeled as consisting of six independent Rayleigh multipaths, with an exponentially decaying profile. A maximum delay spread of 5 μs and maximum Doppler of 30 Hz is assumed. The channel information is sampled every 0.5 ms to update the subchannel and pow er allocation. The total pow er was assumed to be 1 W, the total bandwidth as 1 MHz, and t otal subcarriers as 64. T he average sub channel SNR is assumed to be 38 dB. The number of users for the system varies from 6-12, shown in Fig.2.

Fig.3 s hows the comparison of total capacities between the pr oposed method and other methods. Notice that the capacities increase as the number of users increases. This is t he e ffect o f m ultiuser d iversity gai n, w hich i s more pr ominent in s ystems w ith larger number of users. The proposed method has a consistently higher total capacity than the other methods for all the numbers of users for this set of simulation parameters. This advantage can be attributed t o t he r elaxation of t he p roportionality cons traints, and the ad ded f reedom of assigning the $N^*$ subcarriers.

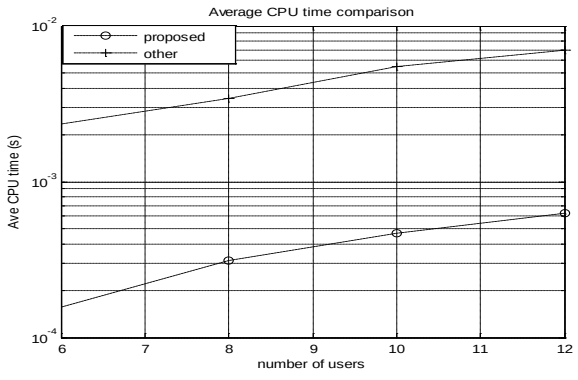


Fig.2 Average CPU time versus number of users

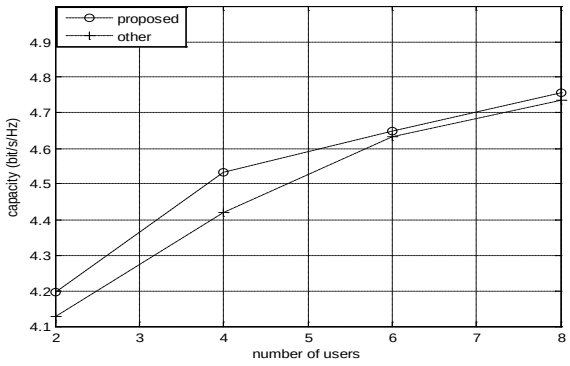


Fig.3 Total capacity versus number of users

## 5. CONCLUSIONS

This paper pr esents a new method t o solve t he r ate-adaptive r esource al location proportional rate constraints for OFDMA systems. It improves on the prev work in this area [ 5] b y dev eloping a nove l s ubcarrier a llocation s cheme t hat ach ieves

SEARCH
Previous Page
Next Page

approximate rate proportionality while maximizing the total capacity. This scheme was also able to exploit the linear case, thus allowing the optimal power allocation to be per formed using a direct algorithm with a much lower complexity versus an iterative algorithm. It is shown through simulation that the proposed method performs better than the previous work in terms of significantly decreasing the computational complexity, and yet achieving higher total capacities, while being applicable to a more general class of systems.

## 6. REFERENCES


1. CY Wong, RS Cheng, KB Lataief, and R D Murch, "Multiuser OFDM System with Adaptive Subc arrier, B it, and Pow er A llocation", *IEEE J. Select. Areas Commun.*, vol. 17, pp. 1747.1758, Oct 1999.
2. J Jang and KB Lee, "Transmit Power Adaptation for Multiuser OFDM Systems", *IEEE J. Select. Areas Commun.* vol. 21, pp. 171.178, February 2003.
3. H Yin and H Liu, "An Efficient Multiuser Loading Algorithm for OFDM-based Broadband W ireless Sy stems", *Proc. IEEE Global Telecommunications Conference*, vol. 1, 2000, pp. 103.107.
4. W R hee and J M C iof_, .I ncrease i n C apacity of M ultiuser O FDM System U sing Dynamic Subchannel Allocation, *Proc. IEEE Vehic. Tech. Conf.*, T okyo, Japan, pp. 1085.1089, May 2000.
5. Z Shen, JG Andrews, and BL Evans, "Optimal Power Allocation in Multiuser OFDM Systems", *Proc. IEEE Global Communications Conference*, December 2003.

# MICROWAVE DIELECTRIC PROPERTIES OF $CEO_2$ FILLED HDPE COMPOSITES FOR MICROWAVE SUBSTRATE APPLICATIONS

*P. S. Anjana [1], V. Deepu[2], P. Mohanan [2] and M. T. Sebastian [1*]*

[1]Materials and Minerals Division, National Institute for Interdisciplinary Science and Technology (Formerly Regional Research Laboratory), Thiruvananthapuram-695019, India.

Email: mailadils@yahoo.com

[2]Department of Electronics, Cochin University of Science and Technology, Cochin-682022, India.

**ABSTRACT:**

HDPE/$CeO_2$ composites (0-0.5 volume fraction) were prepared by melt mixing technique. The effect of filler content on the dielectric properties was studied at 1 MHz and 7 GHz. The dielectric constant and dielectric loss increased with increase in $CeO_2$ content. For 0.5 volume fraction loading of the ceramic the composite has $\varepsilon_r$ of 6.85 and tan $\delta$ of 0.0085 at 7 GHz. Different theoretical approaches have been employed to predict the effective permittivity of composite systems and the results were compared with that of experimental data. The models were fitted for low filler content.

## INTRODUCTION:

The miniaturization and high speed operation have become the predominant technology for electronic components with the development of electronic information technology. Ceramic-polymer composites form a potential material group suitable for producing demanding and functional packages that combine the electrical properties of ceramic and the mechanical flexibility, chemical stability and low temperature processing possibilities of polymers. Fluoropolymeric materials are the most desirable polymer matrix for flexible substrate fabrication due to their superior high frequency electrical properties and excellent temperature and solvent resistance. Polyethylene is a non-polar polymer with a melting temperature of approximately 160°C. Due to its excellent characteristics such as very low dielectric constant ($\varepsilon_r$ = 2.3), low dielectric loss (tan $\delta = 10^{-4}$ at 1 MHz) better chemical resistance and insulating properties, HDPE is well known for applications as an engineering material. Ceria possess good dielectric and thermal properties. It has a dielectric constant of 23, dielectric loss less than 0.0001 at 7 GHz and thermal conductivity of 12 W/m/K. In the present work, an attempt has been made to explore the possibility of using $CeO_2$-filled HDPE as a substrate material for high frequency applications.

## EXPERIMENTAL:

$CeO_2$ (99.9%, IRE) and HDPE (Kerala Plastics) were used as the starting materials to prepare the composites. $CeO_2$ powder is heated at 1000°C to remove any volatile impurities. The starting materials, polyethylene and $CeO_2$ were mixed thoroughly in a kneading machine. The kneading machine consists of variable speed mixer having two counter rotating sigma blades with a gear ratio of 1:1.2 and heating facility up to 350°C. The counter rotating sigma blades ensure fine mixing by applying high shear force on the dough-like mixture. Different volume fractions ($V_f$ = 0 to 0.5) of $CeO_2$ ceramics were added to the melted polyethylene and blended at 170°C for 30 minutes. Thus obtained composite were thermo laminated under a pressure of 200 MPa and 170°C for 15 min. After thermolamination, the composites with desired shapes were polished and their densities were measured using Archimedes method.

Previous Page Next Page

The surface morphology of the composites was studied by scanning electron microscope (JEOL-JSM 5600 LV, Japan). The low frequency dielectric properties (silver electroded samples having dimension 14x1 $mm^2$) were measured by LCR meter (Hioki 3532-50, Japan). The microwave dielectric properties of the sample were measured by the cavity perturbation technique using HP 8510C Network Analyzer (Agilent Technologies, California).

**RESULTS AND DISCUSSION:**

The density of a two-component mixture should depend on the densities of the constituent components and also on their proportion by weight. Fig. 1. depicts the measured and theoretical densities of HDPE/$CeO_2$ composites as a function of volume fraction. The density is measured using Archimedes method and compared with the mixing rule

$$\rho_{eff} = V_f \rho_f + V_m \rho_m \qquad (1)$$

where $\rho_{eff}$, $\rho_f$, $\rho_m$ are the densities of composite, filler and matrix respectively. The experimental values for all volume fractions agree well with the theoretical values. Fig.2. shows the surface morphology and filler distribution of the HDPE/$CeO_2$ composites. It can be seen that $CeO_2$ particles are uniformly distributed throughout the HDPE matrix. For higher volume fraction of the composites, there is aggregation of $CeO_2$ particles. With the increase of filler content, the packing of particles grew denser (Fig. 2(b)).

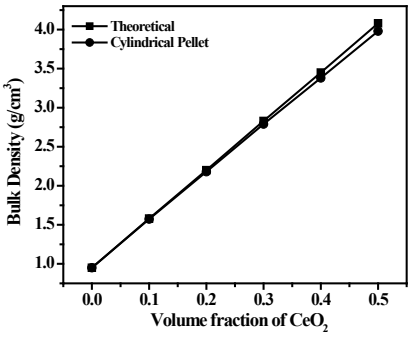


Fig. 1. Variation of density with $V_f$ in HDPE/$CeO_2$ composites

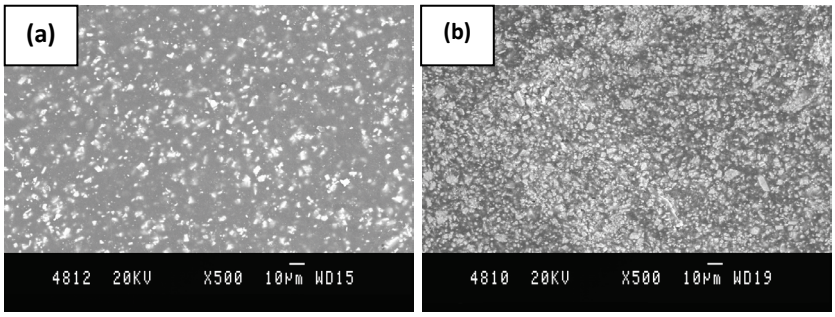


Fig. 2. SEM micrographs of (a) 0.1 $V_f$ (b) 0.5 $V_f$ of HDPE/$CeO_2$ composites

Fig. 3( a) and 3 (b) show the variation of dielectric constant and dielectric loss at 1 MHz and 7 GHz respectively. The dielectric constant and dielectric loss increases with the addition of $CeO_2$ content. The increase in dielectric constant is expected as the ceramics have higher dielectric constant compared to that of HDPE matrix. The dielectric constant increases non linearly as the volume fraction increases from 0.1 to 0.5 for 1 MHz and 7 GHz. Similar variations were reported earlier which confirms that the constituent filler particles are not in parallel combination in the composite.[6] This may be due to the presence of voids in the composite, which is evident from Fig.2. The dipole-dipole interaction increases and contributes to higher dielectric constants as $CeO_2$ fillers come closer at higher filler loading (Fig. 2(b)). When the $CeO_2$ particle is minor and forms a dispersed phase in a $CeO_2$/HDPE composite, the dielectric constants of composites were determined mainly by the continuous matrix instead of the minor filler. The dielectric constant of $CeO_2$/HDPE composites at 7 GHz (2.8 – 6.9) is less than that at 1 MHz (3.2 – 7.3) (±0.2). The dielectric loss of the $CeO_2$/PTFE composites (0.1 - 0.6 VF) at 7 GHz (0.0036-0.0085) is higher than that at 1 MHz (0.0022 - 0.0076). (±1x$10^{-4}$). There are some defects such as air gap and the interface phase between $CeO_2$ and HDPE in the composite materials, which can influence the dielectric

SEARCH
Previous Page
Next Page

constant and dielectric loss of composites.[6] In addition, the increase of $CeO_2$ content causes the increase of interphase between $CeO_2$ and PTFE and hence the influence of interface polarization on the dielectric loss becomes more significant.

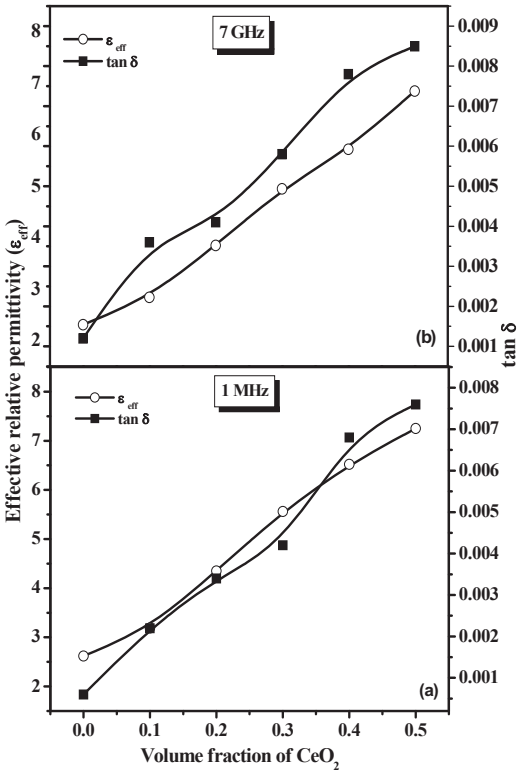


Fig. 3. Variation of $\varepsilon_r$ and tan δ with $V_f$ at 1 MHz and 7 GHz of HDPE/$CeO_2$ composites

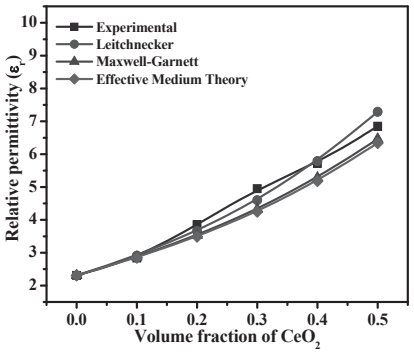


Fig. 4. Experimental and predicted $\varepsilon_r$ of (a) HDPE/$CeO_2$ composites

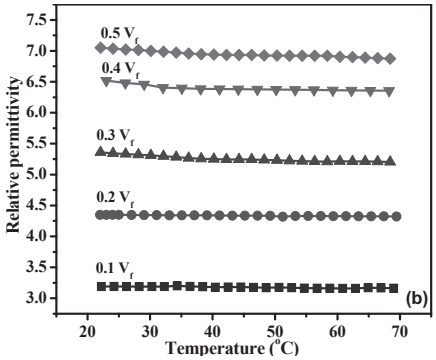


Fig. 5. Variation of $\varepsilon_r$ with temperature for different $V_f$ of HDPE/$CeO_2$ composite

In the present study, following equations were used to calculate the effective dielectric constant of low filler content composites:

I. LeichteneckerEquation:[6]
$$\ln \varepsilon_{eff} = V_m \ln \varepsilon_m + (1-f)\ln \varepsilon_f \quad (2)$$

II. Maxwell-Garnett Equation:
$$\frac{\varepsilon_{eff} - \varepsilon_m}{\varepsilon_{eff} + 2\varepsilon_m} = V_f \frac{\varepsilon_f - \varepsilon_m}{\varepsilon_f + 2\varepsilon_m} \quad (3)$$

III. Effective Medium Theory:[6]
$$\varepsilon_{eff} = \varepsilon_m \left[ 1 + \frac{f(\varepsilon_f - \varepsilon_m)}{\varepsilon_m + n(1-f)(\varepsilon_f - \varepsilon_m)} \right] \quad (4)$$

where $\varepsilon_{eff}$, $\varepsilon_f$, $\varepsilon_m$ are the dielectric constants of composite, filler and matrix respectively and $f$ is the volume fraction of the filler. The predicted values of dielectric constant are compared with that of experimental results at 7 GHz and are shown in Fig. 4. It is seen that for lower volume fractions (up to 0.2 $V_f$) theoretical models hold good and thereafter it deviates from the experimental values. EMT model fits well with the experimental values. Generally all theoretical predictions are valid for low filler contents. This is due to the imperfect dispersion of ceramic particles at higher filler contents and also to the air enclosed by the composites.

SEARCH
Previous Page
Next Page

The variation in dielectric constant of the HDPE and HDPE/$CeO_2$ composites with temperature is shown in Fig. 5. It should be noted that the variation in dielectric constant of HDPE/$CeO_2$ composites is very small. The low decrease in dielectric constant with temperature is due to the large difference in thermal expansion coefficient of HDPE and $CeO_2$ filler, which would disturb the aggregation of polar components causing a decrease in dielectric constant.[6]

## CONCLUSIONS

The HDPE/$CeO_2$ composites were prepared by melt mixing technique. SEM micrographs show that with the increase of filler content, the packing of particles grew denser and indicated the excellent compatibility between HDPE and $CeO_2$ particles. The dielectric constant and dielectric loss increased with the increase in $CeO_2$ content at 1 MHz and 7 GHz. Theoretical model approaches have been employed to predict the effective dielectric constant of the composite systems. The variation of dielectric constant with temperature in HDPE/$CeO_2$ composites is very small. For 0.5 volume fraction loading of the ceramic, the composite has $\varepsilon_r$ of 6.9 and tan $\delta$ of 0.0085 at 7 GHz. Hence the HDPE/$CeO_2$ composite (0.5 $V_f$) can be considered as a possible candidate for microwave substrate applications.

## REFERENCES:


1. M. B. Tian, Substrates for high density package engineering, Tsinghua University press, Beijing, 2003.
2. D. L. Chung, Materials for electronic packaging, Butterworth, Heinemann, Washington, 1995.
3. Y. M. Wang, D. C. Jia, and Y. Zhou, Preparation and properties of $Ba_2Ti_9O_{20}$/PTFE microwave dielectric composites, Piezoelectrics and Accoustooptics, 24, 225, 2002.
4. Y-C. Chen, H-C. Lin, and Y-D. Lee, The effects of Phenyltrimethoxysilane coupling agents on the properties of PTFE/Silica composites, J. Poly. Res., 11**,** 1, 2004.
5. A. J. Bur, Dielectric properties of polymers at microwave frequencies, Polymer, 26, 1985.
6. P. S. Anjana, M. N. Suma, P. Mohanan and M. T. Sebastian, Low Dielectric Loss PTFE/$CeO_2$ Ceramic Composites for microwave substrate applications, Int. J. Appl. Ceram. Tech., 5**,** 325, 2008.
7. J. Zhang, H. Fan, S. Ke, Y. Shi, X. Zeng, M. Bi and H. Huang, Dielectric properties of AlN/polymer composites for electronic substrate application, Key Eng. Mater., 334,1053, 2007.
8. A. H. Sihvola, Effective permittivity of dielectric mixture, *IEEE Trans. Geosci. Remote Sens.*, 26**,** 420, 1988.

# IMPAIRMENT AWARE DYNAMIC LIGHTPATH PROVISIONING/PROTECTION SCHEME FOR IP OVER WDM NETWORK

*P. Goswami[(1)], S. K. Ghosh[*(2)] , and D. Datta[(3)]*
(1) Computer & Informatics Centre
(2) School of Information Technology
(3) Department of Electronics & Electrical Communication Engineering
Indian Institute of Technology, Kharagpur 721302, India
E-mail: partha@cc.iitkgp.ernet.in, skg@iitkgp.ac.in

**ABSTRACT:**

This paper provides a brief overview of point-to-point IP-over-WDM network along w ith a wavelength-routed i mpairment-aware pat h-protected l ightpath provisioning scheme for IP-over-WDM network. This scheme will be used to study the impact of physical impairment parameter and other WDM network settings over the I P ne twork per formance metric s uch as conges tion, scalability, average hop, and average delay.

**INTRODUCTION:**

In t oday's net working i nfrastructure, the ev er-increasing I nternet traffic has al ready superceded t he existing voi ce traffic. The large volume of Internet traffic, with its connections having much wider geographical reach and longer durations than voice traffic, has enhanced t he need f or hi gh-speed w ide-area backbone net work more t han ever bef ore. While r esponding t o t his de mand, nat ional n etworking back bones al l over the w orld have gone t hrough w ide depl oyment of opt ical n etworking s etup, m ostly us ing poi nt-to-point wavelength-division multiplexing ( WDM) t echnology ( as s hown i n Fi g.1). T he I P t raffic comes into the POP today typically through 10-Gbps SONET/SDH OC-192/STM-64 circuits, which are composed of ITU-T specified wavelengths (Currently recommends 81 channels in the C band s tarting f rom 1528 .77 nm and incrementing i n multiples of 50 GHz t o 1560.61 nm.) mul tiplexed through WDM on to a physical f iber. This f iber i s f ed i nto a W DM demultiplexer, which splits out the individual wavelengths. These individual wavelengths are then f ed into t ransponders, w hich conver t t hem f rom op tical t o el ectrical and then t o a standard short-reach w avelength ( 1310 n m). T his op tical-to-electrical-to-optical ( OEO) conversion is used because historically short-reach optics is used for connectivity inside the POP environment. The short-reach light is then typically fed into a short-reach interface of a SONET/SDH cr oss-connect, which r ecovers t he SO NET/SDH cl ocking, per forms any grooming nece ssary, checks for errors, and monitors for loss of signal (LOS) so that it can perform SONET/SDH-level restoration if needed. The SONET/SDH cross-connect also connects IP co re r outer w ith 10 G bps i nterface w hich per forms pe rformance monitoring at Layer-1 t hrough L ayer-3, m onitors f or L OS s o i t can per form M PLS Fas t R eroute ( FRR) restoration, and per forms a L ayer-3 and abov e lookup to route the packet to its destination. On t he aggr egation side t he c ore r outer is typically aggr egating multiple lower-speed l inks and grooming the IP traffic core transport network through 10Gbps interface.

SEARCH

Previous Page Next Page

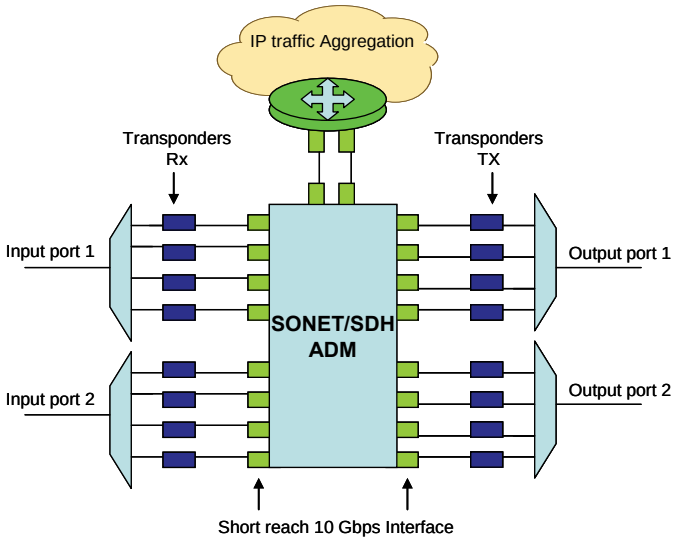


Figure 1 Point to point IP-over-WDM Interconnect Model

There are two types of path followed by IP traffic while entering and exiting a typical service provider point of presence (POP) as shown in Fig.1. The first scenario is IP traffic riding over specific time-slot of a wavelength and needs a Layer-3 lookup at the POP (which will terminate on a router) termed as "router-terminated-traffic". The second is called "pass-through" (or transient) traffic, which stays in the transport domain and bypasses router to travel on to an adjacent POP in the service provider's core network. In case of pass-through traffic today, no grooming is actually needed because the full 10 Gbps is being connected between routers bypassing the POP routers shown in Fig.1. As a result from a connectivity perspective the SONET/ SDH cross-connect is serving essentially as a patch panel. The Pass-Through Traffic volume in the POP has tended to increase and can sometimes is as high as 70 to 80 percent of the overall traffic that the POP handles. Presently, router performs the grooming function by aggregating IP traffic and presenting it to the core transport layer within well-used 10-Gbps links. The router and its associated interfaces can measure errors at layers 1 through 3, collect performance statistics, generate appropriate alarms etc. Again using MPLS FRR, the router can provide 50-ms protection or better and do so much more efficiently than the traditional SONET/SDH protection schemes which waste up to 50 percent of the bandwidth for protection purposes. For these reasons, service providers have already started using manual patching in place of the cross-connect (as shown in Fig.2) to save costs.

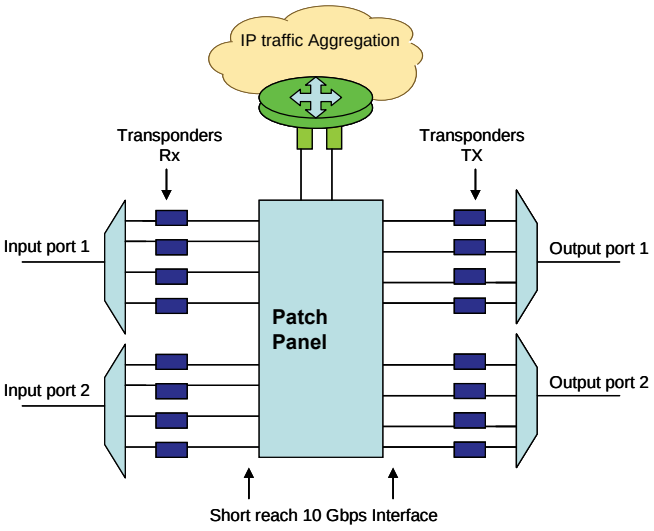


Figure 2 Manual patching in place of the cross-connect

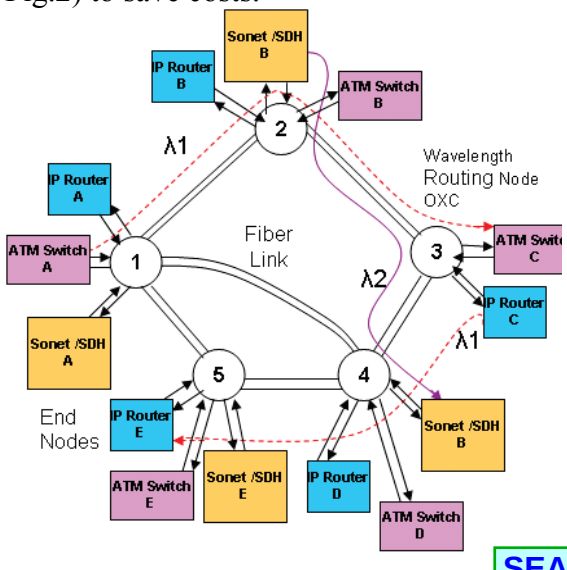


Figure 3 Wavelength-routed optical WDM network

Previous Page Next Page

The rest of the paper is organized as follows. In Sec. II, we describe the fundamentals wavelength r outing, w hile S ec. I II w e have pr oposed t he I mpairment aw are d ynamic lightpath provisioning/protection mechanism for IP over WDM network. Finally, Sec. IV concludes the paper.

## II. WAVELENGTH ROUTED NETWORK:

The above mentioned co mmercially depl oyed I P-over-WDM t echnology i s not suitable f or d ynamic I P t raffic dem and [ 1]. T he bur den of routers i n el ectronic do main i s significantly r educed b y ut ilizing s ome e merging opt ical t echnologies, w hich enabl es t he intermediate nodes in a network to carry out some of the routing functionalities in optical domain itself. Such networks, generally known as wavelength-routed networks, which employ wavelength routing with the use of wavelength add-drop multiplexers (WADM) for ring-based fiber connect ivity, t ypically us ed i n metropolitan net works ( MAN), and opt ical cross-connects ( OXC) for m esh-based fiber connectivity, generally preferred for wide-area backbone networks [ 1], w herein t he transit t raffic at intermediate nodes can be b ypassed i n optical do main i tself. T hus, t he pr oblem of hop -by-hop packet f orwarding ( in e lectrical domain) by IP routers at intermediate nodes can be al leviated in this pr ocess, thanks to the ongoing devel opments i n opt ical multiplexing, dem ultiplexing and s witching t echnologies. However, the electronic networking devices, such as, IP routers, ATM (asynchronous transfer mode) s witches, SD H ( synchronous di gital hi erarchy) or SO NET ( synchronous opt ical network) terminals would remain connected to the WADMs/OXCs to provide the desired networking services. A typical mesh-connected *physical topology* of wavelength-routed networks cons isting of O XCs[1,2] i s s hown i n Fi g. 3. T he end-to-end opt ical connect ivity between var ious node pai rs i n w avelength-routed ne tworks needs to be es tablished b y choosing a s et of *lightpaths*, w ith l ightpaths i mplying a s pecific w avelength of light propagating over a given route between a node pair. The topology formed by these lightpaths, referred t o as *logical topology* in t he l iterature, m ight t urn out t o be s ignificantly di fferent from its underlying physical topology (fiber connectivity).

## III. IMPAIRMENT AWARE DYNAMIC LIGHTPATH PROVISIONING/PROTECTION MECHANISM FOR IP OVER WDM NETWORK:

We as sume a h ybrid node, w hich cons ists of el ectrical I P r outer and opt ical cr oss-connect (OXC) (see Fig. 4). The constituent optical components in this network include a pair of EDFA's and optical power taps, on either side of the OXC at each port, for monitoring purposes apar t f rom t he c rossconnect s witch ( OXC). T he E DFA on t he i nput s ide ( with small-signal gain, compensates exactly for the signal attenuation along the input fiber and the tap losses. The EDFA on the output side (with small-signal gain, compensates exactly for the losses at the crossconnect switch (OXC). Each hybrid node also contains a transmitter array (Tx) and a r eceiver array (Rx), enabling local add/drop of any of the wavelengths at any of the nodes. Every port of electrical IP router is connected to the OXC port via internal fiber. All traffic between nodes is carried over theWDM link. Some of the incoming wavelength will terminate at the electrical IP router after it goes through OXC, other will pass-through the node. A lightpath is established between nodes by setting up the crossconnects along the route between nodes. The lightpath is terminated at the transceiver of electrical IP router part of end nodes.



Previous Page Next Page

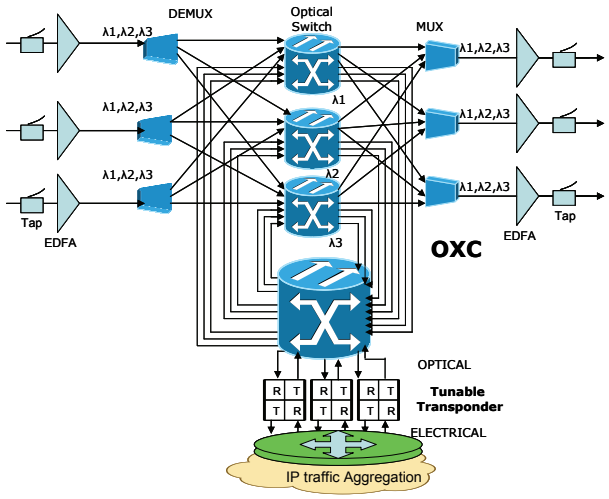


Figure 4: Hybrid IP Over WDM node architecture

In this work, the hybrid nodes are connected through single mode fibers, which employ in- line optical amplifiers for long-distance connectivity. The number of wavelengths per link and the number of transceiver port per node is a limited resource in determining the Lightpath topology (LT). Let N denote the number of nodes, $N_P$ the number of transceiver ports per node and $W$ denote the number of wavelengths in WDM links. The LT should be designed in such a way that a set of traffic demand is efficiently carried. The adequate LT is determined for a given traffic demand matrix under the constraint of the number of wavelengths, the number of transceiver ports and physical impairment parameter. In the proposed method, the network uses impairment aware path-protected lightpath provisioning scheme (See Fig. 5), which dynamically reconfigure the lightpath topology (LT) based on the dynamic traffic demand [1] and estimated signal quality [2] of the lightpath. Each node (Source node $s$) generate flow request $f_t$ ($k$) to different destination node (Destination node $d$) at different instant (at time $t$) where $k$, node pair ID = $s * \mathrm{N} + d$. On arrival of new flow request scheme shown in Fig 5.will be followed. In case of distributed approach each node will periodically measures the traffic carried over the lightpath originating from the node and physical-layer information. For this aim, two main challenges needs to be addressed within the considered distributed scenario: an on-line monitoring system and GMPLS link-state routing protocol extension to include the traffic demand as well as physical-layer information. If the traffic flow over a lightpath or lightpath link quality reaches the threshold limit each node need to initiates a LT reconfiguration procedure. Each node calculates a better LT to reduce the congestion and increase the future scalability of the network.

## IV. CONCLUSION:

Dynamically provisioned wavelength-routed backbone networks can potentially transport several Gbps of data on each lightpath over the fiber-optic physical topology. However, the high capacity of each lightpath in a fiber link has the associated problem that a link failure can potentially lead to the loss of a large amount of data and revenue. All such failures must be dealt with promptly and efficiently. A key requirement for such networks is to develop of a common control plane for both optical and electronic networks with the features of signaling, routing, and link management protocols to enable intelligent fault management. This paper provides a brief overview of a comprehensive impairment aware path-protected lightpath provisioning scheme for IP-over-WDM network. The impac physical impairment parameter and other network settings over the network performance metric such as congestion, scalability, average hop, and average delay can be studied.



Previous Page Next Page

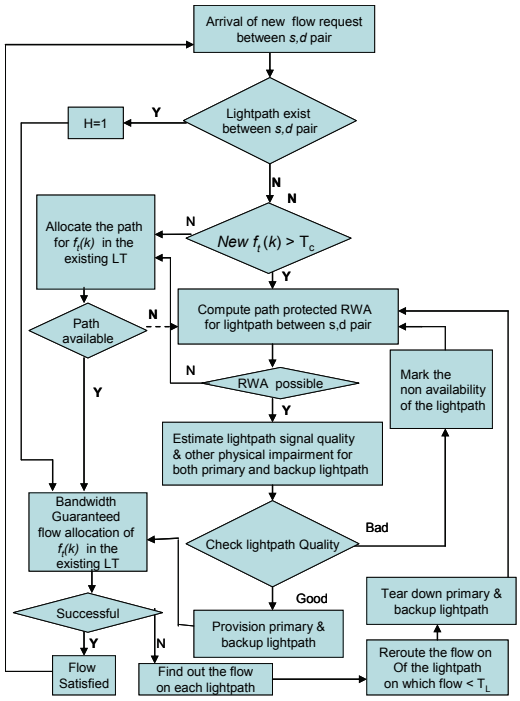


Figure 5: Impairment aware dynamic Lightpath provisioning/protection scheme for IP over WDM Network

## REFERENCE:

1. Gençata, B. Mukherjee, "Virtual-Topology Adaptation for WDM Mesh Networks Under Dynamic Traffic" *IEEE/ACM Transactions on Networking*, Vol.11, No.2, pp.236-247, April 2003
2. Y. Huang, J. P. Heritage, B.Mukherjee,"Connection Provisioning With Transmission Impairment Consideration in Optical WDM Networks With High-Speed Channels" *Journal of Lightwave Technology*, Vol. 23, No. 3, pp 982-993, March 2005

SEARCH

Previous Page

Next Page

# PTFE/CERAMIC FLEXIBLE LAMINATES FOR MICROWAVE SUBSTRATE APPLICATIONS

*K.P Murali[(1)], S. Rajesh[(1)], K. Stanly Jacob[(1)], K.J Nijesh[(1)], P. Mohanan [(2)] and R. Ratheesh[(1)*]*

(1) Microwave Materials Division, Center for Materials for Electronics Technology (C-MET), Dept of Information Technology, Government of India, Athani P.O. Thrissur, Kerala - 680 771, India.
E-mail: ratheeshr@yahoo.com

(2) Dept of Electronics, Cochin University of Science and Tech (CUSAT), Thrikkakkara, Kochi – 22
E-mail: drmohan@ieee.org

## ABSTRACT:

Polymer ceramic composites offer excellent material systems to fulfill the increasing demands in microwave communication applications. Ceramic filled Poly tetrafluroethylene (PTFE) is widely used for the fabrication of printed circuit board in the microwave region because of its low dielectric constant, low loss, high service temperature etc. In the present work PTFE/Ceramic composites have been prepared through SMECH process, a proprietary processing technique developed by C-MET. A wide spectrum of dimensionally stable composite substrates having dielectric constant ( $\varepsilon_r'$ ) ranging from 2.94 to 13.1 with loss tangent (tan δ) from 0.0018 to 0.0055 was realized. The dielectric properties of the composites were evaluated at X-band frequency region by waveguide cavity perturbation technique using Vector Network Analyzer.

## INTRODUCTION

Microwave devices such as low noise oscillators, filters, patch antennas etc. use planar substrates as the basic building block. Most common substrates are 99.6% pure alumina, fiber reinforced or ceramic filled thermoset and thermoplastic materials. Filled thermoplastic materials with superior electrical properties seize the major share of the high frequency circuit materials. Among thermoplastics, poly (tetrafluroethylene) (PTFE) based materials are the front runner for very high frequency applications. PTFE exhibits excellent dielectric properties which are stable over a wide range of frequency together with high service temperature. Open literature regarding the fabrication of such materials are very limited since most of the work in this area is protected by patent [1,2].

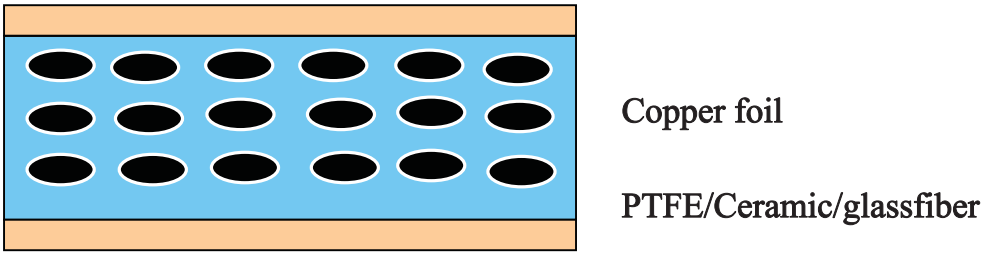


Figure1Schematic of ceramic filled PTFE substrate with Cu cladding

Although PTFE has excellent microwave dielectric properties, as such it can not be used for circuit fabrication due poor dimensional stability as a result of its high coefficient of thermal expansion (CTE ~109 ppm/°C). Often this problem is tackled by incorporating eith glass fiber or ceramic particulates in to it [2]. Ceramic filled PTFE substrates have advantageous over glass fiber filled PTFE composites due to its nearly isotropic dielectric properties. A schematic representation of ceramic filled PTFE composite is shown in figure1.

SEARCH
Previous Page
Next Page

advantageous over glass fiber filled PTFE composites due to its nearly isotropic dielectric properties. A schematic representation of ceramic filled PTFE composite is shown in figure1. In order to obtain nearly isotropic dielectric properties in the composite systems, the ceramic particulates have to be uniformly distributed throughout the polymer matrix. It is difficult to make uniformly filled PTFE composites due to its high melt viscosity ($10^{11}$Ps) through conventional polymer processing techniques like melt extrusion, injection molding etc. [2]. Hence improved processing techniques needs to be evolved to fabricate isotropic flexible laminates in the PTFE composite system.

The availability of commercial ceramic filled PTFE laminates are limited to $\varepsilon_r'$=2.94±0.04, $\varepsilon_r'$=3.0±0.04 $\varepsilon_r'$=6.15±0.15 and $\varepsilon_r'$=10.2±0.25 which are known under the trade name RT/Duroid 6002, 3003, 6006 and 6010 respectively. However this severely restricts the design flexibility of microwave circuits. Moreover, further circuit miniaturization necessitates substrates having dielectric constant > 10.2. In order to accomplish the above objectives, a range of ceramic filled PTFE composite substrates having dielectric constant between 2.94 and 13.1 have been fabricated through SMECH process [3]. The surface of the dimensionally stable composite laminates obtained through SMECH process was chemically etched to obtain better adhesion with copper conducting layer. The conducting copper layer was then laminated over the bare substrate through vacuum lamination.

## EXPERIMENTAL

The ceramic filler materials were prepared through conventional solid state ceramic route using corresponding oxides and carbonates with purity > 99%. Calcined ceramic powders were treated with Phenyl Trimethoxy silane (M/s. Sigma Aldrich, USA) coupling agent to preclude moisture absorption characteristics. The laminates were prepared through sigma mixing (SM), Extrusion (E), Calendering( C) followed by Hot pressing (H) (SMECH) process using 50 mm size PTFE (H71 Grade, HFC India), silane coated ceramic powder and short E-glass fiber ( M/s. Binani Glass, India). The appropriate proportions of starting materials were mixed using a Sigma Mixer comprising of two counter rotating sigma blades. The well mixed dough is then subjected to extrusion to make preforms. The preforms were calendered to less than 100 mm thickness by passing through the rollers of a calendering machine with rpm ratio of 1:1.2. During calendering process, the rollers imparts shear force to the preforms thereby reduces the thickness and ensures uniform distribution of filler materials throughout the polymer matrix. 9 to 10 numbers of such calendered green sheets were stacked one over the other and then hot pressed using a hydraulic laminating press. The optimized processing pressure and temperature were 210 kg/cm$^2$ and 350 $^o$C respectively. Flexible laminates of dimension of 4″x 4″ (LxB) size with 625 mm thickness were obtained after hot pressing.

The relative permittivity and loss tangent of the composites were measured in the microwave frequency region ( X-band) by waveguide cavity perturbation technique using Agilent make PNA E 8362B Vector Network Analyzer [4]. To study the filler matrix interaction, the composites were broken in liquid nitrogen and SEM ( Philips XL-30, The Netherlands) pictures were taken at the fractured surfaces.

SEARCH

Previous Page Next Page

## RESULTS AND DISCUSSIONS

A wide spectrum of dimensionally stable ceramic filled PTFE composites have been fabricated through SMECH process. The dielectric constant and loss tangent of the laminates are measured at X-band (8.2 -12.4 GHz) frequency region by waveguide cavity perturbation technique using a Vector Network Analyzer and the results are plotted in figure 2. Our studies reveal that the fused silica filled PTFE substrates have the lowest dielectric constant whereas highest dielectric constant of 13.1 is obtained for $SrTiO_3$ filled PTFE composites. It is also noted that the loss tangent of the composite system largely depends on the filling fraction and loss tangent of the ceramic particulates. We obtained loss tangent in the range 0.0018 to 0.005 for the composites under study. All the dielectric properties reported are obtained for optimum filler loaded composite systems. At optimum filler loading, the substrates exhibit maximum dielectric constant, better homogeneity, low CTE and acceptable thermal conductivity. The optimum filling fraction in PTFE composites depends on the particle size, size distribution, morphology etc. of the filler. In the present work, special emphasis has been given to control the particle size of the particulate fillers in the range 2-10 mm with wide particle size distribution.

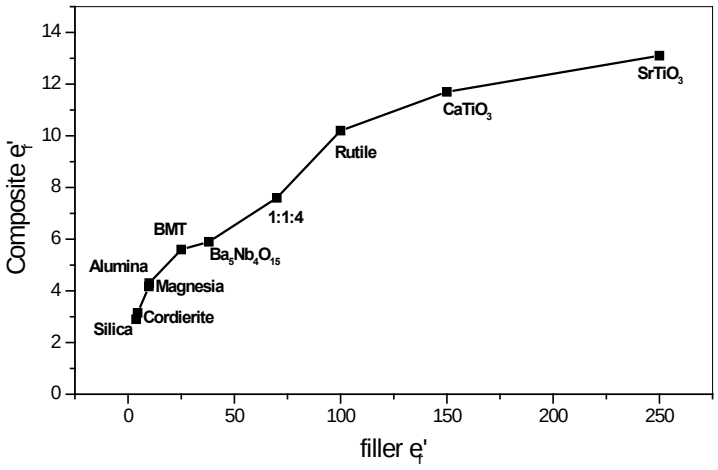


Figure 2. Dielectric constant of particulate fillers and corresponding PTFE composites.

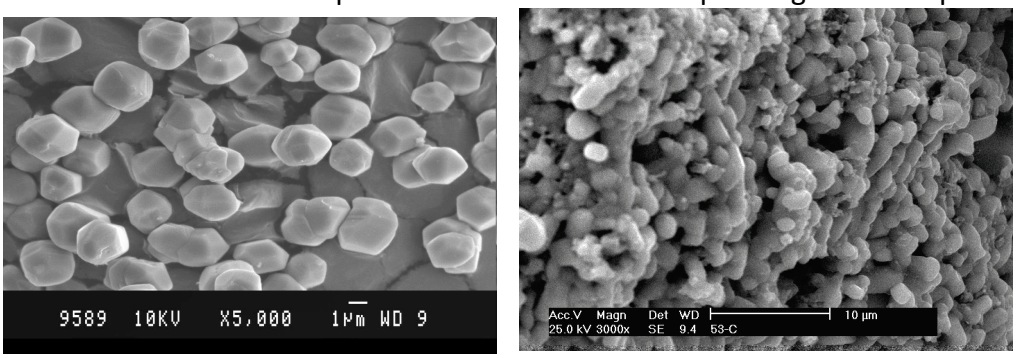


Figure 3. SEM picture of ceramic filler and ceramic filled PTFE composites.

The morphology of the filler and that of filled composites were studied using scanning electron microscopic studies. The composites were freeze fractured using liquid

Previous Page Next Page SEARCH

nitrogen before taking cross sectional SEM pictures. The SEM picture of typical alumina filler and PTFE/alumina composites are shown in figure 3. The uniform distribution of ceramic particulates are clearly observable from the figure. The cross section micrograph does not show any sign of delamination although multilayers of composite green tapes are stacked one over the other to obtain a final thickness of 625 mm. This clearly shows the efficacy of the processing methodology employed for the fabrication of planar PTFE substrates. A photograph of ceramic filled PTFE substrate with copper conducting pattern on both surfaces is shown in figure 4.

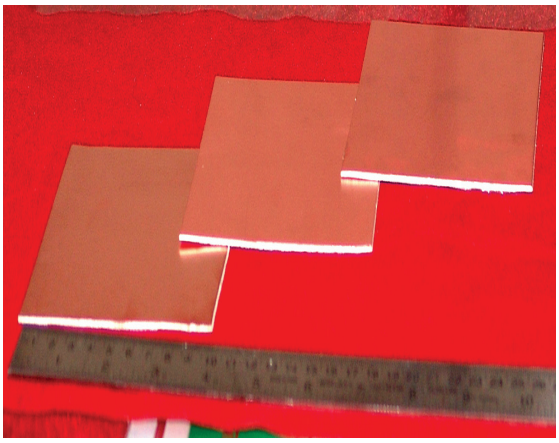

Figure 4. Copper cladded 4x4size PTFE/ceramic substrates

## CONCLUSIONS

Dimensionally stable substrates with dielectric constant ranges from 2.94 to 13.1 were realized in the PTFE/ceramic composite system through SMECH process. The dielectric properties were evaluated using waveguide cavity perturbation technique. The uniform filler distribution of the ceramic particulates in the PTFE matrix are achieved through SMECH process. 35 mm oxygen free copper foils are cladded on the bare substrate through vacuum lamination.

## REFERENCES

1. T.S. Laverghetta , Microwave materials and fabrication techniques, Artech House, Dedham MA, pp 9-55, 1985.
2. D.N. Light, J.R.Wilcox, "Process consideration in the fabrication of fluropolymer printed circuit boards," IEEE T Compon Pack T. part A.,Vol.18, No.1, pp118-26,1995.
3. S. Rajesh, K.P. Murali, R. Ratheesh, "Preparation and Characterization of High Permittivity and Low loss PTFE/$CaTiO_3$ Microwave Laminates" Polym. Comp. ( in press), 2008.
4. D.C. Dube, M.T. Lanagan, J.H. Kim, S.J. Jang, "Dielectric measurements on substrate materials at microwave frequencies using a cavity perturbation technique," J. Appl. Phys., Vol. 63, No.7, pp. 2466-68, 1988.

# RESEARCH SESSION VI

# ANTENNAS I

SEARCH

Previous Page

Next Page

# RESEARCH SESSION VI

## ANTENNAS I

***Chair : Prof. Debatosh Guha, Institute of Radiophysics & Electronics, Kolkata***



SEARCH

Previous Page

Next Page

# INTENSIVE STUDY ON WAVEGUIDE COUPLED MICROSTRIP PATCH ANTENNA.

*Nandkumar M. Shetti and N.H.Ayachit**
Dept. of E&C S.D.M.college of Engg.and Technology Dharwad
*B.V.B. College of Engg. and Technology Hubli
nmshetti2003@yahoo.co.in narasimha1957@yahoo.co.in

**ABSTRACT:**

An entirely new technique has been designed to couple the advantages of both the microstrip pat ch ant enna and r ectangular w aveguide. Pat ch ant enna consists of two patches, one r adiator patch which faces outside, and t he other faces mouth of the rectangular waveguide. This tool is called effective fringing area method. F irst w e cons idered her e w aveguide coupl ed microstrip pat ch antenna as t he par allel load com prising of four el ements .Along w ith t his observed return loss graph and radiation pattern graph with observation table is provided.

## INTRODUCTION:

In t his pa per, a new de sign of w aveguide coupl ed microstrip pa tch antenna i s proposed, w hich i s us eful i n designing co llision avoi dance s ystem becaus e her e r adiation pattern can be steered so that it falls in the next lane thus enabling s tracking of the obj ects. The radiating patch in the proposed design is a simple circular patch. The proposed patch antenna has two patterns on either side. One is radiating patch which is circular which faces outside and t he ot her w hich f aces mouth of the w aveguide pl ays an i mportant r ole in t he designing of the patch antenna.

## CONSTRUCTION:

Patch di mensions i s 40. 785mm x 40.73 mm and cad p oints ar e (10,10),(50.785,10),(10,50.73) and ( 50.78,50.73).Mounting hole co -ordinates i s 30.90 mm x 32.70 mm and cad poi nts ar e ( 14.94,46.715), ( 44.845,46.71), ( 14.94,14.013) and(45.84,14.013).Waveguide di mension i s 22.82 mm x 10.016mm an d cad poi nts are (18.84,25.36), (41.66,25.36), (18.84,35.36) and (41.66,35.36). Iris t ype rectangular ring dimension is 7.60 mm x 7.32 mm and cad points are (26.69, 27.76), (33.01, 27.16), (26.69,32.96) and ( 33.01,32.96).The ci rcular d isk an tenna mounting co -ordinates on radiating s ide of t he pa tch i s (26.68,36.76).The r adius o f t he ci rcular di sk patch ant enna is 4.575mm.The feed point co-ordinates is (26.69,32.96). The distance from feed point to center of circular disk is 1.4mm.P.T.Hole diameter is 0.8mm. Preparation method is photo etching method. Microstrip antenna was constructed for 10 GHz. For this frequency duroid material was pr eferred, s ince t his material i s not f reely avai lable i n I ndia, doubl e s ided gl ass epox y with dielectric constant of 4.2 was used. Dimensions were taken from microwave hand-book. Waveguide coupled microstrip patch antenna was prepared using PTH (plated through hole) method and bot h sides of t he copper w ere t in coat ed. T hickness of t he di electric i s 1.6 and copper thickness is 35 micron. Minimum line thickness possible is 0.25 mm.

SEARCH
Previous Page
Next Page

The study is performed for various geometry by varying feed point ,orientation of the patch and location of the patch as shown in the below figure

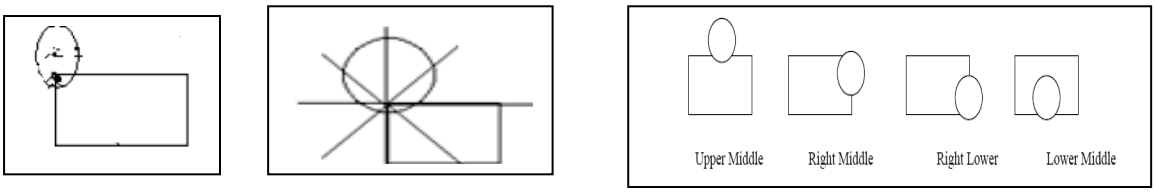


## EXPERIMENTAL SETUP:

10 G Hz m icrowave bench ( GUNN di ode os cillator) i s us ed f or the s tudy o f waveguide-coupled microstrip patch antenna. The antenna is mounted on t he mouth of the waveguide. Radiation pattern measurements were carried out with help of the horn antenna mounted on ar m of the spectrometer. The readings were taken from the horizontal field for every 5 degrees using detector diode .The results were plotted on the polar graph. For return loss measurement, direction couplers of 3db each were used in reflectometer method. For the entire measurement 0-20 micro ammeter used so that square law is obeyed. Totally 12 discrete frequencies were used

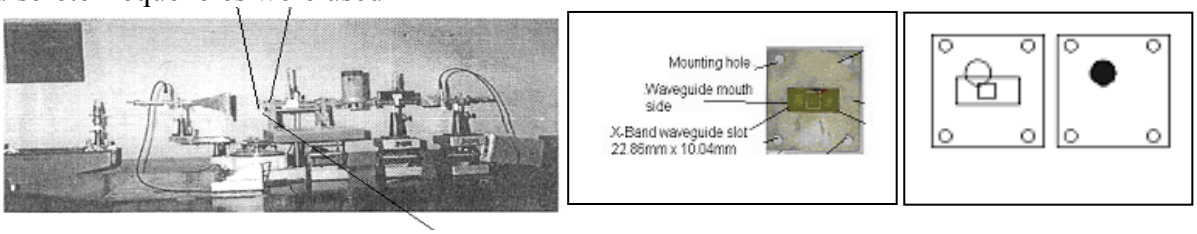


## OBSERVATION:

Return loss graph of patch no 19 Radiation pattern graph

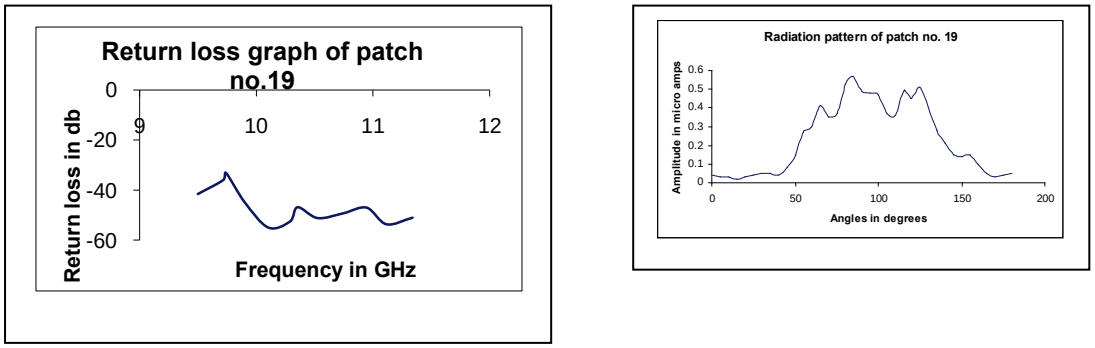


| patch no. | length | Rotation | position | Feed point | Return Loss db | Band width | Polarization | Main peak |
|---|---|---|---|---|---|---|---|---|
| 19 | 7.6 | $0^0$ | Left top corner | 3.8mm | -55.04 | 2.72 | elliptical | $90^0$ |

## ANALYZING USING PARALLEL LOAD MODELING:

Patch is modeled as parallel loads in the waveguide. The admittance of the iris type rectangular patch, admittance of aperture and admittance of radiation patch are calculated using the formula .The rectangular ring pattern on the waveguide side is loaded as a reso ring and the normalized susceptance Bf is given by the equation [3]and Y of aperture in[1].

Figure of equivalent circuit of waveguide coupled microstrip patch antenna

SEARCH
Previous Page
Next Page

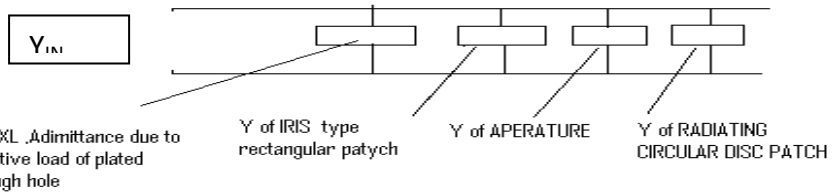


$$xx = \left( \frac{377 \times h \times f \times \log\left( \frac{c}{\pi f r \sqrt{\varepsilon_r}} \right)}{c} \right)$$

$Y_{XL}$=1/XL=admittance due to inductive load of plated through hole

Y of Iris:

$$B_f = \left( \frac{l_g}{a} \right) \cot^2\left( \frac{\beta D}{2a} \right) + \left\langle \frac{p\left(a^2 - D^2\right)}{4AD\cos\left( \frac{\beta D}{2a} \right)} \right\rangle^2 \cdot \left\langle \frac{\left( 1 - \frac{l^2}{4D^2} \right)}{\left( 1 - \frac{l^2}{4a^2} \right)} \right\rangle \left( \frac{4bd}{l_g a} \right) \ln \cos ec\left( \frac{\beta d}{2b} \right)$$

$$+ \left( \frac{l_g}{aD^2} \right) \left( \frac{b^2}{3} + \frac{d^2}{2} - \frac{8bd}{2} \right)$$

$$- \left( \frac{2b^2}{p^2} \right) \sum_{n=1} \left( \frac{\pi p d}{b} \right) \frac{\left( \frac{2np(a-d)}{b} \right)}{n^2}$$

## ANALYZING USING EFFECTIVE FRINGING AREA MODELING:

In t his modeling adm ittance of ci rcular p atch i s not ca lculated, instead near est rectangle formed by the circular disc on the ground plane is considered for calculation. As full ci rcular pat ch w as not over lapping on gr ound pl ane fringing t akes pl ace onl y on those area of circular disk which is backed by ground plane. So fringing takes place by small area, and this fringing is responsible for radiation. Fringing takes place between the lower area of the circular patch and the ground plane. The calculation performed as in [2]

Nearest rectangle formed from effective fringing area

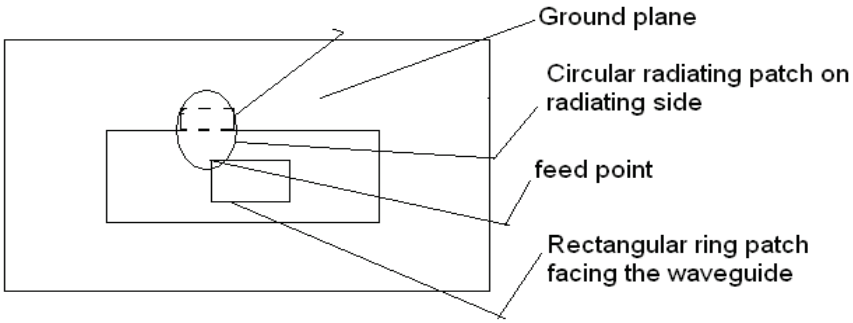


Figure to indicate rectangle formed by considering the effective fringing area

SEARCH

Previous Page

Next Page

## WALL ADMITTANCE.

$$Y_{WY} = Y_W = G_W + jB_W \qquad G_W = 0.00836W / \lambda_0 \qquad B_W = 0.01668 \frac{\Delta l}{h} \frac{W}{\lambda_0} e_e$$

$$e_e = \frac{\varepsilon_{r+1}}{2} + \frac{\varepsilon_r - 1}{2}\left(1 + \frac{12h}{W}\right)^{-1/2}$$

$$\frac{\Delta l}{h} = 0.412 \frac{(e_e + 0.3)\left(\frac{W}{h} + 0.264\right)}{(e_r - 0.250)\left(\frac{W}{h} + 0.8\right)}$$

These formulas were used to calculate the return loss graph for all the 12 discrete frequencies and graph is plotted .In patch no 19 it matches exactly and for other patches error is less.

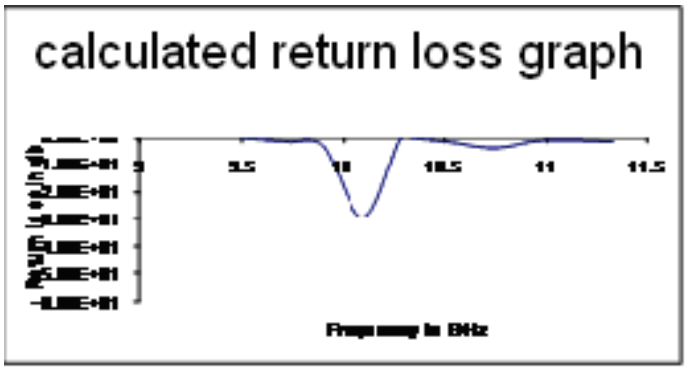


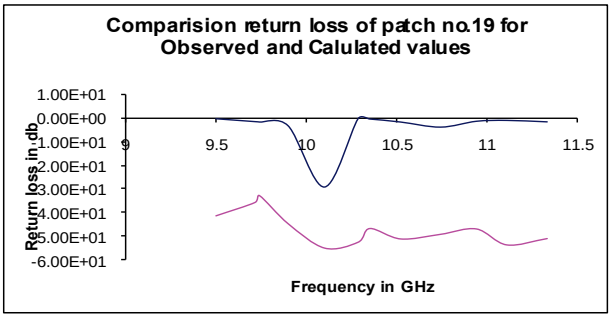


## CONCLUSION:

Successfully tested the new kind of antenna called waveguide coupled microstrip patch antenna Effective fringing area method yields very good results .In patch no 19 both results were 10.102GHz whereas for other three it is in 10% variation .So this method can be used for analyzing of waveguide coupled microstrip patch antenna. More better modeling is possible with the help of method of moments. Here circular disc antenna, along with rectangular iris type patch, at the mouth of the waveguide is looked as metallic conducting body with impedance attachment, embedded in dielectric. The $TE_{10}$ wave from waveguide incident on it is scattered by the conducting body.

## ACKNOWLEDGEMENT:

Authors thank the Management and principal of S.D.M. college of engg. And technology Dharwad for all the support and encouragement shown

## REFERENCES:

1. David M.Pozor ,"Microwave engineering" John Wiely and Sons,1998.
2. J.Bahl and B.Bhatia ,"Microstrip antenna" Artech House ,1980.
3. Kanda, "Iris fed millimeter wave rectangular antenna." IEEE Electromagnetic computability , vol.27, no. 4,pp212 1985

SEARCH

Previous Page Next Page

# DESIGN OF A COMPACT DUAL BAND MICROSTRIP ANTENNA USING GENETIC ALGORITHM

*P.Mythili, S.Mridula and Binu Paul*
Division of Electronics, School of Engineering,
Cochin University of Science and Technology,Kochi-22, India,
mythili@cusat.ac

## ABSTRACT

In this paper the design of a dual band single feed microstrip antenna supporting Wireless communication applications (DCS/PCS/IEEE 802.11b/g) is presented. Genetic Algorithm is used to optimize the multi-objective problem of obtaining the required antenna geometry and the size of the antenna for the frequencies 1.8 GHz and 2.4 GHz. The designed antenna is analyzed using the IE3D™ software and the return loss characteristics and the radiation patterns are reported.

## INTRODUCTION

Modern communication systems such as, Global Positioning System (GPS), Satellite Digital Audio Radio Service (SDARS), Wireless Local Area Networks (WLAN) and Wireless Personal Area Networks (WPAN) usually require antennas with compactness and low cost. They often require dual band operation to support multiple applications. In recent years, the miniaturization of antennas has become more important especially due to the huge demand of small antennas for cellular mobile communication system applications where compact antennas are required to be integrated into very small handsets. Light-weight and low-cost are other important specifications. Many configurations have been proposed till date. Most of them suggest modifications of common well known geometries leading to the reduction of the antenna physical size. However all the proposed structures are based on intuitive solutions and their behavior can be described in terms of known radiation mechanisms. The technique based on Genetic Algorithm (GA), is increasingly applied to electromagnetic design. GA optimization is well suited to working with existing electromagnetic (EM) simulation technologies, often yielding results that achieve the performance targets with a unique structure that is non-intuitive to the antenna designer. Various multiband designs are proposed till date [1 – 6]. However these techniques usually lead to an increase in antenna size or manufacturing cost. GA is used in this work to optimize the multi-objective problem of obtaining the antenna geometry as well as optimize its size to obtain the desired characteristics. The attractiveness of the GA design over the other methods is its ability to achieve the desired performance by a unique patch shape with a single feed as against dual fed and other slotted antennas.

## GENETIC ALGORITHM (GA)

GA's are search and optimization algorithms [7] based on the mechanics of natural selection and natural genetics. A simple flowchart showing the process of GA is shown in Fig. 1.

SEARCH

Previous Page Next Page

## CODING OF THE MICROSTRIP PATCH

A square patch is divided in to n x n cells. All cells have equal dimensions. Each cell is assigned a binary random number '1' or '0' as shown in Fig. 2. A population (initial) with N numbers of such patches is generated in the form of random binary strings. GA is then applied. Each one in the population is analyzed and its resonant frequency is obtained using Integral Equation method.

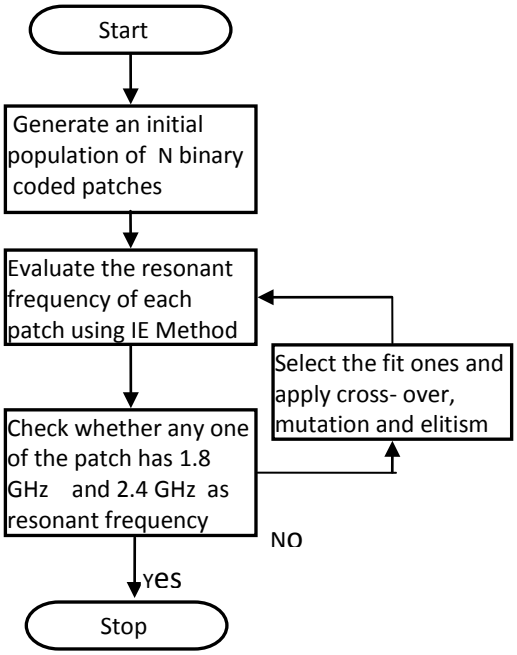


Figure.1 A simple flowchart for microstrip antenna design using GA

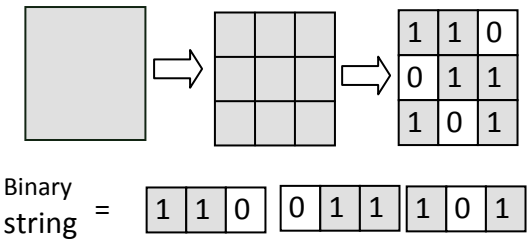


Figure.2 A typical coding of a 3x3 patch

## FITNESS FUNCTION

The fitness of each antenna in the population is evaluated using a fitness function. The fitness function for the antennas whose frequencies do not fall in the range 1.7 to 1.8 and 2.3 to 2.5 GHz is defined by

$$fitness = \left(\frac{1}{error}\right)*100 \quad (1)$$

and rest of the antennas are assigned a fitness given by

$$fitness = \left(\frac{1}{error} + dbfit\right)*100 \quad (2)$$

$$error = \frac{\dfrac{abs\left(f_{target1} - f_{evolved1}\right)}{f_{target1}} + \dfrac{abs\left(f_{target2} - fevolved2\right)}{f_{target2}}}{2} \quad (3)$$

$f_{target1} = 1.8$ GHz and $f_{target2} = 2.4$ GHz for this particular work and $dbfit$ is a small bonus value added to the fitness based on the return loss i.e., performance of the antenna. $f_{evolved1}$ and $f_{evolved2}$ are the evolved frequencies corresponding to each antenna in the population.

## SELECTION PROCESS, CROSSOVER, MUTATION AND ELITISM

Based on the fitness assigned in the previous section the fittest of the population is ... Roulette wheel selection. Single point cross over is used after mutation ...

SEARCH
Previous Page
Next Page

elitism are introduced and the new population is obtained. The chromosomes are once again checked for fitness and the entire process continues until the fit patch with compact dimension satisfying the frequency requirements arrives.

## RESULTS AND DISCUSSIONS

GA was implemented in MATLAB® 7.0. A population size of 20 antennas was considered. Crossover rate is 0.7 and the mutation rate is chosen as 0.1. The Ground plane size of the antenna was 30 x 30 mm and the patch size was 20 x 20 mm. The patch was divided in to 10 x 10 cells of dimension 2 x 2 mm. The microstrip antenna synthesized using GA is shown in Fig. 3. This antenna was obtained in the 5th generation. The return loss curves are shown in Fig. 4.

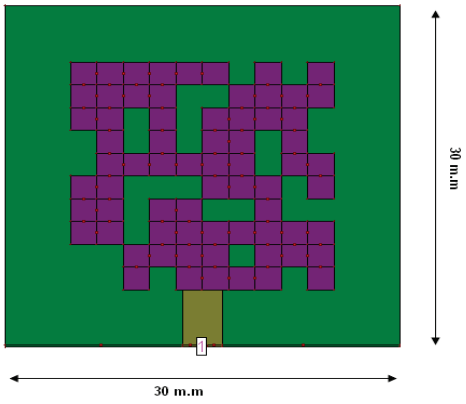


Figure.3 Genetically Designed antenna with f1=1.8GHz and 2.4

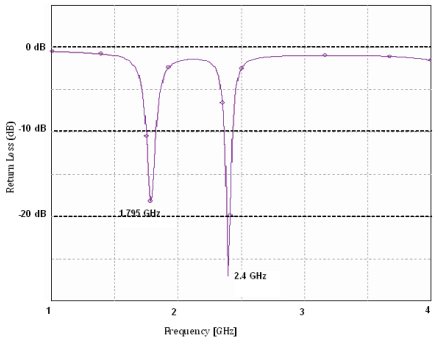


Figure.4 Return loss curves

The radiation patterns of the dual band antenna are shown in Fig. 5.

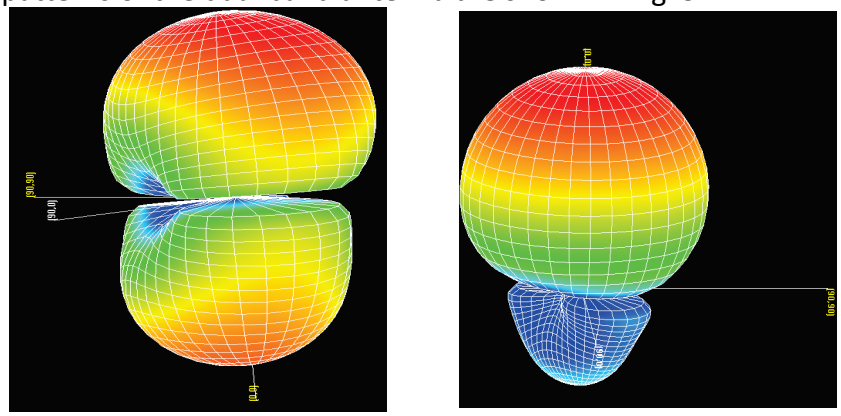

Figure.5 Radiation patterns of the genetic MSA for 1.8 GHz and 2.4 GHz

SEARCH

Previous Page Next Page

## CONCLUSION

A dual band genetic microstrip antenna was successfully designed for 1.8 and 2.4 GHz. Considerable compactness was achieved compared to the dual feed regular rectangular microstrip antenna of dimensions: ground plane = 50 x 50 mm and patch size 28 x 39 mm.

## REFERENCES


1. Constantine A. Balanis, "Antenna theory analysis and design", 2nd Edition
2. Naftali Herscovici, Manuel Fuentes Osorio and Custodio Ceixeiro, "Miniaturization of microstrip rectangular patches using genetic algorithms", IEEE Antennas and Wireless Propagation Letters, Vol. 1, pp. 94- 97, 2002.
3. Frank J. Villegas, Tom Cwik, Yahya Rahmat-Samii, and Majid Manteghi, "A Parallel Electromagnetic Genetic Algorithm Optimization Application for Patch Antenna Design", IEEE transactions on antennas and propagation , volume 52 , No. 9, Sept. 2004.
4. J.Michael Johnson and Yahya Rahmat-Samii "Genetic algorithms in engineering electromagnetics", IEEE Antennas and propagation magazine, volume 39, No. 4, Aug 1997.
5. H. Choo and H. Ling, "Design of multiband microstrip antenna using genetic algorithm", IEEE Microwave and Wireless components letters, Volume 12, No. 9, Sep 2002.
6. Edward E. Altshuler and Derek S. Linden, "Wire antenna designs using genetic algorithms", IEEE Antennas and propagation, volume 39, No. 2, April 1997.
7. D.E. Goldberg, "Genetic algorithms in search, Optimization and machine learning", New York, Addison-Wesley, 2003.


SEARCH

Previous Page Next Page

# SMALL DUAL-FREQUENCY ASYMMETRIC Π SLOT LOADED RECTANGULAR MICROSTRIP ANTENNA USING VERTICALLY ORIENTED RECTANGULAR SLOTS

*Ravi M. Yadahalli[1], Vani R. M.[2], and P.V. Hunagund[3]*
Dept of E &CE, S.D.M. College of Engg and Technology, Dharwad-580 002, India
ravimyadahalli@yahoo.com
[2] USIC, Gulbarga University, Gulbarga- 585 106, India
[3] Department of Applied Electronics, Gulbarga University, Gulbarga- 585 106, India

**ABSTRACT:**

In this paper, a small dual-frequency rectangular microstrip antenna is presented. The proposed design consists of a rectangular microstrip antenna with a pair of asymmetric Π slots close to the non-radiating edges of the patch and vertically oriented rectangular slots. Experimental study was carried out by varying the number of rectangular slots. Using three identical rectangular slots in addition to asymmetric Π slots, a dual frequency operation with significant reduction of both the resonant frequencies is obtained in comparison to conventional rectangular microstrip antenna without slots. The proposed configuration was first simulated using IE3D simulation software package and then verified experimentally. The simulated and experimental results are found to be in good agreement.

**INTRODUCTION:**

In some applications such as mobile satellite personal communication systems, cellular network systems, global position system (GPS), vehicular communication, an antenna needs to be operated at two frequencies which may be too far apart for a single antenna element to operate efficiently at both these frequencies. Also, the antenna has to be compact in size. For this purpose various types of dual-frequency antennas in microstrip configurations have been devised. In the literature survey, various microstrip antennas have been proposed to reduce the size of the antenna or to be used for dual frequency operation. But the combinations of these two objects are rare in literature. In the year 1997, Wong and Yang proposed a small dual frequency microstrip antenna with cross-slot [1]. In the same year, Wong and Chen proposed a compact, dual frequency microstrip antenna. The design consists of rectangular microstrip patch loaded with shorting pin [2]. In the year 1998, Wong and Yang, demonstrated Compact dual frequency operation by cutting microstrip antenna with a pair of bent slots [3]. Other dual frequency operations achieved using a cross-slot loading & two shorting pins are reported by Zhong and Cui [4]. Again in the year 2001, a dual frequency operation was demonstrated by varying spacing between two arms of symmetric Π shaped slots [5]. Recently, Ravi et. al., proposed a compact dual frequency microstrip antenna by varying the length of the arms of the asymmetric Π slots and achieved compact dual-frequency operation with compactness of 25% and 18% in the antenna size [6].

In this paper, we present small dual-frequency asymmetric P slots loaded rectangular microstrip patch antenna. Using the proposed design, dual frequency operation an SEARCH significant lowering of both the resonant frequencies is obtained by varying the number of rectangular slots in the radiating patch.

Previous Page Next Page

## ANTENNA DESIGN

First a reference antenna (RA) which is a rectangular microstrip antenna (L, W) = (30, 20) mm fed by a 50 Ω co-axial feed was designed for 2.37 GHz ($\varepsilon_r$ = 4.3 and h = 1.6 mm). Later, a pair of asymmetric Π slots are etched in the rectangular patch close to its non-radiating edges with a spacing $S_1 = S_2 = 1$ mm. The length of the asymmetric Π slots, $l_{v1} = 8$ mm and their width $w_{v1} = 1$ *mm*. The asymmetric Π slots loaded rectangular patch is in turn embedded using 3 identical rectangular slots in the antenna's radiating patch. These vertically embedded rectangular slots are narrow and have a fixed length of 15 mm. The feed point is located at the centerline of the rectangular microstrip patch, with a distance of $d_f$ from (X, Y) = (0, 0) as shown in Fig.1.

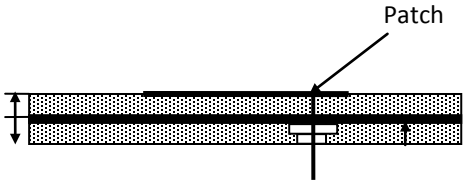


Fig.1: Geometry of Compact dual-frequency rectangular microstrip patch antenna using asymmetric Π shaped slots and rectangular slots (CDFRMSA-AΠR)

## EXPERIMENTAL RESULTS AND DISCUSSION:

Initially the proposed prototype antennas were simulated using IE3D Zeland software for different number of narrow rectangular slots of fixed length [7]. For the simulation of all the microstrip antennas, an infinite ground plane has been assumed. However, for the experiments, size of the ground plane is taken to be more than six times the substrate thickness in all directions with respect to the patch dimensions to reduce the effect of the finite ground plane. Then the proposed prototype antennas were fabricated and measured experimentally using Rohde and Schwarz, Germany Make Vector Network Analyzer of ZVK model (10 MHz to 40 GHz).

The parametric study is carried out by varying the number of vertically oriented rectangular slots in the asymmetric Π slots loaded rectangular patch of CDFRMSA-AΠR. Several proposed antennas with different number of vertically oriented rectangular slots i.e., the cases of antennas with single rectangular slot, two rectangular, and three rectangular slots have been implemented and studied. The corresponding simulated and experimental results are shown in the Table 1. It is seen from the table that when a rectangular slot is inserted at the center of asymmetric Π slots loaded radiating patch, dual frequency operation is obtained. $f_1$ gives a compactness of 34.82% while $f_2$ gives a compactness of 19.27%, when compared to conventional RMSA and the obtained frequency ratio is 2.09.

**Table 1: Simulated and experimental results of CDFRMSA-AΠR**

| Simulated/ **Measured** | $l_{v1}$ , *mm* | **Resonant frequency, $f_r$ (GHz)** | **Return Loss (dB)** | **Bandwidth (MHz %)** | **Frequency Ratio, $f_2/f_1$** | **Reduction in size, %** |
|---|---|---|---|---|---|---|
| **REFERENCE ANTENNA** | | | | | | |
| Simulated | 0 | 2.36 | −16.40 | 95 4.03 | --- | --- |
| **Measured** | | **2.37** | **−24.80** | **60 2.53** | --- | --- |
| **CDFRMSA using a pair of asymmetric Π shaped slots & single rectangular slot** | | | | | | |
| Simulated | 8 | $f_1$ = 1.73<br>$f_2$ = 3.65 | −14.59<br>−12.48 | 68 3.93<br>90 2.46 | 2.10 | 34.92<br>20.20 |
| **Measured** | | **$f_1$ = 1.8**<br>**$f_2$ = 3.775** | **−30.97**<br>**−22.31** | **25 1.38**<br>**75 1.99** | **2.09** | **34.82**<br>**19.27** |
| **CDFRMSA using a pair of asymmetric Π shaped slots & two rectangular slots** | | | | | | |
| Simulated | 8 | $f_1$ = 1.69<br>$f_2$ = 3.58 | −16.13<br>−21.86 | 89 5.2<br>146.7 4.0 | 2.11 | 36.44<br>21.78 |
| **Measured** | | **$f_1$ = 1.75**<br>**$f_2$ = 3.57** | **−22.52**<br>**−11.19** | **43.75 2.5**<br>**58.75 1.64** | **2.04** | **36.56**<br>**23.26** |
| **CDFRMSA using a pair of asymmetric Π shaped slots & three rectangular slots** | | | | | | |
| Simulated | 8 | $f_1$ = 1.63<br>$f_2$ = 3.35 | −17.13<br>−12.51 | 92 5.64<br>72 2.15 | 2.05 | 38.74<br>26.85 |
| **Measured** | | **$f_1$ = 1.6825**<br>**$f_2$ =3.4075** | **−27.85**<br>**−16.17** | **30 1.78**<br>**60 1.76** | **2.03** | **38.92**<br>**26.88** |

Again for etching two vertically oriented rectangular slots at the extreme radiating edges of the patch, both the frequencies reduce still further giving a frequency ratio of 2.04. Further, when three vertical slots are inserted as shown in the figure 1, both the frequencies reduce still further. The variation of return loss with the frequency for the proposed antenna CDFRMSA-AΠR is shown in the Fig.2 and it is seen from the figure that $f_1$ resonates at a frequency, which is 0.61 times that of the conventional antenna giving a size reduction of 38.92% and $f_2$ resonates at a frequency, which is 0.72 times the conventional antenna giving a compactness of 26.88% in the antenna size. Again, it is seen from the table that $f_1$ h SEARCH bandwidth of 1.78% and $f_2$ has a bandwidth of 1.76%.

The radiation pattern of the proposed antenna remains in the broadside direction at $f_1$ = 1.68 GHz. Previous Page adiation pattern at $f_2$ = 3.40 GHz splits into two equal halves, which can find applicatio Next Page synthetic aperture radar (SAR).

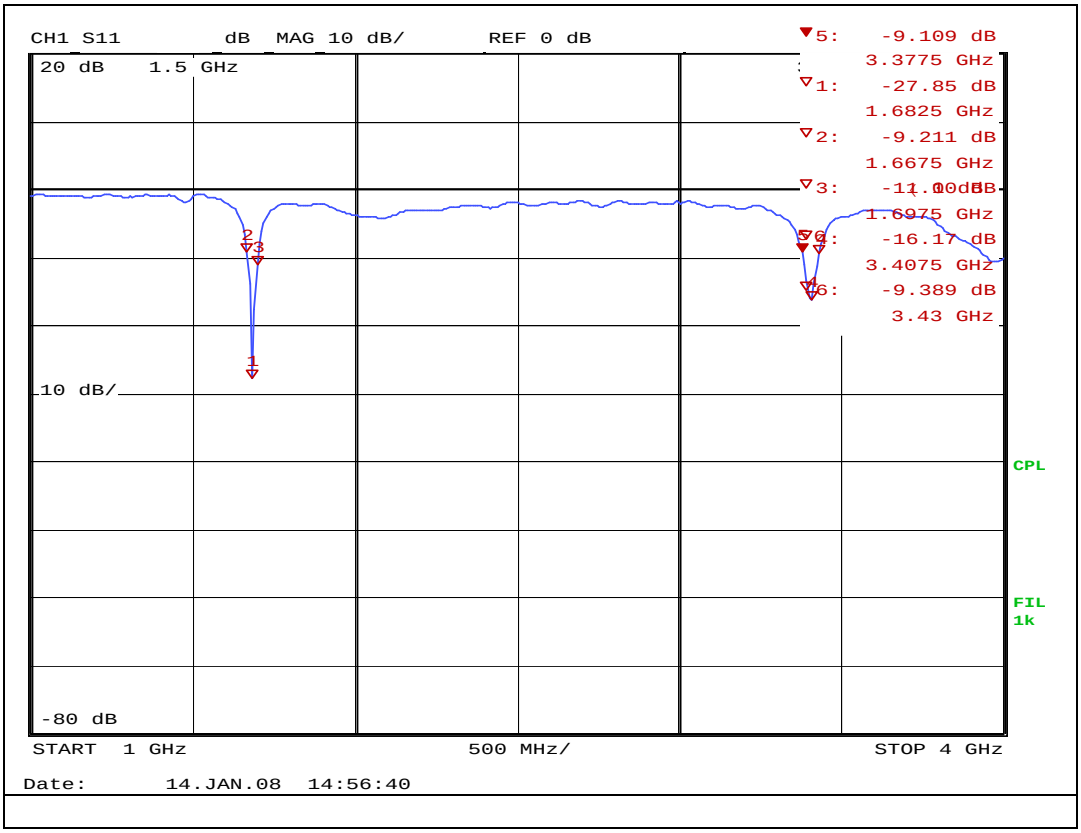


Fig. 2: Variation of return loss Vs frequency for CDFMSA-AΠR

A pair of asymmetric Π shaped slots in the radiating patch of the microstrip antenna can introduce dual-frequency behavi or. A tunable frequency ratio between the two frequencies in the r ange of 2.03 to 2.09 can be obtained by increasing the number of rectangular slots. Moreover, with proposed design, a com pactness of 38.92% and 26.88% is obtained by i ntroducing t hree r ectangular slots, w hen co mpared t o standard r ectangular microstrip antenna without slots (reference antenna).

**CONCLUSIONS:**

A compact dual frequency asymmetric P slots loaded microstrip patch antenna using vertically oriented rectangular slots was designed, fabricated and studied in detail. With the proposed design, a size reduction of 38.92% and 26.88% for the two resonant frequencies is obtained, when compared to standard rectangular microstrip antenna without slots (Reference antenna). A tunable ratio of in the range of 2.03 – 2.09 can be obt ained by increasing the number of rectangular slots.

SEARCH

Previous Page

Next Page

**REFERENCES:**


1. Kin Lu Wong and Kai-Ping Yang, "Small dual-frequency microstrip antenna with cross slot", *Electron Lett.*, Vol.33, No.23, pp.1916-1917, 1997.
2. Kin Lu Wong and W.S. Chen, "Compact microstrip antenna with dual frequency operation", *Electron Lett.*, Vol.33, No.8, pp.646-647, 1997.
3. Kin Lu Wong and Kai-Ping Yang, "Compact dual-frequency microstrip antenna with a pair of bent slots", *Electron Lett.*, Vol.34, No.18, pp.225-226, 1998.
4. Shun-Shi Zhong and Jun-Hai Cui, "Compact dual-frequency microstrip antenna", *IEEE Antennas and Propagation Society International Symp.* Vol.4, pp.2196-2199, 2000.
5. Yi-Fang Lin, Hua-Ming Chen, Chin-Chun Kuo and Kuang-Chih Huang, "Single feed dual-frequency rectangular microstrip antenna with a pair of π slots", *IEEE Antennas and Propagation Society International Symp.*, Vol.4, No. , pp.74-77, 2001.
6. Ravi M. Yadahalli, Usha Kiran K., R. M. Vani, and P.V. Hunagund, "Compact dual-frequency microstrip patch antenna using a pair of asymmetric P-shaped slots", Asian Journal of Physics, Vol.17, No.1, pp. 153-156, 2008.
7. IE3D release 12.1, Zeland Software Inc., 2006.

# MOM ANALYSIS OF BROAD WALL SLOT COUPLED DIELECTRIC RESONATOR ANTENNA

*Abdulla P[1], Y.K.Singh [2], and Ajay Chakrabarty[2]*
(1) School of Engineering, Cochin University of Science and Technology, Kochi, India.
E.mail: abdulla@ece.iitkgp.ernet.in
(2) Department of Electronics and Electrical Communication Engineering, Indian Institute of Technology, Kharagpur, India.
E.mail: yatendra@ece.iitkgp.ernet.in

## ABSTRACT

Broad wall longitudinal slot coupled hemispherical DRA being analyzed using method of moments(MoM) . The slot electric field is described using entire domain sinusoidal basis function and the continuity of tangential magnetic field at the slot aperture is enforced to determine the actual electric field. Thickness of the slot is analyzed using cavity Green's Functions. The computed data are compared with commercial FEM code.

## INTRODUCTION:

It has been shown that dielectric resonator antennas can be used as effective radiators at microwave frequencies where ohmic losses become a serious problem for conventional metallic antennas [1]. DRAs offer several advantages such as small size, low cost, light weight, ease of excitation and ease of integration with active circuitry. They offer wider bandwidth than the microstrip antennas used at the same frequency [2]. Many different feeding mechanisms can be used with DRA, such as the co-axial probe , direct microstrip line feed , aperture coupled by microstripline or coplanar waveguide and conformal strip feed [3]. However, feed line losses of these excitation methods are considerable at millimeter-wave frequencies. Today, the waveguide still plays an important role in microwave and millimeter-wave applications; since the waveguide has metallic walls, it has an excellent shielding between the exterior and interior regions, thus avoiding radiation loss even in the millimeter–wave band. Recently, a new and low loss excitation scheme that employs a rectangular waveguide broad wall slot fed is reported [4], in which analysis is given for the broad wall slot coupled cylindrical dielectric resonator only. Moreover, the DR is analyzed using the body of revolution, which is applicable only for rotational symmetrical structures.

Waveguide slot antennas are widely used as conventional array antennas [5-7]; however, the bandwidth of waveguide slot is narrow. Such narrow bandwidth limits the frequency scanning range for the array. In order to increase the frequency scanning range, the bandwidth should be increased. To increase the bandwidth, the slot is loaded with a dielectric resonator that has very high radiation efficiency. Such a combination creates two coupled resonators that can be designed properly to increase the over all bandwidth and consequently improve the frequency scanning. Moreover antenna miniaturization is the hot topic today. The slot loaded DRA will reduce the effective length of the slot as well as the spacing between the slots, which will bring down the total length of array.

The analysis presented in this paper, the electric field at the slot is assumed to be sum of several sinusoidal functions (basis functions) defined over the entire slot region, weighted by certain complex coefficients. On the basis of this distribution, the transverse magnetic

SEARCH
Previous Page
Next Page

scattered inside the waveguide and cavity are determined. At the boundary of the slot, the magnetic fields must match. On imposing this boundary condition, an equation is obtained with the coefficients of basis functions as unknowns which are solved by using MoM.

**THEORY:**

The geometry of the waveguide broad wall longitudinal slot coupled HDRA is shown in Fig 1. The longitudinal cross sectional view of Fig.1 is given in Fig. 2. We assume that the thickness of waveguide is $2t$ on which HDRA sitting. The considered slot is narrow in $\hat{x}$ direction to eliminate any possible cross-polarization, only variation along z is considered for magnetic field, i.e., the electric field $E_x$ in the aperture varies only in the z-direction and is non-varying in the $x$ direction.

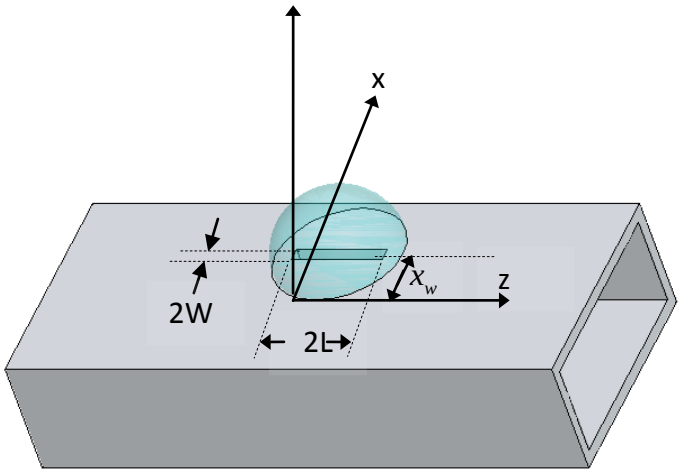


Fig. 1: Broad wall longitudinal slot coupled hemispherical DRA

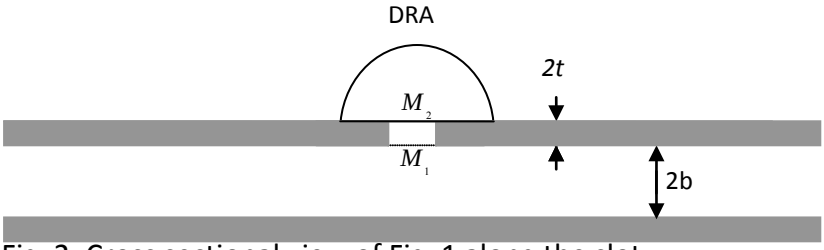


Fig. 2: Cross sectional view of Fig. 1 along the slot

At the region of the slot, the tangential component of the magnetic fields both inside the waveguide and outside (within the DR) should be identical. Invoking the surface equivalence principle, the slot can be closed by a perfect electric conductor which divides the problem into two equivalent problems: the slotted waveguide part and the DRA placed on the infinite ground plane. By applying magnetic boundary conditions at the apertures of waveguide and slot, and slot and DRA, the magnetic field $H(\bar{M})$ can be expressed as:

$$H_z^{WG}(\bar{M}_z^1) + H_z^{SL}(\bar{M}_z^1) - H_z^{SL}(\bar{M}_z^2) = H_z^{inc} \qquad (1)$$

$$H_z^{SL}(\bar{M}_z^1) - H_z^{SL}(\bar{M}_z^2) - H_z^{DRA}(\bar{M}_z^2) = 0 \qquad (2)$$

SEARCH
Previous Page
Next Page

$$H_z^{SL}(\bar{M}_z^1) - H_z^{SL}(\bar{M}_z^2) - H_z^{DRA}(\bar{M}_z^2) = 0 \qquad (2)$$

Where $H_z^{\alpha}\left(\bar{M}_z^i\right)$ ($i$=1,2 and $\alpha = WG, SL, DRA$) is the magnetic fields due the magnetic currents at the aperture $i$, any of the two faces of the thick slot, 1 and 2.

**RESULTS AND DISCUSSION:**

The longitudinal shunt slot milled on the broad wall of X-band rectangular waveguide coupled to hemispherical DRA has been studied. To implement the theory presented in this paper, a general MATLAB code was written capable of analyzing hemispherical DRA excited by a thick slot, kept at the offset $x_w$ in x direction at the broad wall. The DRA is kept centrally to the slot to couple maximum power from the slot. Convergence checks for the moment method solution were performed. It was found that convergence is very stable, and results using number of basis function, N=1 were very close to those using larger N. In this chapter, however, N = 5 is used in all the calculations.

A hemispherical DRA of radius $a_{dr}$ = 7.5 mm, $\varepsilon_r$ =10 and the standard WR90 waveguide with dimensions 22.86 mm × 10.16 mm was used in the computations and the simulations. Fig. 3 and 4 shows the computed and simulated values of reflection and transmission coefficients in dB for a slot dimension of 9.2 mm × 0.8 mm with a thickness of 1.27 mm. The slot is kept at a distance of 8 mm from the center of the waveguide in order to cut the maximum current. Both sides of the broad wall, where slot is milled, additional ground plates are attached to have sufficient space for sitting DRA. The numerically computed results are further compared with the commercial FEM software ( Ansoft HFSS) and CST Microwave Studio [8-9]. The computed resonant frequency is found to be 8.95GHZ. The $S_{21}$ for a single slot is found to be too low and it can increase further by increasing the number of slots in the broad wall, like in an array operation

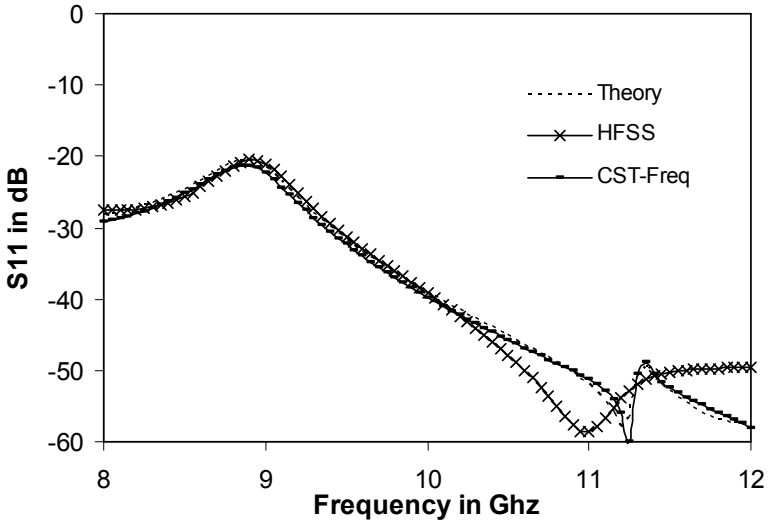


Fig. 3: Comparing computed return loss with HFSS and CST simulations. The parameters of antenna considered are: DRA radius = 7.5 mm; $\varepsilon_r$ = 10; Slot length = 9.2 mm; slot width = 0.8 mm; position of slot from center of waveguide = 8 mm; slot thickness = 1.27 mm. WR90 waveguide, dimensions 22.86 mm × 10.16 mm, width extended ground plane = 30 mm.

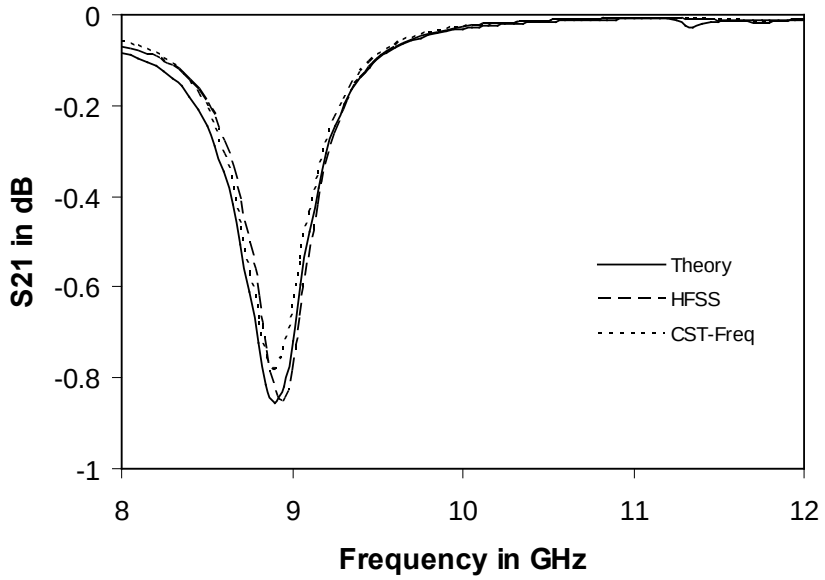


Fig. 4: Comparing computed $S_{21}$ with HFSS and CST simulations The parameters of antenna considered are: DRA radius = 7.5 mm; $\epsilon_r$ = 10; Slot length = 9.2 mm; slot width = 0.8 mm; position of slot from center of waveguide = 8 mm; slot thickness = 1.27 mm. WR90 waveguide, dimensions 22.86 mm´ 10.16 mm, width extended ground plane = 30 mm.

**REFERENCE:**


1. S.A. L ong, M.W. McAllister and L.C. Shen,"The resonant cylindrical dielectric resonator antenna", *IEEE Trans. Antennas Propagt*., vol.31, pp. 406-412, May 1983 .
2. Kishk, A.A., M.R. Zonoubi, and D. Kajfez, "A numerical study of a dielectric disc antenna above grounded dielectric substrate", *IEEE Trans. Antennas Propagt*. vol . 41, No.6, pp. 813-821, 1993
3. K.M. Luk and K .W. Leung, Eds., *Dielectric resonator antennas*, London, U.K.; R.S.Press, 2003.
4. Islam A E shrah, A hamed A Kishk, A .B. Y akovlev and A .W. G lisson. " Theory and implementation of di electric r esonator antenna excited by a w aveguide s lot", *IEEE Trans. Antennas Propagt*, vol.53, No.1, pp. 483-494 , January 2005
5. Collins, R.E., "Field Theory of Guided Waves", IEEE Press, 1991
6. Raju, G.S.N., Chakrabarty, A. and Das, B.N., **"**Studies on wide inclined slots in the narrow wall of rectangular waveguide**"**, *IEEE Trans. Antennas Propagt*., V ol. 38, pp. 24-29, January 1990.
7. Rahmat Samii, Y., "On the question of computation of the dyadic Green's function at the source region in waveguides and cavities", *IEEE Trans. of Microwave Theory and Techniques*, Vol-23, pp. 762-765, Sept. 1975.
8. Ansoft H igh Fr equency Structures Si mulator ( HFSS), ver sion 11.0, A r Corporate. USA
9. CST- (Computer Simulation Technology ) Microwave Studio 2006, Germany


SEARCH
Previous Page
Next Page

# A NOVEL DUAL-BAND FREQUENCY RECONFIGURABLE MICROSTRIP ANTENNA

*Manoj Singh, Student Member, IEEE, Ananjan Basu, Member, IEEE and Shiban K. Koul, Senior Member, IEEE*

Center for Applied Research in Electronics Indian Institute of Technology Delhi, Hauz-Khas, New Delhi-110016, INDIA

mscare_iit@yahoo.co.in, ananjan_b@yahoo.com, shiban_koul@hotmail.com

**ABSTRACT:**

A novel microstrip antenna with reconfigurable resonant frequency capability is proposed. The antenna consists of two radiating rectangular patches, connected by thin metallic strip incorporating a PIN diode in between. By controlling the PIN diode bias voltage, the antenna can be switched between two different frequencies. Both simulation and experimental results indicate that without any additional matching elements, the proposed antenna demonstrates very good input match at both the resonant frequencies.

## I. INTRODUCTION

RECONFIGURABLE microstrip antennas have received considerable attention in the recent years [1-6] for their properties of adapting with change in the environmental and system requirements. To achieve reconfigurability in an antenna RF switching devices, such as PIN diodes, photoconductive switches, micro-electromechanical system (MEMS) switches and FETs are required. Among the available RF switches, PIN diode switch is very popular in microwave circuit applications due to its fast switching speeds, reasonably high current handling capabilities, reliability and ease of modeling. Using PIN diodes for switching, it is natural to investigate frequencies at which a single antenna can resonate under different bias voltages. In principle, there may be very large number of states (resonant frequencies), but the circuit complexity puts a limit for any antenna with more than around 7-8 states. To keep the circuit complexity to bare minimum, with two diodes one may achieve a maximum of 4 states using 2 bias lines. With a single bias line, one can achieve 3 states (positive, negative and 0 bias levels) without introducing any additional circuit elements. This is the motivation behind developing a reconfigurable dual-band antenna.

Full-wave simulations were carried out using the 3D Electromagnetic simulator CST Microwave Studio (Version 8) with good matching for both frequency bands. In the simulations, diode was modeled as metal strips in ON state and was ignored in the OFF state. Although this introduces significant errors, the principle of operation is easily verified. In this paper, we have omitted simulated radiation patterns results due to space constraints.

## II. ANTENNA DESIGN FOR DUAL-BAND FREQUENCY OPERATION

The geometry of a reference patch antenna and the proposed dual–band frequency reconfigurable antenna are shown in Figs. 1 and 2, respectively. The proposed antenna is printed on 0.508 mm ($h$) thick GML substrate having relative dielectric constant $\varepsilon_r$=3.2. The ground plane dimensions are 38.1 x 38.1 mm$^2$. The dimensions of dual-band antenna are $w_1$= 1.2 mm, $w_2$=0.15 mm, $Lp1$ = 7.93 mm, $Wp$=10.3 mm, $Lp2$=2 mm and $G$=8 mm. The input-impedance matching transformer has dimensions of $l_1$ =4.8 mm and $w_3$=0.18 mm. For the design of frequency reconfigurable antenna, we start with conventional microstrip patch antenna as reference antenna in Fig. 1 and calculate the length and width of the p

and λ/4 matching transformer using standard rectangular microstrip antenna design equations for 10 G Hz resonance. To get second resonance, we connect an additional patch of same width as reference antenna but different length using thin metallic strip of length G as shown in Fig. 2. By connecting and disconnecting the metallic strip to the reference patch, we can achieve resonance at the frequency of reference antenna or below that of the reference antenna.

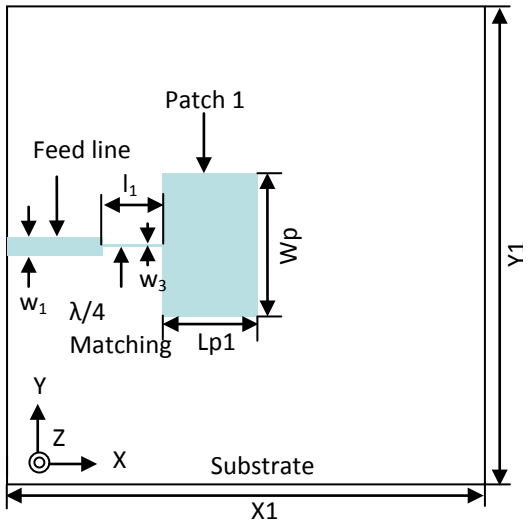


Fig.1. Reference patch antenna

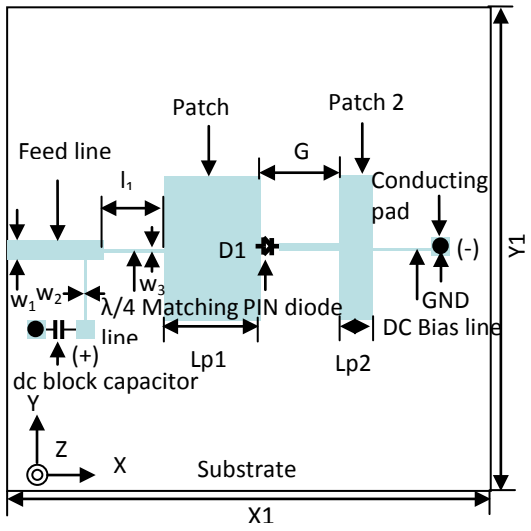


Fig. 2. Proposed reconfigurable antenna

To convert reference antenna into an actual reconfigurable antenna, the metallic strip is connected to reference patch through a diode. In this arrangement, we get resonance at 9.9 GHz and 9.48 GHz by applying reverse bias and forward bias to diode switch. The reason behind this phenomenon is that if we connect an additional element to the reference patch, the antenna will resonate at a frequency that is dependent on the combination of two resonators. The resulting resonant frequency will be different from the resonant frequency of individual antenna elements.

## III. Results and Discussion

The prototype of the proposed two-state reconfigurable antenna was fabricated using conventional photolithography technique. Fig.3 shows the simulated antenna geometry and the photograph of the fabricated antenna structure mounted in a brass test jig. The antenna structure was tested on an automatic vector network analyzer (VNA). Figures 4 and 5 show the simulated as well as measured return loss characteristics of the antenna for dual-band operation under two bias states. It is observed that the antenna exhibits -10dB return loss over two frequency bands at 9.9 GHz, 9.48 GHz. The slight difference in the resonance frequency between measured and simulated results is due to fabrication tolerances and ideal ON-OFF switching method used in the simulations.

SEARCH

Previous Page

Next Page

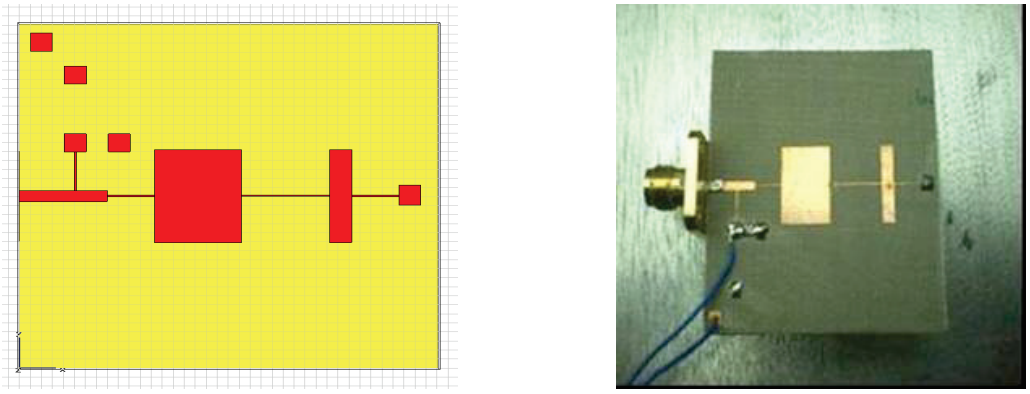

(a) (b)

Fig.3 (a) Simulated Geometry in EM Simulator (b) Photograph of the dual-band frequency reconfigurable antenna mounted in the test jig.

Figure 6 shows the measured radiation patterns at 9.9 GHz and 9.48 GHz for the two switching states. The measurements of the radiation patterns of the antenna were carried out in the anechoic chamber. Here, the y-z plane has been described as E-plane and the x-z plane as H-plane. Polarization was parallel to the feed line in all cases.

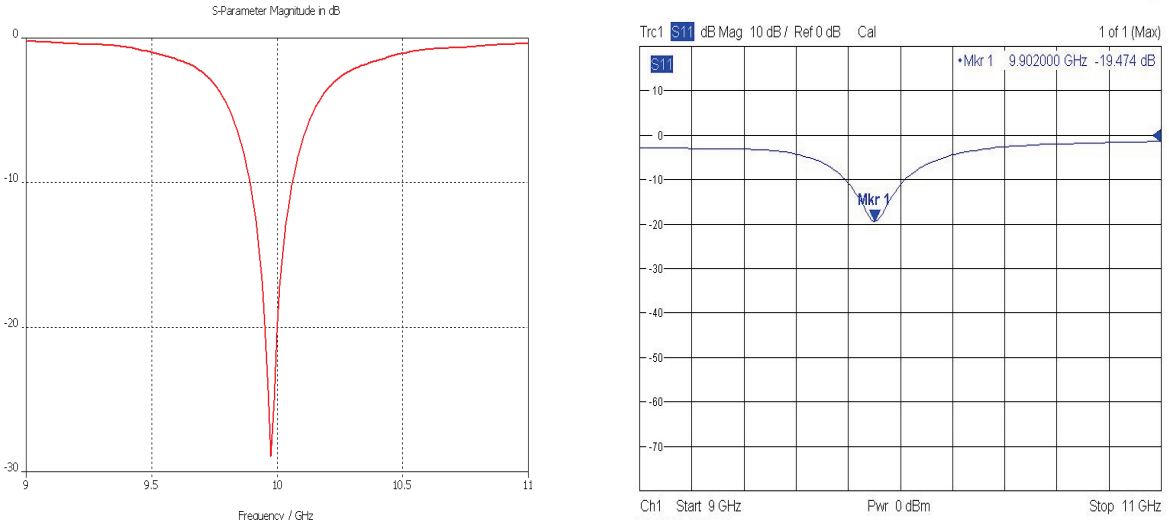


(a) (b)

Fig.4. (a) Simulated return loss under ideal OFF state (b) Measured return loss under reveres bias state.

SEARCH

Previous Page Next Page

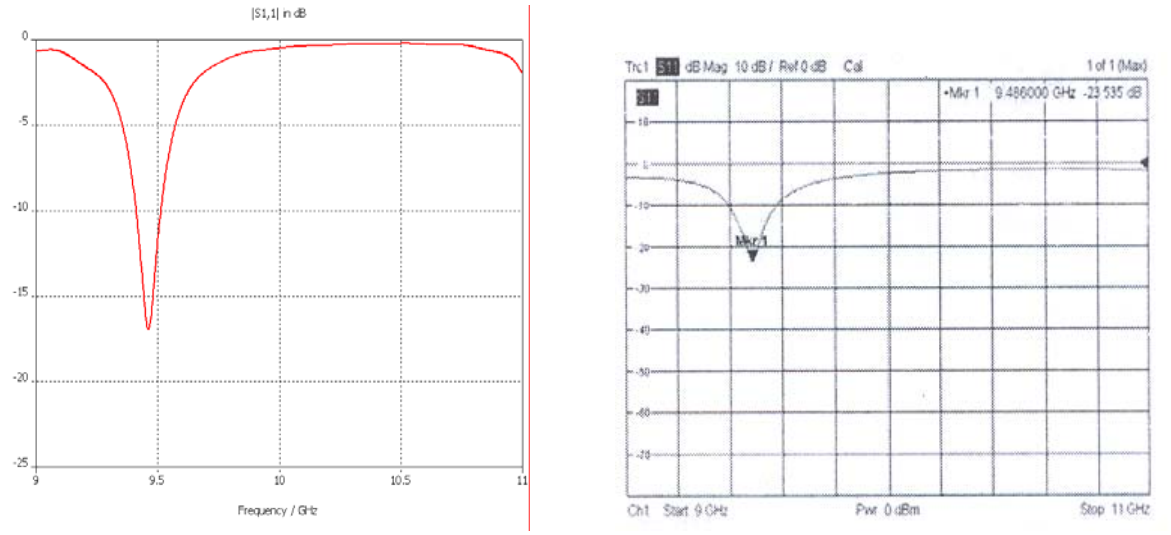


(a) (b)

Fig.5. (a) Simulated return loss under ideal ON state (b) Measured return loss under forward bias state.

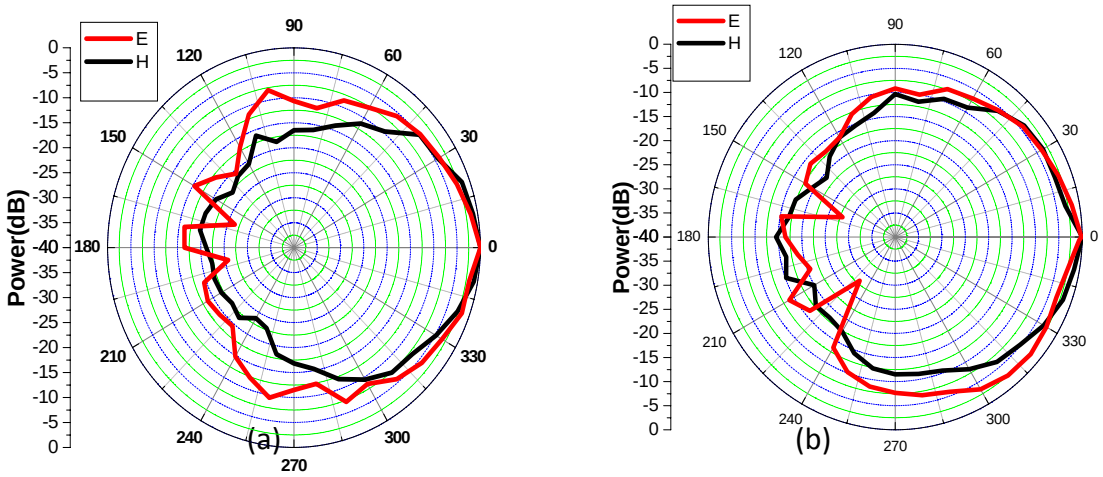


Fig.6. Measured E- and H-plane radiation patterns at (a) 9.9 GHz under reverse bias state (b) 9.48 GHz under forward bias state.

SEARCH
Previous Page
Next Page

## IV. CONLUSION

A novel dual -band f requency r econfigurable microstrip ant enna with s witchable frequency ban d capabilities at X-band has been proposed. Frequency reconfiguarbility is achieved by controlling the bias voltage of the PIN diode. The fabricated antenna shows good agreement be tween t he s imulated and measured r eturn loss char acteristics. T he r eturn l oss versus frequency characteristics indicates that the proposed antenna can be switched over two frequency bands at 9.9 GHz, and 9.48 GHz with frequency tunability up to 414 MHz. Due to its compactness and easy fabrication, the proposed antenna can be useful for commercial X-band wireless communication applications.

## REFERENCE:


1. Chien-Yuan Pan, C hein-Hsiang H uang and T zyy-Sheng H orng, "A new pr inted G-shaped monopole ant enna f or dual -band WLAN appl ications", M icrowave and Optical Technology Letters, Vol. 45, No. 4, pp. 295-297, 2005.
2. C.-J. Wang an d W.-T. T sai, "A slot antenna module for switchable radiation patterns," IEEE Antennas Wireless Propag. Lett., Vol. 4, pp.202–204, 2005.
3. J. T. Aberle, S. H. Oh, D. T. Auckland, and S. D. Rogers, "Reconfigurable antennas for portable wireless devices," IEEE Antennas Propag. Mag., Vol. 45, no. 6, pp. 148–154, Dec. 2003.
4. N. Behdad and K. Sarabandi, "A varactor-tuned dual -band slot ant enna," IEEE Trans. Antennas Propag., Vol. 54, no. 2, pp. 401–408, Feb. 2006.
5. D. Peroulis, K. Sarabandi, and L. Katehi, "Design of reconfigurable slot antennas," IEEE Trans. Antennas Propag., Vol. 53, no. 2, pp. 645–654, Feb. 2005.
6. N. B. J in, F. Y ang, and Y . R ahmat-Samii, "A novel pat ch antenna w ith s witchable slot (PASS): D ual-frequency oper ation w ith reversed c ircular pol arizations," I EEE Trans. Antennas Propag., Vol. 54, no. 3, pp. 1031–1034, Mar. 2006.

# AN INVESTIGATION OF WIDEBAND MICROSTRIPLINE FED HALF SPLIT CYLINDRICAL DIELECTRIC RESONATOR ANTENNA

*C Gopakumar*, Jaimon Yohannan, Ullas G Kalappura, K.T. Mathew*
Microwave Tomography and Materials Research Laboratory,
Department of Electronics, Cochin University of Science and Technology,Kochi-682 022, Kerala, India.
E.mail: ktm@cusat.ac.in.

**ABSTRACT:**

A microstrip line fed dielectric resonator antenna with half split circular cylindrical profile is experimentally investigated. It shows that at optimum parameters, this low profile, small size antenna gives a wideband response similar to that of its full cylindrical counter part with moderate gain but at different frequency. The return loss and radiation pattern of the proposed antenna are measured and studied. The simulated and measured results verify that the proposed antenna offers an impedance bandwidth of 36.7% (from 3.24GHz to 4.70 GHz) and shows a conical radiation patterns.

## INTRODUCTION:

The dielectric resonators (DRs) were originally proposed as antennas in the early 1980s [1] and various configurations, geometrical shapes and feed mechanisms have been investigated in the following years. It provides an efficient radiating structure in the upper microwave and lower millimeter wave frequency bands, where its minimal ohmic loss gives it an inherent advantage over more conventional antennas. It has been shown that a dielectric resonator antenna (DRA) can be excited by either a coaxial probe or a microstrip transmission line [1, 2]. But the bandwidth of a common DRA is typically below 10%. Investigations of the DRA initially concentrated on low permittivity materials (dielectric constant $\varepsilon_{r\sim 5\text{--}30}$) to enhance the radiation capability and antenna bandwidth. Simple and easy excitation arrangements had been reported for various antenna configurations to provide wide bandwidth, flexible polarization adjustment and high radiation efficiency which make DRAs by far superior to conventional microstrip patch antennas [3]. In order to enhance the bandwidth, various techniques have been developed for DRAs, such as coplanar parasitic DRAs [4], stacked DRAs [5], [6] or various shaped DRAs [7].

It is shown here that by selecting optimum parameters like height and breadth of vertical feed-strip and its offset distance from the open end of the microstrip feed line, a wideband response with a moderate gain could be achieved for a half split dielectric resonator antenna which is comparable to the result obtained in its full cylindrical counterpart as reported in [8].

## ANTENNA CONFIGURATION:

The proposed antenna configuration used for the study is shown in Fig.1. A cylindrical circular sector dielectric resonator antenna of radius 2a = 24mm, and thickness d =7.3mm having a dielectric constant of $\varepsilon_{rd}$ = 20.8 is used and is fed by a 3mm wide microstrip transmission line which is fabricated on a microwave substrate of $\varepsilon_{rs}$= 4 with a size of 115mm X 115mm X 1.6mm. DRA is mounted with its curved surface on the substrate symmetrically with the feed line which is directed along Y-axis. Surface area of the antenna from which radiation is emerged is increased due to this configuration. A vertical metallic strip is adhered half circular flat surface of the DRA and is connected with the microstrip li



Previous Page Next Page

a length $L$ from its open end. The width $w$ and height $h$ of the vertical strip line and the offset length $L$ are the key factors that are varied for obtaining the optimum condition for a good result.

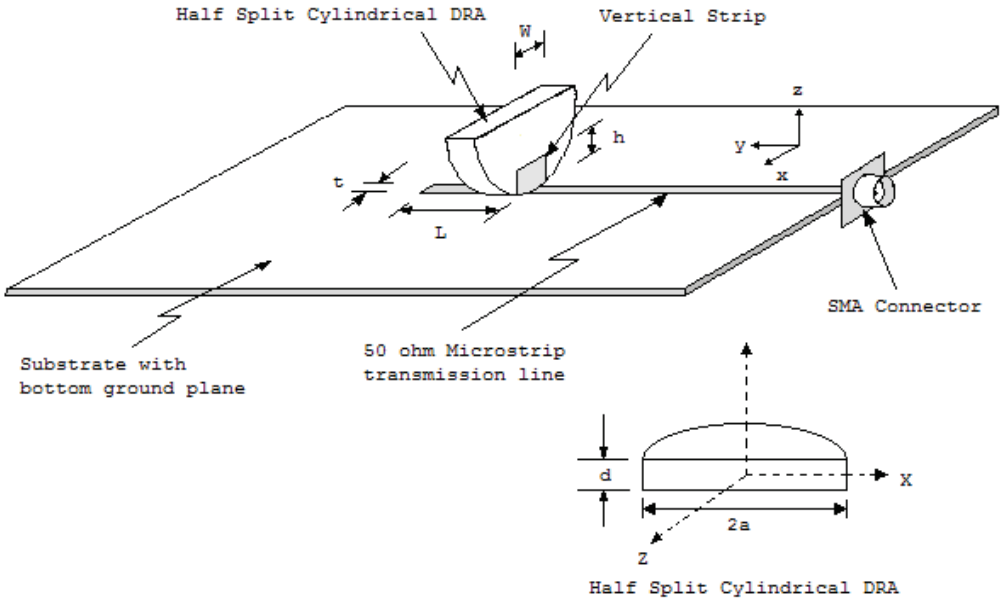


Fig.1 Geometry of the proposed antenna.

**RESULTS AND DISCUSSION:**

The antenna characteristics are measured using an HP 8510C vector network analyzer. Ansoft HFSS is used for computer simulation. $|S_{11}|$ is measured for different values of $L$ for a particular width $w$ and height $h$ of vertical strip. It is found that for an offset length $L$ =13mm, the maximum band width is obtained. Keeping this value unchanged, $h$ is varied for a constant value of $w$ and again the maximum BW is found out. Finally, for these optimum values of $L$ and $h$, the best possible value of $w$ is achieved. Thus it is established that for a combination of $L$ = 13mm, $h$ = 4mm and $w$ = 6mm, a maximum impedance bandwidth of 36.7% is obtained from 3.24 to 4.70 GHz. The broadband response is due to multiple radiating modes having similar radiating properties like $TM_{21\delta}$ mode that are merged together when excited by this arrangement.

Measured and simulated plot of $|S_{11}|$, of the DRA are compared in Fig. 2 and shows that they are in good agreement. The far field radiation pattern of this antenna configuration is shown in Fig. 3. It is apparent that the pattern is conical in shape. Since antenna is placed symmetrical to the feed, XZ plane pattern is seen symmetrical.

SEARCH

Previous Page

Next Page

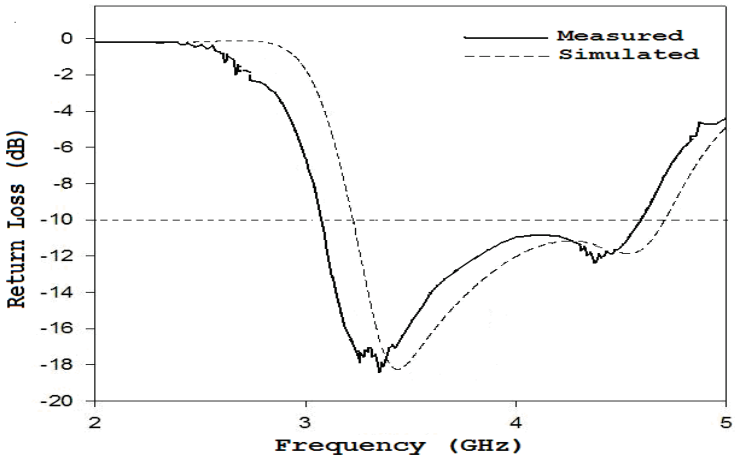


Fig. 2 Return Loss ($S_{11}$) at the optimum feed position.

Different orientations of the antenna with respect to the microstrip line feed is also tried out for studies and verified that the proposed one gives the best result. The antenna gain of this configuration is also studied. It is found that an average gain of 5.7 dB is obtained. The result, however, is omitted here for brevity.

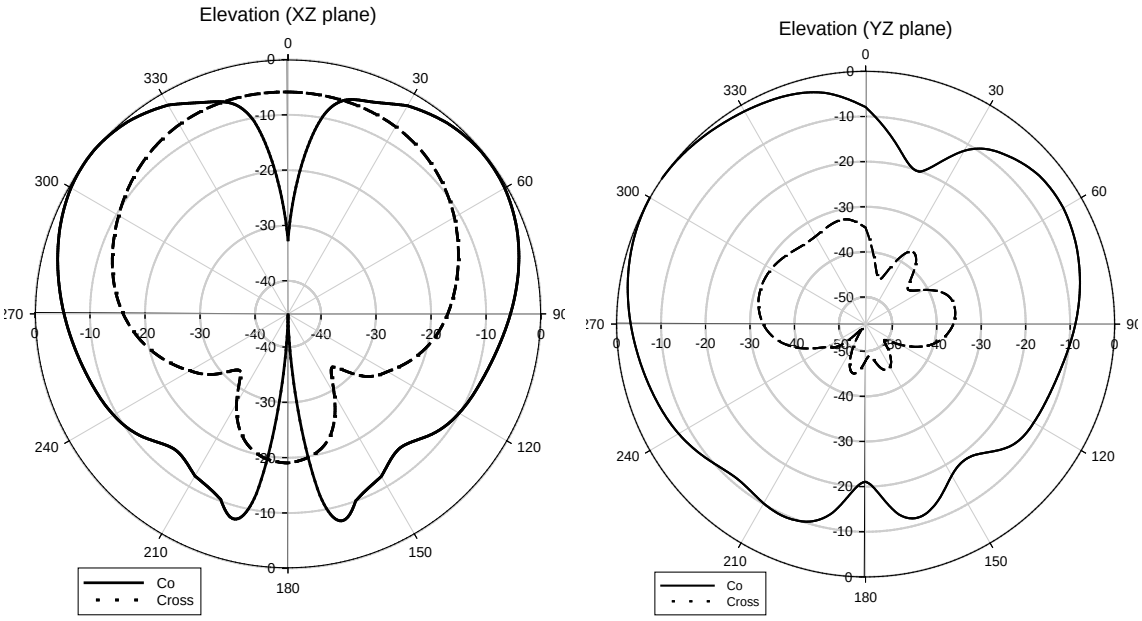


SEARCH

Previous Page

Next Page

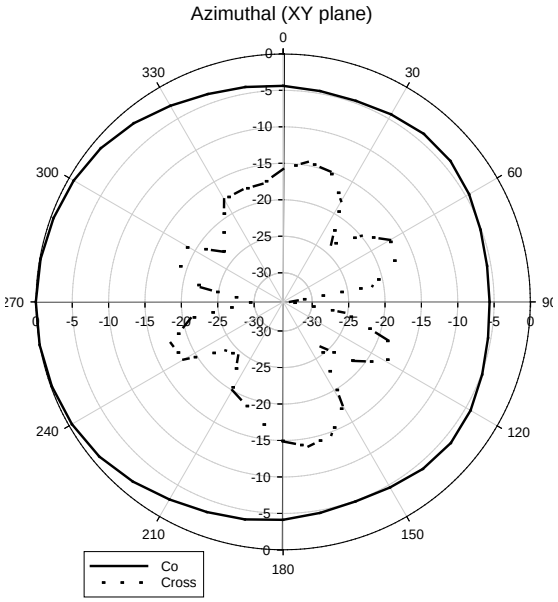


Fig. 3 Measured far field radiation pattern of the Half Split Cylindrical DRA at 4 GHz.

## CONCLUSION:

A compact wideband DRA has been experimentally investigated. The results show that the proposed antenna offers more than 36% impedance bandwidth from 3.24 to 4.70 GHz, which covers several important application bands in WiMAX standard. By optimizing design, it can be used for vehicular and indoor mobile communications. The antenna radiates stable conical radiations within the matching impedance bandwidth. Furthermore, this antenna configuration is very easy to construct and is suitable for integration with MIC's.

## REFERENCE:

1. Long S.A., McAllister M.W., and Shen L.C., "The resonant cylindrical dielectric cavity antenna", *IEEE Trans.,* AP-31, pp. 406-4 12, 1983.
2. St. Martin J.T.H., Antar Y.M.M., Kishk A.A., Ittipiboon A. and Cuhaci M. "Dielectric resonator antenna using aperture coupling", *Electron. Lett.,* 1990.26, pp. 2015-2016
3. R. K. Mongia, A., Ittipibon and M. Cuhaci, "Measurement of radiation efficiency of dielectric resonator antennas", *IEEE Microwave Guided Wave Letters*, Vol. 4, no. 3, pp 80-82, March 1994.
4. Z. Fan andY. M. M. Antar, "Slot-coupled DR antenna for dual-frequency operation," *IEEE Trans Antennas Propag.*, vol. 45, no. 2, pp. 306–308, Feb. 1997.
5. A. A. Kishk, X. Zhang, A.W. Glisson, and D. Kajfez, "Numerical analysis of stacked dielectric resonator antenna excited by a coaxial probe for wideband applications," *IEEE Trans Antennas Propag.*, vol. 51, no. 8, pp. 1996–2005, Aug. 2003.
6. M. H. Al Sharkawy, A. Z. Elsherbeni, and C. E. Smith, "Stacked elliptical dielectric resonator antennas for wideband," in *Proc. IEEE Antennas and Propagation Society Int. Symp.*, vol. 2, 2004, pp. 1371–1374.
7. A. A. Kishk, "Wide-band truncated tetrahedron dielectric resonator antenna excited by a coaxial probe," *IEEE Trans. Antennas Propag.*, vol. 51, no. 10, pp. 2913–2917, Oct. 2003.
8. A.V. Praveen Kumar, V. Hamsakkutty, Jaimon Yohannan and K.T. Mathew, "A Wideband Conical Beam Cylindrical Dielectric Resonator Antenna", *IEEE Antennas and Propagation Letters*, vol. 6, 2007.

SEARCH
Previous Page
Next Page

# COMPACT UNIPLANAR ANTENNA FOR WIDE BAND APPLICATIONS

*Laila.D, Deepu.V,Sujith.R, P. Mohanan *, C K Anandan, and K Vasudevan*
Center for Research in Electromagnetics and Antennas, Department of Electronics,Cochin University of Science and Technology, Kochi-22, Kerala, India
e-mail: drmohan@ieee.org.

**ABSTRACT :**

An Asymmetric Coplanar Strip (ACS) fed uniplanar antenna suitable for broadband applications is presented. The proposed antenna offers a 2:1 VSWR bandwidth greater than 80% from 2.72GHz to 6.57GHz covering the WiMAX, IEEE 802.11a, HIPERLAN2,HiSWANa ban ds. The ant enna has an over all dimension of 22m m X 18m m w hen pr inted on a s ubstrate of di electric constant 4.4 a nd hei ght 1.6m m. T he w ide band width i s obt ained by combining three individual resonances excited by various current paths. The antenna exhibits good radiation characteristics and moderate gain in the entire operating band.

## INTRODUCTION:

The dem and for w ideband ant ennas has exper ienced a boom ing gr owth i n t he wireless industry. Several interesting designs of wide band antennas have been dem onstrated recently. A r esonant aper ture w ith s tacked pat ches of different di electric con stants i s employed for bandwidth enhancement in microstrip antenna[1].The wideband E shape microstrip patch antenna [2] incorporates two parallel slots in the patch to obtain a wide band. This antenna is excited by a probe feed and is mounted on large ground plane. The microstrip fed pl anar Q uasi-Yagi an tenna pr esented [ 3] has a band w idth of 48 %. These m ethods typically enl arge t he vol ume and com plexity of t he ant enna s tructure. Unlike t he abo ve mentioned microstrip configurations, uniplanar antennas are popular due to easy fabrication and easy integration with MMIC's. The coplanar wave guide fed T shaped antenna in [4] has an overall dimension of 37.5 x 80 $mm^2$ having 61.5% band width. The ACS fed monopole antenna in [5] has only a bandwidth of 16 %.

In t his paper we pr esent the opt imized de sign of a simple and co mpact A CS f ed antenna for wideband applications. A very large bandwidth of 82% is obtained within an overall area of 22 x 18 $mm^2$ on a substrate of dielectric constant 4.4 and thickness 1.6 mm.

## ANTENNA GEOMETRY:

Figure.1 shows the geometry of the proposed ACS fed antenna. The antenna is designed on a substrate of dielectric constant 4.4 and height 1.6 mm. In the present design the strip dimensions are taken as $L_1$= 18mm and the width $W_1$= 5mm.The ground plane dimensions ar e $L_2$ = 22 m m, $W_2$ = 6 m m c onsists a gap g of 1 m m. T he ant enna i s f ed between t he po ints $S_1$ and $S_2$.These di mensions ar e chos en af ter exhaus tive s imulation a nd experimental studies f or obtaining wide band width. The resulting antenna exhibits poor impedance matching. To improve the matching a small triangular cut of dimensions Δx X (shown in dotted lines) is inserted in the ground plane. In a compact Asymmetric Coplanar Strip feed the lateral strip width (in this case $W_1$), the ground plane length (in this case $L_2$) and the gap g determine the characteristic impedance [6].

SEARCH
Previous Page
Next Page

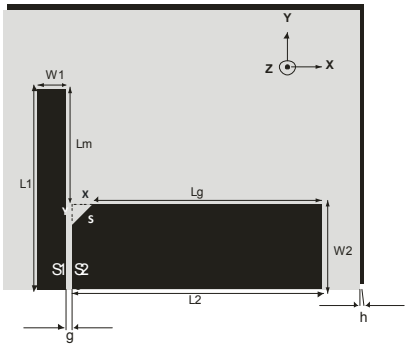


Fig.1. Antenna geometry of the proposed antenna ($L_1$=18mm,$L_2$=22mm,$W_1$=5mm,$W_2$=6mm,g=1mm,$L_m$=12mm, Δx=3mm, Δy=3mm)

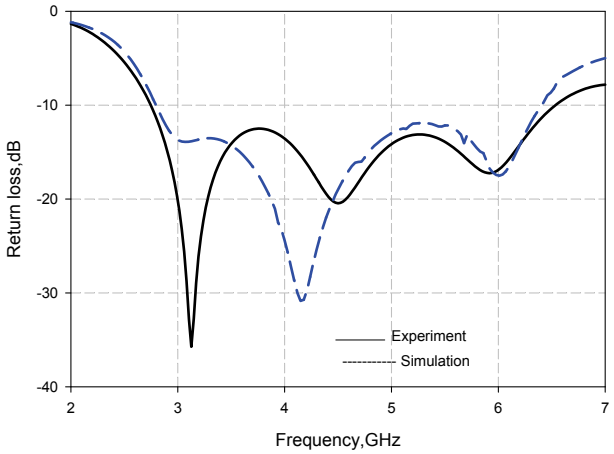


Fig. 2 Experimental and simulated Return loss characteristics of the proposed antenna

## EXPERIMENTAL RESULTS:

The Experimental and Ansoft HFSS simulated return loss curves of the antenna are shown in Figure.2. The proposed antenna exhibits a bandwidth of 82 % from 2.72GHz to 6.57 GHz with good impedance matching. This wide bandwidth is due to the merging of three individual resonances centered at 3.12 GHz, 4.4 GHz and 5.9 GHz. The broad band behavior of the antenna is confirmed by scaling the antenna for different frequencies.

## DESIGN EQUATION:

To design a wide band antenna operating at a center frequency $f_c$, the dimensions $L_v$ and $L_h$ are taken as

$$L_h+L_v = 0.59\ \lambda_c$$

$$L_h = 0.36\ \lambda_c$$

$$L_v = 0.23\ \lambda_c$$

Where $\lambda_c$ is the free space wave length corresponding to the center frequency $f_c$. and $L_h = Lg+\Delta s$ and $L_v = L_m+\Delta y$ .

In the proposed antenna the ground plane width $W_2$ is optimized as 0.27 times the length $L_2$ for maximum bandwidth. Similarly the width $W_1$ is optimized as 0.28 times $L_v$ when the gap g is 1mm. From the series of simulation and experimental studies it is found that the first resonance is due to the total length $L_v+L_h$, the second resonance is mainly due to $L_h$ and the third resonance is mainly due to $L_v$.

SEARCH
Previous Page
Next Page

The gain of the antenna is measured and depicted in figure 4. The average gain of the proposed antenna in the entire band is 3.52dBi.

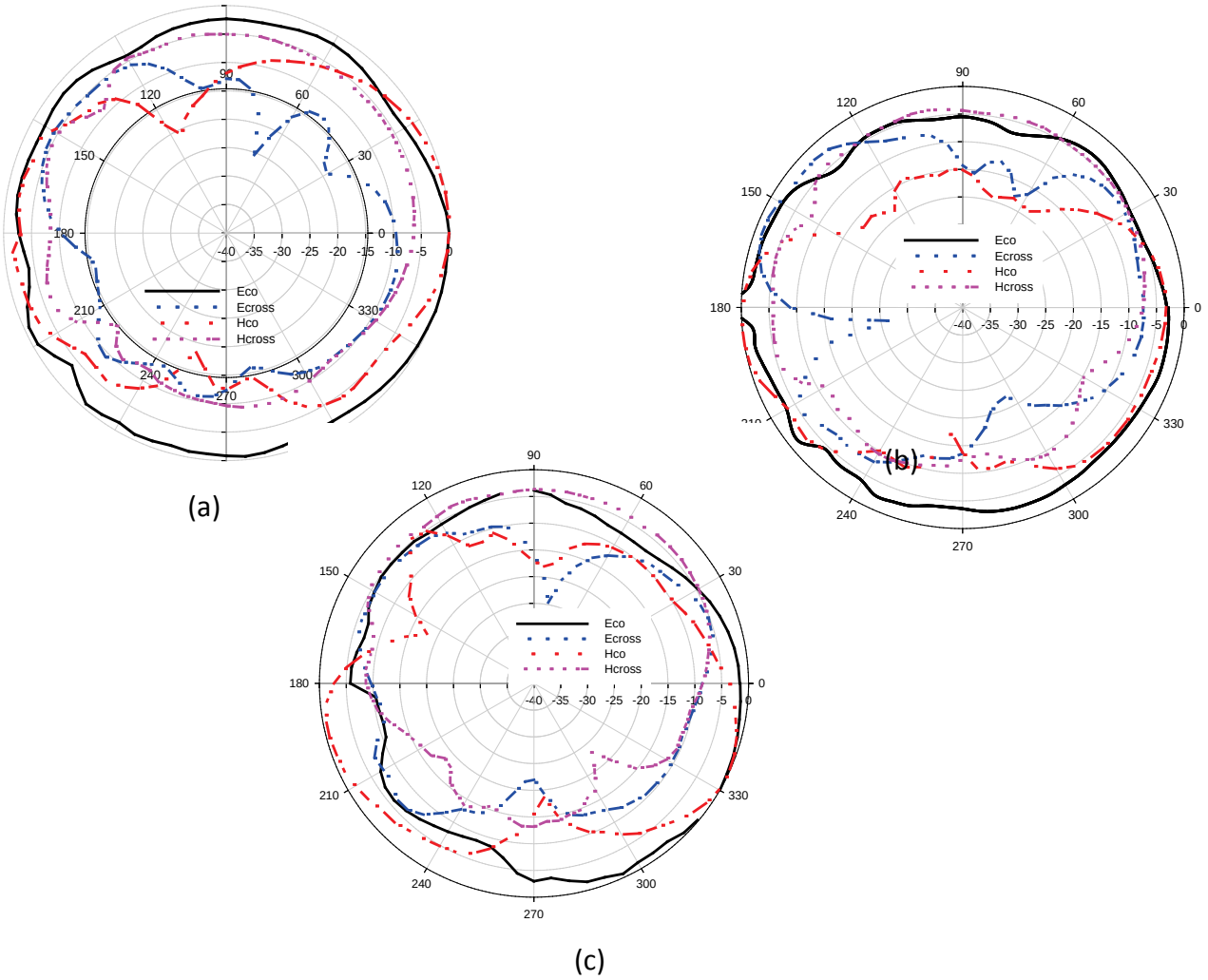


Fig. 3 Measured radiation pattern of the proposed antenna (a) at 3.12GHz (b) at 4.4GHz (c) at 5.92GHz

SEARCH

Previous Page

Next Page

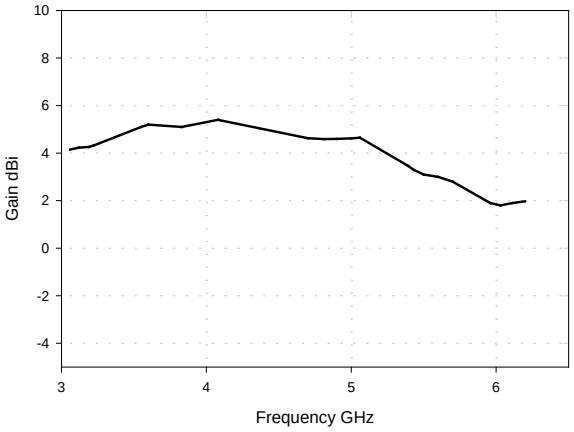


Fig. 4 Measured gain of the proposed antenna

## CONCLUSION:

A simple, compact Asymmetric Coplanar Strip fed antenna operating from 2.72 GHz to 6.57 GHz with 82 % bandwidth is presented. This wide band antenna is obtained from exhaustive optimization studies on a simple ACS fed strip monopole. The antenna exhibits good radiation characteristics with moderate gain in the entire operating band.

## ACKNOWLEDGEMENT

The authors are grateful to UGC, Govt. of India, Kerala State Council for Science Technology and Environment (KSCSTE) and Defence Research Development Organization (DRDO), Govt. of India for providing financial assistance.

## REFERENCES

1. S D Targonski and R B Waterhouse "Design of wide band Aperture stacked patch microstrip antennas", IEEE Trans.Antennas Propag 46( 1998),1245-1251
2. Fan YANG,Xue-Xia Zhang,Xiaoning Ye and Yahya Rahmat-samii "Wideband E shaped patch Antennas for wireless communication" IEEE Trans.Antennas Propag 49 ( 2001),1094-1100
3. Noriaki Kaneda,W.R.Deal,Yongxi Qian,Rod Waterhouse and Tatsuo Itoh " A Broad Band planar Quasi-Yagi Antenna" IEEE Trans.Antennas Propag 50 (2002),1158-1160
4. R B Hwang, "A broadband CPW–fed T–shaped antenna for wireless communications" IEE Proc Microwaves Antenna Propag 151 (2004),537-543
5. Deepu V,Rohith K Raj,Manoj Joseph,Suma M N and P. Mohanan ,"Compact Asymmetric Coplanar strip fed Monopole antenna for multiband applications" IEEE Trans.Antennas Propag 55( 2007),2351-2357.
6. R.Garg.P.Bhartia and I .Bahl "Microstrip Antenna Design Handbook,"Ists ted.Boston,M.A:Artech House(2001),794-795.

SEARCH

Previous Page Next Page

# CROSS PATCH ANTENNA WITH AN X-SLOT FOR POLARIZATION SWITCHING

*Nishamol M S, Sarin V P, Deepu V, Sujith R, P. Mohanan , C K Anandan and K Vasudevan*

Centre for Research in Electromagnetics and Antennas, Department of Electronics, Cochin University of Science and Technology, Cochin-22, India.

E-mail: vasudevankdr@gmail.com

## ABSTRACT:

A novel design of a compact single-feed cross patch antenna with an X-slot for polarization diversity is presented. The antenna generates two orthogonally polarized radiations with center frequencies at 1.2GHz and 1.515GHz. For fixed dual frequency operation, the antenna has an area reduction of 78% and 64% for the respective frequencies compared to standard rectangular patches. The antenna exhibits broadside radiation pattern and has moderate gain for the two bands. Using two PIN diodes at the centre of X slot, it is possible to produce linear (horizontal or vertical) and circular polarization. The polarization state can be switched electrically by setting two diodes to on or off.

## INTRODUCTION:

Microstrip antennas are usually designed for single- mode in linear polarization (LP). However, in some applications, such as satellite communications, circularly polarized (CP) system is more suitable than a LP system because of its indifference to transmitter and receiver orientations. A polarization diversity antenna, which is an example of a multi-function antenna, allows the user to roam any existing network and use a single handset to access a greater number of services. Therefore, these antennas can be utilized to realize frequency reuse. Additionally, polarization diversity of reception is important to counter the effects of fading in communication, especially in mobile communication.

In this letter, we present a technique for obtaining a compact polarization diversity microstrip antenna. Initially, four square regions are cut off from the corners of a rectangular patch resulting in a cross shaped patch, giving a dual frequency dual polarized antenna. To the above cross shaped patch, an X shaped slot is inserted to obtain greater area reduction. The X shape is chosen in order to induce symmetric current distributions for the two modes of TM01 and TM10. In this design, a single proximity feed is used to obtain impedance matching for the two frequencies with orthogonal polarization. This antenna generates two orthogonally polarized radiations with center frequencies at 1.2GHz and 1.515GHz providing greater area reduction with good cross polarization levels and low frequency ratio. Two PIN diodes are inserted at the centre of the X-slot to obtain the final polarization diversity antenna. The polarization state can be switched electrically by setting two diodes to on or off. The design has been successfully implemented and the experimental results are in good agreement with the simulations.

## ANTENNA DESIGN:

The geometry of the proposed antenna is shown in Figure 1. The antenna is fabricated on an Fr4 substrate of thickness ‘h’ (0.16cm) and dielectric constant ‘εr’ (4.4). The design is obtained by removing four square regions of dimension ‘ls’ from

SEARCH

Previous Page Next Page

corners of a rectangular patch of size L x W. An X-slot of length 'lx' and width 'wx' is inserted at the centre of the cross patch. Two PIN diodes are inserted at the centre of the X-slot, to obtain the final antenna. The antenna is electromagnetically coupled using a 50Ω microstrip line. The dimensions of the slot and feed locations are optimized using Ansoft HFSS.

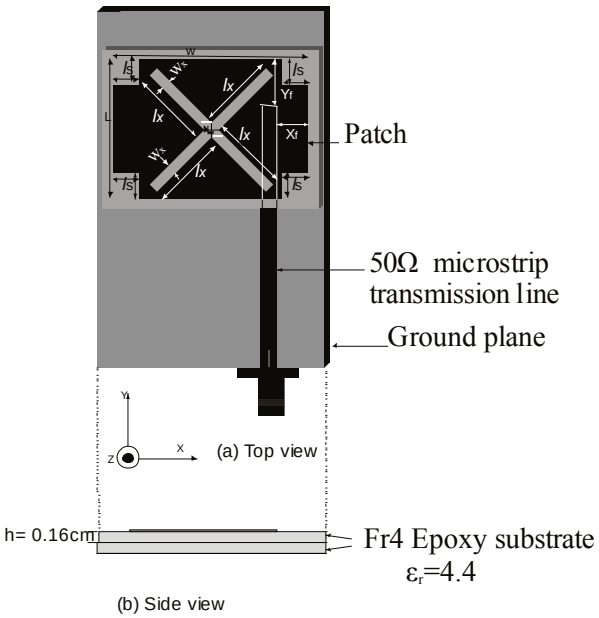


Figure 3 Geometry of the proposed antenna L=30mm, W=42mm, ls=5mm, lx=17.8mm, wx=2mm, h=1.6mm and $\varepsilon_r$ =4.4.

## RESULTS AND DISCUSSION:

The proposed antennas are tested using Agilent HP8510C network analyzer and the reflection coefficient ($S_{11}$) of the cross patch antenna with X-slot is given in Figure 2. The two resonant modes ($TM_{01}$ and $TM_{10}$) with orthogonal polarizations at 2GHz and 2.64GHz are obtained without X-slot. By properly selecting the size of the slot the two resonant frequencies are lowered to 1.2GHz and 1.515 GHz. The transmission coefficient ($S_{21}$) of the antenna is given in Figure 2. It can be seen that, high cross polar level is obtained for the two resonances.

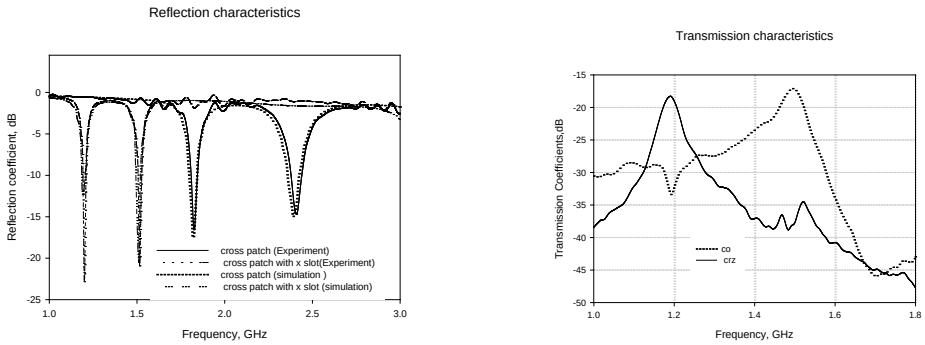


**Figure 4 Reflection and transmission characteristics of the cross patch antenna with X-slot**

The antenna resonates at two frequencies with orthogonal polarization gives an a reduction of 78%for the first frequency and 64% for the second frequency compared to standard rectangular patch. A frequency ratio of 1.26, which is slightly less than the aspect ratio (1.4) of the rectangular patch, is obtained. The E plane and H plane patterns of the two resonant frequencies are given in Figure 3. Good cross polar lev

SEARCH
Previous Page
Next Page

obtained for both the two frequencies. It is observed that, as slot length increases, the operating frequencies are lowered.

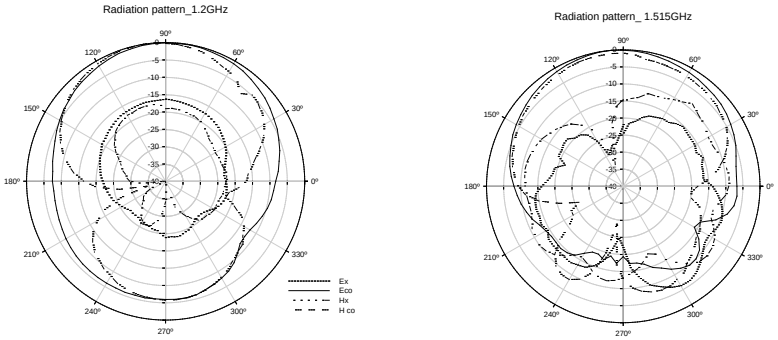


**Figure 5 Radiation patterns of the cross patch antenna with X-slot at two resonant frequencies**

In this study four different sets have been considered. The PIN diode represents a capacitance of 0.35pF in the reverse biased state and behaves almost as open impedance. With applied forward bias, The PIN diode exhibited an ohmic resistance of 1.35Ω and a series inductance of 1.4nH.A dc bias circuit is required to control the on/off mode of diode. Figure 4 shows the return loss of the proposed antenna for each state of the diodes.

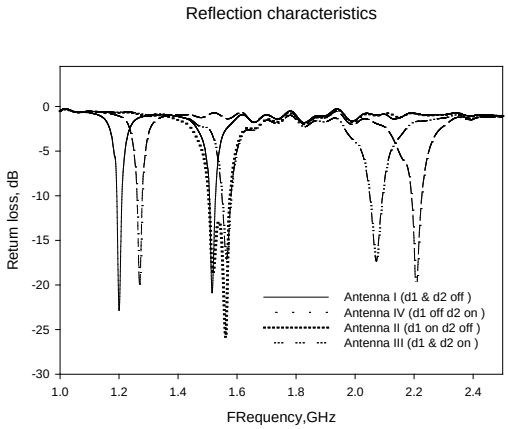


**Figure 6 Return losses for different states of diodes**

The case of the proposed antenna with two diodes off (referred to as antenna I) is first considered. When D1 and D2 are off, the antenna generates two linearly polarized radiations which are orthogonal to each other at 1.2GHz and 1.515GHz respectively.

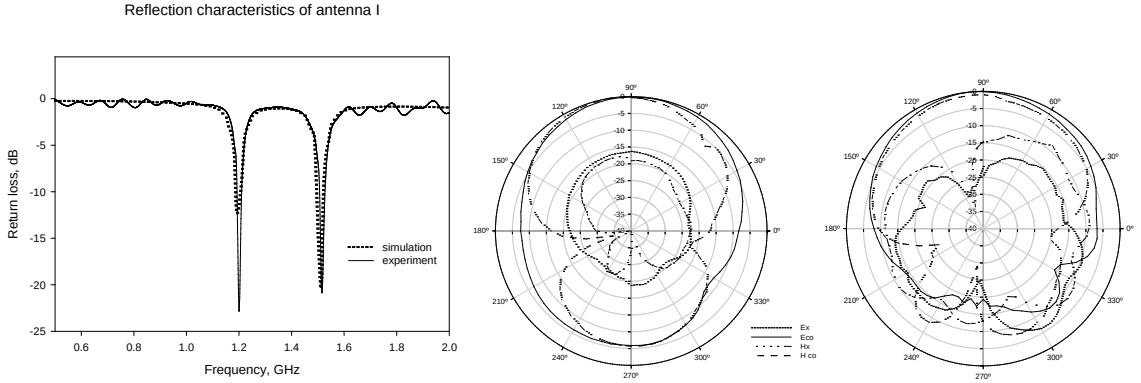


**Figure 7 Return loss and radiation patterns of antenna I**

Previous Page
SEARCH
Next Page

When D1 is switched on while keeping D2 off (referred to as antenna II), the antenna generates a circular polarized radiation from 1.5GHz to 1.572GHz. In this mode, the antenna excites two orthogonally polarized modes with equal amplitude and 90º phase shift, results a circularly polarized radiation. When D1 is off while D2 is kept on (referred to as antenna IV), the antenna generates two linearly polarized radiations which are orthogonal to each other at 1.278GHz and 2.22 GHz respectively.

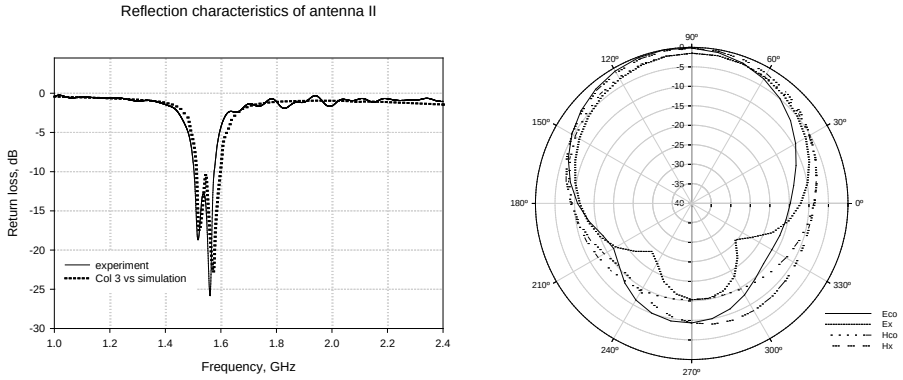


**Figure 8 Return loss and radiation pattern of antenna II**

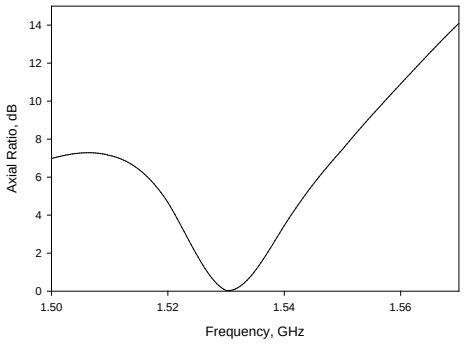


**Figure 9 Simulated Axial ratio for antenna II**

When D1 and D2 are on (referred to as antenna III), the antenna generates two linearly polarized radiations which are orthogonal to each other at 1.572GHz and 2.07GHz respectively.

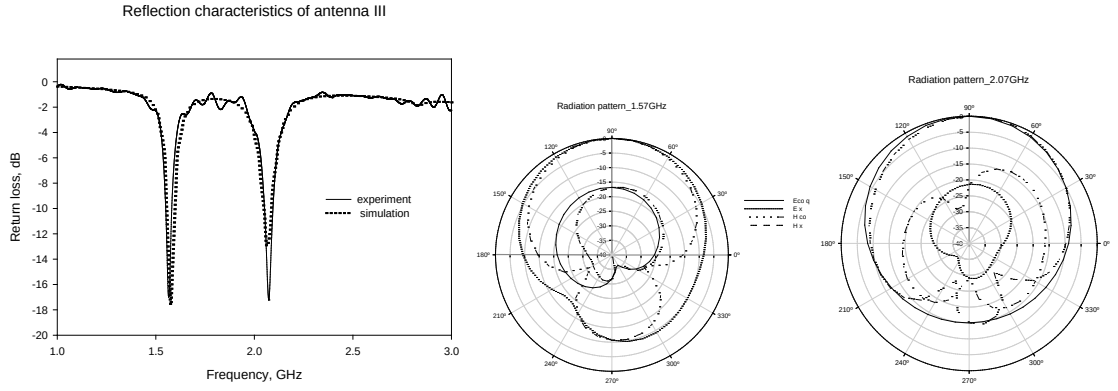


**Figure 10 Return loss and radiation patterns of antenna III**

SEARCH
Previous Page
Next Page

## CONCLUSION:

The high potentiality of a switchable microstrip antenna has been proposed for multi-operation applications. Using PIN diodes, the proposed antenna can produce linear or circular polarization. The antenna has an area reduction of 78% and 64% for the respective frequencies compared to standard rectangular patches. The antenna exhibits broadside radiation pattern and has sufficient gain. The proposed antenna is suitable for satellite communications applications.

## ACKNOWLEDGEMENT:

The authors acknowledge University Grants Commission (UGC), Council of Scientific and Industrial Research (CSIR), Department of Science and Technology (DST), Government of India for financial assistance.

## REFERENCES:

1. Youngje Sung, A corner fed microstrip circular antenna with switchable polarization, ETRI journal, Vol. 30, No. 5, October 2008
2. Kyungho chung, Y. Nam, T. Yun and J. Choi, A Reconfigurable microstrip patch antenna with switchable polarization, ETRI journal, Vol. 28, No. 3, pp. 718-722, pp. 379-382, June 2006
3. N. Jin, Fan Yang and Y Rahmat Samii, A Novel patch antenna with switchable slot (PASS) dual frequency operation with reversed circular polarizations, IEEE transactions on Antennas and Propagation, Vol. 54, No. 3, pp. 1031-1034, March 2006
4. Y J Sung, T U Jang and Y S Kim, A Reconfigurable microstrip antenna for switchable polarization, IEEE Microwave and wireless communication letters, Vol. 14, No. 11, pp. 534-536, November 2004
5. Fan Yang and Y Rahmat Samii, A Reconfigurable patch antenna using switchable slots for circular polarization diversity, IEEE Microwave and wireless communication letters, Vol. 12, No. 3, pp. 96-98, March 2002

SEARCH

Previous Page

Next Page

## RESEARCH SESSION VII
## ANTENNAS II

SEARCH

Previous Page

Next Page

SEARCH

Previous Page

Next Page

# RESEARCH SESSION VII
# ANTENNAS II

***Chair : Dr. K.J. Vinoy,IISc. Bangalore***





Previous Page Next Page

# COMPACT CPW FED ANTENNA FOR MULTIBAND APPLICATIONS

*Sujith R,Deepu.V,Laila D ,Sarin V.P,NishaMol M.S,C.K.Aanandan ,K.Vasudevan and P. Mohanan **

Centre for Research in Electromagnetics and Antennas, CREMA, Department of Electronics, CUSAT
Email:drmohan@ieee.org

## ABSTRACT:

A compact, dual band coplanar waveguide fed modified T-shaped uniplanar antenna is presented. The antenna has resonances at 1.77GHz and 5.54GHz with a wide band from 1.47-1.97GHz and from 5.13-6.48GHz with an impedance bandwidth of 34% and 26% respectively. Also the antenna has an average gain of 3dBi in lower band and 3.5dBi in higher band

## INTRODUCTION

In modern wireless communication system, compact multiband or wideband antennas are in great demand. Various printed monopole antennas satisfying the requirements of low profile and multiband with good impedance matching and omnidirectional radiation pattern have been reported. The stacked T-shaped monopole presented in [1] uses microstrip line as the feed and has a large ground plane. Various CPW fed uniplanar antennas for multiband applications have been reported in [2-6].In this paper a compact modified T-Shaped CPW-Fed monopole antenna is presented. The presented antenna has an overall dimension of 32 x 31 x 1.6 $mm^3$ including the ground plane on a substrate of dielectric constant 4.4. The antenna resonates at 1.77GHz and 5.54GHz and has a wide band from 1.47-1.97 GHz and from 5.13-6.48 GHz covering DCS 1800, DCS 1900/PCS, RFID(5.75-5.85GHz), ISM WLAN 5.2(5.15-5.35GHz), HIPERLAN2(5.47-5.725GHz) and ISM WLAN 5.8(5.725-5.825GHz) communication bands.

## ANTENNA GEOMETRY

Figure 1(a) shows the schematic of the CPW fed optimized compact antenna.

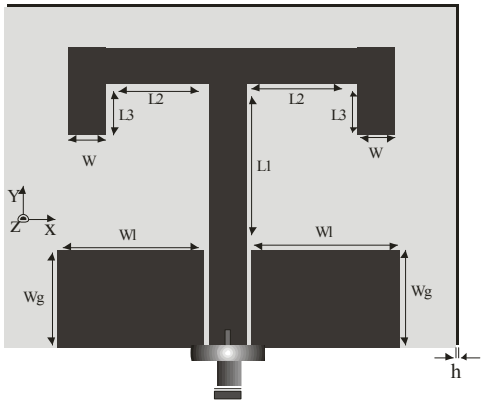


Figure 1(a) Geometry of the proposed CPW-Fed antenna

(L1=18mm, L2=11.5mm,L3=7mm,W=3mm,Wl=14mm,Wg=10mm,h=1.6mm,εr=4.4)

The antenna consists of a T-shaped monopole with two symmetrical vertical strips on both sides. The T monopole has a dimension 21mm (L1+w) x 32mm (2*L2+3*W) while each of the two symmetrical vertical strips has a length of 7 mm (L3). The dimensions of the coplanar waveguide feed are chosen from standard design equations for 50Ω impedance matching. The lateral ground plane dimension of the antenna is optimized as 10 mm (Wg) x

14 mm (Wl) for maximum compactness. The antenna is printed on a substrate of dielectric constant 4.4 and thickness 1.6mm.

## ANTENNA GEOMETRY

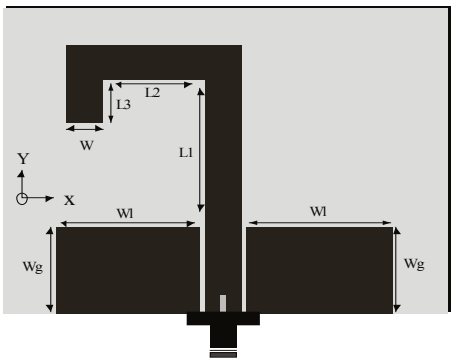


Figure 1(b) (L1=18mm, L2=11.5mm, L3=7mm,W=3mm, Wl=14mm,Wg=10mm,h=1.6mm,εr=4.4)

Since a top-loaded monopole can excite resonances, the antenna shown in figure 1(b) has two resonances but with poor matching. It is showing high capacitive reactance in the desired resonating bands, so by adding an inductive stub (L2+L3) as in figure 1(a) we can improve matching efficiently, resulting in a Modified T-shaped structure. The antenna is tested using HP 8510C Network Analyzer and the simulated and experimental return loss of the final antenna is shown in figure 2(a). The lower band centered at 1.77GHz has a wide bandwidth from 1.47GHz-1.97GHz with a percentage bandwidth of about 34%.The measured impedance bandwidth of the upper band centered at 5.54 GHz with wide bandwidth from 5.13GHz-6.48GHz .

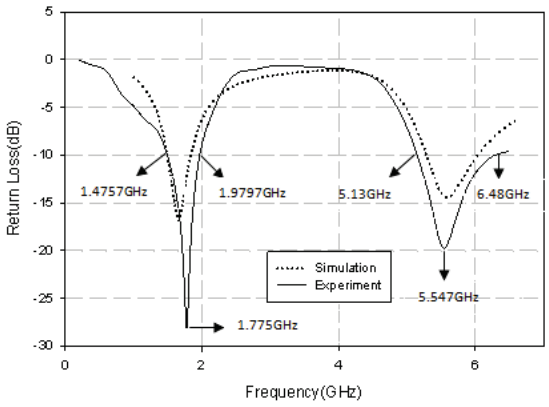


Figure (2) Measured and simulated Return loss of the proposed dual frequency antenna

The current distribution for the centre frequencies of the designed antenna is shown in figure 3. The current distribution on the horizontal arms is equal and opposite and cancels at the far field. So the radiation is primarily due to the y-component and hence it is polarized along y-direction in the two bands. It is also noted that the fundamental mode at 1.77GHz due to the lengths L1+L2+L3 which is nearly equal to λ/4. The second resonance at 5.55GHz is due to the length L1 which is nearly equal to λ/2. This aspect is reconfirmed by conducting experiments with different lengths.

SEARCH
Previous Page
Next Page

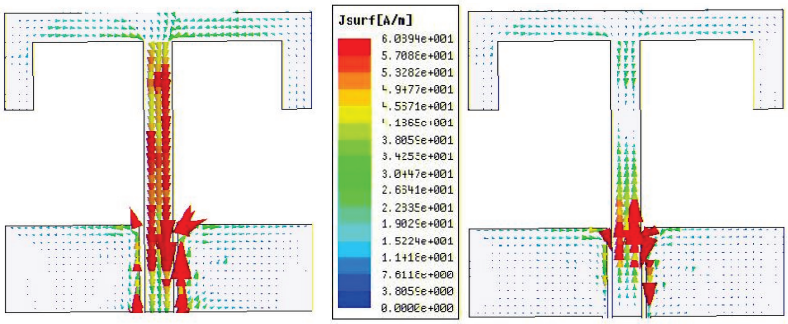


(a) (b)

Figure (3)

Simulated surface current distribution of antenna at (a) 1.77GHz and (b) 5.54GHz

The measured radiation patterns are shown in figure 4 and are nearly omnidirectional. The average gain of the antenna is 3dBi in lower band ( 1.47-1.97GHz) and 3.5dBi in higher band (5.13-6.48GHz) .

## CONCLUSION

A CPW fed planar monopole antenna built on a substrate of thickness 1.6mm and dielectric constant 4.4 for multiband operation has been developed. It is shown that by modifying a monopole additional resonances can be excited. Antenna is showing a 2:1 VSWR for the two bands centered at 1.77GHZ (1.47-1.97 GHz)and 5.54GHz(5.13-6.48GHz) with a impedance bandwidth of 34.15% and 26.31% covering DCS,PCS and ISM WLAN bands with an average gain of 3dBi and 3.5dBi respectively.

## ACKNOWLEDGEMENT

The authors wish to thank Department of Science and Technology (DST), UGC, and Defence Research and Development Organization (DRDO) for providing financial support.

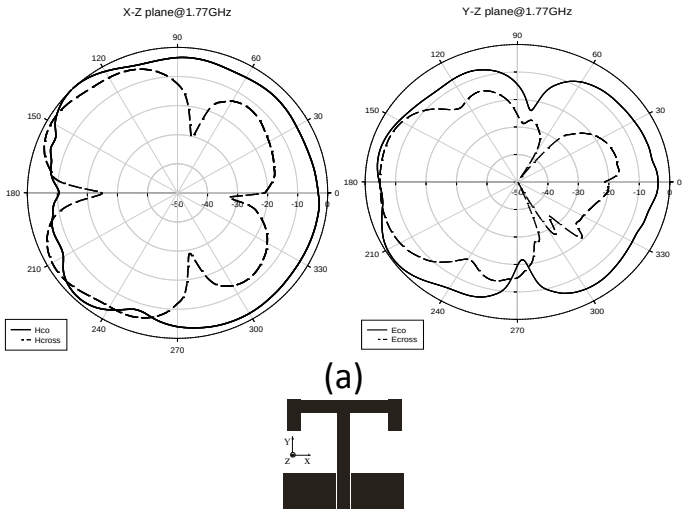


SEARCH

Previous Page Next Page

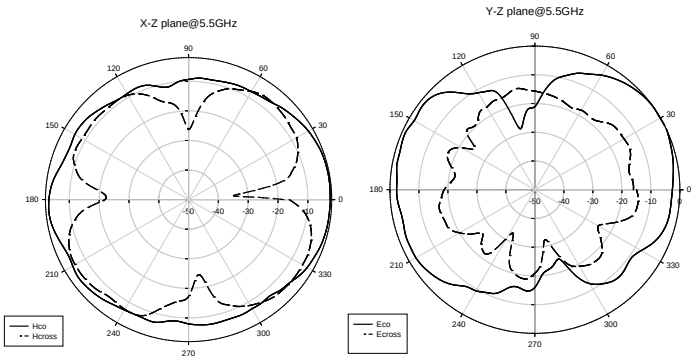


(b)

Figure 5. Measured radiation pattern of the proposed dual frequency antenna at (a) 1.77GHz and (b) 5.54GHz

## REFERENCES


1. Yen-Liang Kuo and Kin-Lu Wong, Printed Double-T Monopole Antenna for 2.4/5.2 GHz Dual-Band WLAN operation, IEEE Trans Antennas Propag 51 (2003), 2187-2192.
2. R.B.Hwang, A broadband CPW-fed T-shaped antenna for wireless communications, IEE proc Microwave Antennas Propag 151 (2004), 537-543.
3. Horng-Dean Chen and Hong-Twu Chen, ACPW-Fed Dual-Frequency Monopole Antenna, IEEE Trans Antennas Propag 52 (2004), 978-982
4. Horng-Dean Chen, Compact CPW-fed dual-frequency monopole antenna, Electron Lett 38 (2002), 1622-1624
5. Sheng-Bing Chen, Yong-Chang Jiao, Wei Wang, and Qi-Zhong Liu, Wideband CPW-Fed uniplanar sleeve-shaped monopole antenna, Microwave Opt Technol Lett 47 (2005), 245-247.
6. Wen-Chung Liu, Broadband dual-Frequency cross-shaped slot CPW-Fed monopole antenna for WLAN operation, Microwave Opt Technol Lett 46 (2005), 353-355.


SEARCH

Previous Page Next Page

# SIMPLE PRINTED ANTENNA WITH REDUCED HEIGHT FOR WLAN/WIMAX APPLICATIONS

*M.Sreenivasan, K.George Thomas*
SAMEER-Centre for Electromagnetics, C.I.T Campus, 2nd Cross Road, Taramani,
*Chennai -600113, India*
E.mail: sreeni_vm@yahoo.com, gt2781964@yahoo.com

**ABSTRACT:**

A new microstrip-fed printed antenna with triple band operation is presented for simultaneously satisfying wireless local area network (WLAN) and worldwide interoperability for microwave access (WiMAX) applications. The antenna consists of a rectangular radiating element fed asymmetrically by a 50Ω microstrip line and a trapezoidal ground plane. Rectangular horizontal strips are attached to the radiating element to form different current paths which make the antenna resonates in WLAN and WiMAX frequency bands. The antenna is simple in configuration outlining an overall dimension of $38 \times 30 \times 0.8$ $mm^3$. The measured 10dB bandwidth for return loss is from 2.23 to 2.65GHz and 3.24 to 6.95GHz, covering all the 2.4/5.2/5.8GHz WLAN bands and 2.5/3.5/5.5 GHz WiMAX bands.

.

## INTRODUCTION:

The interest in research and design of multiband and broadband antennas has increased dramatically in recent years, with the boost in modern wireless communication systems. Several multiband antenna designs for wireless local area network have been reported. The reported popular design configurations meeting the dual band operation for local area network in the 2.4GHz (2.4-2.484GHz) and 5.2/ 5.8GHz (5.15-5.35GHz/5.725-5.825GHz) bands include a microstrip-fed double-T monopole antenna[1], a CPW-fed monopole antenna with two resonant paths [2], a C-shaped monopole antenna with a shorted parasitic element [3], an inverted-L monopole with meandered wire and conducting triangular section [4], a dual band WLAN dipole antenna [5], a branched monopole antenna with a truncated ground plane [6] and a microstrip-fed dual band coplanar antenna [7]. The dual band slot antenna with double T-match stub generates resonance at 2.35-2.55 and 5 -6 GHz [8]. However, none of the above available designs can support worldwide interoperability for microwave access ( WiMAX) application. Various kinds of antennas suitable for WLAN/WiMAX operation were reported. The microsrtrip line fed slot antennas possess advantages such as wide impedance bandwidth, low profile, light weight and easy to manufacture [9],[10]. These printed slot antennas have a disadvantage of being large in size. In [11], authors presented a microstrip fed rectangular monopole with a metallic plate of trapezoid shape placed beneath, to generate the resonances. Also low profile multiband antennas have been reported. The compact slotted CPW-fed antenna [12], embedded by three shape slots produces triple resonant modes at 2.27 -2.62, 5.11 -5.54 and 6.45 -7.64 G[illegible] respectively, with poor radiation pattern performance. In[13], the band-rejected design of a printed open slot antenna for WLAN/WiMAX operation has been investigated.

In this paper, a planar rectangular radiation element with horizontal strips, printed on

Previous Page rate is proposed to achieve triple frequency band operation, covering Next Page

WLAN/WiMAX bands. The antenna is simple in structure with reduced height compared to that of a conventional printed monopole. The paper also provides detailed antenna dimensions and comparison between measured and simulated results.

## ANTENNA CONFIGURATION:

Fig.1.(a) illustrates the evolution of the proposed triple band antenna printed onto a FR4 substrate with thickness of 0.8mm and relative permittivity of 4.4. A rectangular radiation element with horizontal strips of unequal lengths and a 50Ω microstrip feed line are printed on the top of the substrate while a trapezoidal ground plane placed under the microstrip feed line is printed on the bottom of the substrate. The rectangular radiation element was fed asymmetrically in a direction perpendicular to its length '*l*'. The antenna performance was analyzed using High Frequency Structure Simulator (HFSS). Fig.1.(b) shows three different current paths formed in the proposed antenna configuration. The path length of the current path AB, formed by 50Ω feed line, rectangular element and the attached strip with length $l_1$, is equal to 0.5λ and provides the resonance in the 2.4GHz band. Current path AD which is responsible for resonance at 3.5GHz band is formed by 50Ω feed line, rectangular element and the attached strip with length $l_2$ and resonates at a path length of 0.75λ. Similarly resonance in the 5.8GHz band is created by an effective path CD of length equal to 0.5λ which combines the rectangular element (portion of horizontal length and vertical length) and the horizontal strip with length $l_2$. The gap 'g' formed between the ground plane and rectangular radiation elements significantly affects the impedance performance and was optimized by simulation. The upper width of the trapezoidal ground plane $wg_2$ has a significant effect in the 5.8GHz band resonance. On varying the width $wg_2$, the resonance shifts in frequency without affecting first and second resonances. The optimum dimensions of the antenna are shown in fig.1.(a)

## RESULTS AND DISCUSSION:

Fig.2. shows the simulated and experimental results of the return loss for the proposed triple band antenna. A good agreement is seen between the measured and simulated return loss curves. The 10dB bandwidth for the measured return loss reaches 0.42GHz(2.23 - 2.65 GHz) and 3.71 GHz(3.24 - 6.95 GHz) respectively, and can cover the 2.4 - 2.484GHz, 5.15 - 5.35GHz, and 5.725 – 5.825GHz WLAN bands, and the 2.5 – 2.69GHz, 3.4 – 3.69GHz, and 5.25-5.85GHz WiMAX bands. It is to be noted that 3.24-6.95GHz 10dB return loss bandwidth is due to the overlapping of second and third resonances. Fig.3. illustrates the measured radiation pattern in H-plane (x-y plane). It is seen that the antenna possesses omni directional radiation patterns with minimum distortion in the 2.5 and 3.5GHz frequency bands. However, instability seen in 5.5GHz pattern can be attributed to the asymmetrical feeding of the radiation element. E-plane patterns are demonstrated in fig.4. which resemble to dipole patterns. It is worthwhile to mention that at 2.4 and 3.5GHz bands, the shaped trapezoidal ground plane and the rectangular element constitute the radiation structure. Measured peak antenna gain against frequency in the frequency bands of 2-3GHz, 3-4GHz and 5 -6 GHz are plotted in fig.5. (a), (b) and (c). It is observed that antenna exhibits reasonably stable gain over the band of frequencies.

## CONCLUSION:

A small printed antenna is presented for promising triple band operation. With the [illegible] of horizontal strips attached to radiation element, the proposed antenna not offers reduced height but also demonstrates sufficient impedance bandwidth and suitable

SEARCH
Previous Page Next Page

radiation characteristics for the triple frequency band operation, required for WLAN/WiMAX applications.

**REFERENCE:**


1. Y.L.Kuo and K.-L.Wong, " Printed double-T monopole antenna for 2.4/5.2 GHz dual-band WLAN operation" *IEEE Trans. Antennas propag*., vol.51, no.9, pp.2187-2192, Sep.2003
2. T.H.Kim and D.C Park, "CPW-fed compact monopole antenna for dual-band WLAN applications," *Electron. Lett*., vol.41, no.6, pp.292-293, Mar.2005
3. C.-Y.Huang an d P. -Y.Chiu, "D ual band ant enna w ith s horted par asitic element," *Electron. Lett*., vol.41, no.21, pp.1154-1155, Oct.2005
4. H.-D. Chen, J.-S.Chen, and Y.-T.Cheng, " Modified inverted-L monopole antenna for 2.4/5 GHz dual band operation," *Electron. Lett*., vol.39, no.22, Oct.2003
5. Z.Zhang, M.F.Iskander, J.-C. Langer, and J.Mathew, " Dual band WLAN dipole antenna using an internal matching circuit," *IEEE Trans. Antennas Propag*., vol.53, no.5,May.2005
6. M.N.Suma, R.K.Raj, M.Joseph, P.C.Bybi, and P. Mohanan , "A compact dual band branched monopole ant enna for D CS/2.4GHz W LAN appl ications," *IEEE Microw. Wireless Comp. Lett*., vol.16, no.5, pp.275-277, May.2006
7. R.K.Raj, M.Joseph, C.K.Anandan, K.Vasudevan and P. Mohanan, " A new compact microstrip-fed dual-band coplanar antenna for WLAN applications," *IEEE Trans. Antennas Propag*., vol.54, no.12, pp.3755-3762, Dec.2006
8. Y.C.Lin, and K .J.Hung, "D esign of dua l-band s lot an tenna w ith doubl e T -match stubs," *Electron. Lett*., vol.42, pp 438-439, 2006
9. J.Y.Jan and J.W.Su., " Bandwidth enhancement of a printed wide-slot antenna with a rotated slot," *IEEE Trans. Antennas Propag*., vol.53,pp.2111-2114,2005
10. Y.F.Liu, K.L.Lau, Q.Xue, and C.H.Chen, "Experimental studies of printed wide-slot antenna for w ide-band appl ications," *IEEE Antennas Wireless Propag. Lett.,* vol.3, pp.273-275,2004.
11. C.-Y. Pan, T.-S. Horng, W.-S. Chen and C.-H. Huang, "Dual wideband printed monopole antenna for WLAN/WiMax applications," *IEEE Antennas Wireless Propag. Lett.,* vol.6, pp.149-151,2007
12. W.C Liu and H.J Liu, "Compact tri-band slotted monopole antenna with asymmetrical CPW grounds," *Electron. Lett*., vol.42, pp 840-842, 2006
13. W.-S Chen and K.-Y Ku, "Band – rejected design of printed open slot antenna for WLAN/WiMAX operation" IEEE Trans.Antennas. Propag., vol.56,no.4,pp 1163-1169, April 2008.


SEARCH

Previous Page Next Page

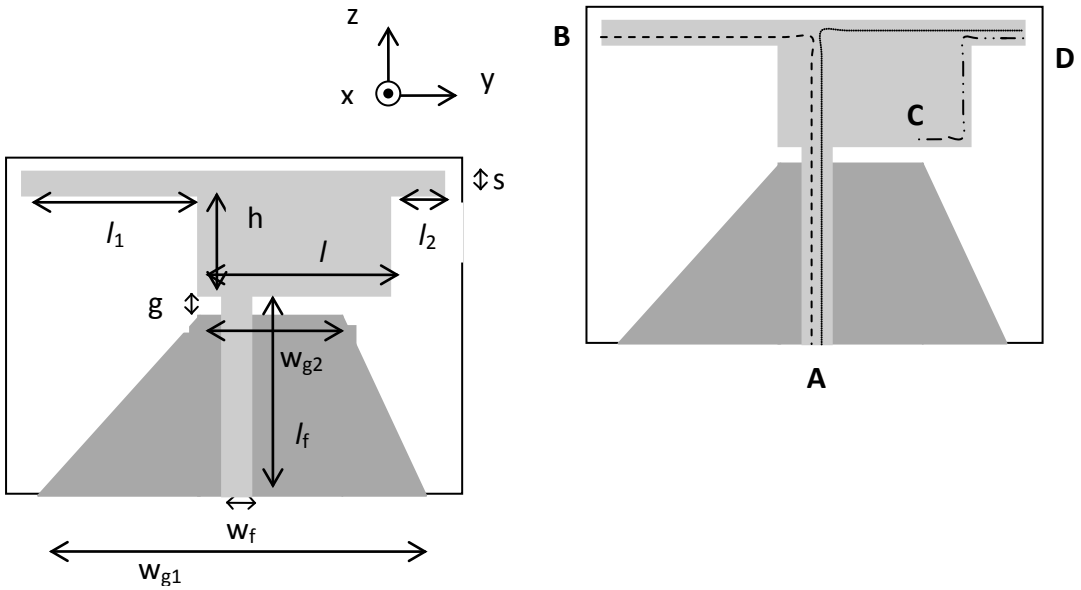


(a) (b)

Fig.1.(a) Configuration of the proposed triple band printed antenna, (b) Different current paths in the proposed antenna
$l_f$ = 17mm, $w_f$ = 1.4mm, $w_{g1}$ = 36mm, $w_{g2}$ = 10mm, g = 1mm, h = 12mm, $l$ = 16mm, $l_1$= 18mm, $l_2$= 4mm, s = 1mm, H = 0.8mm

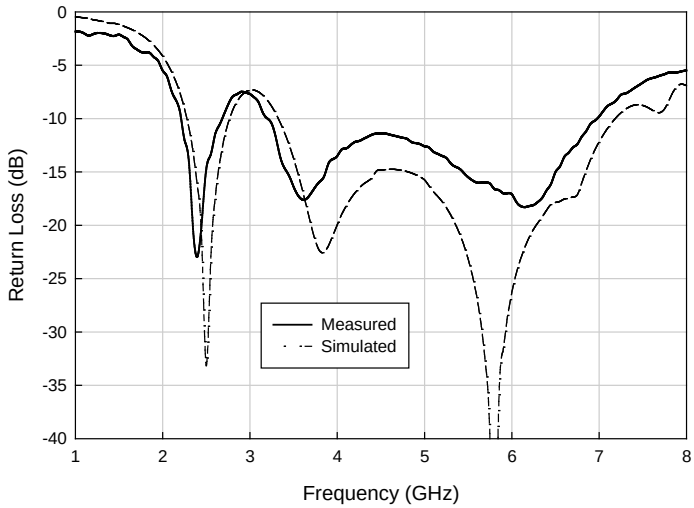


Fig. 2. Measured and Simulated return loss for the proposed triple band printed antenna

SEARCH

Previous Page

Next Page

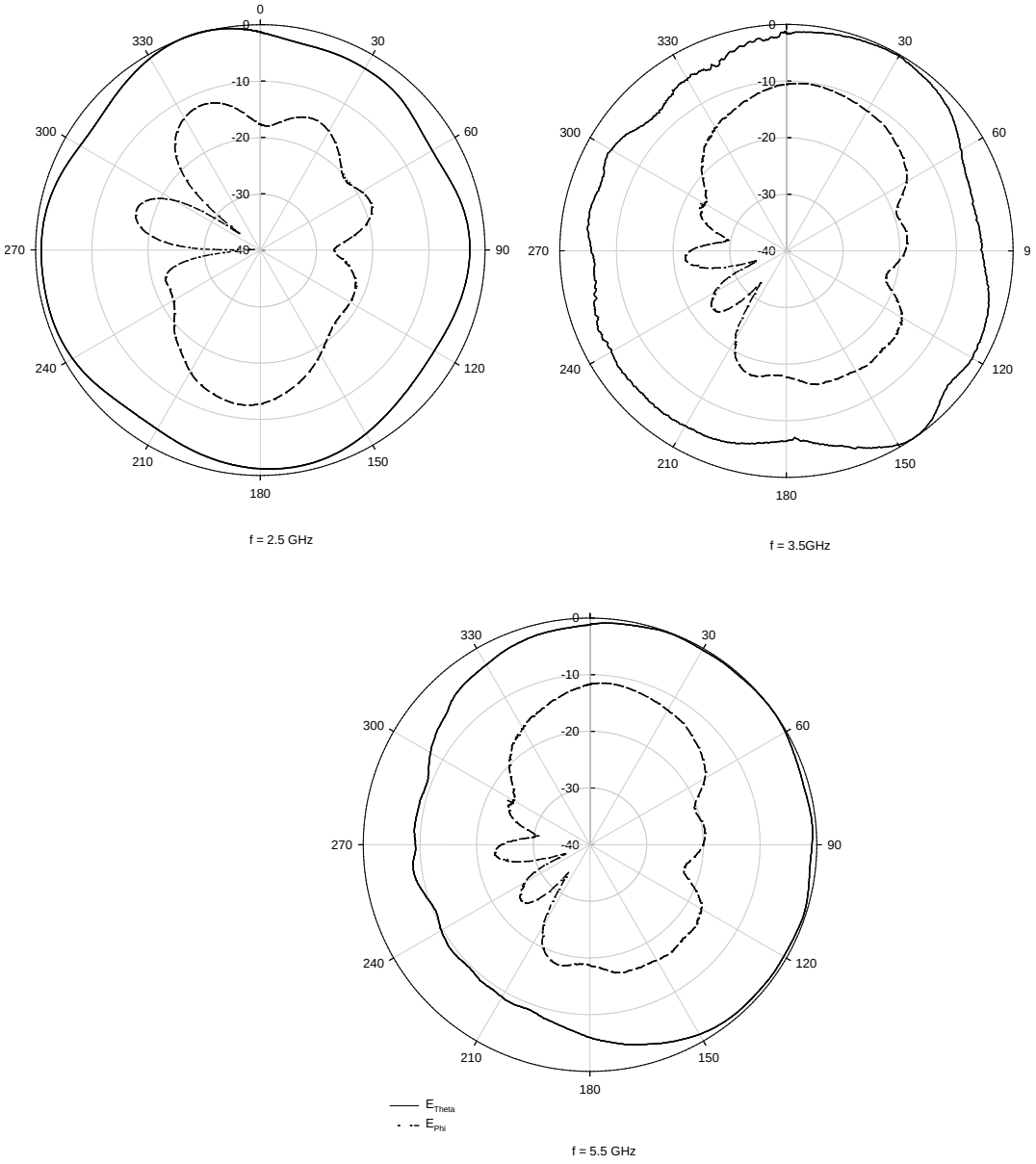


Fig. 3. Measured radiation patterns of the proposed antenna in x-y plane ($E_{Theta}$ and $E_{Phi}$ component )

SEARCH

Previous Page

Next Page

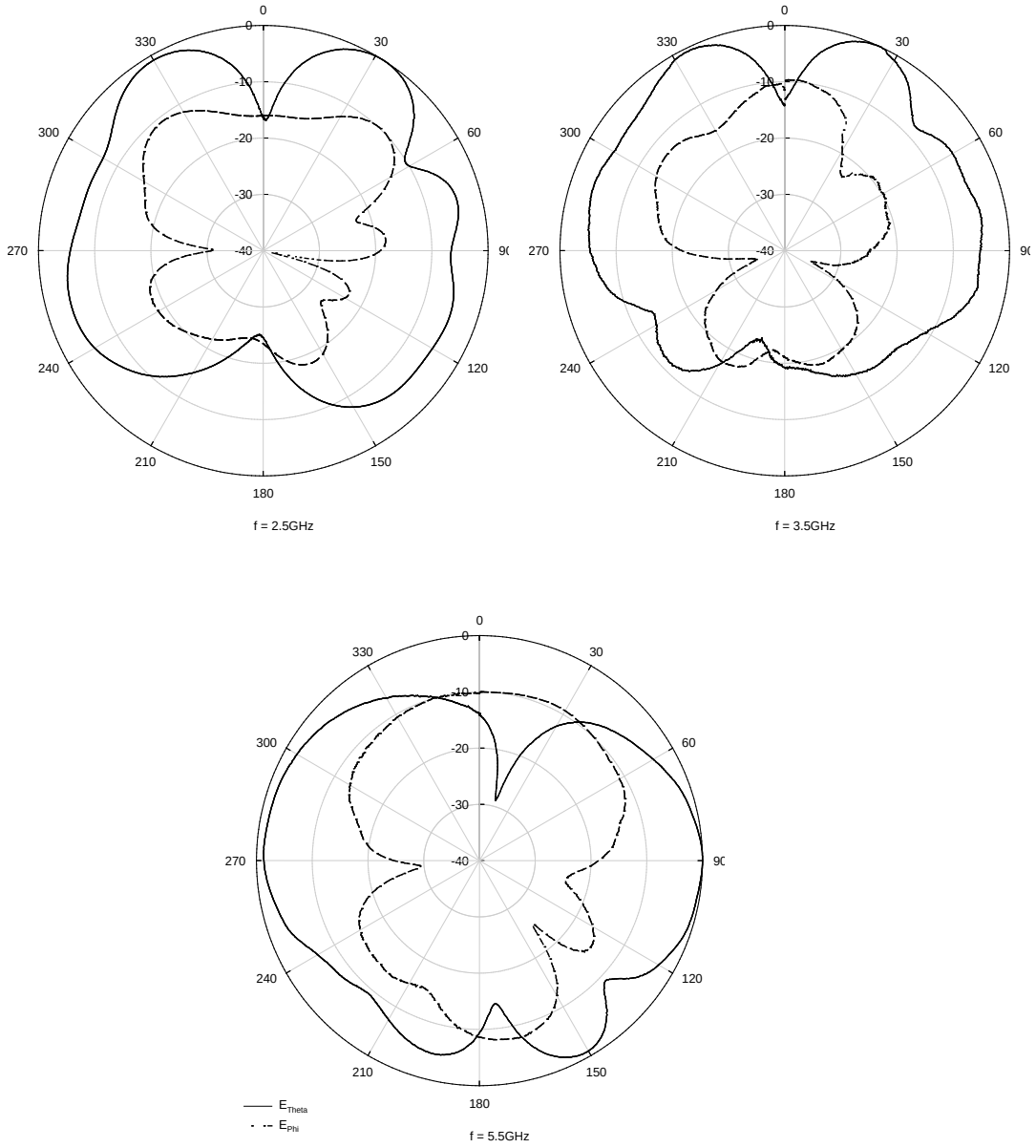


Fig. 4. Measured radiation patterns of the proposed antenna in z-x plane ($E_{Theta}$ and $E_{Phi}$ component)

SEARCH

Previous Page

Next Page

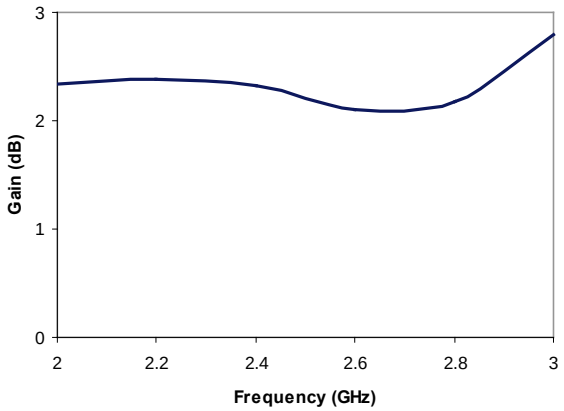


(a)

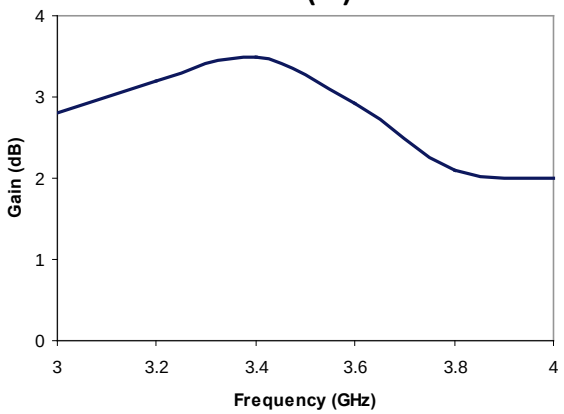


(b)

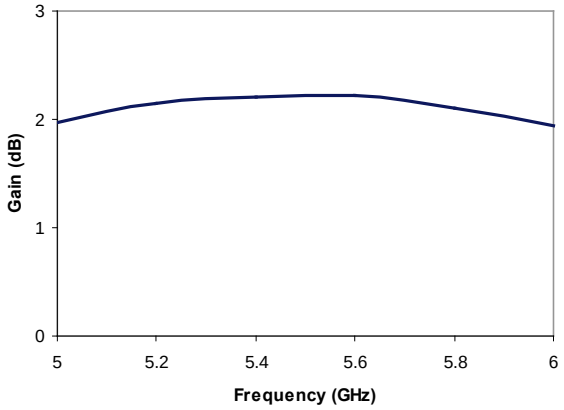


(c)

Fig. 5. Measured peak gains for the proposed antenna in the (a) 2.5GHz; (b) 3.5GHz ; (c) 5.5GHz bands.

SEARCH

Previous Page

Next Page

# BROAD BAND MICROSTRIP ANTENNA FOR WIRELESS APPLICATIONS

*Sarin V.P, Nisha mol M.S, Deepu V, Sujith R, P. Mohanan , C.K Aanandan and K. Vasudevan*

Centre for Research in Electromagnetics and Antennas, Dept. of Electronics, CUSAT, Cochin-22

E.mail: vasudevankdr@gmail.com

## ABSTRACT:

A new electromagnetically coupled broad band printed microstrip antenna covering the 5.2/5.8 GHz WLAN application is presented. The antenna has a dimension of 42mmx55mmx3.2mm when printed on a substrate of $\varepsilon_r$ =4.4 and has a 2:1 VSWR bandwidth of 42% from 4.17 GHz to 6.4 GHz. Details of the design, experimental and simulated results are discussed.

## INTRODUCTION:

The new wireless communication era demand wide band high gain antennas. Eventhough microstrip antennas have a lot of advantages like high gain, low profile ,ease of fabrication etc, their perfomance is seriously limited by their inherent narrow band width.Many techniques have been proposed to enhance the bandwidth of microstrip antennas. [1] and [2] deal with stacked configurations for wide-band operation. A simple E-shaped patch in [3] having a bandwidth of 30.3% and its derivative [4] with 49% area reduction has been reported. Modifications of the E-shaped patch [5] and [6] has been reported recently. Configurtations with modifications in the feed probe [7-9] are also good choices of wide-band microstrip antennas.

In this paper we propose a simple wide-band printed microstrip antenna having a 2:1 VSWR bandwidth of 42.19% from 4.17-6.4 GHz. It covers IEEE 802.11a (5.15-5.35,5.725-5.825 GHz) and HIPERLAN2 (5.45-5.725 GHz) communication bands.

## ANTENNA CONFIGURATION:

The final design is derived from an electromagnetically coupled square patch of dimension $L_1xL_1$ $mm^2$ fabricated on a substrate of dielectric constant $\varepsilon_r$=4.4 and height h=1.6mm. The width of the microstrip transmission line ($W_f$) is designed using standard design equation for the same substrate. A $45^0$ tilted square slot of dimension $L_2xL_2$ $mm^2$ is etched on the above patch. This strucure exhibits poor impedance matching characteristics as shown in fig. 2. The impedance matching can be made better by incorporating a rectangular strip of dimensions $L_3xW_1$ $mm^2$ symmetrically on the top corner of the slot. The final antenna is shown in fig. 1. The ground plane dimension $L_4xL_5$ $mm^2$ is optimised after a set of simulations.

SEARCH

Previous Page

Next Page

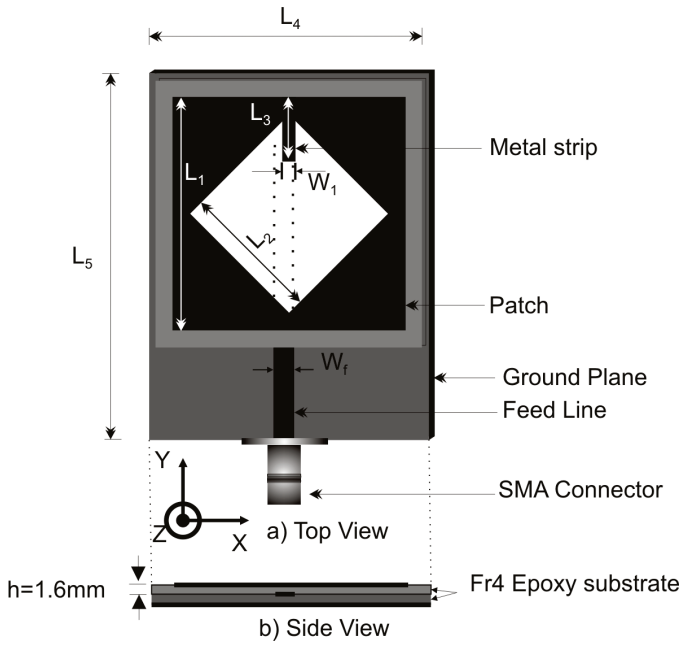


Fig. 1 Geometry of the proposed antenna

## RESULTS AND DISCUSSION:

The simulation and the experimental works of the antenna are done using Ansoft HFSS and Agilent HP8510C Network analyser respectively. The simulated and experimental return loss characteristics of the antenna with and without the metal strip are shown in fig. 2. The length ( $L_3$) and the width ( $W_1$) of the strip are the major parameters affecting the optimum bandwidth of the antenna. Fig. 3 shows the simulated return loss variation with respect to strip length $L_3$. It can be seen that the bandwidth enhancement is achieved by the merging of five bands centered at 4.3 GHz,4.56 GHz, 5 GHz,5.68 GHz and 6.14 GHz respectively. The normalised XZ and YZ plane radiation patterns of the antenna at 4.3 GHz , 5.2 GHz and 5.8 G Hz are shown in fig. 3. The patterns show broadside radiation with good cross polar isolation throughout the band. The cross radiation patterns are conical in shape.The antenna is linearly polarised along the Y-axis in the entire operating band. It can be seen that the surface currents at 4.3 G Hz starts from the metal strip;directed along the upper patch surface symmetrically. This causes field cancellation along the boresight at the far field yielding a reduced gain at lower operating frequencies. The antenna has a peak gain of 6.73 dBi at 5.78 GHz and a least of 3.41 dBi at 4.3 GHz.

SEARCH

Previous Page

Next Page

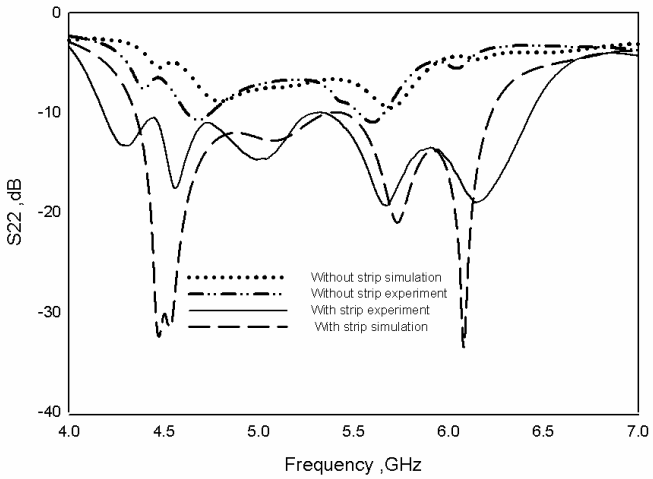


Fig.2 Return loss characteristics of the proposed antenna ($L_1$=35mm, $L_2$=21mm, $L_3$=10mm, $L_4$=42mm, $L_5$=55mm, $W_1$=2mm and $W_f$=3mm)

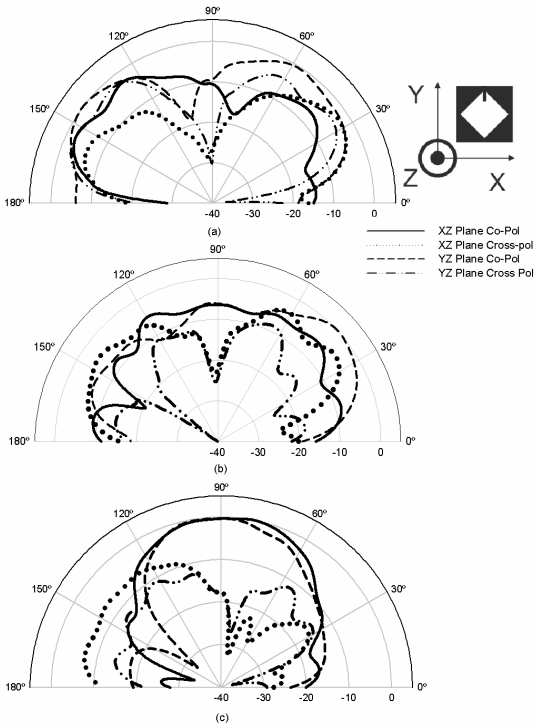


Fig. 3 Radiation patterns of the antenna at a) 4.3 GHz, b) 5.2 GHz and c) 5.8 GHz

SEARCH

Previous Page

Next Page

## CONCLUSION:

A wide-band electromagnetically coupled printed microstrip antenna suitable for 5.2/5.8 G Hz WLAN,HIPERLAN2 and HISWANa appl ications is pr esented. B andwidth enhancement is achi eved by the merging of bands caused by the add on metal strip on a slotted microstrip structure. The presented antenna has a 2: 1 VSWR bandwidth of 42.19% from 4.17 GHz to 6.4 GHz; exhibiting good radiation characteristics.

## REFERENCE:


1. S.D Targonski, R.B Waterhouse, D.M Pozar, "Design of wideband aperture stacked patch microstrip antennas," IEEE Trans. Antennas Propag., vol. 46, no. 9, pp. 1245-1251, 1998.
2. M.A Martin, B.S Sharif, C.C Tsimenidis, "Probe fed stacked patch antenna for wideband applications," IEEE Trans. Antennas Propag., vol. 55, no. 8, pp. 2385-2388, 2007.
3. Fan Yang, Xue-Xia Zhang, Ziaoning Ye, Yahya Rahmat-Samii, "Wide-bannd E-shaped patch antennas for wireless communications," IEEE Trans. Antennas Propag., vol. 49, no. 7, pp. 1094-1100, 2001.
4. Ricky Chair, Chi-Lun Mak, Kai-Fong Lee, Kwai-Man Luk, Ahmed A. Kishk, "Miniature wide-band half U-slot and half E-shaped patch antennas," IEEE Trans. Antennas Propag., vol. 53, no. 8, pp. 2645-2652, 2005.
5. Diego C aratelli, R enato C icchetti, G iorgi B it-Babik, A ntonio Far aone, "A per turbed E - shaped patch antenna for wideband WLAN applications," IEEE Trans. Antennas Propag., vol. 54, no. 6, pp. 1871-1874, 2006.
6. Yuehe Ge, Karu P. Esselle, Trevor S. Bird, "A compact E-shaped patch antenna with corrugated wings," IEEE Trans. Antennas Propag., vol. 54, no. 8, pp. 2411-2413, 2006.
7. Yong-Xin Guo, Michael Yan Wah Chia, Zhi Ning Chen, Kwai-Man Luk, "Wide-band L-probe fed circular patch antenna for conical-pattern radiation," IEEE Trans. Antennas Propag., vol. 52, no. 4, pp. 1115-1116, 2004.
8. Jongkuk Park, Hyung-gi Na, Seung-hun Baik, "Design of wideband aperture stacked patch microstrip antennas," IEEE Antennas wireless Propag. Lett., vol. 3, pp. 117-119, 2004.
9. Chi-Lun Mak, Hang Wong, Kwai-man Luk, "High-gain and wide-band single-layer patch antenna for wireless communications," IEEE Trans. Vehicular. Tech., vol. 54, no. 1, pp . 33-40, 2005.


SEARCH

Previous Page Next Page

# EFFECT OF SLOT ON GROUND PLANE FOR WIDEBAND OPERATION

*M Veereshappa[1],R B Konda[2], S K Satnoor[2] , S N Mulgi[2] and P V Hunagund[2]*
[1]Department of Electronics, L.V.D.College, Raichur – 584 101, Karnataka, India.
[2]Department of PG Studies and Research in Applied Electronics,
Gulbarga University, Gulbarga - 585 106, Karnataka, India.
E.mail: veereshappam@yahoo.com

## ABSTRACT:

A complementary ground rectangular microstrip antenna (CGRMSA) is proposed for dualband operation having wider upper operating band than the lower. If the slots are introduced in the conducting patch of CGRMSA the lower operating band becomes wider than the upper band and overall impedance bandwidth becomes 8.6% more when compared to CGRMSA. Further, replacing the ground plane by parallel slot patch, a 32.47% of impedance bandwidth is achieved without affecting the nature of radiation characteristics. These antennas may find applications in WLAN. The design concept of antennas is presented and experimental results are discussed.

## INTRODUCTION:

The microstrip antennas are very popular because of their attractive features, such as low profile, lightweight, and ease in fabrication and can be deployed for a wide verity of applications in microwave communication. However, microstrip antennas inherently have narrow impedance bandwidth, which is one of the main drawback. A number of approaches have been reported in the literature for dual band operation required for blue tooth, mobile, wireless local area network (WLAN), global system for mobile communication (GSM) and global position satellites (GPS) applications[1,2]. But in this study a simple technique has been used to achieve the same.

## DESCRIPTION OF ANTENNA GEOMETRY:

The art work of antennas are sketched by using computer software Auto-CAD 2004 and are fabricated on low cost glass epoxy substrate material of thickness $h$ =1.66 mm and permittivity $\varepsilon_r$ = 4.2.

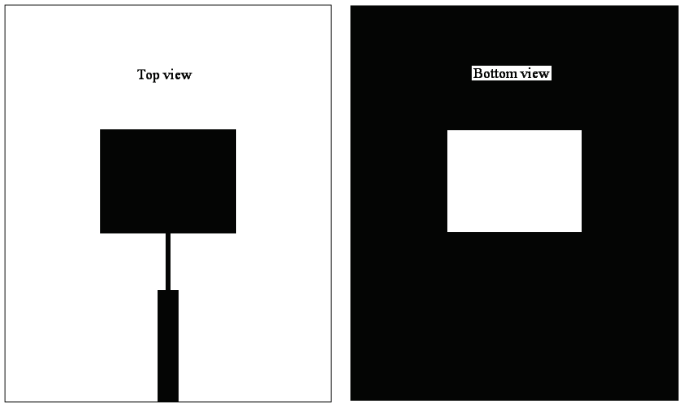


Fig. 1 Geometry of CGRMSA

SEARCH
Previous Page
Next Page

The geometry of CGRMSA is shown in Fig. 1. In this antenna the copper area exactly below the patch of same dimension on the ground plane is removed. The antenna is fed through microstripline. The quarter wave transformer is used between patch element and microstripline for matching the impedance[3]. In the top-view, the length and width of patch are 1.57 and 2.067 cm, length and width of quarter wave transformer are 0.858 and 0.053 cm and length and width of microstripline are 1.692 and 0.316 cm respectively. The complementary ground parallel slot rectangular microstrip antenna (CGPSRMSA) consists of two equal parallel slots in the conduction patch. The length and width of slots are 1.11 and 0.277 cm respectively. These slots are kept at a distance of 0.23 cm from the width and 0.4 cm from the length of the patch. The geometry of this antenna is as shown in Fig. 2.

The geometry of ground parallel slot rectangular microstrip antenna (GPSRMSA) is shown in Fig. 3. In this antenna the ground plane is replaced by the top view geometry shown in Fig. 2 but microstripline feed is replaced by a connicting strip. The top view geometry of Fig. 3 is same as that of Fig. 1.

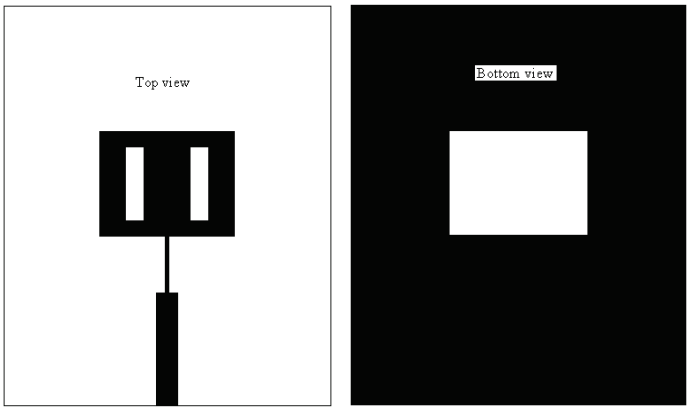


Fig. 2 Geometry of CGPSRMSA

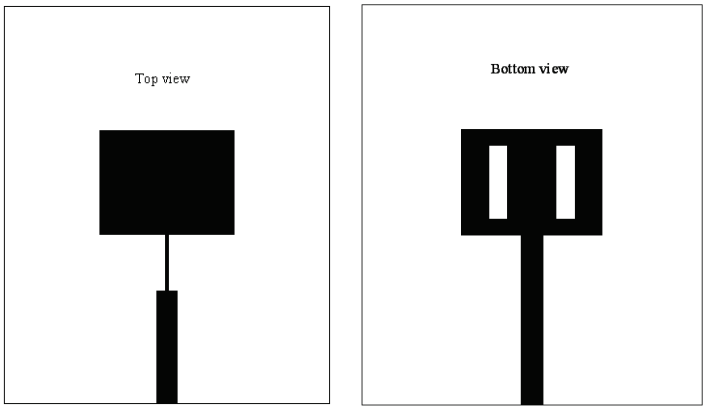


Fig. 3 Geometry of GPSRMSA

## EXPERIMENTAL RESULTS:

The impedance bandwidth over return loss less than –10dB for the proposed antennas is measured for 1 to 6 GHz. The measurement is taken on Vector Network Analyzer (Rohde & Schwarz, Germany make ZVK model). The variation of return loss versus frequency of CGRMSA and CGPSRMSA is as shown in Fig. 4. From this figure it is seen that the antenna CGRMSA resonates for two bands of frequencies having magnitude ($BW_1$)3.45% and ($BW_2$) 4.85%. This dual band property is due to patch and complementary ground makes the patch resonates for two bands of frequencies. The dual band operation of this antenna may find applications in WLAN, where two bands can be used independently for transmit/receive operations. Further from the same figure it is seen that, the antenna CGPSRMSA resonates for two bands of frequencies. But in this case the lower resonating band becomes wider than the upper band as against in case CGRMSA, this is due to addition of parallel slots in the conducting patch. The overall bandwidth is ($BW_3$+$BW_4$) 9.98% which is 8.6% more when compared to CGRMSA. The variation of returnloss versus frequency of

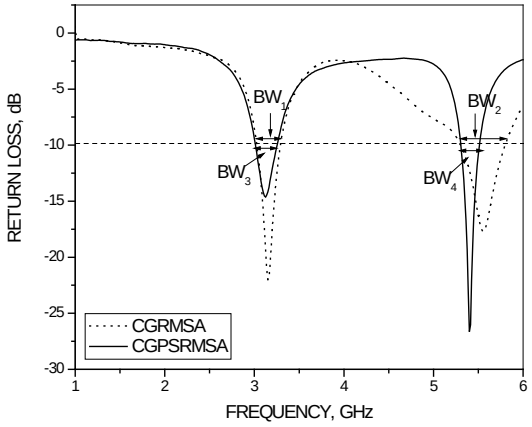


Fig. 4 Variation of return loss versus frequency

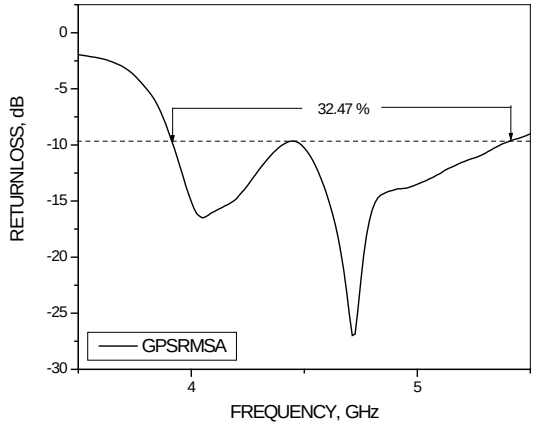


Fig. 5 Variation of return loss versus frequency

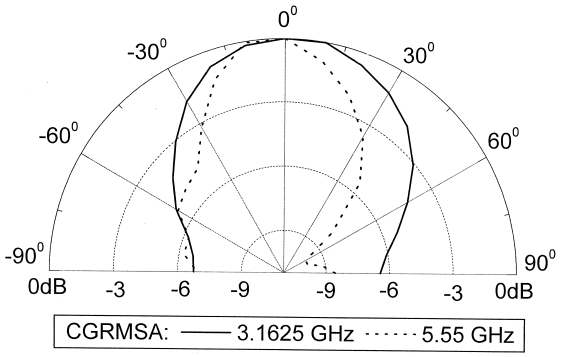


Fig. 6 Typical radiation pattern measured at 3.16 and 5.55 GHz

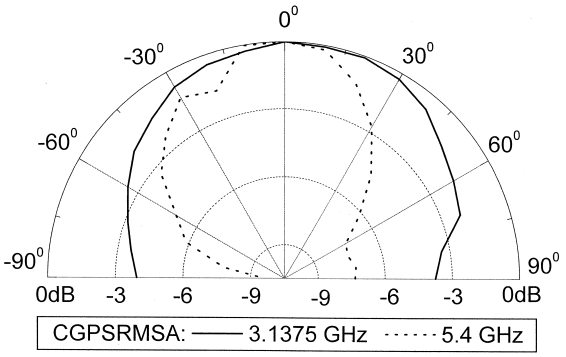


Fig.7 Typical radiation pattern measured at 3.13 and 5.4GHz

SEARCH

Previous Page

Next Page

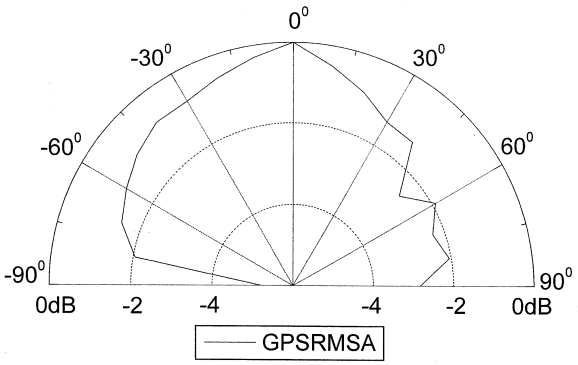


Fig. 8 Typical radiation pattern measured at 4.71 GHz

GPSRMSA is as shown in Fig. 5. From this figure it is seen that the antenna gives a wide bandwidth of 32.47%. This band can be used single or dual as the case may be[4]. Hence it is quite clear that, the new technique proposed for the construction of GPSRMSA is very much effective in enhancing the bandwidth of antenna.

The typical co-polar radiation patterns of CGRMSA, CGPSRMSA and GPSRMSA measured for their resonate frequencies are shown in Fig. 6 to Fig. 8 respectively. From these figures it is clear that the antenna shows broadside radiation pattern. Hence the nature of radiation pattern remains the same in spite of enhancement in their impedance bandwidth.

## CONCLUSION:

From the detailed experimental study it is concluded that, the dual band operation of antenna may be achieved by placing a simple slot at the ground plane having dimension same as that of radiating patch. The inversion of operating band may be achieved by inserting parallel slot on the conducting patch. However, if ground plane is replaced by parallel slot patch two operating bands merges and becomes single wideband. The proposed antennas are simple in their design and fabrication and uses low cost substrate material. These antennas may find applications in WLAN.

## ACKNOWLEDGEMENT:

The authors would like to thank Dept. of Science & Technology (DST), Govt. of India, New Delhi, for sanctioning Network Analyzer to this Department under FIST project.

## REFERENCES:

1. S Maci and G Biffi Gentili, "Dual-frequency patch antennas", IEEE Antennas and Propag. Magz.,Vol. 39, No. 6, pp.13-18,1997.
2. Dong-Uk Sim, Jung-Ick Moon, and Seong-Ook Park, "An internal triple-band antenna for PCS/IMT-2000/Bluetooth applications", IEEE Antennas and Wireless Propag. Lett.,Vol. 3, 2004.
3. Bahl I J and Bhartia P, Microstrip Slot Antenna, *Microstrip Antennas,* Dedham, MA: Artech House, New Delhi, 1981.
4. Ghz R afi an d Shaf ai L , " Wideband V -slotted di amond-shaped microstrip pa[illegible] antenna", Electron Lett., Vol. 40, No. 19, 2004.



Previous Page Next Page

# A NOVEL PENTA-FREQUENCY MICROSTRIP ANTENNA

*Arindam Deb* [1] *and Bhaskar Gupta* [2]
KIIT University, Bhubaneswar- 751024, India,
Email: arindamdeb2008@rediffmail.com
*(2)Jadavpur University, Kolkata-700032, India*
E-mail: gupta_bh@yahoo.com

**ABSTRACT:**

A new rectangular microstrip antenna is proposed that has five resonant frequencies in the range 1-4 GHz, specifically at 1.092, 1. 98, 2.616, 3.144, 3.762 GHz. Simulation of the structure was done using IE3D. The antenna uses air substrate and two slots of equal dimensions are cut across each other in the form of a Christ-cross.

**INTRODUCTION:**

Small size multifrequency patch antennas, which are easy to manufacture and cost effective, are in demand in the mobile communication industry. A large number of multi-frequency antennas for this purpose were reported. All these antennas use some sort of slots cut into the patch along with the probe feed at a certain optimally chosen point to achieve the desired objective. A dual-frequency equilateral triangular microstrip antenna with a slit is reported in [1] with $\hat{I}_r$ =4.4 . Similarly a small dual frequency microstrip antenna with cross-slot is also reported in [2] that uses the substrate with same value of $\hat{I}_r$. Again a compact planar quad frequency microstrip antenna was reported in [3] that uses a substrate with $\hat{I}_r$ = 2.22. In this paper, we present a novel design of a microstrip antenna that has five resonant frequencies in the range 1-4 GHz. The antenna has two slots of equal dimensions cut across each other perpendicularly in the form of a Christ-cross. It uses air as its substrate to simplify fabrication and reduce cost.

**ANTENNA DESIGN:**

The antenna rectangular patch as shown in the fig. 1 has length L and width W. Two slots are used. While the vertical one has length $L_s$ and width $W_s$, the horizontal one has length $W_s$ and width $L_s$. The former is centered at the center of the patch while the other slot's center lies F mm above the center of the former as shown in the figure. The probe feed is situated at distance x from the vertical bisector and distance y from the topmost edge of the patch. The patch is at a height h above an infinite ground plane.

SEARCH

Previous Page Next Page

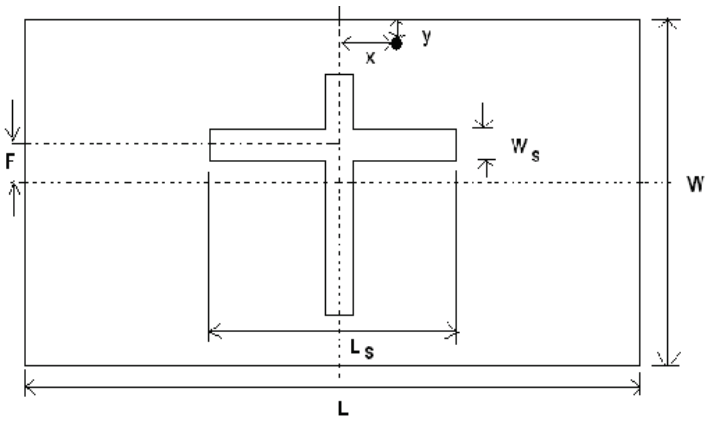


Figure 1

Table 1. (Dimensions in mm)

| L | W | Ls | Ws | F | x | y | h |
|---|---|---|---|---|---|---|---|
| 110 | 60 | 45 | 5 | 5 | 10 | 2 | 6 |

## SIMULATION RESULTS:

The antenna shows five resonant frequencies as shown in figure 2.

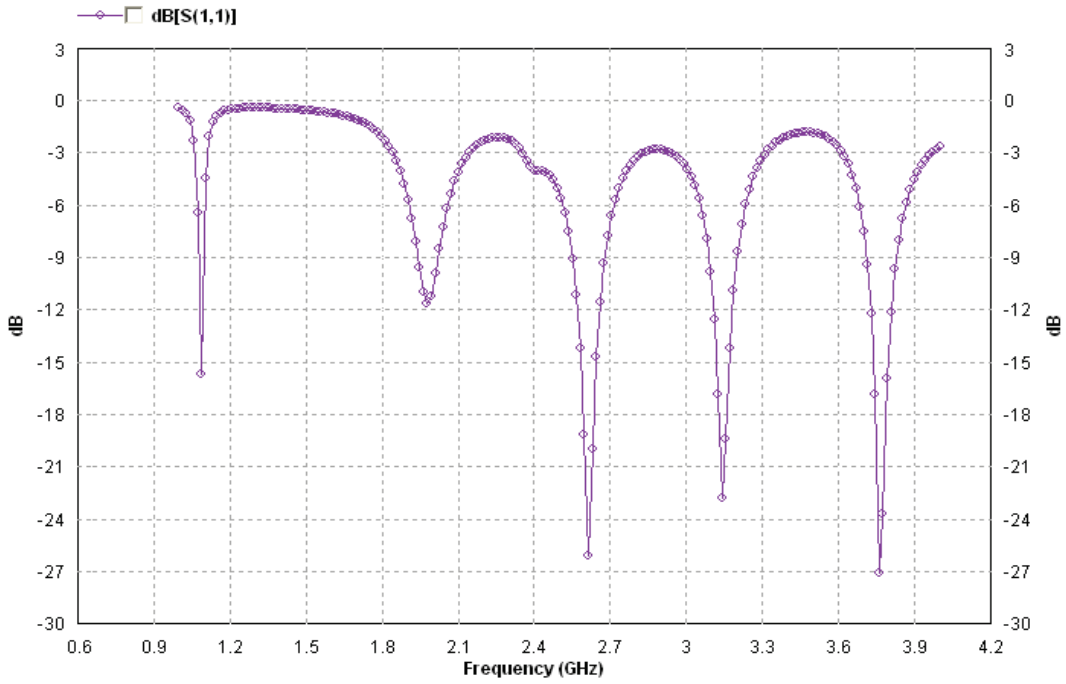


**Figure 2.**

The simulation results depict $S_{11}$ of -16dB at 1.092 GHz, -11.88dB at 1.98 GHz, -26.2 GHz, -22.8 dB at 3.144 GHz and -27 dB at 3.762 GHz. The radiation patter the above resonant frequencies are shown in figures 3, 4, 5, 6, and 7.

SEARCH
Previous Page
Next Page

At 1.092 GHz, it is nearly a single frequency operation because the bandwidth at this frequency is negligible. For 1.98, 2.616, 3.144 and 3.762 GHz bandwidths obtained are 0.057 GHz ( percentage bandw idth: 2.88) , 0. 109 G Hz ( percentage ban dwidth: 4.17) , 0.096(percentage bandw idth: 3.05) G HZ and 0.1 G Hz ( percentage bandwidth: 2. 66) respectively.

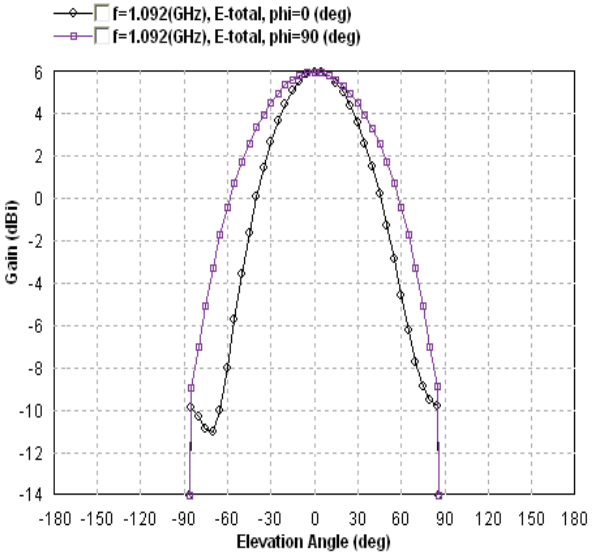

Figure 3

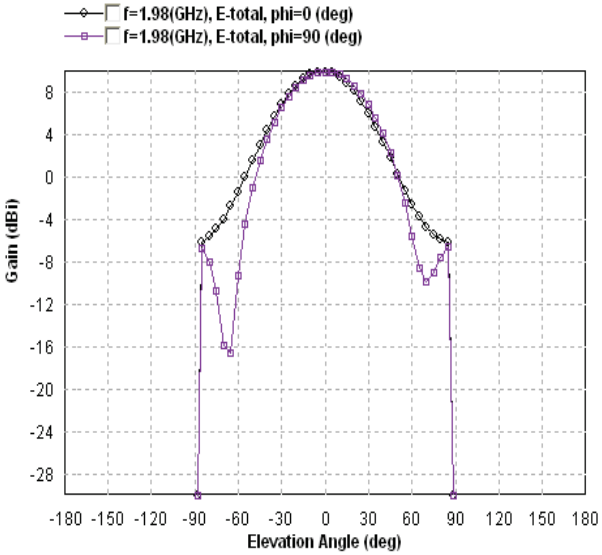

Figure 4

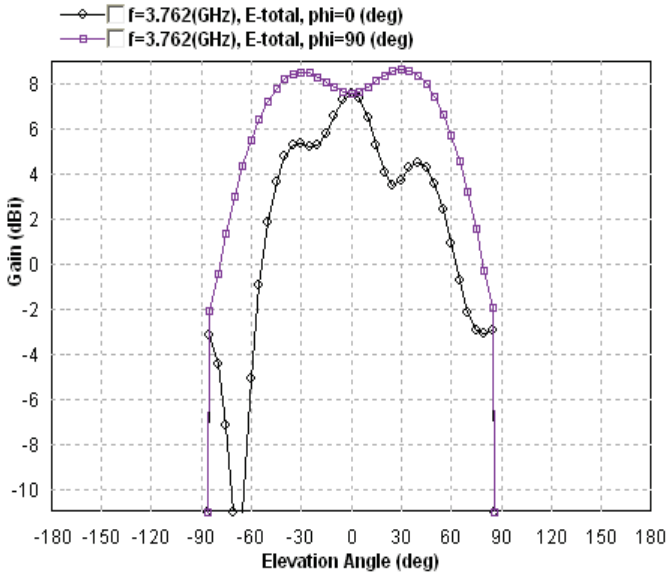

Figure 7

Figures 3, 4 and 6 s how the regular radiation pattern. Figure 7 i s almost close to the regular shape. However for figure 5, there is a broadside null.

SEARCH

Previous Page

Next Page

## CONCLUSION:

A new rectangular microstrip antenna is proposed with air as its substrate so that the manufacturing cost is substantially reduced. The antenna used two rectangular slots cut perpendicularly across each other in form of Christ-cross.

## REFERENCE:


1. K.L. Wong, S. T. Fang, and J.H. Lu, "Dual-frequency equilateral triangular microstrip antenna with a slit ", Microwave and Optical Technology letter, Vol 19, No.5, 348-350, 1998.
2. K.L. Wong and K.P. Yang, "Small dual-frequency microstrip antenna with cross- slot", Electronics letters, Vol .33, No. 23, pp. 1916-1917, 1997.
3. A. A. Abdelaziz, "A compact planar quad-frequency broad –band rectangular microstrip patch antenna", Microwave and Optical Technology letters, Vol .50, No.1 pp 22-24, 2008.

# T-SHAPED MONOPOLE LOADED WITH DIELECTRIC RESONATOR ANTENNA FOR WIDEBAND COMMUNICATION

Saswati Ghosh[1] and Ajay Chakrabarty[2]
(1) Kalpana Chawla Space Technology Cell, IIT, Kharagpur-721302, W. B., India.
E.mail: saswati@ece.iitkgp.ernet.in
(2) Department of E & ECE, IIT, Kharagpur-721302, W. B., India,
E.mail: bassein@ece.iitkgp.ernet.in

## ABSTRACT:

The performance of a T -shaped monopole loaded with dielectric resonator antenna (DRA) is studied for wideband communications. The length of the monopole and load arm is adjusted for a certain DRA dimension to achieve a 10 dB bandwidth of 110%. The return loss characteristics and radiation pattern of the antenna is presented. The results are achieved using Method of Moment-based software WIPL-D. The simulated results are compared with the measured result for a prototype antenna.

## INTRODUCTION:

The monopole loaded with dielectric resonator antenna (DRA) has found wide application as broadband antenna [1 - 2]. The guideline for the design of this antenna was presented in recent literature [2]. Also the simple loaded wire antennas (e.g., inverted L, T, I and C antennas) are used for wideband communication [3]. In the present work, a hybrid antenna using T-shaped monopole loaded with DRA is presented. The design guidelines for the DRA are followed from the literature [2]. The electromagnetic software WIPL-D Pro v5.1 is used for the simulation of return loss and radiation pattern [4]. The simulated results for return loss are verified with the measured results from a prototype antenna.

## ANTENNA GEOMETRY:

The antenna configuration is shown in Fig. 1. It consists of a thin T-shaped monopole and an annular DRA, both sharing the same axial reference and mounted on a ground plane. The T-shaped monopole is designed to have a resonance at the lower end of the frequency band, while the DRA is designed to have a resonance near the upper end of the desired spectrum range. The combined effect of the T antenna and DRA produces the intermediate resonance and maintains the 10 dB return loss over a wide frequency range.

## RESULTS:

For the simulation, the antenna is considered to be connected with a delta-gap source of 1Volt. The result for the return loss versus frequency of the T-shaped monopole / DRA is compared to a simple monopole in Fig. 2. The dimensions of the antennas studied in this section are presented in Table 1. The variation in return loss with the change in the main-arm length of the T-antenna is presented in Fig. 3.

The prototype antenna is fabricated for experimental verification [5]. The dimens SEARCH of the prototype antenna are presented in Table 1. The design parameters of the prototype are as follows: L = 12 mm; 2L1 = 6 mm; s = 0.84 mm; a = 5 mm; b = 1.49 mm; r = 0.65 mm; h = 6 mm ; $\varepsilon_r$ = 10. A circular finite ground plane of radius 50 mm is used for the measurement Previous Page n between the simulated and measured return loss using HP 8757 C network Next Page

analyzer is presented in Fig. 4. The radiation patterns in the vertical plane of the antenna are presented in Fig. 5.

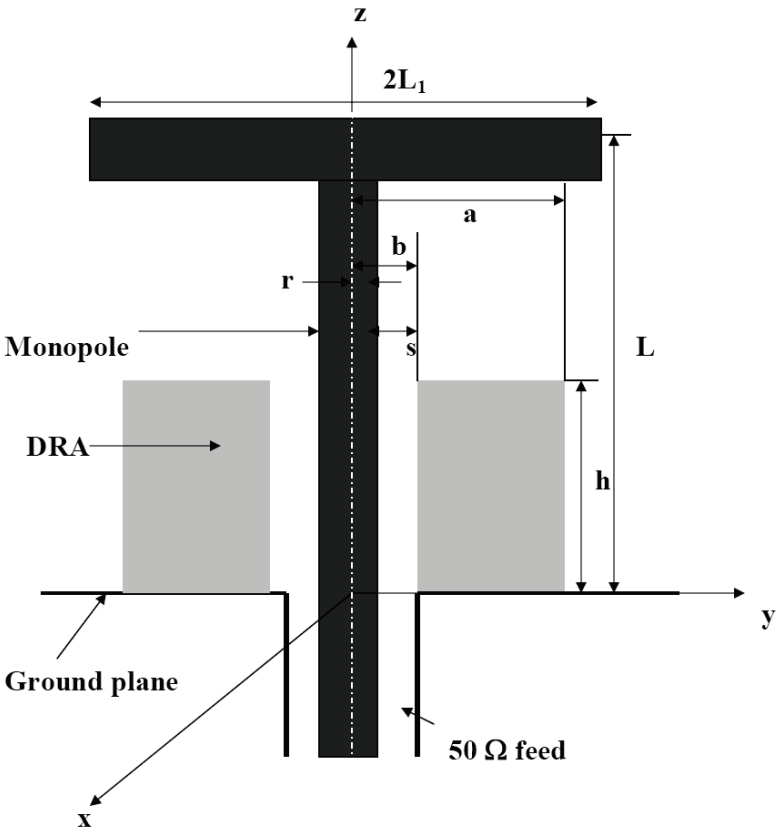


*Fig. 1 Cross section of a DRA loaded T-shaped monopole.*

*Table I Antenna Parameters of Different Antennas*

| *Shown in* | *Name* | *Antenna Parameters (all dimensions in mm) (Refer Fig. 1)* | | | | | | | |
|---|---|---|---|---|---|---|---|---|---|
| | | *L* | *2L1* | *s* | *a* | *b* | *r* | *h* | *e* |
| *Fig. 2* | *T-monopole* | *12* | *6* | *-* | *-* | *-* | *0.65* | *-* | *-* |
| | *T-monopole / DRA* | *12* | *6* | *0.84* | *5.0* | *1.49* | *0.65* | *6* | *10* |
| | *Monopole* | *15* | *0* | *-* | *-* | *-* | *0.65* | *-* | *-* |
| *Fig. 3* | *Design#1* | *11* | *8* | *0.84* | *5.0* | *1.49* | *0.65* | *6* | *10* |
| | *Design#2* | *12* | *6* | *0.84* | *5.0* | *1.49* | *0.65* | *6* | *10* |
| | *Design#3* | *13* | *4* | *0.84* | *5.0* | *1.49* | *0.65* | *6* | *10* |
| | *Design#4* | *14* | *2* | *0.84* | *5.0* | *1.49* | *0.65* | *6* | *10* |
| *Fig. 4* | *Prototype* | *12* | *6* | *0.84* | *5.0* | *1.49* | *0.65* | *6* | *10* |
| *Fig. 5* | *T-monopole / DRA* | *12* | *6* | *0.84* | *5.0* | *1.49* | *0.65* | *6* | *10* |

*DISCUSSIONS:*

The D RA-loaded T -shaped m onopole ant enna s hows a wider bandw idth ( 10 dB bandwidth of 110%) compared to a monopole or T-shaped monopole and al so to a DRA-loaded monopole (Fig. 2). Fig. 3 shows that by suitably adjusting the load-arm and main-arm sired bandwidth can be achieved. A good agreement between the measured

simulated result is obtained (Fig. 4). Also Fig. 5 shows a monopole-like radiation pattern over the impedance bandwidth.

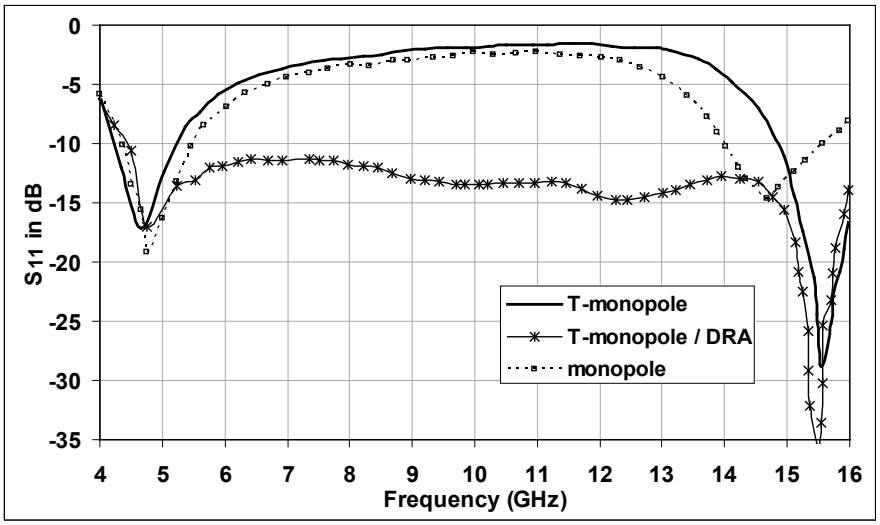


**Fig. 2. Return loss versus frequency plot of T-shaped monopole / DRA.**

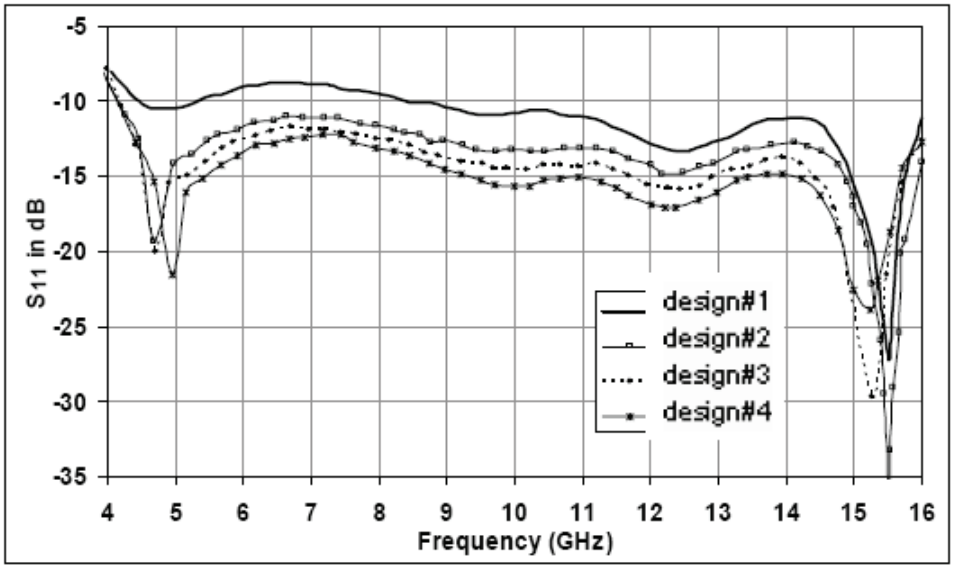


SEARCH

Previous Page

Next Page

*Fig. 3 Return loss versus frequency of T-shaped monopole / DRA with varying main arm and load arm length.*

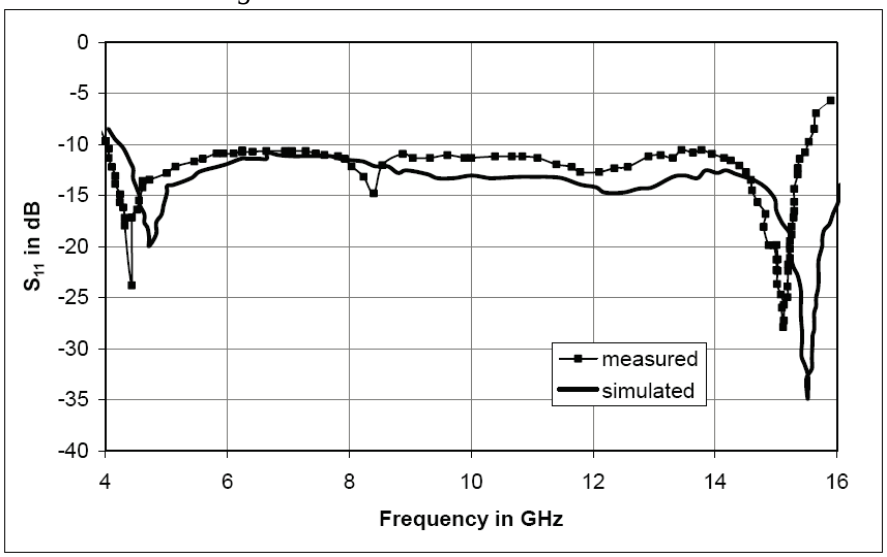


*Fig. 4. Return loss versus frequency of prototype antenna with dimensions given in Table 1.*

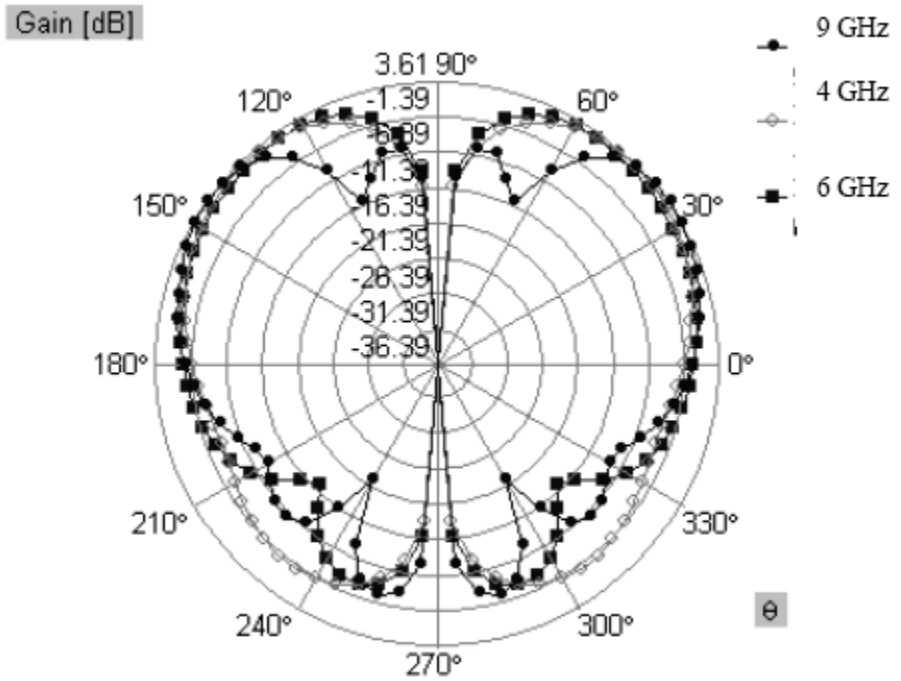


*Fig. 5 Radiation pattern in the vertical plane at different frequencies.*

*CONCLUSION:*

The wideband performance of a hybrid antenna consisting of a thin T-monopole and an annular DRA is studied. This antenna may be used for wideband trans-receive system.

SEARCH

Previous Page

Next Page

**ACKNOWLEDGEMENT:**

The authors would like to acknowledge the financial support given by Department of Science and Technology, New Delhi, India.

**REFERENCE:**

1. Marc L apierre, Y ahia M .M. A ntar, A . I ttipiboon, A . Pet osa, "U ltra W ideband Monopole/Dielectric R esonator A ntenna," I EEE M icrowave and W ireless C omponents Letters, Vol. 15, No. 1, January 2005.
2. Debatosh G uha, Y ahia M .M. A ntar, A . I ttipiboon, A . Pet osa, D avid L ee, "Improved Design G uidelines f or t he U ltra W ideband M onopole-Dielectric R esonator A ntenna," IEEE Antennas and Wireless Propagation Letters, Vol. 5, pp. 373-376, 2006.
3. T. L. Simpson, "The theory of top-loaded antennas: Integral equations for the currents," IEEE Trans. Antennas and Propagation, vol. AP-19, 186–190, March 1971.
4. B. M . K olundzija, J . S. O gnjanovic, T .K. Sar kar, W IPL-D s oftware: E lectromagnetic Modeling of Composite Metallic and Dielectric Structures –Software and User's Manual, Artech House, pp.1-332.
5. Saswati Ghosh, Ajay Chakrabarty, "Ultra Wideband Performance of Dielectric Loaded T-shaped Monopole Transmit and Receive Antenna / EMI Sensor", accepted for IEEE Antennas and Wireless Propagation Letters, 2008.

SEARCH

Previous Page Next Page

# ANALYTICAL AND NUMERICAL EVALUATION OF CHARACTERISTIC IMPEDENCE OF NON- COPLANAR FIN ANTENNA

*Bavishna Balagopal*(1) and Raji S Nair(1)*
*(1) Dept. of Electronics, Cochin University of Science and Technology, India – 682022*
Email*: bavishna.balagopal@gmail.com

**ABSTRACT:**

A theoretical method of finding the characteristic impedance of a non-coplanar fin antenna is presented. In this problem, the spherical geometry can be mapped on a plane, thus reducing the problem to finding the solution of Laplace's equation by using Conformal mapping techniques. Verification of the method is provided by comparing it with an alternative numerical technique namely Boundary Element Method.

An Infinitely long non-coplanar fin antenna belongs to the class of structures which support spherical TEM waves. The problem of determining the electric and magnetic fields due to a given antenna configuration is essentially one of solving Maxwell's equations subject to the appropriate boundary conditions for the surface. A conical structure is one for which the surface can be specified solely in terms of the spherical angles $q$ and $f$, in which case the excited wave in the structure is a TEM spherical wave. This means that by a suitable choice of variables, Maxwell's equations may be reduced to the Laplace equation in two dimensions given by

$$\left[\sin q \frac{d}{dq}\left(\sin q \frac{d}{dq}\right)+\frac{\partial^2}{\partial f^2}\right]\tilde{O}(q,f)=0 \quad \text{-------- (1)}$$

where $\tilde{O}$ is the hertz potential. Thus the non–zero component of the electric and magnetic fields corresponding to the TEM mode excited in the structure are given by

$$Eq=\frac{1}{r}\frac{\partial^2\tilde{O}_{er}}{\partial r\partial q} \quad ; \quad Hq=\frac{jwe}{r\sin q}\frac{d\tilde{O}_{er}}{df}$$

$$Ef=\frac{1}{r\sin q}\frac{\partial^2\tilde{O}_{er}}{\partial r\partial f} \quad ; \quad Hf=\frac{-jwe}{r}\frac{d\tilde{O}_{er}}{dq}$$

SEARCH

Previous Page Next Page

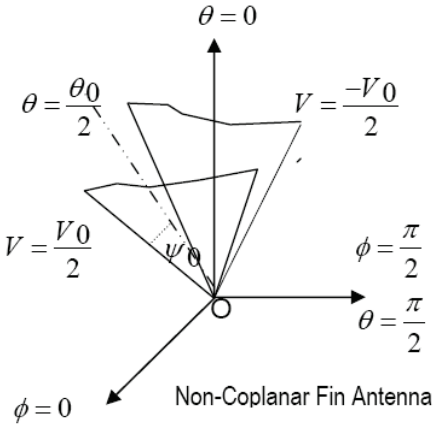


**Figure 1:**

In this way, the original 3-D problem of determining the electric or magnetic field due to a given conical antenna structure can be reduced to one of solving Laplace's equation for the scalar function $\tilde{O}(q, f)$ in two dimensions, subjected to the appropriate boundary conditions prescribed by the structure, which is given by

$$\tilde{O}(q,f) = \frac{jV_0}{2k}$$ For any point P $e$ S1

$$= \frac{-jV_0}{2k}$$ For any point P $e$ S2.

Thus conformal mapping technique may be applied to determine the solution of (1) in the case of a non-coplanar fin antenna.

Thus by mapping the antenna onto a suitable 2-D structure, the impedance can be obtained by considering the capacitance of the associated static field distribution. The required mapping relation is $r = \tan\frac{q}{2}; f = f_c$, this transform maps the surface of any sphere r = constant into the $(r, f_c)$ plane. For a non-coplanar fin antenna this transforms the plane into a set of equations of a family of circles centered on the U-axis through points $v \pm 1$ and family of circles centered on the v-axis as shown in figure 2: (a)

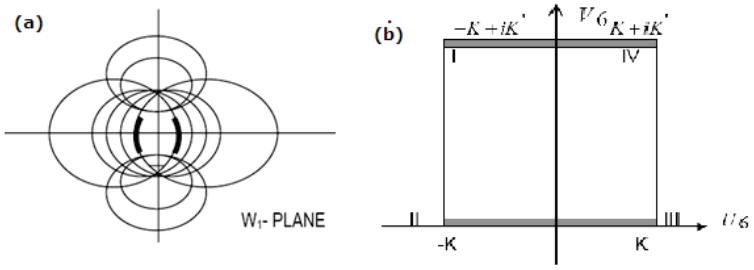


**Figure 2: (a) (b)**

SEARCH
Previous Page
Next Page

Subjecting this obtained result to a series of transformations consisting of bilinear transformation, logarithmic mapping, Schwarz - Christoffel transformation along with elliptic integrals of the first and third kind, we get our desired mapping as shown in figure 2: (b).

Thus the original, non-coplanar fin structure has been mapped onto a pair of parallel plates as shown above. It follows that the electric field is uniform within the rectangle with the potential being given by

$$\tilde{O}(q,f) = \frac{-jV_0}{2k}\left[1 - \frac{v6}{K'}\right],$$

The Characteristic Impedance of the configuration can be directly obtained from the final transformation as $Z_0 = h\frac{d}{b}$, where 'd' is the distance between the plates and 'b' is the width of the plates. Now the same can be verified using the numeric technique namely Boundary element method (BEM).

The finite element method (FEM) and Method of moments (MOM) have become the two most popular methods of numerical analysis of electromagnetic problems. The choice between the two numerical techniques depends on the particular problem. A hybrid method called BEM, have been proposed that allows the use of both MOM and FEM, with the aim of exploiting the strong points in each method. It basically involves obtaining the boundary-integral equation from the Green's identity and solving this by a discretization procedure similar to that used in regular FEM analysis. Since the BEM is based on the boundary integral equivalent to the governing differential equation, only the surface of the problem domain needs to be modeled. Thus the dimension of the problem is reduced by one as in MOM.

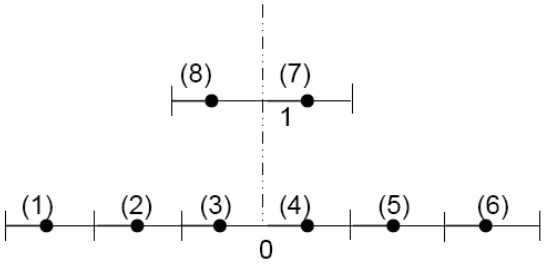


**Figure 3:**

The fundamental solution for potential is $u^*(x,X)$ and the fundamental solution for flux is given by $q^*(x,X)$. Hence the Green's function is given by,

$$u^*(x,X) = \frac{-1}{2p}\ln|x_i - X_i| = \frac{-1}{2p}\ln(r)$$

$$q^*(x,X) = \frac{-1}{2p}\cdot\frac{(x_i - X_i)}{|x_i - X_i|^2}\cdot n_i = \frac{-1}{2pr}\cdot r_i n_i$$

We obtain the boundary integral equation as,

$$c(x)u(x) + \int_G q^*(x,X)u(x)\,dG = \int_G u^*(x,X)q(x)\,dG$$

, where $c(x) = \left(1 - \frac{a}{2p}\right)$ *for* x Î G

= 1 *for* x Î W

$= \quad 0 \qquad for\ x \in G, x \in W$

An analytical solution of the integral in equation (12.9) is only possible for very simple cases. Here, instead the boundary is divided into segments –the so called boundary elements – and the boundary variables are interpolated by piecewise continuous functions, e.g., polynomials, so that an approximate calculation of the boundary integrals becomes possible. This approach is called Discretization. The discretized form of boundary equation is then given by

$$c(x)u(x)+\sum_{e=1}^{E}\sum_{m=1}^{M}\left(-u_m^{(e)}\int_{G^{(e)}} f_m q^* dG\right)=\sum_{e=1}^{E}\sum_{m=1}^{M}\left(-q_m^{(e)}\int_{G^{(e)}} f_m u^* dG\right)$$

This can equivalently be represented as,

$$\begin{bmatrix} \hat{H}_{11} & H_{12}..... & H_{1N} \\ H_{21} & \hat{H}_{22}..... & H_{2N} \\ M & M & M \\ H_{N1} & H_{N2}..... & \hat{H}_{NN} \end{bmatrix} \begin{bmatrix} U_1 \\ U_2 \\ M \\ U_N \end{bmatrix} = \begin{bmatrix} G_{11} & G_{12}..... & G_{1N} \\ G_{21} & G_{22}..... & G_{2N} \\ M & M & M \\ G_{N1} & G_{N2}..... & G_{NN} \end{bmatrix} \begin{bmatrix} q_1 \\ q_2 \\ M \\ q_N \end{bmatrix}$$

For the case of two unequal parallel slots of finite length arranged as shown

Assembling the known and unknowns we end up with the usual form of the matrix equation, AX=B, in terms of the H and G matrix. The matrix X gives the charge distribution of the system, which ultimately gives the capacitance of the system. This is substituted in the basic equation of the characteristic impedance. This result can be compared with the analytical value of characteristic impedance. The characteristic impedance of the system is plotted in figure 4.

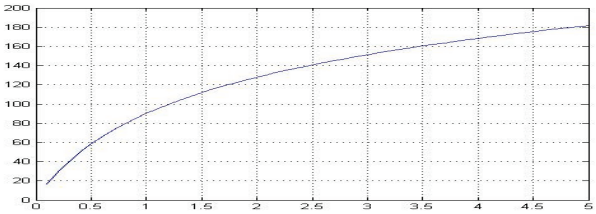


**Figure 4:**

**ACKNOWLEDGMENT**

The authors acknowledge the support of Mr. Subhankar Ghose, Scientist-c, EMI/EMC division, LRDE, DRDO, Banglore, especially for the discussions and intellectual input into this work.

**REFERENCES**

1. A. P. Lambert, "Calculation of the characteristic impedance of tem horn antennas using the conformal mapping approach", IEEE transactions on Antennas and Propagation vol. 43, no. 1,January 1995.
2. R. L. Carrel, "The characteristic impedance of two infinite cones of arbitrary cross section," ire transactions on Antennas and Propagation, vol. Ap-6, pp. 197-201, 1958.
3. H. M. Shen, r. W. P. King, and t. T. Wu, "v-conical antenna," IEEE transactions on s and Propagation, vol.ap-36,pp. 1519-1525, 1988

SEARCH
Previous Page
Next Page

# WIDEBAND APERTURE COUPLED RECTANGULAR MICROSTRIP ARRAY ANTENNA FOR RADAR APPLICATIONS

*R B Konda, S K Satnoor , M Veereshappa, S N Mulgi and P V Hunagund*
Department of PG Studies and Research in Applied Electronics,
Gulbarga University, Gulbarga - 585 106, Karnataka, India.
E.mail: rajendrakonda@rediffmail.com

**ABSTRACT:**

An eight-element slot rectangular microstrip array antenna (ESRMA) using corporate feed arrangement is proposed for triple band operation for radar applications where antenna is required to operate at two or more discrete band of frequencies. If ESRMA is fed through aperture, the coupling enhances the impedance bandwidth at each operating bands. The overall impedance bandwidth is found to be 29.61%, with improved radiation characteristics. The design concept of antennas is presented and experimental results are discussed.

## INTRODUCTION:

Dual or triple band frequency operations have gained wide attention in radar communication particularly in synthetic aperture radar ( SAR). The application of modern radars working in C-band and X-band needs not only to achieve large-scale scanning and early warning but also track targets exactly as soon as finding them. At the same time, broader bandwidth is needed for anti-jamming. To fulfill these requirements, the antennas of modern radars should possess both broader bandwidth and beams[1]. These can be met by aperture-coupled microstrip patch array antenna based on low-permittivity, low-weight and low-cost substrates. In this study a triple band operation of ESRMA is achieved in X-band (8.2 to 12.4 GHz) by using a simple eight-element slot array configuration. Further the bandwidth at each operating band is enhanced, by energizing the elements of ESRMA through aperture coupling.

## DESCRIPTION OF ANTENNA GEOMETRY:

The antennas are sketched by using computer software Auto-CAD 2002 and are fabricated on commonly available glass epoxy substrate material of thickness $h$ =1.66mm and permittivity $\epsilon_r$ = 4.2. The elements of ESRMA are fed by using corporate feed technique. This technique has been selected because of its simplicity and it can be simultaneously fabricated along with the antenna element. At the center of radiating elements in ESRMA an optimum slot is embedded which is parallel to the width of radiating element for enhancing the impedance bandwidth. The length $L_s$ and width $W_s$ of slot is taken, as $\lambda_o/4$ and $\lambda_o/16$ respectively, were $\lambda_o$ is the free space wavelength in cm. This slot is considered as a wide slot, as its width is comparable to its length. The wide slot is selected because it is more effective in enhancing impedance bandwidth when compare to a narrow slot[2]. Among the various broad banding techniques the aperture coupled technique receives much attention; mainly due to the additional advantage that, separate substrate can be used for the feed circuit which helps in designing desired feed network for energizing the antenna element through coupling slots placed on the ground plane[3]. The slots, which are used in the radiating

Previous Page Next Page

elements of ESRMA, are used on the ground plane in the form of coupling slots to energizing the elements of aperture coupled eight element rectangular microstrip antenna (AERMA).

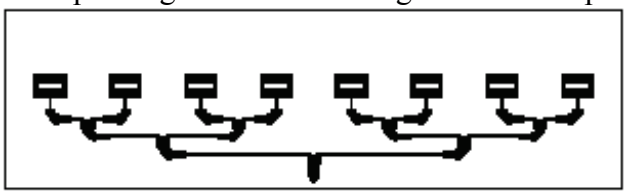

Fig. 1 Geometry of ESRMA

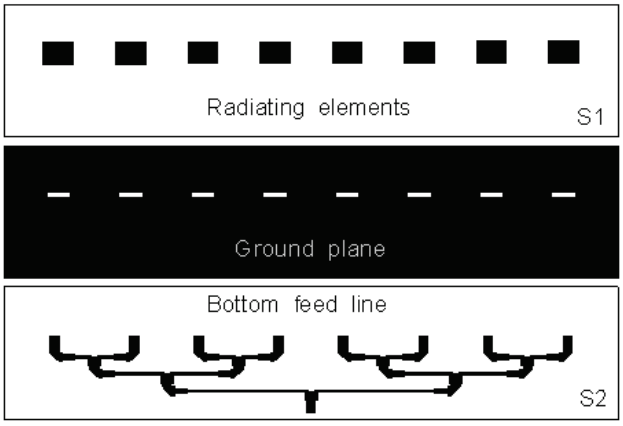


Fig. 2 Geometry of AERMA

Figure 1 shows the geometry of ESRMA. The radiating elements are placed at a distance of $3\lambda_o/4$ in order to add the radiated power in free space by individual elements. However, the distance between two elements is taken in terms of multiple of half wavelength. But in this case $3\lambda_o/4$ has been selected in order to accommodate corporate feed arrangements between the radiating elements. The corporate feed arrangement consists of matching transformer, quarter wave transformer, microstrip bend and power divider and is used for better impedance matching between feed and radiating element which reduces the loss in the feed line. At the tip of microstrip line feed a 50 Ωcoaxial SMA co-axial connector is used for feeding the microwave power.

The geometry of AERMA is as shown in Fig. 2. The radiating elements are etched on the top surface of substrate $S_1$. The corporate feed arrangement is etched below the substrate $S_2$ having the same dielectric constant ($\varepsilon_r$) and thickness ($h$) as that of $S_1$. The coupling slots are placed on the top of the substrate $S_2$ exactly at the tip of 50 Ω microstrip feed line of corporate feed arrangement. The substrate $S_2$ is placed below the substrate $S_1$. The radiating elements on the topside of substrate $S_1$ energizes through coupling slots placed on the topside of substrate $S_2$ that is the ground plane. This arrangement forms aperture coupling.

## EXPERIMENTAL RESULTS:

The impedance bandwidth over return loss less than –10dB for the proposed anten is measured for X-band frequencies. The measurement is taken on Vector Network Analyzer (Rohde & Schwarz, Germany make ZVK model). The variation of return loss versus frequency of ESRMA is shown in Fig. 3. The antenna resonates for triple bands $BW_1$, $BW_2$ and $BW_3$. The $BW_2$ is due to the fundamental resonance of the driven elements. The additional

resonance $BW_1$ and $BW_3$ are due to the effect of slot inserted in the driven elements which acts as secondary resonance[4,5]. The overall impedance bandwidth ($BW_1$+$BW_2$+$BW_3$) is found to be 6.53 % i.e. 590 MHz.

The variation of return loss versus frequency of AERMA is also shown in Fig. 3. It is seen from this figure that, the antenna again resonates for triple band of frequencies $BW_4$, $BW_5$ and $BW_6$. The magnitude of $BW_4$ is 1.25, $BW_5$ is 1.99 and $BW_6$ is 16.27 times more when compared to $BW_1$, $BW_2$, and $BW_3$ respectively. This enhancement in impedance bandwidth is due to the combined resonance effect of radiating element and the coupling slots that couples energy from the feed line to the radiating elements. The coupling slot can be either resonant or non-resonant. If it is resonant, the current along the edges of the slot introduces an additional resonance, which adds to the fundamental resonance of radiating element, causes enhancement in the impedance bandwidth[4,5]. The overall impedance bandwidth ($BW_4$+ $BW_5$ + $BW_6$) is found to be 29.61% i.e. 3030 MHz, which is 4.53 times more when compared to the impedance bandwidth of ESRMA.

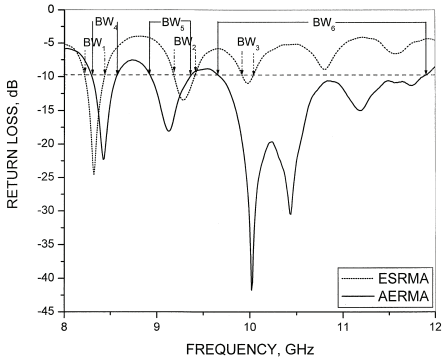


Fig. 3 Variation of return loss versus frequency

In order to calculate the gain, the power received $P_s$ by the pyramidal horn antenna and the power received $P_t$ by ESRMA and AERMA is measured independently. With the help of these experimental data the gain of antenna under test $G_T$ in dB is calculated using the formula, $(G_T)_{dB} = (G_s)_{dB} + 10 \log (P_t/P_s)$where, $G_s$ is the gain of pyramidal horn antenna. From this, the gain of ESRMA and AERMA is found to be – 0.27 dB and –1.34 dB respectively. Since the impedance bandwidth of AERMA increases the gain decreases. The decrease of gain is mainly because the radiating patches in the aperture-coupled feeding are not directly connected to the feed network.

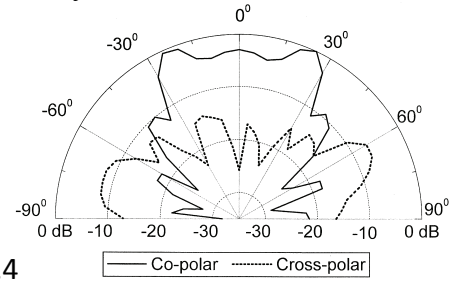


Fig.4

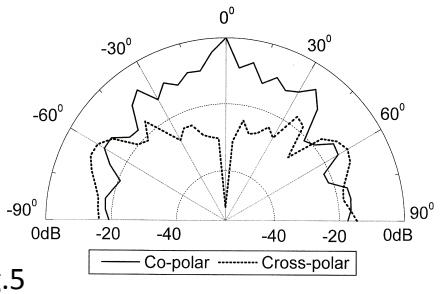


Fig.5

Fig. 4 Variation of relative power versus azimuth angle ESRMA

Fig. 5 Variation of relative power versus azimuth angle AERMA

SEARCH

The co-polar and cross-polar radiation patterns of ESRMA measured at 8.32 GHz and AERMA measured at 10.3GHz are shown respectively in Figs 4 and 5. From these figur

Previous Page Next Page

is seen that patterns are broad sided with cross-polar level better than –10 dB indicating linear polarization of radiation. It is seen from Fig. 5 that, the power level for the cross-polar of AERMA is quite low when compared to the cross-polar power level of ESRMA as seen in Fig. 4. This improvement in radiation pattern is due to aperture coupling.

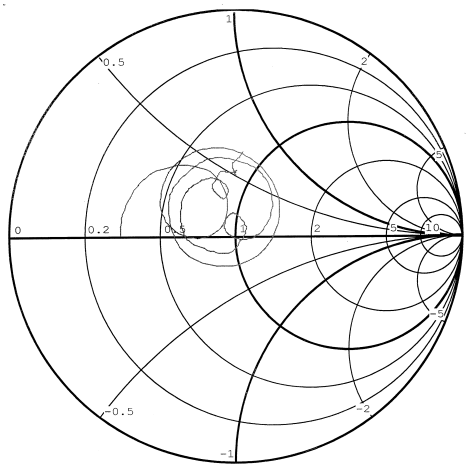


Fig. 6 Input impedance of AFRMA

Since, AERMA gives wider impedance bandwidth when compared to ESRMA, for the validation its input impedance is measured on Vector Network Analyzer, as shown in Fig. 6. From this figure it is seen that the impedance loci has three central loops that accounts for its wideband operation.

**CONCLUSION:**

From the detailed experimental study it is concluded that the triple band operation of ESRMA can be enhanced considerably through aperture coupling. This overall impedance bandwidth is 4.53 times more than that of ESRMA. These proposed antennas are simple in design and fabrication and uses low cost substrate material. These antennas may find extensive use in radar communication particularly in SAR.

**ACKNOWLEDGEMENT:**

The authors would like to thank Dept. of Science & Technology (DST), Govt. of India, New Delhi, for sanctioning Network Analyzer to this Department under FIST project.

**REFERENCES:**

1. Zhu Qi and Bao Liang, "Design of microstrip antenna with broader bandwidth and beam", Antenna and Propag Society Intr Symp., 3A, pp. 617-620, July 2005.
2. Bahl I J and Bhartia P, Microstrip Slot Antenna, Microstrip Antennas, Dedham, MA: Artech House, New Delhi, 1981.
3. David M Pozar, "Analysis of an infinite phased array of aperture coupled microstrip patches", IEEE Trans Antennas and Propag, Vol. 37, No. 4, pp. 418- 425, April 1989.
4. Gh Z Rafian d Shaf ai L , " Wideband V -slotted di amond-shaped microstrip pat ch antenna", Electron Lett., Vol. 40, No. 19, Sept. 2004.
5. Jeen-Sheen Row, "Dual-frequency triangular planar inverted-F antenna", IEEE Trans Antennas & Propag, Vol. 53, No. 2, pp. 874-876, Feb.2005.



Previous Page Next Page

# DUAL FREQUENCY MICROSTRIP ARRAY ANTENNA FOR SAR

*S L Mallikarjun, R B Konda, R G Madhuri and P M Hadalgi*
Dept. of PG Studies and Research in Applied Electronics,
Gulbarga University, Gulbarga – 585 106, Karnataka.
mslakshetty@rediffmail.com

**ABSTRACT:**

A new type of dual-frequency rectangular microstrip array antenna is presented, which is designed by using a simple corporate feed arrangement. Comparing with the conventional rectangular patch antenna, the bandwidths for dual-frequency both are extended to 6.3 and 1.6 times and the gain is increased to 7.40 dB with an -3dB beam width of $31^0$. The experimental measurements are taken and are presented.

## INTRODUCTION:

Patch antennas are popular for their well-known attractive features, such as low profile, light weight, and compatibility with monolithic microwave integrated circuits. Their main disadvantage is an intrinsic limitation in bandwidth, which is due to the resonant nature of the patch structure.

Patch antennas are well suitable for systems to be mounted on airborne platforms, like Synthetic-aperture radar (SAR). From these applications, a new motivation is given for research on innovative solutions that overcome the bandwidth limitations of patch antennas. In applications in which increased bandwidth is needed for operating at two separate sub-bands, a valid alternative to the broadening of total bandwidth is represented by dual-frequency patch antennas. Indeed, the optimal antenna for a specific application is one that ensures the matching of the bandwidth of the transmitted and/or the received signal.

When the system requires operation at two frequencies too far apart, dual-frequency patch antennas may avoid the use of two different antennas; a typical case is that of SAR. As is well-known, the present SAR antenna employs different arrays for each band. The trend of SAR antennas of the future generation is to cover at least two of the three bands with a dual frequency antenna. This would reduce weight and surface, thus improving the possibilities of accommodation under the launcher fairing.

In principal, dual-frequency planar antennas should operate with similar features, both in terms of radiation and impedance matching, at two separate frequencies. Obtaining these features by using planer technologies is not a straightforward matter, particularly when the intrinsic structural and technological simplicity of patch antennas is to be presented[1,2].

In this paper, a new type of dual-frequency microstrip array antenna is proposed. The dual-frequency behavior is obtained by means of two radiating elements, each of them supporting strong currents and radiation at the resonance.

## ANTENNA CONFIGURATION:

The proposed antennas are designed using low cost glass epoxy substrate material having dielectric constant $\epsilon_r = 4.2$ and thickness $h = 0.16$ cm. The artwork of these antennas is developed using computer software AutoCAD. The antennas are fabricated using photolithographic process.



Previous Page Next Page

Figure 1 shows the geometry of conventional rectangular microstrip antenna (RMSA) designed for the resonant frequency of 9.4 GHz with dimensions ($L$, $W$) = (0.66, 0.98) cm. The antenna is fed by microstrip line feeding. This feeding has been selected because of its simplicity and it can be simultaneously fabricated along with the antenna element. Further this planer feed makes the structure suitable for integration with associated microwave circuitry. A quarter wave transformer of dimensions ($L_t$, $W_t$) = (0.42, 0.05) cm is used for better impedance matching between microstrip feed line of dimensions ($L_f$, $W_f$) = (0.41, 0.32) cm and radiating element. At the tip of microstrip line feed a 50W coaxial SMA connector is used for feeding the microwave power.

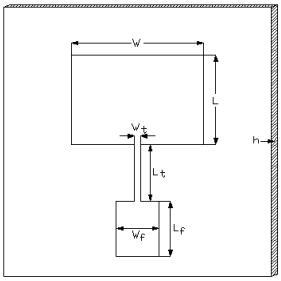


Fig. 1 Geometry of RMSA.

Figure 2 shows the geometry of two-element rectangular microstrip array antenna (2RMSAA). The elements of this array antenna are exited through corporate feed arrangement. This feed arrangement consists of two-way power divider made up of 70W matching transformer of dimension ($L_{70}$, $W_{70}$) = (0.41, 0.16) cm, used between 100 W microstrip line of dimension ($L_{100}$, $W_{100}$) = (0.83, 0.07) cm and 50W microstrip line of dimension $L_f$ and $W_f$. The array elements are kept at a distance of $D = 5\lambda_0/6$ (i.e. 2.66 cm) from their center point. This optimized distance is selected in order to achieve minimum side lobes in the radiation pattern[3].

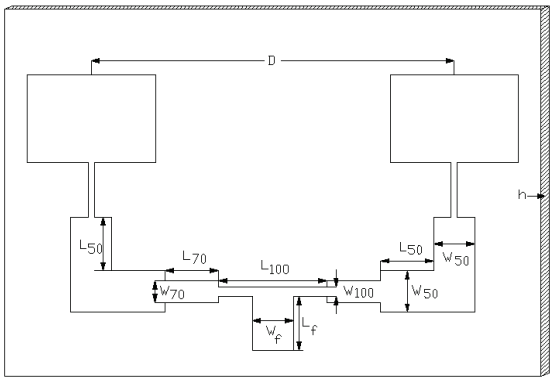


Fig. 2 Geometry of 2RMSAA.

SEARCH
Previous Page
Next Page

## EXPERIMENTAL RESULTS:

The impedance bandwidths over return loss less than –10dB for the proposed antennas are measured. The measurements are taken on Vector Network Analyzer (Rohde & Schwarz, German make ZVK Model). The variation of return loss versus frequency of RMSA, and 2RMSAA is shown in Fig. 3 for the sake of comparison. From this graphs the impedance bandwidth is calculated by using the equation

$$BW = \left[\frac{f_H - f_L}{f_C}\right] 100\%$$

where, $f_H$ and $f_L$ are the higher and lower cut-off frequencies of the band respectively, when its return loss becomes -10 dB and $f_c$ is the center frequency of band.

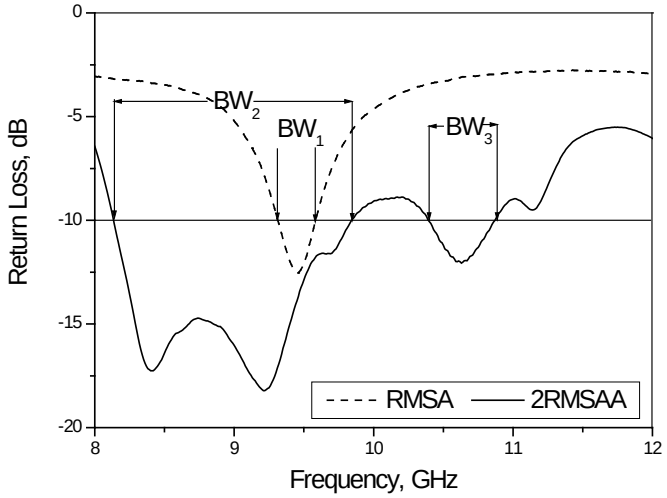


Fig. 3 Variation of return loss versus frequency.

From Fig. 3. It is clear that the experimental impedance bandwidth ($BW_1$) of RMSA is found to be 290 MHz i.e. 3.07 %. The overall impedance bandwidth of 2RMSAA which is resonating for two bands ($BW_2$ + $BW_3$) is found to be 17920 MHz i.e. 24.23 %, which is 7.9 times more when compared to conventional RMSA in terms of percentage.

Further from Fig. 3 it is also clear that impedance bandwidth ($BW_2$) of 2RMSAA is found to be 17400 MHz i.e. 19.33 % and the impedance bandwidth ($BW_3$) of 2RMSAA is found to be 520 MHz i.e. 4.9 % which are respectively 6.3 and 1.6 times more when compared to conventional RMSA. The dual-band is due to the array configuration of two elements, which resonates at its own frequencies[4].

SEARCH

Previous Page

Next Page

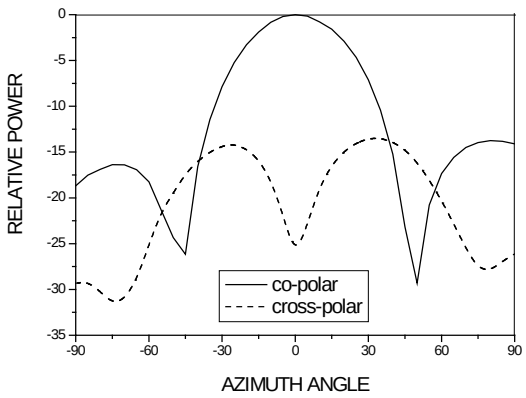


Fig. 4 Variation of relative power versus azimuth angle of 2RMSAA at 9.21 GHz.

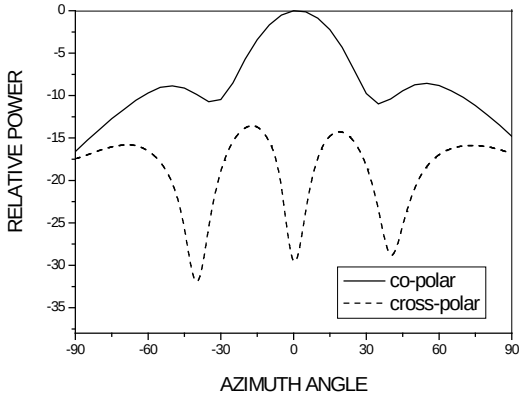


Fig. 5 Variation of relative power versus azimuth angle of 2RMSAA at 10.63 GHz.

Fig. 4 and Fig. 5 shows the co-polar and cross-polar radiation patterns of the proposed antenna, measured at the operating frequencies. From the figures it is clear that the antenna is showing broad side radiation characteristics with cross-polar level less than -15 dB at both the operating frequencies. The HPBW of the proposed antenna is calculated and is found to be $31^0$ which is much lesser when compared to the conventional RMSA ($70^0$).

In order to calculate the gain, the power received ($P_s$) by the pyramidal horn antenna and the power received ($P_t$) by RMSA and 2RMSAA are measured independently. With the help of experimental data, the gain of antenna under test ($G_T$) in dB is calculated using the formula,

$$(G_T)_{dB} = (G_s)_{dB} + 10 \log (P_t/P_s)$$

where, $G_s$ is the gain of pyramidal horn antenna. It is seen that the gains of RMSA and 2RMSAA are 4.78 dB and 7.40 dB respectively, which shows that the gain of 2RMSAA is 1.55 times more. This indicates that the gain of proposed antennas is quit high when compared to the gain of conventional RMSA. This shows the use of array configuration also improves the antenna gain considerably[5]. The input impedance profile of 2RMSAA is as shown in Fig.6.

## CONCLUSION:

From the detailed study it is clear that, the proposed antenna is quite, simple in design and fabrication and quite good in enhancing the impedance bandwidth and gain at X-band when compared to RMSA without changing the nature of radiation pattern. This antenna is also superior as it uses low cost substrate material. This antenna is more suitable where limited antenna real estate is available in phased array, in modern communication and may find applications in SAR.

## ACKNOWLEDGEMENT:

We thank to the authorities of Department of Science and Technology (DST), Govt of India, New Delhi, for sanctioning the FIST Project to the Department of Applied Electronics, Gulbarga University, Gulbarga.

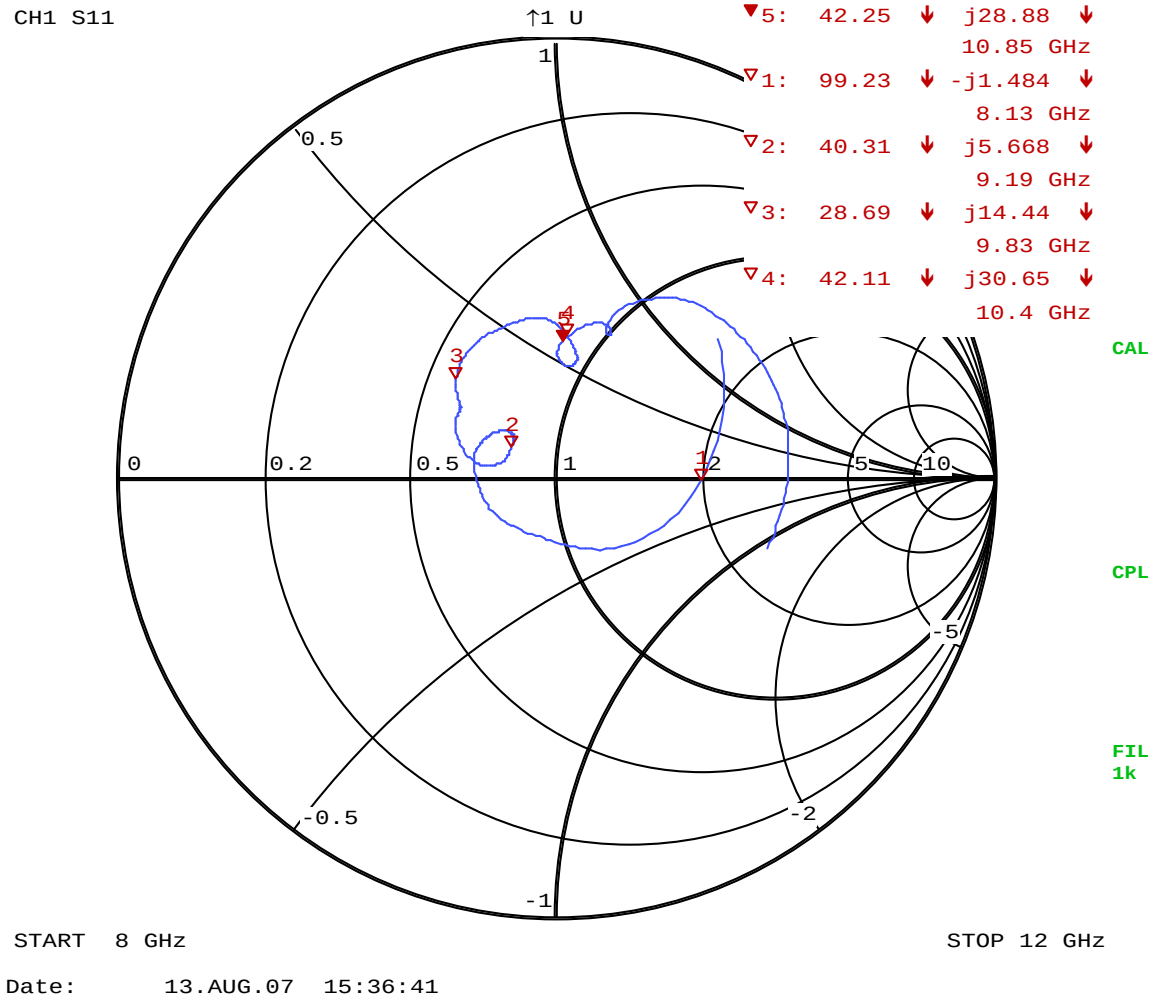


Fig. 6 Input impedance of 2RMSAA.

**REFERENCES:**


1. Shun-Shi Zhong and Jun-Hai Cui, "Compact dual-frequency microstrip antenna", IEEE Antennas and prop. Soci. Int. Symp., Vol. 4, pp. 2196-2199, 2000.
2. S. Maci and G. Biffi. Gentili, "Dual-frequency patch antenna", IEEE Antennas and prop. Magz., Vol.39, No.6, pp. 13-18, 1997.
3. I. J. Bhal and P. Bhartia, "Microstrip antennas" Artect house, New Delhi. pp. 230-234 , 1980.
4. H. Legay, L. Shafai, "Planar resonant series-fed arrays", IEE proc. Microw Antennas propag., Vol. 144. No. 2, pp. 67-72, 1997.
5. Kametani Koichi et al., "Development of X-band Microstrip array antenna for NeLS satellite", Proc. of Space Sci. and Tech. conf., Vol. 46, No. 3, pp. 883-888, 2002.


SEARCH

Previous Page

Next Page

# RADAR CROSS SECTION OF A NOVEL RFID TAG

*Thomaskutty Mathew [1], M. A. Ziai [2], and John Batchelor [2]*
[1]School of Technology and Applied Sciences, Mahatma Gandhi University, Regional Centre, Edappally, Kochi, India
[2]Department of Electronics, University of Kent, Canterbury, UK
[1]drtkmathew@yahoo.co.in

**ABSTRACT:**

The development of a novel RFID tag operating at 869 MHz and its performance evaluation using simulated Radar Cross Section (RCS) are presented. The RCS of the tag antenna is evaluated over azimuth and elevation angular ranges for three cases of load: short, matched load and open. The tag exhibits appreciably good differential RCS between its switching states over wide azimuth angular ranges and over the entire elevation angular ranges. The measured read range variations over the azimuth and elevation angular ranges are also presented to validate the simulated results

## INTRODUCTION:

Radio frequency identification (RFID) is an automated wireless data collection technology which is widely being used as a substitute for barcodes [1]. Recently there has been intense research on RFID technology in the UHF band (860-960 MHz) and is widely getting popular in the identification of objects in the various supply chains around the world. Several papers have been published on UHF RFID tags and their performance evaluation in terms of Read range in a particular reader [2] - [4]. This method of evaluation has a drawback that read ranges may vary with different readers as the reader systems of different companies have different sensitivities. A suitable method for evaluation of RFID tags is by method of Radar Cross Section (RCS) evaluation and has been attempted by some researchers recently [5] – [6]. In this paper we present a novel RFID tag operating at 869MHz and the evaluation of its RCS over azimuth and elevation angular ranges using electromagnetic simulation with CST microwave studio. The measured read range of the tag is also presented to validate the simulated RCS results

## RCS OF RFID TAGS: .

In an RFID system, the tag changes its reflectivity in order to convey its stored identity and data to the reader. This is referred to as the differential RCS. The tag varies its RCS by changing the impedance match of the antenna between two states, usually matched load and short. The backscattering RCS of an RFID tag antenna is given by [5]

$$\sigma_{1,2} = \frac{\lambda^2 G^2 R a^2}{\pi [Z_a + Z_{c1,2}]^2} \quad \text{---------- (1)}$$

Where λ is the wavelength, G is the tag antenna gain and Za=Ra+jXa is the complex antenna impedance. $Zc_1$ and $Zc_2$ are the complex RFID impedances.

The vector differential RCS of the tag is given by [6] as

$$\Delta\sigma = \frac{\lambda^2 G^2}{4\pi} |\rho_1 - \rho_2|^2 \quad \text{---------- (2)}$$

where $\rho_1$ and $\rho_2$ are the complex power reflection coefficients given by

$$\rho_{1,2} = \frac{z_{c_{1,2}} - z_a^*}{z_{c_{1,2}} + z_a} \quad \text{---------- (3)}$$

Knowing the value of $\Delta\sigma$, the read range may be calculated from the classical radar range equation as

$$R_{max} = \left[ \frac{P_t G_t^2 \lambda^2}{(4\pi)^3 P_{r,min}} \Delta\sigma \right]^{\frac{1}{4}} \quad \text{---------- (4)}$$

This shows the dependence of Read range on the differential RCS of the tag.

## METHODOLOGY AND EXPERIMENTAL SET-UP:

The configuration of the RFID tag is shown in fig.1. The tag consists of an antenna and a chip with terminal impedance of $Z_c$=128-j577. The electromagnetic power from the antenna is maximally delivered to the tag chip when antenna has a conjugate impedance of the chip. The parameters L1, L2, L3, W1, W2, and W3 are properly tuned using CST microwave studio simulations to get a conjugate match with the chip at resonant frequency 869MHz. The experimental model was made with optimised parameters $L_1$=90mm, $L_2$=29mm, $L_3$=35mm, $W_1$=1mm, $W_2$=7mm and $W_3$=4mm on an FR-4 substrate with dielectric constant $\varepsilon_r$=4.9 and thickness h=3.44mm.The backscattered RCS of the tag for different cases of load is computed over azimuth and elevation angular ranges using CST microwave studio. The read range measurements of the RFID tag were performed inside an anechoic chamber using a reader with 500mW of ERP operating at 869 MHz. The read range is defined as the maximum distance from which a tag can be detected by the reader and it depends on the differential RCS of the tag between the two switching states.

## RESULTS AND DISCUSSIONS:

The simulated results for the variation of RCS of the RFID tag at 869 MHz over azimuth and elevation angular ranges is illustrated in fig. 2(a) and 2(b) respectively. In each case computed results are given for the antenna connected to different cases of the load: short, matched load and open. It can be seen from fig.2(a) that RCS of the tag antenna is maximum at θ=0 for all three cases of the load and falls off on either side of maximum. The typical maximum values are -17.41 dBsm, -23.03 dBsm and -27.91 dBsm for load impedances with short, matched load and open respectively. This gives a differential RCS of 5.62 dBsm between the short circuited and matched load cases. It is also evident that differential RCS becomes negligibly small for azimuth angles above 70. The difference in RCS between the short circuited and matched load cases is the main factor which determines the read range of the RFID tag. It can be seen from fig. 2(b) that Backscattering RCS is nearly constant over the elevation angular ranges in each case of load impedance. It is also clear that the differential RCS between the two states of the tag antenna also remains constant which should give almost constant read range over the elevation angular ranges. The measured read range variations of the tag antenna at 869 MHz over azimuth and elevation angular ranges are illustrated in figures 3 (a) and 3(b) for different cases of the load. F SEARCH fig. 3(a) it is clear that the read range is maximum at θ=0, where the differential RCS is maximum. The tag read range becomes small with azimuth angles on either side and becomes zero at the extremes. This is in agreement with the simulated results of fig. 2 (a). It may be Previous Page n fig.3 (b) that the read range remains almost constant over the elevation an Next Page

ranges with a maximum of 285cms at Φ=0. This is in good agreement with the simulated RCS results in Fig.2(b).

## CONCLUSIONS:

The Radar Cross Section of a novel RFID tag at 869 M Hz is computed using CST microwave studio for different cases of load impedance. The measured results for the read range of the tag agree well with the variations in the RCS. The RCS simulation of the tag is found to be a good technique in evaluating the performance of the RFID tag. The tag exhibits good read range over the entire elevation angular range and over wide azimuth.

## ACKNOWLEDGEMENTS:

Authors wish to acknowledge the encouragement and support received from Mr. Martin Fogg, RF Tags, Oxfordshire, UK

## REFERENCES:

1. K.Finkenzeller, RFID Handbook, 2nd edition. John Wiley & son, England 2003
2. K V S Rao, P.V. Nikitin and S.F Lam, "Antenna design for UHF RFID tag: a review and a practical application" IEEE Trans. on Antennas & Propagation, Vol. 53, No. 12, 3870-3876, Dec 2005.
3. C. Diugwu, J. Batchelor and T homaskutty M athew "Complementarity in the optimization of RFID dipole tag antenna" IEEE Int. symp. on Antennas & Propagation Digest. San Diego, USA, July 2008. pp. 1-4.
4. S. Chen and K. Lin, "Performance of a folded dipole with closed loop for RFID applications" Proc. of PIERS 2007, Prague, Czech Republic, 329-331
5. K.Penttilla, M. Keskilammi, L. Sydanheimo and Kivikoski, "RCS analysis for passive RFID systems. IEE Proc.- Microwave, antennas, propagation. Vol. 153, No. 1, 103-109, February 2006.
6. P.V. Nikitin, K.V.S Rao and R.D. Martinez, "Differential RCS of RFID tag" Electronics Letters, Vol. 43, No. 8, pp. 256-257, April 2007

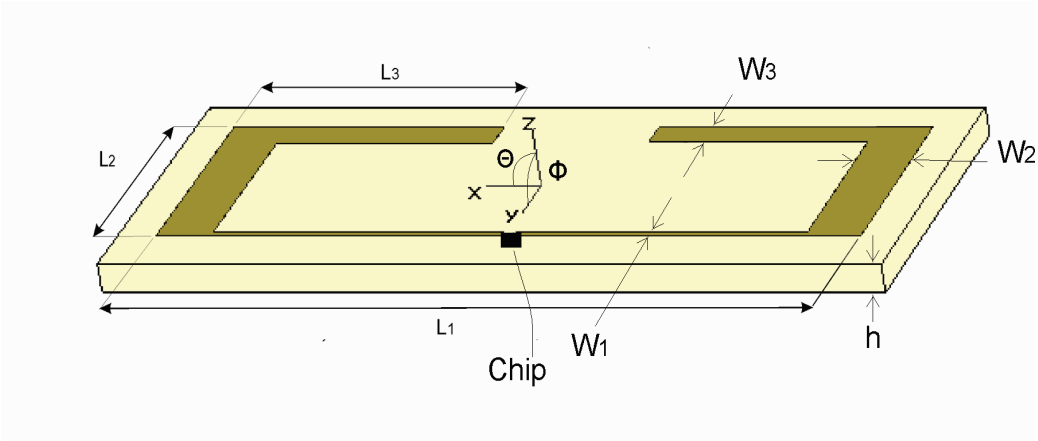


Fig.1 Schematic diagram of the RFID tag antenna.

SEARCH

Previous Page

Next Page

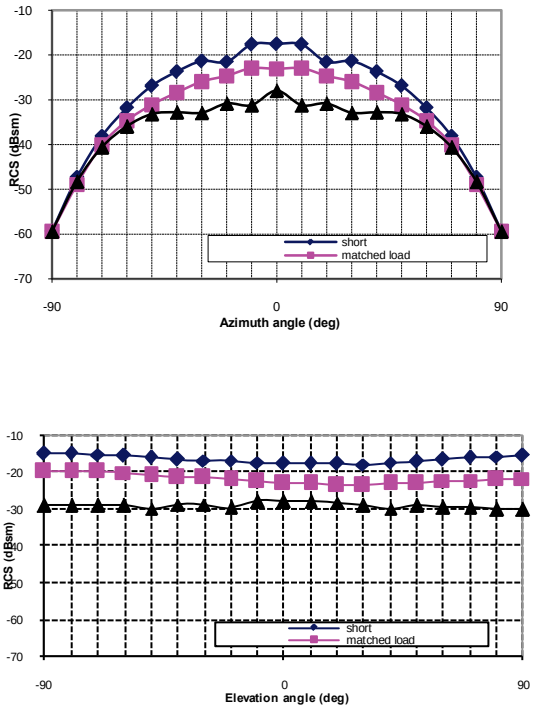


Fig.2 Simulated results for the Variation of backscattered RCS with angle for the RFID tag at 869 MHz for various load impedances (a) RCS Vs azimuth angle for Φ=0 (b) RCS Vs elevation angle with θ=0

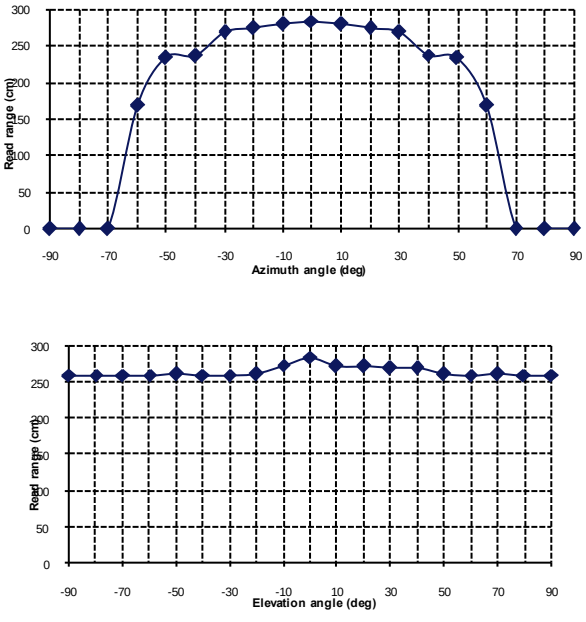


Fig.3 Measured variation of read range with angles for the RFID tag at 869 MHz (a) Read range Vs Azimuth angle with Φ=0 (b) Read range Vs Elevation angle with θ =0

SEARCH

Previous Page

Next Page

# ANALYSIS OF MULTILAYER PATCH ANTENNA WITH TWO PARASITIC ELEMENTS

*J. A. Ansari[1], Prabhakar Singh[1], Nagendra P. Yadav[1] and B. R. Vishvakarma[2]
[1]Department of Electronics & Communication, University of Allahabad, Allahabad, India
[2]Department of Electronics Engineering, I. T. BHU, Varanasi, 221005, India
E-mail: jaansari@rediffmail.com, E-mail : brvish@bhu.ac.in

## ABSTRACT:

The analysis of stacked patch antenna with two parasitic elements is presented. The antenna shows improved radiation and directivity by 6.57 dB as compared to single layer patch antenna. The bandwidth of the antenna is found to depend on various parameters such as $h_1$, $h_2$ and s. The proposed results are compared with the IE3D simulation and reported experimental results.

## INTRODUCTION:

In the present paper an attempt has been made to improve the antenna bandwidth and gain by stacking two parasitic elements over the fed patch in a multilayer planar structure. Various antenna parameters such as input impedance, VSWR, return loss and radiation pattern are calculated for different value of air gap spacing and separation between two parasitic elements. The entire investigation is based on circuit theory concept. Theoretical results obtained from the analysis are compared with the IE3D simulation and experimental results, the details of which are given in the following sections.

## ANTENNA DESIGN AND EQUIVALENT CIRCUIT:

The side view of the proposed antenna configuration is shown in Fig. 1 with the corresponding current distribution at centre frequency 3.011 GHz (Fig. 2).

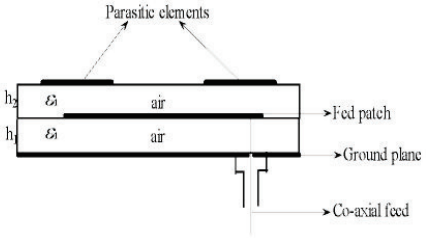


Fig.1 Side view of proposed antenna in two layer configuration

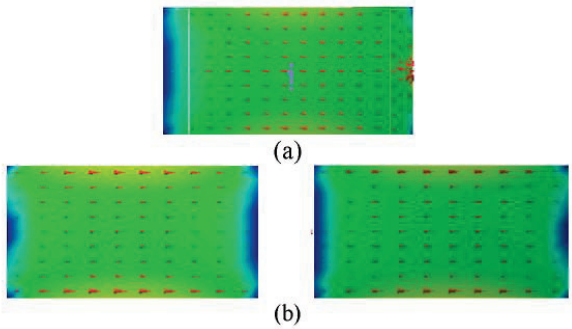


Fig.2 Current distribution at centre frequency 3.011 GHz (a) fed patch and (b) two parasitic elements

SEARCH
Previous Page
Next Page

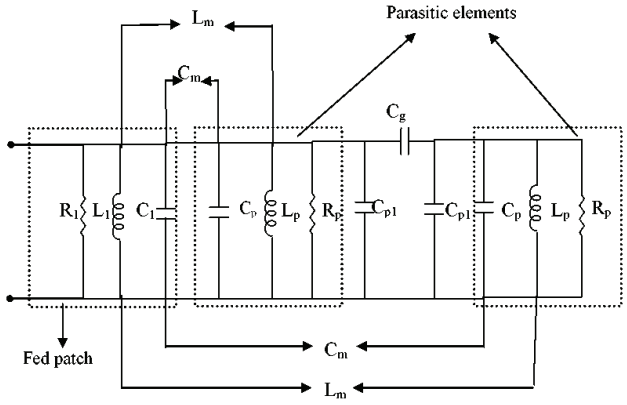


Fig. 3 Coupled equivalent circuit of proposed antenna

Since the stacked parasitic patches are excited through electromagnetic coupling by fed patch, the value of capacitance ($C_2$), inductance ($L_2$) and resistance ($R_2$) for identical stacked parasitic elements canbe given as [2].

Thus the equivalent circuit of the stacked patch with two identical parasitic elements can be given as shown in Fig. (3). The coupling inductance ($L_m$) and capacitance ($C_m$) are calculated by [5]. Now using the equivalent circuit (Fig. 3) total input impedance of the proposed antenna can be calculated.

## RADIATION PATTERN:

The radiation pattern of the rectangular patch can be given as [6]. The radiation pattern for the stacked patch antenna can be obtained with the assumptions

(a) the slot voltage of the parasitic elements are $k_c$ times the slot voltage of the driven patch.

(b) the distance between two patches is very small compared to the wavelength and hence the radiation from the two patches are in same phase.

Further the radiation pattern for the stacked two identical parasitic elements can be obtained as

$$E_p(\theta) = AF \times E_1(\theta) \quad \text{--- (2)}$$

$$E_P(\phi) = AF \times E_1(\phi) \quad \text{---(3)}$$

where AF is array factor and calculated by [7] and $E_1(\theta)$ & $E_1(\varphi)$can be obtained by multiplying coupling coefficient ($k_c$) in equation given by [6]. Hence the radiation pattern for the proposed antenna can be given as

$$E(\theta)_T = E(\theta) + E_p(\theta) \quad \text{---(4)}$$

$$E(\phi)_T = E(\phi) + E_P(\phi) \quad \text{--- (5)}$$

## DESIGN SPECIFICATIONS FOR THE PROPOSED ANTENNA:

Substrate material used – air; Dielectric constant ($\varepsilon r1$ ,$\varepsilon r2$ )-1.0; Thickness of substrate ($h_1$)- 5 mm; Design frequency ($f_r$)- 3.0 GHz; Length of the fed patch (L)- 50mm; Width of the fed patch (W)- 30 mm; Thickness between fed and parasitic patch ($h_2$)- 5 mm; Length of the parasitic patch (Lp)- 36 mm; separation between parasitic elements (s) -52 mm ;Width of the parasitic patch (W)- 30 mm; Feed point location-(24 mm,0).

SEARCH
Previous Page
Next Page

## DISCUSSION OF RESULTS:

Variation of VSWR as a function of frequency is shown in Fig. 4 for different value of s for given value of $h_1$ and $h_2$. From Fig. 4 it is found that the bandwidth of the antenna depends directly on the value of s. Both the theoretical and simulated results for a given value of $h_1$, $h_2$ and s are shown in Fig. 5. It is observed that the theoretical results are in close agreement with the simulated results using IE3D software [8].

The variation of VSWR for multilayer antenna is shown in Fig. 6 with frequency along with simulated and reported experimental results [9] for a given value of antenna dimensions. It is evidently clear that the proposed theoretical results are in close agreement with the reported experimental results however there is slight variation in the simulated results.

The radiation pattern for the stacked antenna is given in the Fig. 7 for different frequencies along with simulated results. It is found that the stacked antenna shows enhanced radiation (6.57 dB higher) as compared to single layer patch antenna. However the stacked patch antenna shows variation in maximum power radiation within 1 dB with frequency. Further it is noted that the stacked antenna shows improved directivity as compared to simple patch.

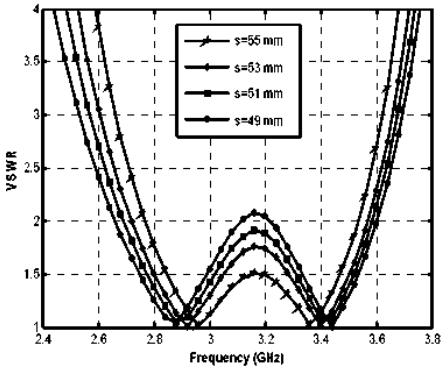


Fig. 4 Variation of VSWR with frequency for different value of gap s, ($h_1$= 5 mm, $h_2$=5mm)

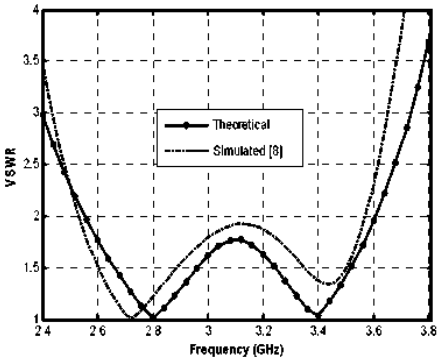


Fig. 5 Graph of VSWR verses frequency ($h_1$=4 mm, $h_2$=9 mm, s=52 mm)

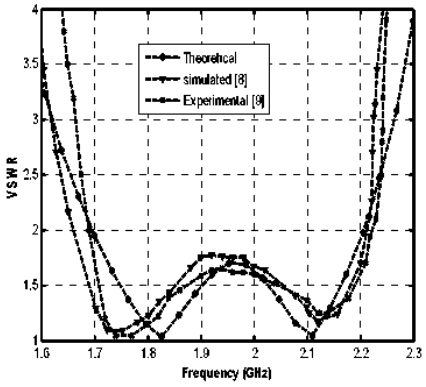


Fig. 6 Theoretical graph of VSWR along with simulated and experimental results ($h_1$=4mm, $h_3$=11mm, $h_2$=$h_4$=1.59mm, s=50 mm, $\varepsilon_{r1} = 1, \varepsilon_{r2} = 4.3$)

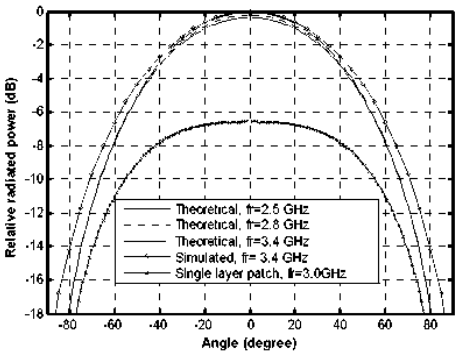


Fig. 7 Radiation pattern at different frequencies

SEARCH
Previous Page
Next Page

## 6 REFERENCES


1. Z.F.Liu et al., "A method for designing broadband microstrip antenna in multilayered planar structures," IEEE Trans. Antenna and Propagation, vol. 47(a), pp.1416-1420, 1999.
2. J. Bahal and P.Bhartia, "Microstrip Antenna," Bosten. MA, Artech house, USA, 1988.
3. M. Meada ., "Analysis of gap in microstrip transmission lines," IEEE Trans. Antenna and Propagation, vol. 32,pp.1375-1379,1972.
4. A.Gopinathand Gupta C., "Capacitance parameter of discontinuities in microstrip lines," IEEE Trans. On Microwave Theory and Tech., vol. 26, pp.831-836, 1978.
5. F.E. Terman, "Electronic & radio Engineering," Kogakusha, Tokyo, Japan (1995) ,pp. 15. K.R.Corver and J. Mink., "Microstrip antenna technology," IEEE Trans. Antenna and Propagation, vol. 29,pp.1-24,1981,.
6. C.A. Balanis, " Antenna theory analysis and design," 2ed edition, Wiely, New York ,1997 IE3D simulation software, Zeland Inc., USA, Version 14.05, 2008.
7. Girish Kumar & K.P. Ray, "Broad band microstrip antenna," Artech house, Baston, London, pp.184-187, 2003.

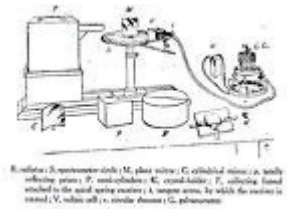

# INVITED TALKS

SEARCH

Previous Page

Next Page

SEARCH

Previous Page

Next Page

# A SUPER-RESOLUTION METHOD OF SOURCE RECONSTRUCTION USING NEAR FIELD ANTENNA MEASUREMENTS

*Tapan K. Sarkar*
Department of Electrical Engineering and Computer Science
Syracuse University, Syracuse, NY 13244 USA
Phone: + 315 443 3775, Fax: + 315 443 4441
tksarkar@syr.edu

**ABSTRACT:**

A computational technique based on near-field to far field transformation is presented. This can be more versatile and accurate than the conventional modal expan sions. The established method for near-field to far-field transformation has been the modal expansion method. The primary drawback of the technique is that when a Fourier transform is used, the fields outside the measurement region area is assumed to be zero, particularly in the planar and cylindrical cas e. C onsequently t he f ar-fields ar e accur ately det ermined onl y over a particular angular sector which is dependent on the measurement configuration. A s imple and accur ate i ntegral equat ion s olution w hich represents an alternate method for computing far-fields from measured near-fields is p resented. The basic i dea is to replace the radiating antenna by equivalent el ectric and /or magnetic cur rents w hich r eside on a f ictitious surface and encompasses the antenna. These equivalent currents are assumed to r adiate i dentical f ields as the or iginal ant enna i n t he r egion of i nterest. Using the surface equivalence principle different types of the E-field integral equation ( EFIE) have been devel oped. T he m ethod of moments ( MoM) has been ut ilized t o t ransform t he i ntegral equa tion i nto a matrix one and the conjugate gr adient ( CG) pr ocedure has been applied to s olve i t nu merically. Hence, this procedure is not limited by the Nyquist sampling criteria nor by the pr esence o f evanes cent waves w hich m ay m ake source r econstruction using current procedures unstable. Accurate far-fields over large elevation and azimuthal ranges have been c alculated f rom simple measurements bas ed on planar and spherical scanning.

## INTRODUCTION:

Near field antenna measurements are widely used in antenna testing since they allow for accur ate measurements of ant enna pat terns i n a cont rolled envi ronment. T he ear liest works ar e bas ed on t he modal expansion m ethod in w hich t he f ields r adiated by t he t est antenna are expanded i n terms of planar, cylindrical or spherical wave functions and t he measured near fields are used to determine the coefficients in the expansion [1–4]. Here, we focus our at tention pr imarily on planar near f ield measurements. A pr oblem o f t he pl anar modal expansion technique is that the fields outside the measurement region are assumed to be zer o. T his as sumption r esults i n a s ystematic er ror in t he com putations i nvolved i n planar modal expansion theory. If the measurement plane is of dimension $L \times L$ and the source plane ( the plane w hich encom passes the s ources) i s of di mension $D \times D$ , t hen t he planar modal expans ion t heory hol ds up t o an ang le $\theta$ , w hich i s gi ven by $q = \tan^{-1}[(L - D)/$ where $d$ is t he s eparation di stance bet ween t he two pl anes [ 5]. An al ternate method o f

computing far-fields from measured nearfields has recently been explored [6,7] utilizing an equivalent magnetic current approach. This method utilizes the measured near field data obtained on the $L \times L$ measurement plane to determine equivalent currents on the $D \times D$ source plane which encompass all sources. These equivalent currents may then be used to image the sources on the antenna if desired (for fault diagnosis) and also to compute the far fields. This is in distinction to the planar modal expansion method where the far fields are computed first and then they are Fourier transformed to the source plane to image the sources [8]. The objective of this paper is to demonstrate that the truncation error in the equivalent current approach is smaller as one transfer the data from the measurement plane to the source plane before Fourier transforming it to compute the far fields. Hence, the results for the equivalent current approach should hold over a larger azimuth angle $\theta$ than the planar modal expansion method.

## EQUIVALENT CURRENT APPROACH:

For the integral equation approach, a fictitious source plane is considered of the same dimension as the measurement plane but translated a distance $d$ towards the sources. So the source plane is located at $z = 0$ . As outlined in [7] an equivalent magnetic current of strength $2m$ is placed on the source plane at $z = 0$ . The factor of 2 arises due to the application of the equivalence principle to a magnetic current radiating in the presence of a perfectly conducting ground plane. On this source plane, we put fictitious magnetic currents. The basic philosophy here is that if one knows the complex values of the magnetic currents on the source plane, one can evaluate the fields at the measurement plane. Conversely, if the measurement fields are known, then one can find the complex amplitudes of the magnetic currents $m$ put on the source plane mathematically.

$$E_{meas,x} = \iint_{-\infty}^{\infty} 2m_y(x', y', z' = 0)\frac{\partial G(r, r')}{\partial z'}\,dx'dy'$$

$$E_{meas,y} = \iint_{-\infty}^{\infty} 2m_x(x', y', z' = 0)\frac{\partial G(r, r')}{\partial z'}\,dx'dy' \qquad \frac{\partial G(r, r')}{\partial z'} = \frac{e^{-jk_0|\bar{r}-\bar{r}'|}}{4\pi|\bar{r}-\bar{r}'|^2}(z - z')\left[jk_0 + \frac{1}{|\bar{r}-\bar{r}'|}\right]$$

where $|r - r'|$ is the distance between the source point and the field point. Observe here, $z = 0$ and $z = d$ . Now if we take the two dimensional Fourier Transform of both sides,

this results in $\iint_{-\infty}^{\infty} E_{meas,x}(x, y, z = d)\, e^{j(k_x x + y k_y)}\,dxdy = 2\tilde{m}_y(k_x, k_y)\,\tilde{g}(k_x, k_y)$ where $\tilde{m}_y$ is the two dimensional Fourier Transform of the magnetic currents located at the source plane and $\tilde{g}$ is two dimensional Fourier transform of the derivative of the Green's function

$$\tilde{G}(k_x, k_y, z, z') = \frac{-j}{2k_0}\, e^{j|z-z'|\sqrt{{k_0}^2-{k_x}^2-{k_y}^2}} \quad ; \quad \mathrm{Re}\left\{\sqrt{{k_0}^2-{k_x}^2-{k_y}^2}\right\} \geq 0 \quad \mathrm{Im}\left\{\sqrt{{k_0}^2-{k_x}^2-{k_y}^2}\right\} < 0$$

In the transform domain, the derivative of the spectral Green's function with respect to $z$ yields: $\frac{\partial}{\partial z'}\tilde{G}(k_x, k_y, z, z') = \frac{1}{2}\mathrm{sgn}(z - z')\, e^{j|z-z'|\sqrt{{k_0}^2-{k_x}^2-{k_y}^2}}$ where sgn(z) is the signum function. Since $z = 0$ and $z = d$ $\tilde{g}(k_x, k_y) = \frac{1}{2}\, e^{-jd\sqrt{{k_0}^2-{k_x}^2-{k_y}^2}}$ . Hence, it becomes clear that

$$\tilde{M}_y(k_x, k_y, z = d) = \tilde{m}_y(k_x, k_y, z = 0)\, e^{-jd\sqrt{{k_0}^2-{k_x}^2-{k_y}^2}} \qquad \tilde{M}_x(k_x, k_y, z = d) = \tilde{m}_x(k_x, k_y, z' = 0)\, e^{-jd\sqrt{{k_0}^2-{k_x}^2-{k_y}^2}}$$

So if the information on the measurement plane were available, then the integral equation approach is basically to transfer the measurement data to the source plane and then take the Fourier transform to the far field. However, if the measurement plane is finite in size then the transfer of the data from $z = d$ plane to $z = 0$ plane utilizing the Fourier transform is not accurate because of the truncation error. Therefore we utilize an alternate transformation

SEARCH Previous Page Next Page

to go to the source plane. This alternate transformation is utilized in the integral equation approach through the utilization of the Green's function. Theoretically, this reduces the truncation error problem introduced by the two dimensional Fourier transform.

When the measurement plane is finite in nature then the method of moments is utilized to solved for $m_x$ and $m_y$ . The unknowns are replaced by elementary dipoles. This is a good approximation as long as the source and the measurement planes are separated by a wavelength (i.e. $d = \lambda$ ) [11]. Secondly, the use of dipoles eliminates the need for integration of the matrix elements in the evaluation of the impedance matrix. The two decoupled equations are then solved as matrix equations [6,7,11]:

$$[E_{meas,x}] = [Z_{yx}][m_y]$$

$$[E_{meas,y}] = [Z_{xy}][m_x]$$

These matrices can be very large. However the equations can be solved very efficiently utilizing the FFT and the conjugate gradient method as outlined in [7]. Also the solution of the above two equations are decoupled and the solution can be done simultaneously. Typically for 6400 unknowns for $m_x$ or $m_y$ the number of iterations taken to provide acceptable solution is about 10. Since per iteration, two two-dimensional FFT is computed, the integral equation method is about 20 times slower than the modal expansion method for 6400 unknowns. Typically on a PC this amounts to a few seconds of CPU time for the modal expansion method as compared to several minutes of CPU time for the integral equation method to solve for the unknown magnetic currents $m_x$ and $m_y$ at the source plane. Once these magnetic currents are known, the far field can easily be computed utilizing the FFT.

## APPLICATION TO EXPERIMENTAL DATA:

As an example, we consider experimental data for a microstrip array. This microstrip array consists of 32×32 uniformly distributed dipoles over a 1.5m×1.5m surface. The operating frequency is 3.3 GHz. The array is considered in the $x - y$ plane. The $x$ and $y$ components of the electric near fields are measured on a plane 3.24m×3.24m at a distance of 35cm from the array. There are 81×81 measured points at a distance of 4cm apart. This planar near field data was provided by Dr. Carl Stubenrauch of NIST [10]. If the planar modal expansion method is applied on the 81×81 measured data points, the computed far field will be accurate up to $\tan^{-1}(87/35) = 68^\circ$ [5]. The results obtained using modal expansion method was compared with the integral equation method as outlined in [7]. In [7], it was seen that the agreement between the two methods were good up to $\pm 60^\circ$ and acceptable in the rest of the elevation range.

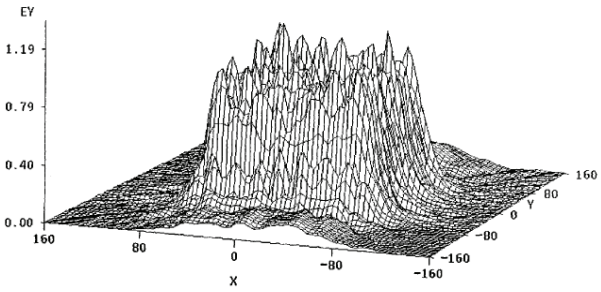


Fig. 1 Amplitude of y component of measured electric near-field for a 32 × 32 patch microstrip array.

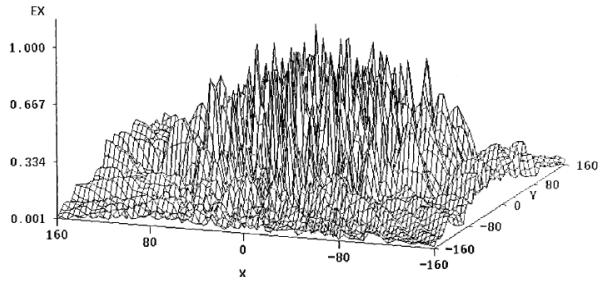


Fig. 2 Amplitude of x component of measu electric near-field for a 32 × 32 patch microstrip array.

SEARCH
Previous Page
Next Page

To demonstrate that by transferring the measured data to a fictitious surface, we are indeed reducing the truncation error, we take only 41×41 samples discarding 75% of the data. Therefore, we are considering the data only over a 1.64m ×1.64m measurement plane. By observing the magnitudes of the two components of the electric field (namely *Ey* in Fig. 1 and *Ex* in Fig. 2. The amplitude of the normalization component for *Ex* is 23.8 dB below that for *Ey* ) it is clear that taking 41×41 points introduces significant truncation error if we were to take the direct Fourier transform of the data in the conventional modal expansion method. The Figs. 1 and 2 are for all the 81×81 data points. Hence by considering only 41×41 data points in Figs. 1 and 2, one is incurring a large truncation error in the conventional modal expansion method. If the modal expansion method is applied to the 41×41 data points, the calculated far fields would be accurate upto $\tan^{-1}(7/35) = 11.3^0$. For the integral equation approach, we consider a 41×41 magnetic dipole array uniformly distributed over a 1.64m×1.64, surface at the $z = 0$ plane. From the 41×41 measured near-field sampled data, we compute the amplitudes of the 41×41 magnetic dipoles utilizing CGFFT [7]. The 2*D* Fourier transform was then utilized to find the far fields. Fig. 3 provides $E\varphi$ ($\varphi = 0$) utilizing the modal expansion method with the original 81×81 points and the integral equation approach with only 41×41 data points. It is seen that for the two results agree till ±40° and beyond that the agreement is reasonable. Therefore, by reducing the data by as much as 75% it is still possible to get reasonable results utilizing the integral equation technique. For this case 41×41 data points, the CGFFT method takes about 10–12 iterations to provide an acceptable solution for the magnetic dipoles. Since the CGFFT method requires two 2D-FFT per iteration, the CGFFT method is slower than the modal expansion method by a factor 20–24 minutes as compared to seconds of the modal techniques. Fig. 4 provides $E_\theta$ ($\varphi = 90^\circ$) utilizing the modal expansion on the original 81×81 measured points whereas the integral equation has been applied to the central 41×41 points only. Again, the two curves agree till ±40° and the agreement is reasonable outside that region. These are the two principal planes co-polar pattern. Next we look at the cross-polar pattern. Fig. 5 provides $E_\theta$ ($\varphi = 0^\circ$) utilizing the modal expansion on the 81×81 points and the integral equation approach utilizing 41×41 data points. Even though the cross-polar pattern is 40 db down, reasonable agreement is seen upto ±40°. Fig. 6 provides $E_\theta$ ($\varphi = 90^\circ$) utilizing the modal expansion and the integral equation approach. Because this pattern is 60 dB down, the accuracy of both the methods are being compared at a level which corresponds to the noise level. Even then, agreement is reasonable!

Limited experimentation utilizing experimental data illustrates that it is possible to go beyond the truncation error introduced by the measurement process, by transferring the measurement plane to a source plane containing equivalent sources on a plane closer to the source. It is important to point out that the integral equation method is not creating information that is not there in the measured data. The integral equation method has less truncation error as the processing is different from the conventional modal expansion method. Since the integral equation method is a model-based-parameter-estimation technique, it will always provide higher resolution than the conventional modal expansion method which is FFT based.

SEARCH

Previous Page Next Page

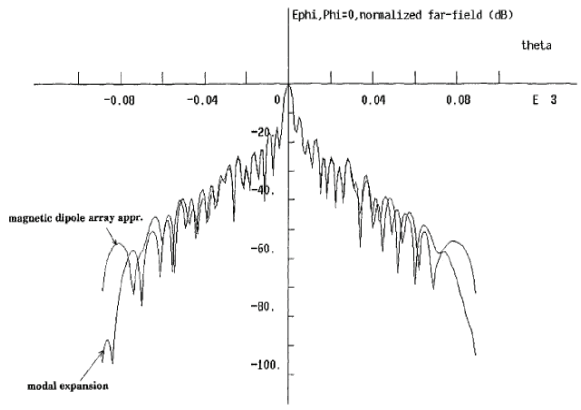


Fig. 3 Co-polarization characteristic for $\Phi = 0^{\circ}$ cut for a 32 × 32 patch microstrip array using planar modal expansion method (81 × 81data points) and equivalent magnetic dipole array approximation (41 ×41 data points).

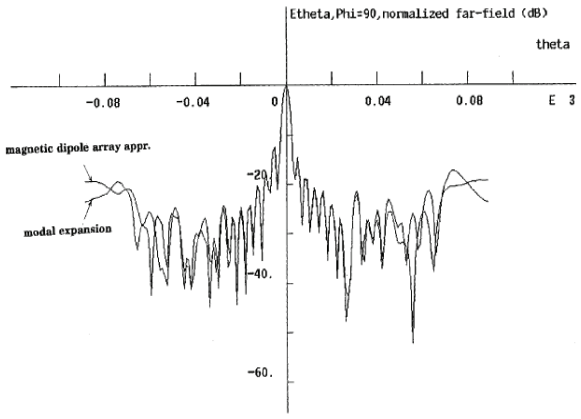


Fig. 4 Co-polarization characteristic for $\Phi = 90^{\circ}$ cut for a 32 × 32 patch microstrip array using planar modal expansion method (81 × 81 data points) and equivalent magnetic dipole array (41 ×41 data points ).

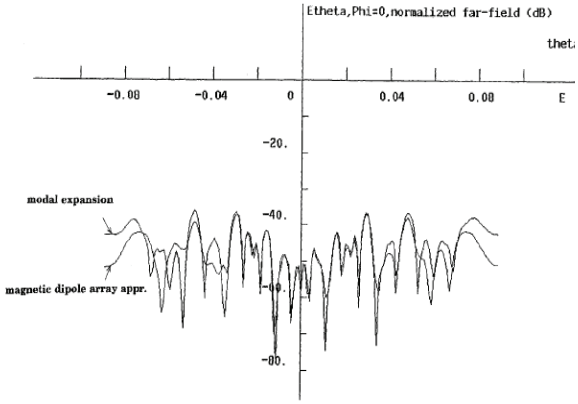


Fig 5. Cross-polarization characteristic for $\Phi = 0^{\circ}$ cut for a 32 × 32 patch microstrip array using planar modal expansion method (81 ×81data points) and equivalent magnetic dipole array approximation (41 ×41 data points).

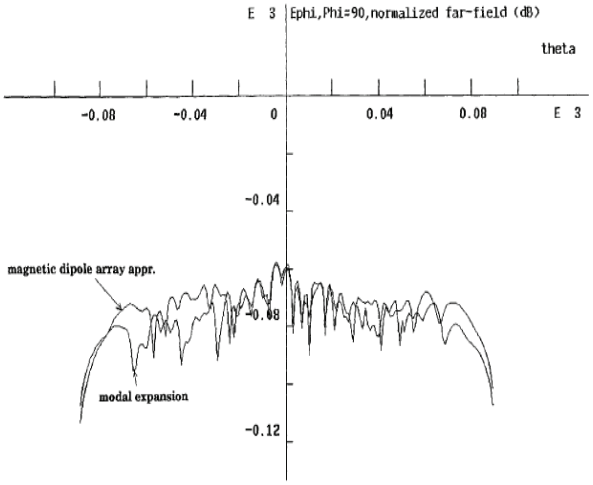


Fig 6. Cross-polarization characteristic for $\Phi = 90^{\circ}$ cut for a 32 × 32 patch microstrip array using planar modal expansion method (81 ×81data points) and equivalent magnetic dipole array approximation (41 ×41 data points).

## CONCLUSION:

The integral equation approach can provide a reduction of the truncation error caused by performing measurements on a finite plane. This is achieved by transforming and shifting

SEARCH
Previous Page
Next Page

the measured data to a plane which is much closer to the sources. Once the equivalent magnetic currents are found on the source plane, the Fourier techniques can be used to compute the far fields from the magnetic currents. So the price one pays in utilizing the integral equation approach over the modal expansion method is that the integral equation approach takes about 20–25 times more CPU time to produce the far fields for the same number of data points. This estimate has been obtained from the limited cases run in this paper. However, the integral equation approach requires fewer measured data points than the conventional modal expansion method to provide comparable numerical accuracy in the far fields when applied to the same near-field data. So the total measurement time in the integral equation method is less to achieve equivalent numerical accuracy in the far field result compared to the conventional modal expansion method.

**REFERENCE:**


1. D. T. Paris, W. M. Leach, Jr., and E. B. Joy, "Basic theory of probe-compensated near-field measurements," *IEEE Trans. On Antennas and Propagation,* Vol. AP-26, No. 3, 373–379, 1978.
2. E. B. Joy, W. M. Leach, Jr., G. P. Rodriguez, and D. T. Paris, "Applications of probe-compensated near-field measurements," *IEEE Trans. on Antennas and Propagation,* Vol. AP-26, No. 3, 379–389, 1978.
3. A. D. Yaghjian, "An overview of near-field antenna measurements," *IEEE Trans. on Antennas and Propagation,* Vol. AP-34, No. 1, 30–45, 1986.
4. J. J. H. Wang, "An examination of the theory for planar nearfield measurements," *IEEE Trans. on Antennas and Propagation,* Vol. AP-36, 746–753, 1988.
5. A. C. Newell, "Error analysis techniques for planar near-field measurements," *IEEE Trans. on Antennas and Propagation,* Vol. AP-36, No. 6, 754–768, 1988.
6. S. Ponnapalli, "Near-field to far-field transformation utilizing the conjugate gradient method," *Application of Conjugate Gradient Method in Electromagnetics and Signal Processing,* in PIER 5, T. K. Sarkar, ed. New York, VNU Science Press, Ch. 11, Dec. 1990.
7. P. Petre and T. K. Sarkar, "Planer near-field to far-field transformation using an equivalent magnetic current approach," *IEEE Trans. of Antennas and Propagation,* 1348–1356, Nov. 1992.
8. Y. Rahmat-Samii, "Surface diagnosis of large reflector antennas using microwave holographic metrology: An iterative approach," *Radio Science,* Vol. 19, 1205–1217, Sept–Oct, 1984.
9. P. C. Clemmow, *The Plane Wave Spectrum Representation of Electromagnetic Fields,* Pergamon Press, 1966.
10. C. Stubenrauch, [private communication]
11. P. Petre and T. K. Sarkar, "Planar near-field to far field transformation using an array of dipole probes," *IEEE Trans. On Antennas and Propagation,* Vol. 42, 534–537, April 1994.


SEARCH

Previous Page Next Page

# BROADBAND DIELECTRIC RESONATOR ANTENNAS

*D. Guha*[1] *and Y. M. M. Antar*[2]

[1]Institute of Radio Physics and Electronics, University of Calcutta,
92 A P C Road, Kolkata 700 009, India.
e-mail: dguha@ieee.org

[2]Department of ECE, Royal Military College of Canada, Kingston,
Ontario, K7K 7B4, Canada.
e-mail: antar-y@rmc.ca

## INTRODUCTION

Dielectric resonator Antenna (DRA) has been an active area of research for the last two decades. Two exclusive books on DRAs [1], [2] have been published and almost all relevant topics are discussed. Although in many cases, DRA is regarded as an alternative to microstrip patch, although its resonance mechanism, resonant modes and radiation characteristics are totally different. Operation over a large frequency band is a common requirement. In recent years, one major wing in DRA research has been focused to exploring different techniques to enhance the impedance bandwidth. Some are similar to those used in microstrip antennas. Some approaches are completely new. Some techniques are application based and some are based on DRA geometries. However, each technique has an individual philosophy or reason behind. Such a discussion was provided in an article by one of the present authors in connection with describing the band width widening techniques of microstrip antennas [3].

In this article, we intend to describe the techniques which have already been explored and demonstrated in open literature to achieve wideband operation of DRAs. The techniques vary with the nature of radiation (broadside/oblique/monopole-like), polarization (linear/circular) and application (wireless/GPS/EMI/Satellite/Ultra-wideband). All possible types and examples will be discussed in short.

## THE TECHNIQUES

The basic approaches and the practical way to implement those are shown below:

| Approach | How to implement | Example |
|---|---|---|
| Lowering Q value | Using low dielectric constant material | |
| | Cutting slots | [4] |
| | Removing material by shaping a DR | [5], [6] |
| Matching of input impedance | Metal strip/tape on DR surface excited by a probe | [4] |
| | Feeding by microstrip line with matching network | [7]-[9] |
| | Using shaped aperture/slot as feed | [10] |
| | Using parasitic metal strip or DR | [11], [12] |
| Multiple resonances | Using multiple DRs in stacked/embedded configuration | [13], [14] |
| | Using optimized shaping of single DR | [15] |
| | Using DR-metal hybrid structure | [16] |
| | Using DR-feed hybrid structure | [17] |
| | Using DR-DR composite structure | [18], [19] |

SEARCH
Previous Page
Next Page

## BROADBAND MONOPOLE-TYPE DRA

Monopole-like DRA was conceived using centre-fed ring resonator [20], [21]. A hybrid geometry has been investigated recently as an ultra wideband antenna [22], [23]. This is a combination of an electric monopole and a dielectric ring resonator as shown in Fig. 1. A single antenna is demonstrated to operate over a frequency range covering GSM to UMTS or PCS to WLAN. This hybrid DRA is of very sleek configuration and is ideal for desktop or any hidden application.

One recent design uses four-element planar array of cylindrical DRA's [18] and exploits the symmetry of the dominant $HEM_{11d}$ mode in the composite structure to generate symmetrical oblique radiation pattern, like a simple monopole. A prototype is shown in Fig. 2. Nearly 29% impedance bandwidth ( $S_{11}$<-10 dB ), which is approximately double the normal bandwidth of an electrical monopole has been achieved. The optimum DRA dimension appears to be approximately 0.6 $\lambda_0$ by 0.1 $\lambda_0$. This new antenna designed for any wireless band like, WLAN or PCS will be highly suitable for hiding under a low profile planar structure or for indoor ceiling mount applications.

Another composite DRA structure recently investigated as a wideband monopole-like radiator is shown in Fig. 3 [24]. This employs newly introduced half-hemispherical shape of a dielectric resonator. Two half-hemispherical DRA segments, one being directly excited by a coaxial probe are apparent from the photograph. About 35% impedance bandwidth with 5 dBi peak gain and 99.08% radiation efficiency is achieved from an antenna measuring nearly 0.5 $\lambda_0$ by 0.2 $\lambda_0$, $\lambda_0$ being the wavelength corresponding to the center of the operating band. This high-efficiency is a significant factor that makes DRAs superior compared to metallic or printed wireless antennas, commercially available at present.

## BROADBAND DRA FOR WIRELESS APPLICATIONS

Inverted L-shaped triangular [5] and cylindrical [6] geometries are demonstrated to operate over four wireless bands ( DCS, PCS, UMTS and WLAN). They employ the dominant HEM mode with lower effective permittivity and radiates along the broadside of the structure. The shaped cylindrical DRA investigated in [6] is shown in Fig. 4. Similar results are also available for triangular DRA [5]. Although they are volume wise little bulky, but from the efficiency point of view, about 20% improvement is apparent if compared with the microstrip variants.

## BROADBAND CIRCULARLY POLARIZED DRA

There is also some interest in using circularly polarized (CP) antennas for wireless communication. A comb-shaped CP-DRA has recently been proposed with single probe excitation [4]. This shows a simple as well as compact DRA geometry that can operate over nearly 4% axial ratio bandwidth (<3dB) with about 3.5 dBi peak gain. The experimental investigation has been performed using a prototype with small size ground plane (~0.9$\lambda_0$).

## CONCLUSIONS

We have tried to provide a very brief sketch of bandwidth widening techniques explored so far for the DRAs. A few examples are described based on the first hand experience of the present authors. Various geometries, related analysis and applications will be presented in more details.

Previous Page Next Page

## REFERENCES


1. K. M. Luk and K. W. Leung, Dielectric Resonator Antennas, Hertford-shire, U.K.: Research Studies Press Ltd., 2002.
2. A. Petosa, Dielectric Resonator Antenna Handbook, Artech House, 2007
3. D. Guha, "Broadband Design of Microstrip Antennas: Recent Trends and Developments," invited paper in J. Facta Universitatis, Special issue, vol. 3, No. 15, pp. 1083-1088, 2003.
4. L. C. Y. Chu, D. Guha and Y. M. M. Antar, "Comb-shaped wideband dielectric resonator antenna," Electronic Letters, vol. 42, no. 14, pp. 785-786, 6th July, 2006.
5. T. A. Denidni, Q. Rao, and A. R. Sebak, "Broadband L-Shaped Dielectric Resonator Antenna," IEEE Antennas and Wireless Propagation Letters, Vol. 4, pp. 453-454, 2005.
6. L. C. Y. Chu, D. Guha and Y. M. M. Antar, " Air gap loaded ultra wideband dielectric resonator antenna for commercial wireless bands" in Int. Sym. Antenna Technology and Applied Electromagnetics & Canadian Radio Sciences (URSI/CNC) Montreal, July, 2006.
7. Sreedevi K. Menon *et al*, "wideband cylindrical dielectric resonator antenna excited using an L-strip feed", Microwave and Opt. Technol. Lett., Vol. 42, No. 4, August 2004.
8. M. N. Suma *et al*, "rectangular dielectric resonator antenna on a conductor-backed co-planar waveguide", Vol. 45, No. 2, April, 2005.
9. Chih-Yu Huang *et al*, "Planar array composed of two linearly polarized dielectric resonator antennas for circular polarization" Microwave and Opt. Technol. Lett. Vol. 21, No. 5, June, 1999.
10. Sreedevi K. Menon *et al*, "L-strip-fed wideband rectangular dielectric resonator antenna", Microwave and Opt. Technol. Lett. Vol. 45, No. 3, May, 2005.
11. Fu-Ren Hsiao *et al*, "A broadband very-high-permittivity dielectric resonator antenna for WLAN application in the 5.2 GHz band", Microwave and Opt. Technol. Lett. Vol. 32, No. 6, March, 2002.
12. K.W. Leung, K.M. Luk, K.Y. Chow and E.K.N. Yung, "Bandwidth enhancement of dielectric resonator antenna by loading a low-profile dielectric disk of very high permittivity," Elect. Left. Vol. 33, No. 9, pp. 725-726, 24th Apr. 1997.
13. A. A. Kishk, X. Zhang, A. W. Glisson, and D. Kajfez, "Numerical analysis of stacked dielectric resonator antennas excited by a coaxial probe for wideband applications," IEEE Trans. Antennas Propagat. , vol. 51, no. 8, pp. 1996-2006, August 2003.
14. A. A. Kishk, "Experimental study of broadband embedded dielectric resonator antennas excited by a narrow slot," IEEE Antennas Wireless Propagat. Lett., vol. 4, pp.79-81, 2005.
15. A.A. Kishk, "Wide-band truncated tetrahedron dielectric resonator antenna excited by a coaxial probe," IEEE Trans. Antennas Propagat., vol. 51, no. 10. pp. 2913-2917, Oct. 2003.
16. K. P. Esselle and T. S. Bird, "A Hybrid-Resonator Antenna: Experimental Results," IEEE Trans. Antennas Propagat., Vol. 53, No.2, pp.870-871, Feb. 2005.
17. A. Buerkle, K. Sarabandi, and H. Mosallaei, " Compact slot and dielectric resonator antenna with dual-resonance, broadband characteristics," IEEE Trans. Antennas Propagat., Vol. 53, No.3, pp. 1020- 1027, March 2005.
18. D. Guha and Y. M. M. Antar, "Four-element cylindrical dielectric resonator antenna for wideband monopole-like radiation," IEEE Trans. Antennas Propagat., Vol. 54, N0. 9, pp. 2657-2662, Sept. 2006.


SEARCH
Previous Page
Next Page

19. D. Guha and Y. M. M. Antar, "New half-hemispherical dielectric resonator antenna for broadband monopole-type radiation," IEEE Transactions on Antennas and Propagation Vol. 54, N0. 12, pp. 3621-3628, Dec. 2006.
20. S. W. Ong, A. A. Kishk, and A. W. Glisson, "Wideband disc-ring dielectric resonator antenna," Microwave and Optical Technology Letters, vol. 35, no. 6, p p. 425 -428, December 2002.
21. S. H. Ong, A. A. Kishk, and A. W. Glisson, "Rod-ring dielectric resonator antenna: Research Articles" Int. J. RF and Microwave Computer-Aided Engineering Vol. 14, No. 6 pp. 441 – 446, Nov. 2004.
22. M. Lapierre, Y. M. M. Antar, A Ittipiboon and A. Petosa, "Ultra wideband monopole/ dielectric resonator antenna," IEEE Microwave Wireless Comp. Lett. Vol. 15, No. 1, pp. 7-9, Jan. 2005.
23. D. Guha, Y. M. M. Antar, A. Ittiboon, A. Petosa, and D. Lee "Improved design guidelines for the ultra wideband monopole-dielectric resonator antenna," IEEE Antennas and Wireless Propagation Letters, Vol. 5, pp. 373-376, 2006.

Figure 1: Ultra wideband monopole-DRA [22], [23].

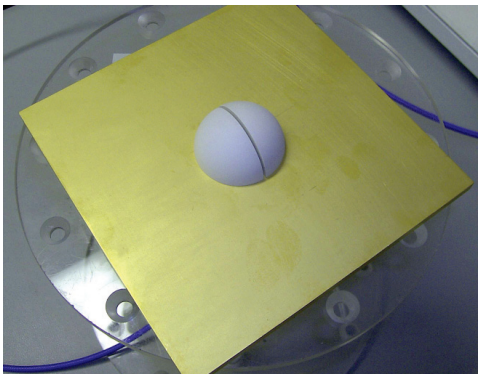

Figure 3 : Two-element half-hemispherical DRA: wideband monopole-type antenna [19]

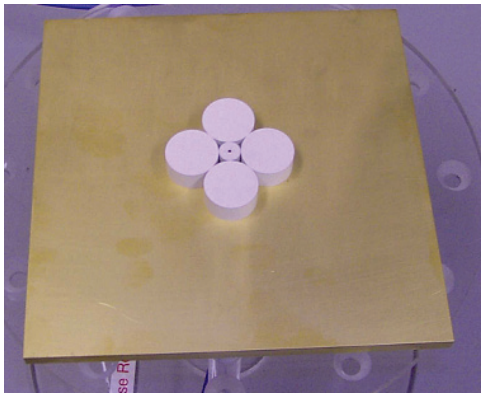

Figure 2 : Four-element Cylindrical DRA: wideband monopole-type antenna [18]

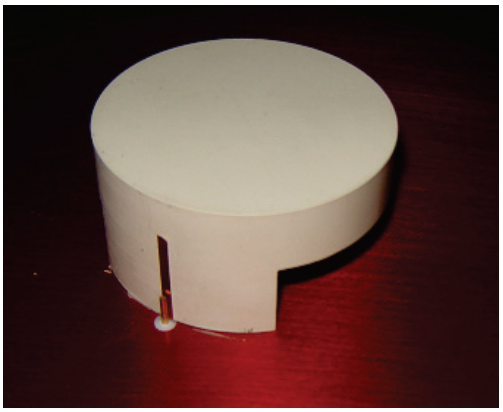

Figure 4 : Shaped DRA designed as wireless antenna [6]

SEARCH
Previous Page
Next Page

# HIGH POWER MICROWAVE TUBES – INDIAN CONTEXT

*SN JOSHI*
CENTRAL ELECTRONICS ENGINEERING RESEARCH INSTITUTE, PILANI
(A CSIR Laboratory)
snjoshi_15@yahoo.com, snj@ceeri.res.in

## ABSTRACT

Microwave Tubes came into prominence around World War – II, when Pulse Magnetrons were substantially used for RADAR Systems. Thereafter, other devices like Klystrons, Backward-wave Oscillators, Crossed Field Amplifiers; Traveling Wave Tubes were invented and used in various systems. As the Conventional Microwave Tubes have limitations of fabrication at higher frequencies particularly beyond 100 GHz due to the smaller geometries of components, another class of device known as Fast-wave Devices has come into prominence, which can be used up to very high frequencies and up to very high power levels. In the area of Conventional Microwave Tubes (Slow-wave Devices), significant enhancement in their performance capabilities has taken place in terms of achieving very high powers (1.0 MW CW) with very high efficiencies (~ 70%), extremely large bandwidth (~ 3 octaves), reliable performance and long life (15 – 20 years). This has mainly been possible due to (i) advent of sophisticated 3-D CAD tools (ii) better analytical concepts and design methodologies (iii) micro-fabrication techniques and availability sophisticated equipment (iv) availability of high current density cathodes and high energy magnets (v) availability of special materials, ceramics and their composits and (vi) better thermal management of devices (vii) growth of technologies. Merger of vacuum and semiconductor technologies is the need of the future particularly for devices in THz range.

Apart from the conventional applications of these devices in various sectors like defence, space, atomic energy, industries, health etc., newer application areas requiring very high power (1.0 MW CW) up to very high frequencies (170 GHz) are emerging. They include (i) Accelerator Driven Sub-critical System (ADSS) of DAE (ii) International Thermonuclear Experimental Reactor (ITER) Programme with participation of seven countries including India (iii) SST-II and National Fusion Programme of DAE (iv) Linear Accelerator Programme of DICT (SAMEER) for Bio-medical Applications (v) Space Programme of ISRO requiring transponders at various frequencies.

All above programmes mentioned at (i) to (iv) require very high power (1.0 MW CW) devices in the frequency range of 350 MHz to 170 GHz and all of them have very long-range applications.

To cater to above National needs CEERI has undertaken a major programme with the support of CSIR for design and development of very high power (~ 250 kW CW) and high frequency (120 GHz) devices. While CEERI is the nodal agency, four other sister laboratories of CSIR namely CGCRI, Kolkata; CMERI, Durgapur; NPL, New Delhi; and CSIO, Chandigarh are participating in this programme which has an outlay of Rs. 4 crores. Another major multi-institutional project with the support of DST has been undertaken by CEERI as the nodal laboratory. Other participating organizations are IT, BHU, Varanasi; IIT(R), Roorkee; SAMEER, Mumbai; and IPR, Gandhinagar. The mandate of this project is design and development of 42 GHz, 200 kW (CW) Gyrotron, a fast-wave device. It

addition to above multi-institutional programmes CEERI has undertaken number of other sponsored projects from DAE, DRDO, DICT and ISRO relating to conventional Microwave Tubes. CEERI has also formal collaboration with international agencies as well as with other academic agencies in the country.

In addition to organizations mentioned above, MTRDC, an R &D Laboratory of DRDO has been working on high power Gyro Devices as well as on other HPM devices in collaboration with BARC, Mumbai; DAVV, Indore and other organizations. They are also engaged in design and development of other Conventional Microwave Tubes and have developed them successfully particularly for Defence. BEL, Bangalore is the only prestigious Public Sector Undertaking in the country for productionization of these devices. They have close collaborations with CEERI and MTRDC in the area of Microwave Tubes.

# GTD TECHNIQUES AND ITS APPLICATIONS TO PROBLEMS IN ANTENNAS AND PROPAGATION

*Subrata Sanyal*
Department of Electronics and Electrical Communication Engineering
Indian Institute of Technology Kharagpur,
India- 721302
ssanyal@ece.iitkgp.ernet.in

## INTRODUCTION:

The wireless revolution led by the development in mobile communication has led to the ever increasing demand for capacity-enhancing techniques such as microcells and adaptive antenna technology which call for realistic directional channel models. Most wireless connectivity is via non-line-of-sight paths that experience multipath propagation. Such wireless channels experience degradation from fading gains and changing phases.

Multipath propagation is a fundamental and capacity-limiting problem whose mechanism must be thoroughly understood in order to design efficient wireless systems. It is now widely recognized that the (semi-) empirical propagation prediction models used for the planning and optimization of conventional, macrocellular networks are not suitable if microcells or adaptive antennas are deployed [1].

The complex nature of urban microcellular and indoor picocellular environments makes it necessary to take into account the geometrical and electromagnetic properties of the different obstacles existing within the propagation environment. After reflection and scattering, diffraction is an important mechanism, and various diffraction theories are often used to explain multipath propagation phenomena in mobile environments [2].

Keller's GTD [3]: is an extension of GO that accounts for diffraction phenomenon. Like geometrical optics it assumes that light travels along certain straight curved lines called rays. But it introduces various new ones, called diffracted rays, in addition to the usual rays.

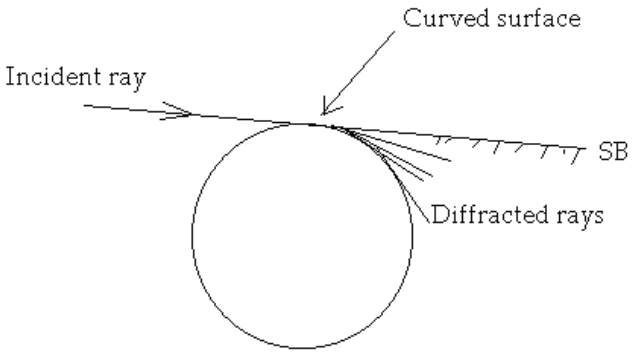


The basic "postulate" in Keller's GTD and its extensions uniform asymptotic theory (UAT) of diffraction [4] and uniform theory of diffraction (UTD) [5] is that at high frequencies or short wavelengths diffraction is a locally determined phenomenon, that is, the diffracted field is determined by the local properties of the incident field and the diffracting obstacle at the point of diffracti
This postulate underlies the idea of "canonical" problems such as the problem of diffraction by a half-plane, an infinite wedge etc., that are, simpler problems (possibly permitting an exact solution) which have the same local features as the diffraction problem at hand.

SEARCH
Previous Page
Next Page

The H alf-plane pr oblem: When the incident wave is normal to the edge of t he s creen, t he di ffracted wave is cylindrical with the edge as its axes.

When the incident ray is oblique to the edge, the resulting diffracted wave is conical.

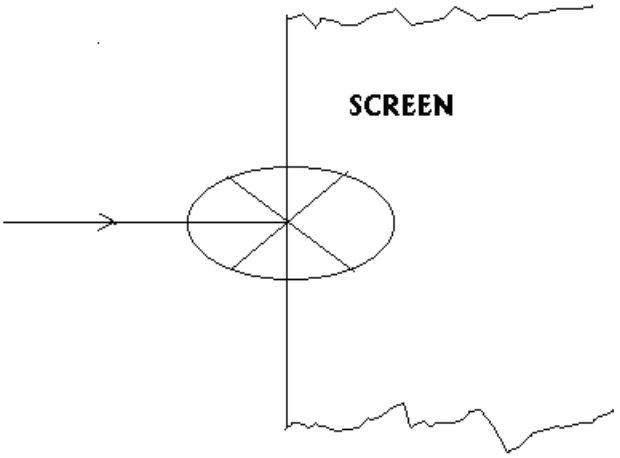


**Half plane diffraction:**

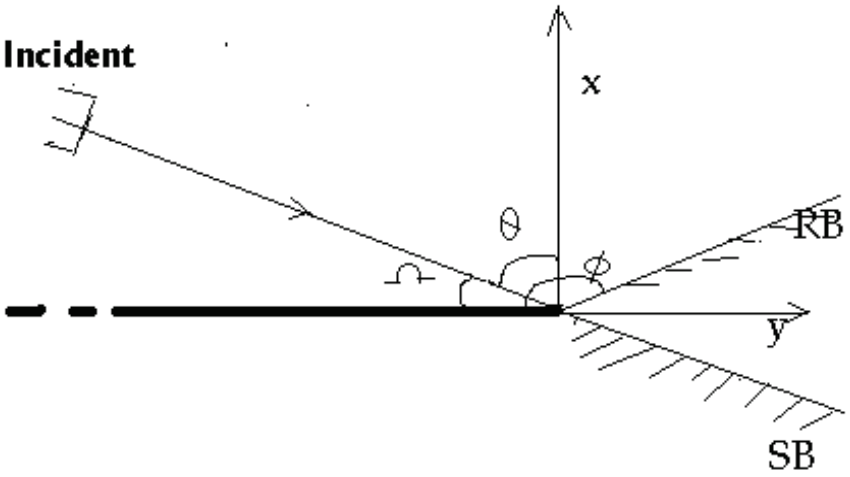


Figure : Field diffracted by half plane

Incident electric field is assumed to be an uniform plane wave with phase referred to origin of the form given as below.

$$E^{inc} = e^{-jk(y\sin\phi - x\cos\phi)}$$

$$E^{ref} = -e^{-jk(y\sin\phi + x\cos\phi)}$$

$$E^{diff} = DE^{inc} r^{-1/2} e^{-jkr}$$

Where

$$D = -\frac{e^{-jp/4}}{2\sqrt{2pk}\sin\beta}\left[\sec\frac{1}{2}(\phi - \omega)\mp\sec\frac{1}{2}(\phi + \omega)\right]$$

- \- sign when $E^{inc}$ is parallel to edge or soft B.C. or Dirichlet B.C.
- \+ sign when $H^{inc}$ is parallel to edge or hard B.C. or Neumann B.C.
- Here $\beta$ is the angle between the incident ray and the edge which in this case is: $\pi/2$.

SEARCH
Next Page
Previous Page

However Keller's GTD fails at the incident and reflection shadow boundary transition regions. The main variants of GTD overcoming this failure are the UTD and the UAT.

**UNIFORM THEORY OF DIFFRACTION:**

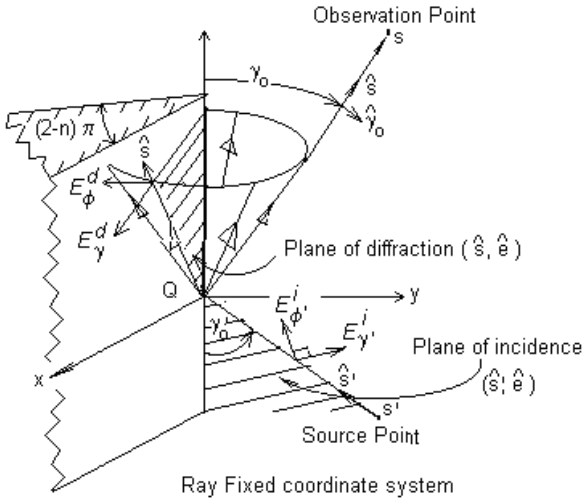


Consider a ray incident on the edge of a perfectly conducting wedge. The diffracted field in matrix form can be written as

$$[E^d] = [D]\ [E^i]\ A(r)\exp(-jkr)$$

where $[E^d]$ and $[E^i]$ are column matrices consisting of the scalar components of the diffracted and incident fields respectively. [D] is a square matrix of the appropriate scalar diffraction coefficients, and r is the distance from the wedge edge to the observation point and A(r) is a spreading factor. Now in general $[E^d]$ will have three scalar components $E^d\rho$, $E^d\phi$, $E^dz$ when edge fixed coordinate system is used. [D] in this case will be three by three matrix. However, when ray-fixed coordinate system is used, there is no component of the diffracted field in the direction of the diffracted ray tube since the incident field is not allowed to have a component in the direction of the incident ray tube. It follows that there are only two possible components of the diffracted field, $E^d\beta$ and $E^d\phi$, and only two components of the incident field, $E^i\beta$ and $E^i\phi$. Clearly [D] is a two by two matrix. In this case [D] has nonvanishing terms on the main diagonal. Thus for plane wave incidence in the ray-fixed coordinate system:

$$\begin{bmatrix} E_s^d(s) \\ E_h^d(s) \end{bmatrix} = \begin{bmatrix} -D_s & 0 \\ 0 & -D_h \end{bmatrix} \begin{bmatrix} E_s^i(Q) \\ E_h^i(Q) \end{bmatrix} A(s)e^{-jks}$$

Thus the ray-fixed coordinate system is the natural coordinate system to be used for wedge diffraction. A compact dyadic diffraction coefficient is used for scattering of electromagnetic waves incident on edges formed by perfectly conducting curved or planer surfaces

SEARCH

Previous Page Next Page

$$D_{s,h} = \frac{e^{-jp/4}}{2n\sqrt{2pk}\sin g_0'} \begin{bmatrix} \cot\left(\frac{p+(f-f')}{2n}\right)F[kLa^+(f-f')] + \\ \cot\left(\frac{p-(f-f')}{2n}\right)F[kLa^-(f-f')] \\ \left\{ \begin{matrix} \cot\left(\frac{p+(f+f')}{2n}\right)F[kLa^+(f+f')] \\ +\cot\left(\frac{p-(f+f')}{2n}\right)F[kLa^-(f+f')] \end{matrix} \right\} \end{bmatrix}$$

**Where $(2-n)p$, is the wedge angle, n=2 for half plane, $f'$ and $f$ are the angle of incident ray and diffracted ray with the plane respectively and**

$$a^{\pm}(f \pm j') = 2\cos^2\left(\frac{2np N^{\pm} - (f \pm j')}{2}\right)$$

Where $N^{\pm}$ are the integers, which most nearly satisfy the equations,

$(2np N^{+}) - (j \pm f') = p$ **and** $(2np N^{+}) - (j \pm f') = -p$

**With**

$$F(x) = j2\sqrt{x}e^{jx}\int_{\sqrt{x}}^{\infty}\exp(-jt^2)\,dt$$

where the spatial attenuation factor A(s) is defined as

$$A(s) = \begin{cases} \frac{1}{\sqrt{s}} & for, plane, cylindrical \\ \left[\frac{s'}{s(s'+s)}\right]^{1/2} & for, spherical, incidence \end{cases}$$

## APPLICATION OF GTD TECHNIQUES:

GTD techniques have been applied extensively to problems of radiation and scattering. Some examples of these are: horn antennas in [6-8], radar cross section in [9] and propagation in [2]. In [6 – 8] the horn was modeled as a dihedral corner reflector with parallel plate wave guide modes or with line source excitation to accurately predict the horn radiation pattern. In [9] it was shown proper application of GTD could be useful in predicting scattering from curved plates. GTD and its extensions have proved to be a powerful tool in solving radiation and scattering problems. Current developments in GTD is driven by the requirements of mobile communication, leading to efficient urban environment ray tracing algorithms and towards diffraction coefficients that address the problem diffraction by obstacles like imperfectly conducting buildings, vegetation etc.

SEARCH

Previous Page Next Page

## REFERENCES


1. M.R.J.A.E. Kwakkermaat et al "High-Resolution Angle-of-Arrival Measurements on Physically-Nonstationary Mobile Radio Channels", IEEE Trans. Antennas Propagat. Vol.56, No.8, pp2720-2729, Aug. 2008
2. Susanne Loredo et al., " Accuracy analysis of GTD/UTD radio channel modeling in indoor scenarios at 1.8 GHz and 2.5 GHz", IEEE Trans. Antennas and Propagat. Magazine, vol.43, No.5, pp35-51, October 2001.
3. J.B.Keller, "Geometrical Theory of diffraction," J.Opt. Soc. Amer., vol. 52, pp. 116-130, Feb. 1962.
4. Ahluwalia, D .S., L ewis, R .M. and B oersma, J . " uni form a symptotic t heory of diffraction by a plane screen,' SIAM J. Appl. Math., vol. 16, pp.783-807, 1968.
5. Kouyoumjian R. G. and Pathak P.H., "A uniform theory of diffraction for an edge i n a perfectly conducting surface." Proc. IEEE, vol. 62, No 11, pp 1448 – 1461, Nov.1974.
6. J. S. Yu, R. C. Rudduck, and L. Peters Jr., "Comprehensive analysis for E-plane of horn antennas by edge diffraction theory," IEEE Trans. Antennas Propagat., vol . 14, no. 2, pp. 138-149, Mar. 1966.
7. J. S. Y u and R . C . R udduck, "H -plane pat tern of a py ramidal ho rn," I EEE T rans. Antennas Propagat., vol. 17, no. 5, pp. 651-652, Sept. 1969.
8. S. Sanyal and A. Bhattacharyya, "UAT analysis of E-plane near and far- field patterns of electromagnetic horn antennas," IEEE Trans. Antennas Propagat., vol. 32, no. 2, pp . 187-189, Feb. 1984
9. S. Sanyal and A. Bhattacharyya, "Electromagnetic scattering by a curved plate-Solution by uni form as ymptotic t heory of di ffraction," A ntennas and Pr opagat., I EEE T rans., vol. 31, no. 5, pp. 817-819, Sept. 1983


SEARCH

Previous Page Next Page

# COMPUTATIONAL ELECTROMAGNETICS (CEM) FOR AEROSPACE APPLICATIONS: FROM CONFORMAL ARRAYS AND RADOMES TO METAMATERIALS AND ACTIVE RCS REDUCTION

*Dr.Rakesh Mohan Jha*
Computational Electromagnetics Lab. (CEM Lab.)
Aerospace Electronics and Systems Division (ALD)
National Aerospace Laboratories (NAL-CSIR)
Bangalore 560017 India
Email: jha@nal.res.in

## ABSTRACT:

The analysis of antennas and EM wave propagation for aerospace applications is distinct from that of the classical antenna analysis which is often done in the free-space environment. In the case of aerospace applications, electrically large scatterers are frequently present, and cannot be ignored. This presentation starts with high-frequency scattering and diffraction phenomena, and the ray tracing approach to unifying the various EM performance parameters such as the mutual coupling, radiation pattern and the radar cross section (RCS) of aerospace bodies. The Geodesic Constant Method (GCM), which is an analytical three-dimensional ray tracing technique, is discussed w.r.t. the evolutionary trends in advanced EM applications for aerospace engineering. Further the examples of conformal arrays facilitated by the GCM and airborne radomes are also discussed.

The emerging trends of metamaterials for radomes, and the active RCS reduction for aerospace applications, are discussed. This is enabled by the extension of ray tracing applications. This talk is primarily based on the author's work reported in open literature. Yet another motivation for this talk is to describe the current activities of the CEM Lab., and finally draw the attention of the audience towards a simple but contemporary research problem.

SEARCH

Previous Page

Next Page

# AUTHOR INDEX



SEARCH

## S



## T



## U



## V



SEARCH

Previous Page

Next Page

## SUBJECT INDEX



SEARCH

## S



## T



## U



## W



## Π